# Coexistence, cooperation and communication

## modeling the complex lives of bacteria

Heilmann, Silja

*Publication date:*
2012

*Document version*
Early version, also known as pre-print

*Citation for published version (APA):*
Heilmann, S. (2012). *Coexistence, cooperation and communication: modeling the complex lives of bacteria*. (Københavns Universitet, Niels Bohr Institute ed.).

# COEXISTENCE, COOPERATION AND COMMUNICATION

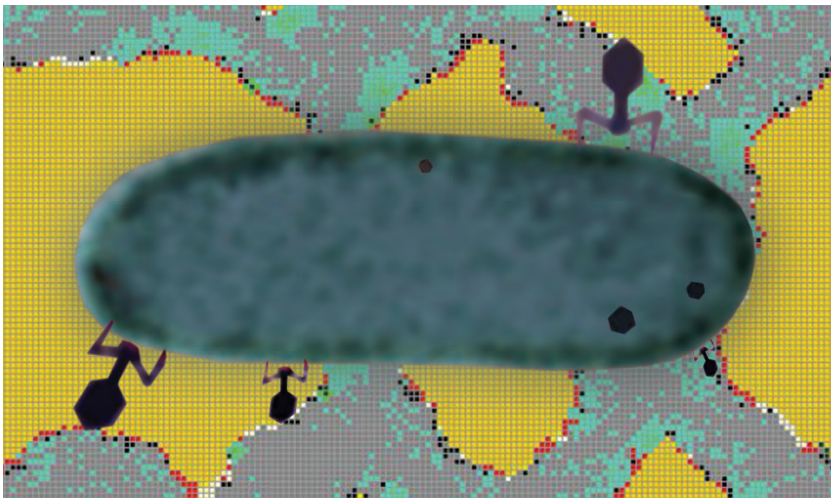

MODELING THE COMPLEX LIVES OF BACTERIA

SILJA HEILMANN

SUPERVISOR KIM SNEPPEN

PHD SCHOOL OF SCIENCE · FACULTY OF SCIENCE · NIELS BOHR INSTITUTE · CENTER FOR MODELS OF LIFE · UNIVERSITY OF COPENHAGEN · DENMARK · 30 JUN 2012

The picture on the cover is an digital collage using a screen shot, from one of the simulations in this thesis, as background. Collage courtesy of artist Hannah Heilmann. Graphical design of the cover, courtesy of graphical designer Sigrun Gudbrandsðottir

for farmor[1]

[1] My biggest idol, who actually saw Niels Bohr lecture in Auditorium A.

# Contents

## List of Publications

1. **Silja Heilmann**, Kim Sneppen, Sandeep Krishna. Sustainability of Virulence in a Phage-Bacterial Ecosystem. *J. Virol.,* 84:3016–3022, 2010.

2. **Silja Heilmann**, Kim Sneppen, Sandeep Krishna. Coexistence of phage and bacteria on the boundary of self-organized refuges. *Proc. Natl. Acad. Sci. (USA), in press*, 2012.

3. Josephine R. Chandler, **Silja Heilmann**, John E. Mittler and E. Peter Greenberg. Acyl-homoserine lactone-dependent eavesdropping promotes competition in a laboratory co-culture model. *ISME J., in press*, 2012.

4. **Silja Heilmann**, Sandeep Krishna and Benjamin Kerr. Accelerating returns from public goods favor quorum sensing in bacteria. *Manuscript in progress.* 2012.

# Abstract

The current knowledge of bacterial ecology and population dynamics in the wild is minimal compared to the amount of information gathered about gene regulation in bacteria on a single cell basis. In this thesis, we formulate several different simple models in order to address some of the questions regarding bacterial ecology and population dynamics, which are still largely unanswered.

We start with the question of how bacteria manage to coexist with virulent phage, a seemingly over-efficient bacterial predator. We explore several known phage behavioral mechanisms via an individual-based, stochastic, spatial ecosystem model and try to assess whether or not these mechanisms enhance coexistence. We find that mechanisms which increase the heterogeneity of spatial distribution of the phage and bacteria, also seem to allow coexistence for a broader range of model parameters. A particularly interesting phenomenon is found when we allow phage to mutate their latent time - the time between infection and the moment where offspring burst out of the bacterial host. Here, we see that the phage which have the highest fitness over long time spans, have a different latent time than those which compete best for new hosts locally. This is due to the fact that the phage which are very efficient at acquiring new hosts tend to wipe out their resources locally and then die out. Consequently there exists a negative selection mechanisms against very efficient killers, which ensures that more mediocre killers prevail in the long run in a spatial system.

We also experiment with different ways of implementing bacterial refuges in which conditions are harsher for the phage in the ecosystem model. When refuges are both fixed in space, and when they form dynamically due to a density dependent mechanism, we find that the presence of refuges greatly expands the range of parameters which allows for coexistence. The condition for facilitating phage and bacterial coexistence on the edges of the refuges are those parameters which inside the refuge make phage so inefficient that they cannot sustain themselves, while in regions of low bacterial density (i.e. on the edge of bacteria colonies or in empty space); phage parameters should be such that phage here are so over-efficient that they would not be able to coexist with the bacteria alone. We find that coexistence on the edges of bacterial refuges in our model share many characteristics with real ecosystems: (i) highly efficient virulent phage with relatively long lifetimes, high infection rates, and large burst sizes (ii) large, stable, and high

density populations of phage and bacteria (iii) a fast turnover of both phage and bacteria (iv) stability over evolutionary timescales despite imbalances in the rates of phage versus bacterial evolution.

Next, we address questions regarding factors that could influence the behavior of bacteria cooperating by producing and excreting common goods. It was been found that common good production is often conditioned by so-called quorum sensing (QS) signals among bacterial cells in a population, but exactly why and when this type communication is beneficial is still unclear. Using a simple 1D model, we analytically determine how the functional form of the benefit gained by having different amounts of common good in the environment, influences the need, or lack thereof, for QS regulation. We find that when benefits initially accelerate, in other words, when the functional form of the benefit versus common good concentration is convex, there exists a critical population number $C_C$ *below* which common good production will not be advantageous, and a critical diffusion constant $D_C$ *above* which common good production will not be advantageous. We also find that having a production strategy which differs from the optimal one comes at a great cost when benefit initially accelerate, which suggests that QS regulation of a common good might be more crucial in this case. We then test the prediction of the 1D model using a stochastic 2D spatial model of quorum sensing cells which can excrete common goods. This model confirms that QS regulation of common good is especially advantageous when the functional form of the benefit versus common good concentration is convex and further shows that the presence of a "cheat", who does not produce common good but nonetheless enjoys the benefits, makes QS regulation crucial for the fitness of the cooperator.

Lastly, we explore a specific scenario of bacterial common good production and communication in which two enemy bacterial species produce QS regulated antibiotics in order to gain a competitive advantage over each other. There exists experimental evidence that some bacterial species condition common good production, not just on their own QS signal, but also on that of the enemy species, a phenomenon which has been termed "eavesdropping". Laboratory experiments with our model system consisting of two species of quorum sensing antibiotic producers, one of which eavesdrops on the other, suggest that a bacterial species may get a competitive advantage by eavesdropping. We construct several simple mathematical models and use these to map out the regions in parameter space where eavesdropping is advantageous and where it is not, and discuss the implications of our model results for the evolution of eavesdropping mutants.

Given that empirical data on bacterial ecology and population dynamics is incomplete, our work not only strengthen existing hypotheses, but also enables us to posit new theories which we hope will in-turn inspire new experiments to test our predictions.

# Dansk resumé

Den nuværende viden om bakterielle økosystemer og deres populationsdynamik i naturlige miljøer er relativ lille i forhold til den store mængde informationer som er opsamlet om bakteriel genregulering på enkelt celle-niveau. Vi har i denne afhandling formuleret en række forskellige simple modeller for at besvare spørgsmål, der vedrører bakterielle økosystemer og populationsdynamik og som stadig er ubesvarede.

Vi starter med spørgsmålet om, hvordan en bakterie formår at sameksistere med en virulent phag - et tilsyneladende overeffektivt rovdyr for bakterien. Vi udforsker flere kendte phag adfærdsmekanismer via en individ-baseret stokastisk og todimensional økosystem model, og forsøger at vurdere, hvorvidt disse mekanismer forbedrer evnen til sameksistens. Vi observerede, at mekanismer som forøger heterogeniteten af den rumlige phag- og bakteriefordeling synes at tillade sameksistens for en bredere vifte af parametre. Vi fandt et særligt interessant fænomen, da vi tillod phagerne at mutere med hensyn til deres latens tid - tidsrummet mellem infektionens start og det tidspunkt hvor phagafkommet bryder ud af den bakterielle vært. De phager, der har optimale overlevelsesevner på langt sigt, har en anden latens tid, end de phager, som er mest konkurrencedygtige når det gælder hurtig udnyttelse af nye lokale bakterielle værter. Dette skyldes, at en phagtype, som meget effektivt erhverver sig nye værter, også har en tendens til at udslette ressourcer lokalt og derefter dø ud. Denne negative selektionseffekt, der virker på de meget effektive bakteriedræbere sikrer, at mere middelmådige dræbere sejrer i det lange løb, når de lever i et rumligt system.

Vi har eksperimenteret med at indføre forskellige arter af bakterielle tilflugtssteder i vores model, hvori betingelserne er hårdere for phagerne. Både når tilflugtsstederne er fastsat i modellens rum, og når de dannes dynamisk grundet en bakteriel densitetafhængig mekanisme, finder vi, at tilstedeværelsen af tilflugtssteder i høj grad udvider spændevidden af parametre, som tillader sameksistens. Betingelsen for at få bakterier og phager til at sameksistere på kanterne af tilflugtsstederne er blot at parametrene inde i tilflugtsstederne gør phagerne så ineffektive, at de ikke kan overleve. Mens regionerne, hvor bakterietætheden er lav (dvs. på kanten af bakterie kolonierne eller udenfor dem) er sådan at phagerne er for effektive til at kunne sameksistere med bakterier alene. Vi observerede at sameksistensen mellem phager og bakterier på kanten af bakterielle tilflugtssteder deler karakteristika med rigtige økosystemer på følgende punkter:

(i) højeffektive phager med forholdsvis lange levetider, høje infektions rater og store mængder afkom (ii) store, stabile populationer med høj densitet af både phager og bakterier (iii) en hurtig omsætningrate for både phager og bakterier (iv) stabilitet over evolutionære tidskalaer trods ubalance mellem hastighederne af h.h.v. phagens og bakteriens evolutions-rater.

Vi tager dernæst fat på spørgsmål vedrørende faktorer, som påvirker adfærden hos bakterier, der samarbejder ved at udskille molekyler, der udgør et fælles gode. Det er blevet observeret eksperimentelt, at en bakteriel "fælles gode" produktion ofte er betinget af såkaldte quorum sensing (QS)-signaler der sendes mellem de bakterielle celler i en population, men præcist hvorfor og hvornår denne type kommunikation er gavnlig, er stadig uklart. Ved hjælp af en simpel endimensionel model, bestemmer vi analytisk, hvordan den funktionelle form af de opnåede fordele ved at have forskellige mængder af fælles gode i miljøet påvirker behovet for, eller mangel på samme, for QS-regulering. Vi finder, at når fordelene accelererer, som funktion af koncentrationen af det fælles gode (altså når den funktionelle form af fordele versus koncentrationen af fælles gode er konveks) findes der et kritisk populationsantal, $C_C$ *under* hvilken fælles gode produktion ikke længere er fordelagtigt, og at der findes en kritisk diffusionskonstant $D_C$ *over* hvilken fælles gode produktion ikke længere er fordelagtigt. Vi observerer også, at bakterietyper som har en fælles gode produktionsstrategi der adskiller sig fra den optimale, har store omkostninger, når den funktionelle form af fordele versus koncentration af fælles gode er konveks; et faktum, der antyder at QS-regulering af et fælles gode, kunne være meget afgørende i netop denne situation. Vi tester derefter forudsigelserne fra vores endimensionelle model med en todimensionel stokastisk model af celler, der udsender QS-signaler og som kan udskille fælles gode molekyler. Denne model bekræfter, at QS-regulering af det fælles gode er fordelagtig, særligt når den funktionelle form af fordele versus koncentrationen af fælles gode er konveks. Modellen viser yderligere at tilstedeværelsen af en "snyder", en bakterietype som ikke producerer det fælles gode men ikke desto mindre nyder fordelene, bevirker at QS-regulering bliver endnu mere afgørende.

Endelig har vi udforsket et bestemt scenarie med bakteriel kommunikation og fælles gode produktion. Scenariet forekommer, når forskellige bakteriearter producerer QS reguleret antibiotika for at opnå en konkurrencemæssig fordel i forhold til hinanden. Der er blevet observeret eksperimentelt, at nogle bakteriearter ikke bare lader antibiotika produktion afhænge af deres eget QS-signal, men også af fjendtlige arters signaler - et fænomen kaldet "aflytning". Laboratorieforsøg med vores model, der består af to arter af QS-signalerende antibiotika producenter, hvoraf den ene aflytter den anden, antyder, at en bakterieart kan opnå en konkurrencemæssig fordel ved hjælp af aflytning. Vi konstruerer dernæst flere matematiske modeller og benytter disse til at kortlægge de regioner i parameterrummet, hvor aflytning giver en fordel, og hvor det giver en ulempe. Til slut diskuterer vi konsekvenserne af vores resultater for udviklingen af

aflyttende mutanter.

Modellerne i denne afhandling har gjort det muligt at formulere en række hypoteser omkring bakterielle økosystemer og populations dynamik; et område hvor eksperimentel data er utilstrækkelig og sporadisk. Vi håber at disse ideer vil inspirere eksperimenter der kan be- eller afkræfte deres validitet i nær fremtid.

# Introductory remarks

## The complex lives of bacteria and why we care

Bacteria are found everywhere on earth in staggering numbers, volume, and diversity[2]. Some of them form an integrated indispensable symbiotic part of the human body[3], while others can cause illness or death. Some are employed in our food and medicinal industries and a majority of the rest are busy in the oceans photosynthesizing, utilizing $CO_2$ to produce oxygen.

A few select bacterial species have been studied extensively in laboratories during the past century and have helped mankind reach great insights into the molecular basis of life. Much is now known about the inner genetic workings of these species, but still very little is known about general bacterial behavior and population dynamics in the wild. Only recently have we acquired the technology, such as high resolution imaging techniques, high throughput gene sequencing and methods for sorting and imaging single cells, which may begin to help us gain a better understanding of bacterial wildlife. The study of bacterial ecology and population dynamics is thus at a very interesting stage, where we may use knowledge about specific mechanisms working inside the cells and start formulating questions about how these mechanism affect a species on a population level in a natural setting. This is a stage where I think simple models could be highly instrumental in leading the way to help us think about these unexplored systems in new ways and perhaps inspire us to design experiments that we would not have thought of otherwise.

[2] A rough estimate of: the total number of bacteria on the planet is $10^{30}$ [143], the total weight of carbon stored in bacterial cells is $350 - 550 \cdot 10^9 tonne$ [143] and the number of bacterial species is $10^5 - 10^7$ [36],

[3] If a human body was a democracy, (and not the neuron-ruled oligarchy that seems to be the case), bacteria would have the majority vote. (Paraphrased from a speaker I sadly forgot the name of).

## A map of this thesis

### Part I

Part I of the thesis deals with questions regarding coexistence between bacteria and their virulent phages. In Chapter 1, we explore different phage behavioral mechanisms which enhance coexistence by facilitating heterogeneity in an otherwise homogeneous spatial environment. In Chapter 2, we further explore spatial heterogeneity by modeling phage-bacteria dynamics in the presence of bacterial refuges; we model refuges both as fixed in space and forming dynamically through a density dependent mechanism. Finally, we explore the nature of the co-evolutionary arms race that can develop in the presence of self-organized bacterial refuges.

### Part II

Part II deals with questions regarding bacterial production of common goods and bacterial communication mechanisms. In Chapter 3, we analytically explore important factors which could influence the behaviour of bacteria producing and excreting public goods. We also attempt to assess the circumstances under which a microbe may benefit from making common good production conditional on communicative cues from other common good producers in the environment. In Chapter 4, we build on the findings from Chapter 3 using a spatial model of common good producing and communicating bacteria; we also introduce a "cheat", a bacterial species which does not incur the cost of common good production but enjoys the benefits, and investigate how the presence of a cheat influences optimal cooperative and communicative behaviour. In Chapter 5, we explore a specific system where the bacterial common goods are antibiotics which are used to combat other bacterial species living in the same habitat. We are interested in probing the phenomenon of bacterial "eavesdropping" - the fact that some bacteria species make antibiotic production depend not just on communicative cues passed between themselves, but also on cues picked up from communication between enemy bacteria.

Biological background information for the models in this thesis will be embedded in the text where appropriate, often mainly in the separate introductory parts of each chapter.

# Part I

# Coexistence

# Chapter 1

# Coexistence of bacteria and virulent phage

## 1.1 Introduction

### 1.1.1 A puzzlingly effective and omnipresent predator

Phage-bacteria ecosystems are found almost everywhere on the planet: in oceans, in soil, on plants and even inside the human body. Phage, together with bacteria, constitute an amount of biomass comparable to that of all plant matter on the planet. Even though phage are easily the most abundant and genetically diverse organism on the planet [12], a remarkable number of questions about how phage and bacteria interact in the wild remain unanswered.
The replication strategies of phages fall into two major categories, virulent and temperate. A temperate phage has the ability to integrate its DNA into the host chromosome, where it is then copied along with the bacterial DNA during cell division. This strategy allows the phage to slow down, or completely stop killing the bacteria, thus reducing the risk of driving its host to extinction. Virulent phage, however, lack this ability. Instead they use the strategy of rapidly replicating within the bacterial cell, lysing it and releasing a large burst of offspring. The time between infection and lysis is known as the latent time of the phage, and the number of offspring released is correlated to this duration. Typically, the latent time is around one bacterial generation [65], during which on the order of a hundred offspring are produced, thereby giving virulent phage an extremely high predator-prey conversion factor compared to most macroscopic ecosystems. Thus, they seem to be remarkably efficient, perhaps even over-efficient, predators.

**The puzzle of virulence.** Questions related to phage bacteria coexistence, population dynamics, and evolution have been extensively studied both theoretically and experimentally: e.g. in [21; 127; 53; 16; 59; 141; 142], yet it remains a puzzle exactly how virulent phage avoid driving their bacterial prey to extinction [17; 104]. Consider, for example, the highly effective T4 phage. For the sake of argument let us assume a burst size of 100 offspring upon lysis.

On average, not more than a single phage out of each burst of 100 should survive to infect another bacterium, or else the phage would rapidly outgrow the bacteria and drive them to extinction. The half-life ($t_{1/2}$) of a free T4 phage particle has been measured to be approximately 10 days in LB[1] at $37°C$ ([28]). Therefore, on average, at least $t_{1/2} = log2(100) \approx 2$ months should pass between infections to prevent runaway phage growth - a time span that seems highly unreasonable for many of the environments where phage and bacteria interact at high densities, such as soil or biofilm. Even a more considered calculation, inserting the above half-life measurement into more realistic Lotka-Volterra-like predator-prey models, does not change the conclusion that T4 and other virulent phages appear to be far too effective predators for coexistence to be feasible [46]. It is, however, an undisputed fact that virulent phages and bacteria have coexisted for eons and still do so everywhere around us and inside us. It is estimated that virulent phage constitute approximately half of the existing phage types on the planet, and they appear to be the dominant type in marine ecosystems [124].

### 1.1.2 The Red queen effect

Perhaps the most prominent explanation for how virulent phage manage to coexist with their bacterial hosts is that they are continuously engaged in a finely balanced co-evolutionary arms race where bacteria constantly avoid extinction by evolving resistance to existing phage and the phage then counter evolve to attack resistant bacteria. This hypothesis, first formulated by Van Valen ref. [130], is known as the "Red Queen" effect. The name is taken from the scene in Lewis Carroll's novel "Through the Looking-Glass, and What Alice Found There" (1871) where Alice is participating in the "Red Queen's race" and running as fast as she can but remaining in the same place. It is a metaphor for an evolutionary arms race where competing species are constantly improving specific fitness while still not improving overall survivability over time in general due to the fact that every specific fitness increase in the prey is counteracted by a similar specific fitness increase in the predator. The Red Queen effect as an explanation for bacteria coexisting with virulent phage has, however, been criticized on the grounds that the rates of evolution of phage and bacteria are not necessarily symmetric [97; 66; 72]. Recent measurements appear support this argument. In soil, for instance, phage appear to be "ahead of the bacteria in the co-evolutionary arms race" [134]. For the Red Queen argument to work, it is necessary that at every stage the phage and bacteria must coexist, without either becoming extinct in order to allow resistant bacteria to evolve. In our view, therefore, although co-evolution is responsible for very long term coexistence between virulent phage and bacteria, (see e.g. [16; 141]) it is also

[1]LB: Lysogeny broth, a nutritionally rich medium used for growth of bacteria.

important to explore non-evolutionary mechanisms that can stabilize predator-prey populations on a shorter time scale.

### 1.1.3 Spatial models

In order to explore mechanisms which enhance coexistence of virulent phage and their bacterial hosts, we have formulated various version of an individual-based stochastic spatial ecosystem model. While we do examine models where the phage and bacteria are repeatedly mixed (mimicking serial cultures or a well-mixed broth), for most of the simulations we use models where the phage and bacteria exist in a two-dimensional space.

Historically, phage-bacterial ecosystem models have often ignored the issue of space, utilizing zero-dimensional approaches such as ordinary differential equations (e.g., see references [7; 18; 69; 68; 78; 121]). However, many real phage-bacterial ecosystems are found in environments with a complex spatial structure, such as soil, biofilms, or wounds in animal and plant tissue. Schrag and Mittler [109] showed that coexistence between virulent phage and bacteria is feasible in a chemostat but not in serial cultures, due to biofilm refuge formation on the walls of the chemostat. Further, experiments done by Brockhurst et al. [12] indicate that reduced phage dispersal can prolong coexistence for virulent phage and bacteria in spatial environments by creating ephemeral refuges for the bacteria. Kerr et al. [59] introduced a simple cellular automaton to model fragmented populations of phage and bacteria in which coexistence was more easily achieved when migration was spatially restricted. Thus it seems introducing spatial dimensions, which allow a degree of heterogeneity in the environment, is an important extension to the often used zero-dimensional predator-prey framework.

### 1.1.4 A map of this chapter

First, in section 1.2, we introduce two models of an ecosystem consisting of one bacterial species and one virulent phage species. In one model the ecosystem is in a two dimensional space, while in the other it is in a well-mixed space. In section 1.3.2, we investigate the effect on coexistence of confining the phage and bacteria to a 2D geometry vs. having a more well-mixed situation, by comparing the behavior of the two models.

Then in sections 1.3.3 and 1.3.5 we explore a series of mechanisms that phage could incorporate into their behavior to enhance coexistence. These can broadly be classified as "hardwired" (where every phage follows the same deterministic strategy) versus "adaptive" (where each phage potentially behaves differently, thus allowing the population to explore different options). We have chosen to look at three specific mechanisms as examples of these categories: (i) phage effectiveness would be reduced if they were unable to register whether they were infecting live

or dead bacteria (a hardwired behavior); (ii) phage could prolong their latent time depending on certain information from the environment (also a hardwired behavior, but a more "active" sort; T4 is known to use such a lysis inhibition strategy), and (iii) phage offspring could have altered latent times due to particular mutations (an adaptive behavior). These mechanisms are described in more detail in sections 1.3.3 and 1.3.5, where we compare their effects in both the spatial and the well-mixed model.

These sections reinforce the well known fact that the latent time of virulent phage is a key parameter that affects their dynamics. In section 1.3.4 we show that for a virulent phage with an inexhaustible supply of host bacteria there is an optimal value for the latent time and burst size. In section 1.3.5 we then show how this optimal value changes when the bacteria are not an inexhaustible resource but have their own population dynamics which both regulates and is regulated by the dynamics of the phage population.

## 1.2 Models

### 1.2.1 Basic model

In the basic model, virulent phage and bacteria interact on an $L \times L$ grid of sites with periodic boundary conditions. Each site in the grid can either be empty or occupied by a single bacterium (each grid site thus has a carrying capacity of one bacterium). The bacterium may be healthy, infected by a phage, or dead. In addition, there can be any number of free phage particles at the site. Time proceeds in discrete steps, $\Delta t$. Precise timers control bacterial cell division and the lysis of an infected bacterium, which releases a burst, $\beta$, of free phage. Other processes are random, e.g., death and diffusion of phage, and are modeled as Poisson processes, (see details in Appendix 1 section 5.6.1).

In each time step, the following can happen.

1. **Bacterial replication.** A bacterium with at least one empty adjacent site will attempt to divide in every time step after the current time has become greater than the value of its replication timer. The probability of replication is set to be proportional to the number of empty neighbor sites. Once a bacterium divides, one daughter cell remains in the original site, and the other is placed randomly in one of the adjacent empty sites. The replication timers of both cells are reset to the current time plus replication time $T$, a parameter which thus sets the growth rate of the bacteria.

2. **Bacterial infection.** A healthy bacterium that shares its site with some free phage may be infected with a probability $p_\alpha$, which depends on the number of phage at the site, the

infection rate per phage per bacterium $\alpha$ and the decay rate of the phage $\delta$. (Note that this means that superinfection – infection by another phage of an already infected cell – is not allowed in the Basic model). The number of free phage at that site is then reduced by one, and the lysis timer of the newly infected bacterium is set to $\tau$ (the latent time of the infecting phage) and starts counting down from that value.

3. **Bacterial lysis.** An infected bacterium will die when its lysis timer has counted down to zero. The number of phage at that site increases, upon lysis, by the burst size $\beta$.

4. **Phage decay.** Free phage die with a probability $p_\delta$ per phage, which depends on the phage decay rate $\delta$.

5. **Phage diffusion.** Each free phage may jump to a neighboring site with a probability $p_\lambda$ which sets the phage diffusion constant.

The burst size increases with latent time: $\beta = \gamma(\tau - \epsilon)$. This formula models the constant rate of replication ($\gamma$) of phage, after a minimum preparatory time ($\epsilon$) usually referred to as the eclipse time [52]. The values of the parameters and the size of the basic time step depend on the choice of phage and bacterial species. With *Escherichia coli*, a reasonable choice is a time step of $10min$, a replication time $T$ of 300 min (i.e., 30 time steps), and an area of $1\mu m^2$ per grid site.

### 1.2.2 Basic model with phage infecting dead and already infected bacteria

This variant is completely similar to the basic model, except that we do not immediately remove bacteria that die to to lysis. The dead bacteria stick around after lysis but decay exponentially with the rate $\delta_B$. They do not block the growth of healthy bacteria, i.e. a replicating bacterium treats a site with a dead bacterium as an empty site. In this model, phage are allowed to "infect" dead bacteria as well as previously infected bacteria. When this happens, this phage disappears from the system – the dead or infected bacterium is left unchanged. The value of $\delta_B = 0.01\Delta t^{-1}$ used in the simulations, results in dead bacteria staying in the system for roughly three bacterial generations before decaying, unless they are overrun by newly replicated bacteria. These choices are explained further in section 1.3.3.

### 1.2.3 Basic model with lysis inhibition

In this version of the model, there are no dead bacteria but phage are allowed to infect previously infected bacteria. Phage can detect such multiple infections. Every time a phage infects an

already infected cell, lysis of this cell is postponed by 8 time steps. We set an upper limit of 200 time steps beyond which lysis cannot be postponed, which gives a maximum burst size of 1330 phage. These choices are explained in more detail in section 1.3.3.

### 1.2.4 Basic model with phage latent time evolution

In this version of the model, the latent times of the phage is allowed to mutate. In each burst of new phage a small fraction (0.5%) have a different latent time from that of the parent phage (and therefore also a different burst size). These new latent times are chosen randomly and uniformly from the range 0 to 50 time steps. The other 99.5% inherit the same latent time as the parent phage. Additionally, 0.5% of bursts are comprised entirely of latent time mutants. (This is done to mimic the fact that occasionally a latent time mutation happens at an early stage of in phage production – this is explained in more detail in section 1.3.5). Burst size for each new phage is calculated from the same formula used in the Basic model, $\beta = \gamma(\tau - \epsilon)$, unless the latent time $\tau$ is less than the eclipse time $\epsilon$, in which case the burst size is zero.

### 1.2.5 Well-mixed model

The well-mixed model is similar to the Basic model, except that (i) upon bacterial cell division, newborn bacteria are placed in a randomly chosen empty grid site, rather than an adjacent empty site, (ii) the probability of a healthy bacterium replicating after $T$ time steps is proportional to the number of empty neighbours averaged over all healthy bacteria, rather than the number of empty sites adjacent to that bacterium, and (iii) newborn phages, released when an infected bacterium is lysed, are randomly placed all over the grid. This results in continuous mixing of the phage and bacteria populations while at the same time ensuring that the two models are as similar as possible to allow for straightforward comparison. We also looked at versions of the Well-mixed model with all of the above phage behavioral mechanisms implemented, i.e. phage infecting dead and already infected bacteria, lysis inhibition and latent time evolution.

## 1.3 Results

### 1.3.1 Coexistence region

The color map in fig. 1.1 shows the average steady-state uninfected bacterial density per grid site $B$ (i.e. fraction of sites occupied by uninfected bacteria), for simulations of the Basic model with various combinations of $\delta$ (degradation rate of phage) and $\alpha$ (infection rate per phage per bacterium). In the deep-red region in fig. 1.1, the phage are so inefficient[2] that they die out and the bacteria subsequently grow to carrying capacity. In the deep-blue region, the phage are so efficient that they drive the bacteria to extinction and then die out themselves. In the middle region, where $0 < B < 1$, coexistence of bacteria and phage is stable. The size of this region in the $\delta$-$\alpha$ parameter plane is a way of quantifying how easily coexistence is achieved in the models we examine, since $\delta$ and $\alpha$ are the main parameters which determine the overall effectiveness of the phage.
It is interesting to note that coexistence in the Basic model requires much higher values of $\delta$ (0.1 to $0.4 min^{-1}$ for, say T4) than has been measured in laboratory conditions. This suggests that the effective death rate for phage may be much higher in real ecosystems than in the laboratory. The typical dynamics of the Basic model involve one or more bacterial colonies that grow at a rate determined by their replication time. These colonies are invaded by phage that move in traveling infection fronts that sweep through the colonies. The speed of the infection front depends on the effectiveness of the phage, i.e., on $\delta$ and $\alpha$. If the phage die too quickly or infect very inefficiently, they go extinct. Conversely, if the phage live a long time or infect quickly, then the infection front may propagate even faster than the bacterial growth front.

**Ecosystem dynamics.** Within the coexistence region, there is considerable variation in the dynamics of the ecosystem, as shown in the four snapshots in figure 1.2. At point A, right at the edge of the coexistence region, the phage infection front in fact travels faster than the bacterial growth front. Nevertheless, there is coexistence because the infection fronts leave behind healthy bacteria often enough to keep the bacterial population from going extinct. However, at point A there is considerable variation in bacterial density with time because the bacteria typically form a small number of big colonies which are then decimated by the fast moving infection fronts. Increasing $\delta$ or decreasing $\alpha$ from point A moves the system deeper into the coexistence region to points B and C, respectively, where there is a higher average bacterial density. Point B, in stark contrast to point A, is characterized by many small intermixed

[2] Henceforth we use the term 'phage efficiency' to mean the phage growth rate in an environment where the bacterial density is kept constant. Parameters that influence phage efficiency are, for example, the infection rate $\alpha$, the burst size $\beta$, the phage degradation rate $\delta$, and the phage diffusion constant.

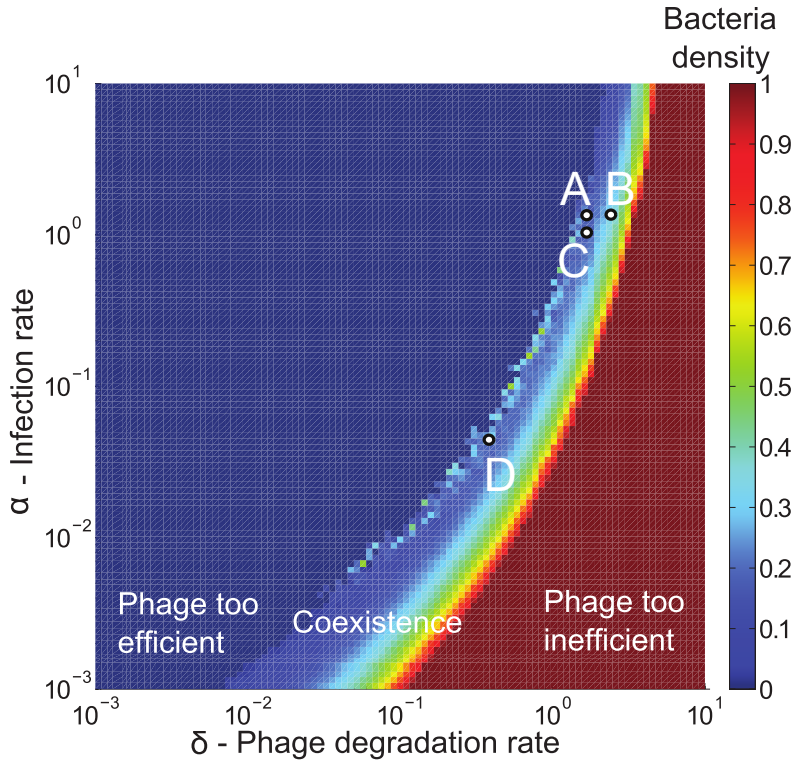


Figure 1.1: **Coexistence region in the $\alpha$-$\delta$ parameter plane. Left:** $\delta$ is the degradation rate of the phage, and $\alpha$ is the infection rate for a phage that occupies the same lattice site as a bacterium (see Appendix 1 section 5.6.1 for details on model implementation). The color map shows the average steady-state bacterial density, $B$, per grid site for simulations with various combinations of $\alpha$ and $\delta$. In the dark-red region to the right, the phage are so inefficient that they die out and the bacteria subsequently grow to carrying capacity. In the dark-blue region on the left, the phage are so efficient that they drive the bacteria to extinction and then die out themselves. In the middle region, where $0 < B < 1$, coexistence of bacteria and phage is stable. The jaggedness of the boundaries, in this and subsequent plots, arises because only a single simulation was done for each $\alpha$-$\delta$ pair. Doing more simulations does not significantly alter the position and shape of the coexistence region.

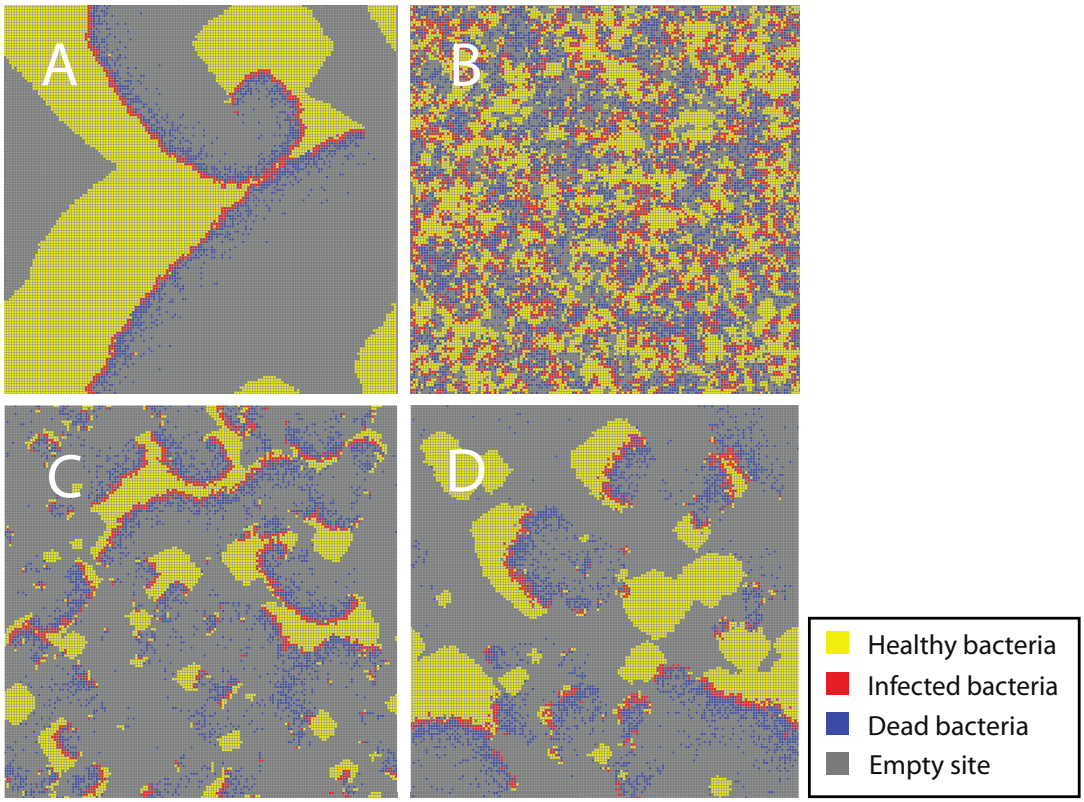


Figure 1.2: **Moving around in the $\alpha$-$\delta$ parameter plane.** Snapshots of simulations at the points marked on the left side plot. At point **A** the phage infection front travels faster than the bacterial growth front. Nevertheless, there is coexistence because the infection fronts leave behind healthy bacteria often enough to keep the bacterial population from going extinct, but there is considerable variation in bacterial density with time. Point **B** is characterized by many small intermixed domains of bacteria and phage and their total populations are quite stable with relatively small fluctuations. At point **C** bacteria survive a passing infection front more often than at point A (because of the lower infection rate) and, therefore, the bacterial domains are smaller and more dispersed. The dynamics at point **D** are very similar to the dynamics at point C because they lie on the same isocolor line (lines of constant bacterial density). Grid size used in simulations was $100 \times 100$. Initial conditions consisted of 5% of the grid sites occupied by healthy bacteria and 0.5% of sites occupied by infected bacteria, randomly chosen.

domains of bacteria and phage, and their total populations are quite stable with relatively small fluctuations. At point C, bacteria survive a passing infection front more often than at point A (because of the lower infection rate) and, therefore, the bacterial domains are smaller and more dispersed than at point A. Qualitatively similar patterns and dynamics are observed as one moves along isocolor lines (i.e., lines of constant bacterial density) to lower $\delta$ and $\alpha$ values. Thus, the dynamics at point D are very similar to the dynamics at point C. At very small $\delta$ values ($\delta \leq 10^{-4}$), however, the system starts behaving like a well-mixed system because the phage are able to diffuse across the entire grid before either dying or infecting.

### 1.3.2 Coexistence is more easily achieved in the Basic model than in the Well mixed model

Figure 1.3 compares the coexistence regions for the Basic and Well mixed models, keeping all parameters other than $\delta$ and $\alpha$ fixed at their default values. The coexistence region is approximately 20% smaller for the Well mixed model than for the Basic model. The right boundary of the coexistence region coincides for both models and is situated where the time between infections is so long that on average only one phage per burst survives (see Appendix 1 section 5.7 for derivation of an analytical expression for the right side boundary). The left boundary, however, is situated further to the left for the Basic model than for the Well mixed model, meaning that in a 2D geometry the bacteria can coexist with far more effective phage than in the Well mixed model. In fact, in the Well mixed model the left boundary corresponds to the onset of high-amplitude oscillations in the populations. These oscillations cause the bacterial numbers to periodically fall to extremely low levels. Each time this happens there is a finite probability that all the remaining bacteria will be infected before they divide so, sooner or later, high amplitude oscillations like these cause the bacteria go extinct. For the same parameter values, the Basic model shows damped or low-amplitude oscillations and therefore coexistence.

### 1.3.3 Hardwired phage behavioral mechanisms which enhance coexistence

Figure 1.4 shows the coexistence regions when two hardwired mechanisms are implemented in the Basic model (see section 1.2). Both impede phage infection and dispersal, but in different ways.

**Phage infecting dead and previously infected bacteria.** First, the left panel in Fig. 1.4 shows what happens if phage simply cannot distinguish between healthy and infected/dead bacteria - they infect whatever they come into contact with and when that is a dead or previously infected bacterium, the phage effectively dies. Traditionally, phage-bacterial models ignore the

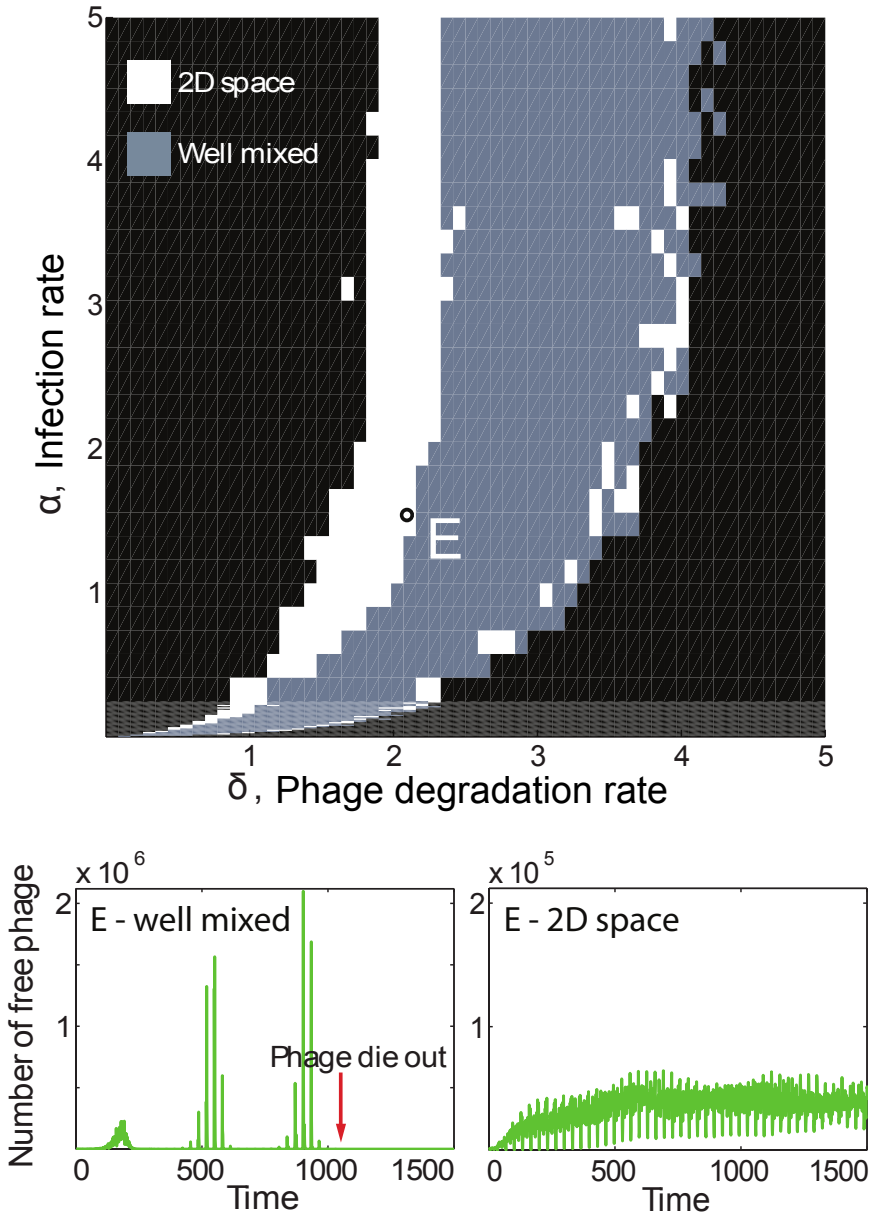


Figure 1.3: **Space enhances coexistence. Top:** Outline of coexistence regions for the Basic (2D space) and Well mixed models plotted on top of each other. In the white region, there is coexistence only in the Basic model. In the gray region, there is coexistence in both models. The area of the gray region is around 20% smaller than the area of the white region signifying that coexistence is more easily achieved in a 2D geometry than in a well mixed system. **Bottom:** The green curves show the total number of free phage in the Basic and Well mixed models as a function of time, for the parameters corresponding to the point marked E in the top panel. In the Basic model the population quickly settles to a stable level, with some fluctuations. In contrast, the Well mixed model exhibits oscillations with increasing amplitude that eventually drive the bacterial population, and subsequently the phage, to extinction.

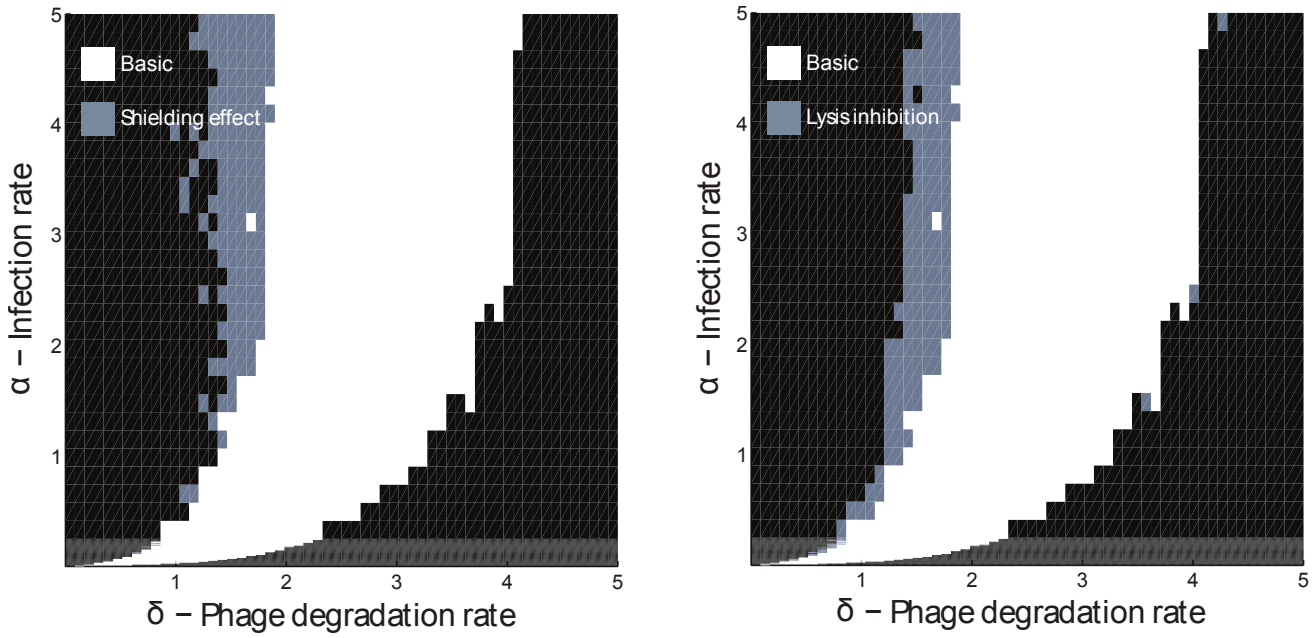


Figure 1.4: **Effects of two hardwired phage strategies on the coexistence region.** In both plots, the white region corresponds to parameters where there is coexistence in the Basic model both with and without the two phage strategies, while the gray region shows where there is coexistence only when the corresponding phage behavior is implemented. **Left:** Phage infect live, dead, and infected bacteria alike (see section 1.2.2). **Right:** Multiple infections of the same bacterial cell result in delayed lysis (see section 1.2.3).

interaction of phage with dead and infected bacteria [89; 69; 121; 18]. It has, however, been proposed that the build up of bacterial debris could hinder phage diffusion, protect live bacteria, and enhance coexistence [7; 97]. This is indeed the effect we see in the left panel in fig. 1.4 at the left boundary of the coexistence region. In contrast, the right boundary is unaffected because here the phage population is relatively low, on the verge of extinction, while the bacterial population is very close to the carrying capacity so infection of previously infected or dead bacteria is rare.

**Lysis inhibition.** The right panel in figure 1.4 shows the effect of a more "active" strategy, where the phage can detect multiple infections and delay lysis. T4 is known to use such lysis inhibition [11; 33]. Through a mechanism involving the anti-holin protein rI, T4 delays lysis by 5 to 10 min whenever the cell becomes super infected with an additional T4 phage (Ryland Young, Texas A&M University, personal communication). We implement this effect in the Basic model by allowing phage to infect already infected cells. Whenever this happens, lysis is postponed by 8 time steps. However, we set an upper limit of 200 time steps beyond which lysis cannot be postponed. This gives a maximum burst size of $1,330$ phage, which approximately corresponds to the maximum phage production possible using the resources available in a single bacterium [33]. This mechanism also boosts coexistence, as shown in the right panel in fig. 1.4. Again, the right boundary is unaffected because super infections are rare here. The possibility of infecting dead and infected bacteria effectively increases $\delta$ for the phage, whereas delaying lysis upon super infection effectively decreases $\alpha$ (by reducing burst size per phage). Either way, the result is shifting the left boundary of the coexistence region further to the left compared to the Basic model.

**Hardwired phage behavioral mechanisms in the Well mixed model.** We also tried implementing these two behavioral strategies in the Well mixed model. However, with the degradation rate of dead bacteria fixed at $\delta_B = 0.01$, we saw no significant effect of letting the dead and infected bacteria act as sinks for phage. $\delta_B$ would have to be much lower, i.e. the dead bacteria would have to remain in the system for much longer, for any effect to be visible. This result emphasizes how the same mechanism can produce different outcomes when implemented in a spatial and a non-spatial model.

### 1.3.4 Optimal latent time

The latent time $\tau$ is the duration between infection and lysis. It has been shown experimentally that the phage proteins which cause lysis, called holins, control the timing of lysis with very high precision ($\pm 1 min$) and that point mutations within the holin gene can significantly alter

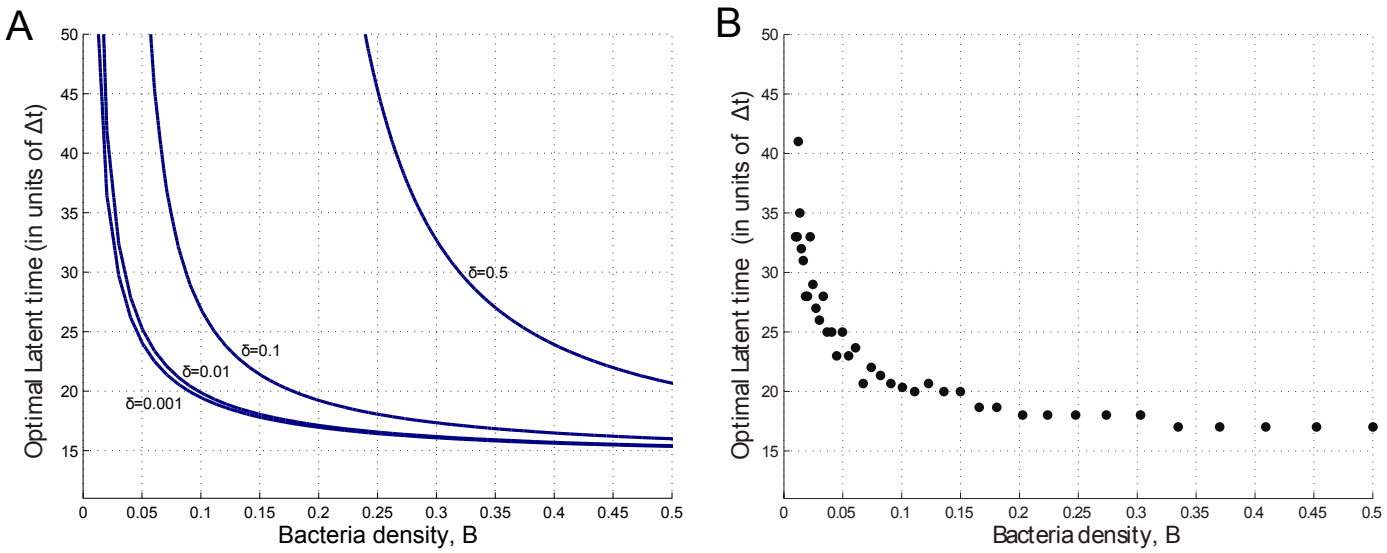


Figure 1.5: **Optimal latent time as a function of bacteria density, when host density is constant. A:** Optimal latent time, $\tau_{opt}$, as a function of the constant bacterial density in a well mixed environment (equation 1.3), for different values of the phage degradation rate, $\delta \in [0.001, 0.01, 0.1, 0.5]$ (with $\alpha = 1.0$ kept fixed). For low bacterial density, phage with long latent times (and thus large burst sizes) have highest fitness, while at high bacterial densities phage with low latent times and small burst sizes do well. When the phage degradation rate is increased $\tau_{opt}$ tends to shift towards higher values. **B:** Optimal latent time as a function of bacterial density when a phage infection front propagates through a bacterial lawn of fixed density. Each point corresponds to the position of the tallest maximum of a distribution like the one shown in fig. 1.6 and fig. 1.8B when averaged over 40 simulations done for each value of $B$. Parameters used for these simulations were $\alpha = 1.0$ and $\delta = 0.001$.

the lysis time without changing this precision [137]. Experimental studies have also shown that phage kept at a high constant bacterial density will very quickly evolve to have a shorter latent time [47]. The fact that the latent time of a phage is a highly malleable genetic trait [149] makes it an interesting choice for evolutionary change in a model study. A short time span after infection the production of phage progeny starts inside the cell at a constant rate $\gamma$; the time span between infection and the onset of phage production is termed the eclipse time $\epsilon$. Because phage are produced at a constant rate, the burst size $\beta$ is a linear function of the latent time [65]:

$$\beta = \gamma(\tau - \epsilon) \tag{1.1}$$

The generation time $T_P$ of the phage is the sum of the latent time $\tau$ and the duration of the diffusive extracellular search for a new host. Both burst size $\beta$ and generation time $T_P$ are thus a function of the latent time $\tau$. Maximizing phage growth is therefore a question of

simultaneously minimizing generation time and maximizing burst size. This presents a tradeoff since reducing latent time decreases generation time while increasing latent time increases burst size. In a well mixed system with a constant bacterial density, $B$, the average time for a new phage to find and infect a bacterium is $(\alpha B)^{-1}$, therefore phage growth can approximately be described by:

$$P(t,\tau) = P_0\left(\beta \exp\left(\frac{-\delta}{\alpha B}\right)\right)^{t/T_P} \tag{1.2}$$

$$= P_0\left((\tau-\epsilon)\gamma \exp\left(\frac{-\delta}{\alpha B}\right)\right)^{t/(\tau+\frac{1}{\alpha B})} \tag{1.3}$$

Where $P(t,\tau)$ is the phage population size and $P_0 \equiv P(t=0)$.
By solving[3] $\lim_{t\to\infty}\left[\frac{\partial}{\partial\tau}\left(\frac{\partial P}{\partial t}\right)\right] = 0$, we can determine the latent time, $\tau_{opt}$, which maximizes[4] the phage growth rate, $\frac{\partial P}{\partial t}$.This optimum satisfies:

$$\frac{1}{\alpha B}\left(\frac{1+\tau_{opt}\alpha B}{\tau_{opt}-\epsilon}+\delta\right) = \log\left[\gamma\left(\tau_{opt}-\epsilon\right)\right] \tag{1.4}$$

and is plotted in fig. 1.5A. We see that for low bacterial density, phage with long latent times (and thus large burst sizes) have highest fitness, while at high bacterial densities, phage with short latent times and small burst sizes do best, consistent with the experimental observations in [47; 30; 112; 2].

**Selection pressure.** When $f(\tau) \equiv \frac{\partial P}{\partial t}\big|_{t=t'}$ (for any fixed $t' \gg \tau_{opt}$) is plotted as a function of $\tau$, it will peak very close to $\tau = \tau_{opt}$. The sharper the maximum, the higher is the selection pressure acting at those parameters, because a sharp peak means that a small change in latent time $\tau$ makes a large change to the phage growth rate. The sharpness of the peak at $\tau = \tau_{opt}$ can be quantified by $S = \left|\left(\frac{\partial^2 f}{\partial\tau^2}\right)_{\tau=\tau_{opt}}\right|$ and we see in fig. 1.7 that $S(B)$ increases with increasing $B$, consistent with the observations and conclusions in [47][5].

**Phage infection front propagating through a bacteria lawn of constant density.** In real life phage probably rarely encounter environments with perfectly constant bacterial den-

[3] For $t \to \infty$, $\tau_{opt}$ does not depend on $t$.

[4] Several other studies have outlined a procedure for determining $\tau_{opt}$ (see e.g. [1]), however the actual derivation done here (which includes the effect of phage degradation) has not to our knowledge been published anywhere.

[5] In ref. [47] they perform experiments where they let phage T7 evolve towards the optimal latent time in both high and low host density environments. They find that T7 evolve quickly to a value near the optimal latent time in the case of high host density, but fail to detect any noticeable phenotypic evolution for the phages at low host density. They too comment on the fact that the strength of selection is greater for high density than for low, and that this may be the reason why they do not see any significant change towards the optimal latent time during the limited time span of the experiment.

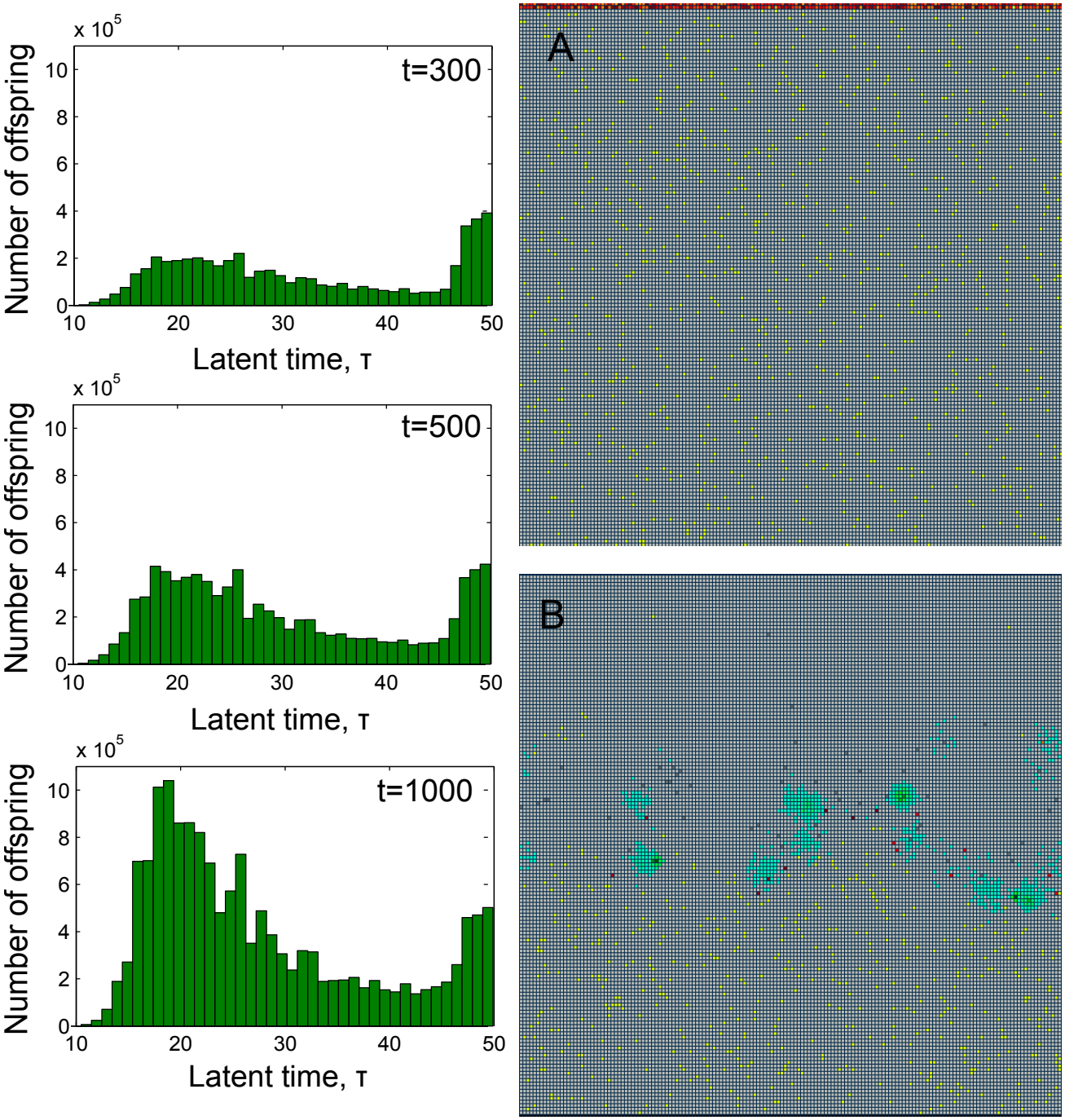


Figure 1.6: **Determining optimal latent time for a phage infection front propagating through a lawn of bacteria of constant density. Left:** The three plots show the phage distribution at different points in time. Note that the peak of the distribution at higher latent times is tallest early in the race, whereas later the local maximum at lower latent time catches up and then takes the lead. **A:** Initial condition used for the spatial simulations where an infection front was allowed to spread down through a bacterial lawn of constant density. The upper line of infected bacteria contains equal numbers of infected bacteria with latent times taking integer values in the range 11 to 50 time steps, randomly arranged along the line. Throughout the simulation 0.5% of each new batch of phage had a new mutant latent time different from the parent phage, drawn randomly and uniformly from the range $\tau \in [0, 50]$. Light red signifies bacteria infected with short latent time phage and darker red signifies bacteria infected with long latent time phage. **B:** Snapshot of the moving infection front. Diffusing free phages are depicted by shades of green, with darker greens corresponding to higher phage numbers at that site. Initial bacterial density in the lawn for these plots was $B = 0.043$.

sity, partly because of external environmental factors and partly because the phage themselves strongly influence bacterial density. One could however imagine that phage would encounter situations where an infection front propagates through a region of near constant density of bacteria, similar to a phage infection front spreading through a lawn of bacteria on an agar plate. In order to assess what the optimal latent time is in this situation we did simulations where an initial straight line of infected bacteria were allowed to burst and spread phage down through an area of constant bacterial density (see 1.6A). The initial line contained equal numbers of infected bacteria with latent times taking integer values in the range 11 (one more than the eclipse time which is fixed at 10) and 50 time steps, randomly arranged along the line. A small fraction of each new burst of phage were then mutated to have a different latent time (and therefore also a different burst size) from the parent phage. (The latent times of 0.5% of the phage from each burst are chosen randomly and uniformly from the range 0 to 50 time steps. The other 99.5% inherit the same latent time as the parent phage. Additionally, 0.5% of the bursts are comprised entirely of latent time mutants). The optimal latent time was determined at the end simply by counting which phage type managed to produce most offspring during the course of a simulation (the final data shown in fig. 1.5B is an average over 40 simulations done for each value of $B$).

**Bimodal phage distribution.** In these simulations the phage which burst right at the edge of the front will effectively feel a density of one half that of the actual density of the lawn. The bacteria infected with phages which have longer latent time however will not burst right at the edge of the moving front but always some distance behind since the pace of the front is set by the phage with low latent times. This means that these long latent time phage effectively feel a lower density of bacteria. The phage with very long latent times are well equipped to deal with a low density of host because of their large burst sizes. Phage with medium latent time on the other hand succumb since they can not keep up with the fastest phage and cannot compete with the high latent time phage in the low host density left behind the propagating front. Thus, the effect the moving front race has on the distribution of phages is that it makes it bimodal, one peak at low latent times and one at high, see fig. 1.6. This effect is especially pronounced for relatively low bacterial densities of $0.01 < B < 0.1$. Over longer time spans, the peak at low latent times always becomes the tallest and the curve for optimal $\tau_{opt}$ (now defined as the position of the highest peak) versus density turns out to be qualitatively very similar to the analytical result shown in fig. 1.5.

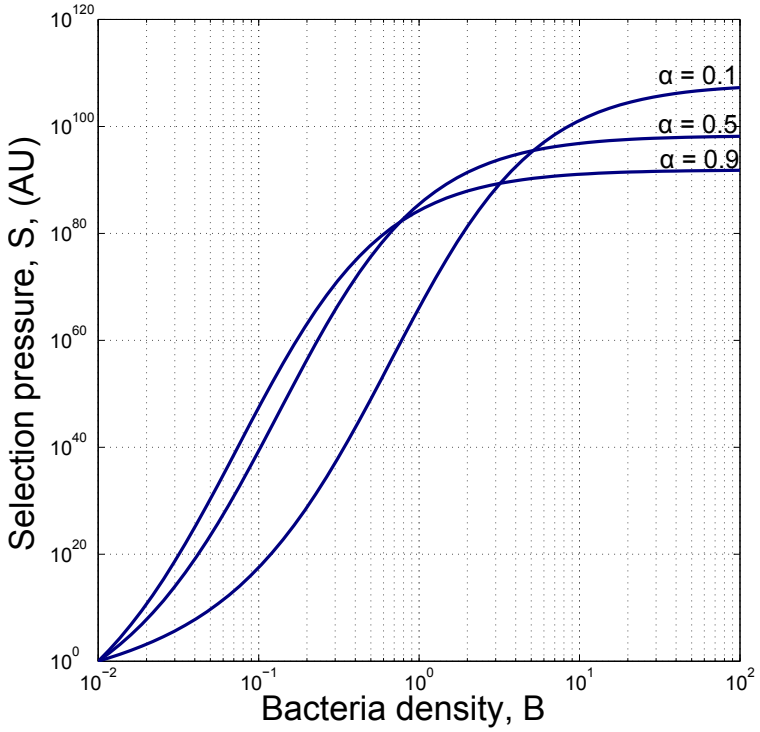


Figure 1.7: **Selection pressure increases with host density.** Selection pressure $S = \left| \left( \frac{\partial^2 f}{\partial \tau^2} \right)_{\tau=\tau_{opt}} \right|$ (where $f(\tau) \equiv \frac{\partial P}{\partial t}\big|_{t=t'}$ and $t' \gg \tau_{opt}$, see equation 1.3 and 1.4), plotted as a function of the bacterial density, $B$, for different values of the phage infection rate $\alpha \in [0.1, 0.5, 0.9]$. Parameters used for plot: $t' = 1000$, $\epsilon = 10$, $P_0 = 1$, $\gamma = 7$, $\delta = 0.001$.

### 1.3.5 An adaptive phage behavioral mechanism which surprisingly can enhance coexistence

The above analytical calculation and simple spatial simulation gives a first simple idea about the trade off and associated optimal phage latent time in the specific situation of a constant bacterial density environment. We wished to go further and asses what constitutes optimal phage latent time behavior in the more complex setting of the dynamic Basic model where bacterial density is not constant but continuously fluctuating and strongly influenced by the phage density.

**Implementing phage latent time mutability.** We modified the Basic model to, once again, allow a small fraction of the phage progeny of each burst to mutate to have a different latent times (and therefore also a different burst size) from the parent phage. (The latent times of 0.5% of the phage from each burst are chosen randomly and uniformly from the range 0 to 50

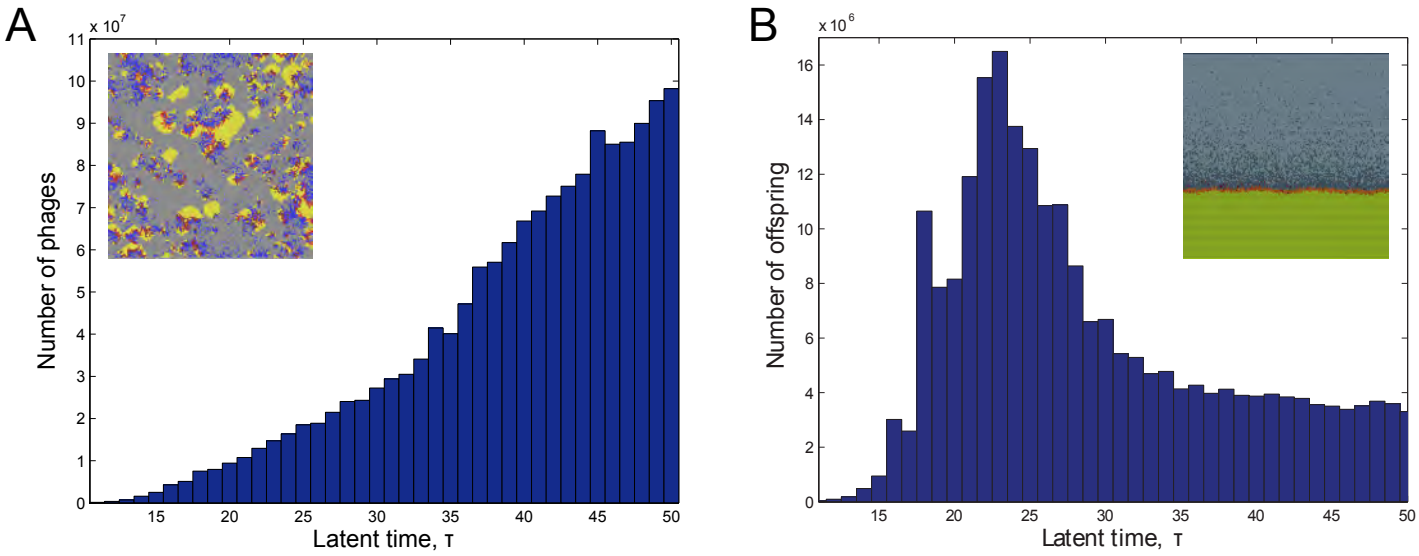


Figure 1.8: **Optimality depends on the context. A:** The cumulative distribution of phage offspring as a function of latent time for simulations of the Basic model, with latent time mutability, over 50,000 time steps (counted after the dynamics had reached steady state). (The distribution has been corrected for the constant level of production that all phage types experience because of the level of random mutation - this means that the column of phages with $\tau = 11$ is only comprised of the phages with $\tau = 11$ that have infected once and produced offspring, not including the random number of phages in each burst that just happened to get $\tau = 11$). The average bacterial density for a steady state in these simulations was $B = 0.15 \pm 0.025$, but the average bacterial density experienced by the phage is probably much higher due to the fact that the bacteria form colonies and that phage are usually released on the edge or close to the edge of a colony. **B:** The cumulative distribution of phage offspring as a function of latent time for simulations, with latent time mutability, where a phage infection front has propagated through a bacterial lawn of maximal density (i.e. $B = 1.0$). The maximum of the distribution corresponds to the optimal latent time for that particular bacterial density. For relatively high bacterial densities ($B > 0.1$) the bimodality of the distribution is not very pronounced - as seen here where the second maximum at higher latent times is not visible (compare with fig. 1.6, at $t = 1000$). Parameters used in both plots were $\alpha = 1.0$ and $\delta = 1.5$ (corresponding to point C in fig. 1.1).

time steps. The other 99.5% inherit the same latent time as the parent phage. Additionally, 0.5% of the bursts are comprised entirely of latent time mutants. See section 1.2.4).

**Latent time mutability enhances coexistence in the Basic spatial model.** The left panel in Fig. 1.9 shows that implementing this adaptive mechanism actually enhances coexistence in the spatial model. It is not intuitively obvious why this strategy helps. When the bacterial density is kept fixed, we saw earlier that the phage will, in general, evolve towards an "optimal" latent time which maximizes the rate with which they spread in that density, thus also maximizing the rate at which they kill bacteria. For lower bacterial densities $0.01 < B < 0.1$ we saw that the fitness distribution became bimodal (albeit with the tallest peak still at short latent time).

**Optimal latent time on short and long time scales.** However, in this variant of the Basic model, the phage who perform best in the long run turn out to be the ones with long latent times and large burst sizes (see fig. 1.8A). Initially one could be tempted to conclude that the effective bacterial density seen by a phage in the Basic model must then be relatively low since we saw before that low bacterial density tends to select for long latent times. It is hard to asses exactly what bacterial density the phage on average experience in the Basic model but just from looking at the simulations (see e.g. insert in fig. 1.8 on the left) we can conclude that it has be a relatively high density, because phage are usually released right at or close to the edge of a colony which has a density close to $B = 1$. The phage distribution for runs with an infection front spreading over a lawn with this kind of high density has a very clear peak at a short latent time ($\tau_{opt} \approx 23$, see fig. 1.8B) and the bimodality of the distribution is not prominent. Thus, this cannot explain why long latent time phage do best in this variant of the Basic model – phage with a $\tau$ around this optimum ($\tau_{opt} \sim 23$) should form infection fronts which move faster than the growth front of a bacterial colony. One then also wonders why the host population is not wiped out by the appearance of these optimal "efficient killers," resulting in an overall reduction of coexistence compared to the Basic model with a single, constant latent time. The reason this does not happen and why the long latent time phage do best in the long run is, it seems, that when an "optimal" phage mutant arises in a colony it quickly wipes it out and subsequently goes extinct if it cannot quickly find another colony nearby to infect.

**A negative selection effect against efficient killers.** Thus, when the bacterial population is split into many small colonies, there is effectively selection *against* very efficient phage, even though they outperform the long latent time phage locally when looking at one isolated colony. In turn, the very existence of phage with different latent times makes the system self-organize

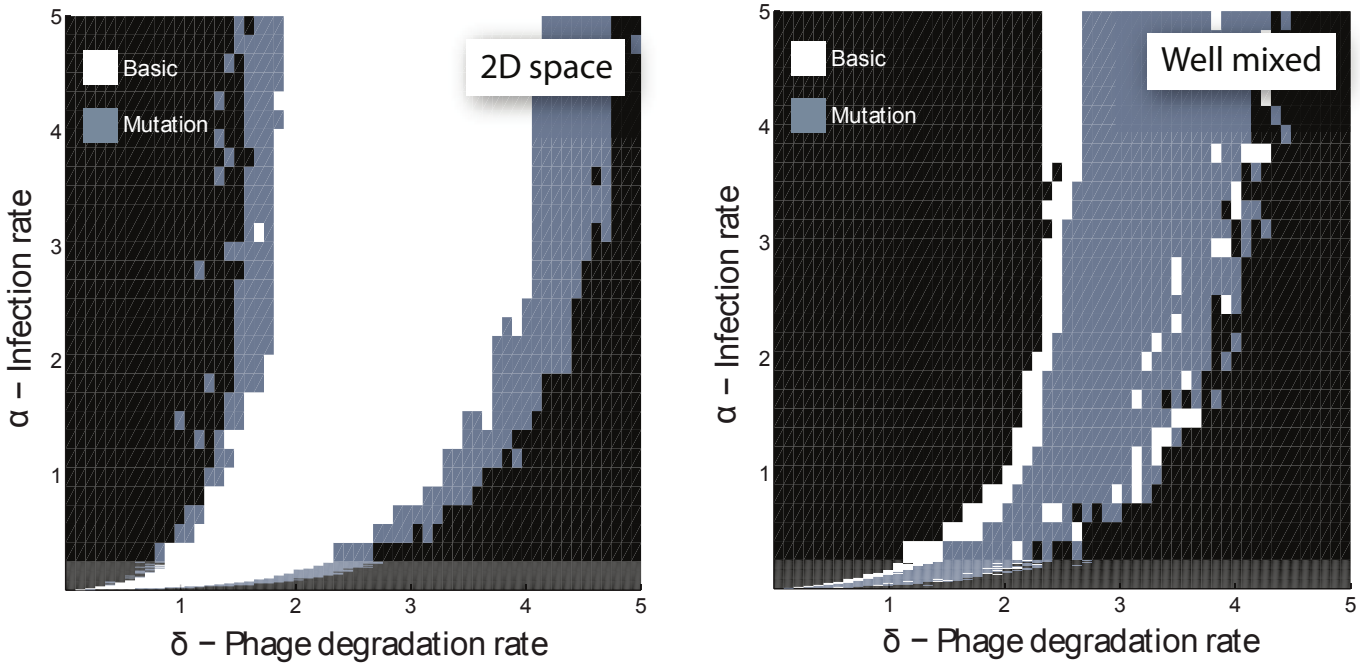


Figure 1.9: **Effect of an adaptive phage strategy where latent times are allowed to mutate. Left:** The white region corresponds to parameters where there is coexistence in the Basic model both with and without latent time mutability, while the gray region shows where there is coexistence only when latent time mutability is implemented. **Right:** The gray region corresponds to parameters where there is coexistence in the Well-mixed model both with and without latent time mutability, while the white region shows where there is coexistence only when latent time mutability is *not* implemented.

to have a larger number of small bacterial colonies compared to the Basic model, as shown in Fig. 1.10D, without which there would be no negative selection against these "optimal" phage mutants.

**Latent time mutability decrease coexistence in the Well mixed model.** In contrast, in the Well-mixed model, the optimal phage mutants that arise have access to the entire bacterial population so there is no negative selection to restrain them. This, along with the increased oscillations we observe when implementing the adaptive strategy of latent time mutability in the Well-mixed model, makes coexistence harder to achieve in this version of the model than in the absence of this mechanism (Fig. 1.9 right panel).

## 1.4 Discussion

### 1.4.1 Space and heterogeneity boosts coexistence

The comparison between the different versions of the Basic and Well mixed models shows that space boosts coexistence - even uniform two-dimensional space, without any built-in heterogeneity such as permanent bacterial refuges. Spatial heterogeneity arises spontaneously as a result of the dynamic interaction between the bacterial growth fronts and the propagating phage infection fronts and is crucial for enhancing coexistence. In the Well-mixed model, which lacks this heterogeneity, the infection and burst events are more prone to happen in synchrony for the whole system, often resulting in large-amplitude oscillations that destroy coexistence. In the Basic model, each small bacterial colony might experience oscillations or big population fluctuations, but on a larger spatial scale these average out because the life cycles of the phage attacking separate colonies quickly become desynchronized and uncorrelated. When looking at figure 1.1 and 1.2, we see that moving from point A deeper into the coexistence region to point B (by increasing $\delta$) or point C (by decreasing $\alpha$) results in more heterogeneity (as shown by the snapshots in the figure).

**Phage infecting dead and previously infected bacteria.** When phage can infect dead or previously infected bacteria, their $\delta$ is effectively increased. Thus, one would expect this behavioral mechanism to increase heterogeneity compared to the Basic model. This is exactly what we see in Fig. 1.10, which shows snapshots of the ecosystem for the Basic model and the different strategies, for the same parameter values. That shielding by dead bacteria enhances coexistence has been observed before in models that lack space [7; 97]. However, in these models, to see a significant effect, the dead bacteria must remain in the system for quite long times. In our Basic model, the enhancement of coexistence is much more dramatic. Even when the degradation rate of the dead bacteria is such that we cannot see any enhancement of coexistence in the Well mixed model (see fig. 5.15 Appendix 1), we still see a distinct enhancement in the Basic model. This is because the free phage and dead bacteria are typically co-localized in the Basic model, because both are "created" by the same events.

**Lysis inhibition.** The mechanism of lysis inhibition also works in slightly different ways in the Basic and Well mixed models. It has been previously argued that this mechanism could enhance coexistence in the following way: the original infecting phage interpret super infection as a sign that phage outnumber host cells in the external environment [99], whereupon delaying lysis gives the few bacteria left alive out there an additional chance to reproduce, thereby reducing the risk of driving them to extinction [122]. This reasoning breaks down in the well mixed case

because lysis inhibition also creates ticking "time bombs" – multiply super infected bacteria that release a huge number of phage when they eventually burst, which counteracts the effect of allowing bacteria more time to replicate. In the Basic model, however, these time bombs are typically left behind by the moving infection front so when they do lyse and release a huge number of phage, these phage are generally relatively far from susceptible bacteria. (We did observe some enhancement of coexistence in the Well mixed model also when lysis inhibition is implemented (see fig. 5.15 Appendix 1), but here it occurs because the strategy of delaying lysis desynchronizes burst events and therefore dampens oscillations).

**Optimal latent time in a constant bacterial density.** From simple analytical arguments about phage growth in a well mixed environment with constant bacterial density, it is seen that phage face a tradeoff when "choosing" a latent time, because short latent times decrease generation time while long latent times increase burst size. If the host density is high and the time taken by diffusive search for new hosts is short, the phage can achieve exponential growth, instead of linear growth inside one cell, by bursting early and infecting neighbouring cells. On the other hand, if host density is low the phage is better off using the resources inside each bacterium to the fullest; basically the burst size needs to be large enough to ensure that the diffusive search is successful and at least one new host is infected per burst. Several experimental studies have dealt with phage fitness and its dependence on the density of host [47; 30; 112; 1] and our observations are in line with their experimental observations and their general conclusions about the trade off associated with an optimal latent time.

**Optimality in the setting of a propagating infection front.** In the simple spatial simulations where an infection front was allowed to propagate through a lawn of bacteria of constant density, we saw the same general trend as the well mixed analytical argument predicts. However, for relatively low bacterial densities ($0.01 < B < 0.1$) there was an interesting twist: the fitness distribution had more than one local maximum. The first peak at short latent times appears to be at a value close to what would maximize the front speed. The second peak at longer latent times is harder to understand, but the following speculative argument may hint at the explanation:
The pace of the infection front is set by phage with short latent times and bacteria infected with longer latent time phages will burst at different distances $x = f(\tau)$ from the infection front, where $f(\tau)$ is an increasing function of $\tau$. Let $\tilde{B}(\tau)$ denote the bacterial density at which phage with latent time $\tau$ are optimal in a well-mixed system, which can be calculated from equation 1.4 ($\tilde{B}(\tau)$ is a decreasing function of $\tau$). Let $B(x)$, a decreasing function of $x$, denote the bacterial density left behind a passing infection front at a distance $x$ from the position of

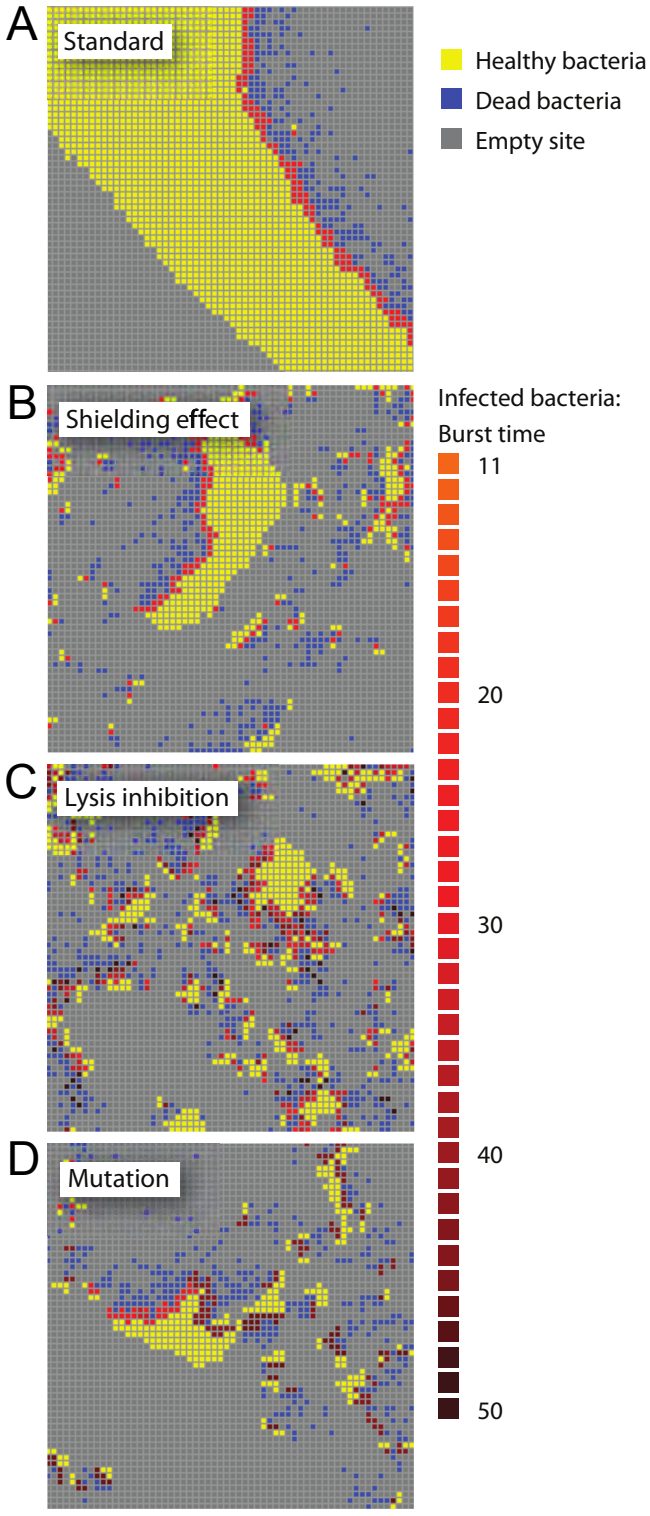


Figure 1.10: **Heterogeneity and enhanced coexistence go hand in hand.** Close-up views of ecosystem snapshots of the Basic model for parameters corresponding to point A in fig. 1.1. **A:** Basic model (phage latent time is fixed at 30 time steps). **B:** Phage infect live, dead, and infected bacteria alike (phage latent time is fixed at 30 time steps). **C:** Basic model with delayed lysis upon super infection (phage latent time is 30 time steps but increases by 8 time steps upon each super infection). **D:** Basic model with latent time mutability (phage latent time can mutate to any value in the range 0 to 50 time steps). Light red/orange cells are bacteria infected by phage with shorter latent times, while dark red/brown cells are bacteria infected by phage with long latent times. Free phage are not shown.

the front (we assume this is not a function of time, which may not always be accurate). Then there will be at most one value of $\tau = \tau^*$, such that $2B\left[f\left(\tau^*\right)\right] = \tilde{B}\left(\tau^*\right)$, unless $2B[f(\tau)]$ and $\tilde{B}(\tau)$ are the exact same function. We speculate that these curves do intersect and this is the value of the second peak, but have not yet confirmed this by measuring the function $B(x)$ from the simulations.

This second peak is especially pronounced for relatively low bacterial densities of $0.01 < B < 0.1$. For higher densities the effect is probably still there but the fitness difference between the first effective fast phage at the tallest peak and the slower phage at the second peak is so big that the bimodality of the distribution no longer is visible in data from our simulations. This is due to the fact that the strength of the selection pressure (quantified by $S = \left| \left( \frac{\partial^2 f}{\partial \tau^2} \right)_{\tau=\tau_{opt}} \right|$, where $f(\tau) \equiv \frac{\partial P}{\partial t}\big|_{t=t'}$, for a $t' \gg \tau_{opt}$, see equation 1.4 and fig. 1.7) is much greater for high densities, which is also mentioned in the experimental study, ref. [47]. For relatively low bacterial densities we do, however, see clear selection for both low and high latent times while phages with medium latent times do poorly, something which to our knowledge has not previously been observed by others. Clearly, in some spatial environments it would then pay off to have a combination of low and high latent times; an observation which could have implications for which combinations of different phages would be most efficient at killing bacteria in a spatial environment like human tissue, and therefore perhaps relevant for the phage therapy research area. Also, the situation of the simple spatial simulation is very similar to a phage infection front spreading through a lawn of bacteria on an agar plate, and since countless experimental procedures rely on the counting and measuring of plaques formed by phage infection fronts, our way of calculating the selection pressure phages experiences during such a population race could prove useful.

**Survival of the mediocre killers.** An interesting aspect of implementing the adaptive strategy of latent time mutability in a spatial setting is that it exhibits selection against the most efficient killers in the system. In the dynamic setting of the Basic model, whenever phage that have the highest fitness in a constant high bacterial density environment appear through mutations, they will deplete resources locally and subsequently die out. More "prudent" long latent time phages, on the other hand, will do better on average because they do not wipe out the bacteria in their vicinity but only kill at a slow enough pace which allows the bacteria time to reproduce or merge with another colony. This is despite the fact that the high latent time phage are no match for the more effective low latent time killers whenever, by chance, they end up side by side in the same colony.

This part of the study thus emphasizes that one must be careful in assessing what is "optimal" behavior for a phage. Calculations that try to determine optimal latent times, for instance, of-

ten take the short-term view of maximizing the phage population growth rate [134; 149], which is what we did in the derivation of 1.4 and in the interpretation of the data from the simple spatial simulations (data shown in e.g 1.8B). Recognizing the risks of making such assumptions has led others to suggest extending the notion of fitness to include "environmental inheritance" [40]. The data from the simulations of the Basic model with latent time mutability implemented supports this point of view: for long-term survival in a spatial environment, virulent phage must ensure that their offspring inherit an environment with sufficient resources.

## 1.5 Take home messages

Latent time optimality and selection pressure for phage at constant host density:

- There exists an optimal phage latent time that depends on host density and phage efficiency.
- High host density (or high phage infection rate) selects for phages with low latent times, but small changes in host density do not shift the optimum latent time much.
- Low host density (or low phage infection rate) selects for phage with long latent times and small changes in host density will shift the optimum latent significantly.
- The selection pressure acting on phage to drive them towards the optimal latent time is much greater at high host density than at low.
- The selection pressure acting on phage in an infection front, moving through a 2D lawn of bacteria at relatively low density, will select for both phage with low and high latent times but not phage with intermediate latent times, i.e. the latent time distribution becomes bimodal.

The effect of phage behavioral mechanisms on coexistence

- When phage are allowed to "infect" previously infected and dead bacteria, coexistence is enhanced. This effect is more pronounced for a spatial setting that for a well-mixed system.
- Lysis inhibition enhances coexistence in both well-mixed and spatial systems.
- Phage latent time mutability enhances coexistence in a spatial system but reduce it in a well-mixed system.

- Survival of the mediocre killers: phage which are the most efficient killers/competitors locally, in a spatial system, are not the ones which do best over long time spans. In the long run more prudent phage prevail because they do not drive their hosts to extinction locally.

# Chapter 2

# Life on the edge: Coexistence of phage and bacteria on the boundary of self-organized refuges

## 2.1 Introduction

### 2.1.1 The importance of refuges

In the previous chapter, we saw that coexistence of a virulent phage and its host is possible, but only in a relatively narrow range of the phage degradation rate $\delta$ and infection rate $\alpha$ values (see figure 2.1). We explored mechanisms which broadened the coexistence region and thus boosted coexistence, but even with these effects implemented, the overall narrowness of the region still indicates that coexistence in the different versions of the Basic model is relatively fine tuned and may therefore be sensitive to larger evolutionary or environmental changes which perturb the parameter values affecting phage efficiency. Coexistence of phage and bacteria in the wild has been observed to have the following properties: (i) highly efficient virulent phage with relatively long lifetimes [28], high infection rates and large burst sizes [65], (ii) large, stable and high density populations of both phage and bacteria [6; 123] , (iii) a fast turnover of both phage and bacteria [123], and (iv) stability over evolutionary timescales despite imbalances in the rates of phage vs. bacterial evolution [97; 66; 72; 134]. The coexistence which we observe in the Basic model and its' variants, however, does not satisfy all these properties together. In particular, we need to make at least one phage efficiency parameter quite different from what is observed; either the infection rate or burst size must be very low, or the degradation rate very high. Even then, we cannot achieve high densities of phage and bacteria together with a high turnover of their populations. Thus, the main question of how a virulent phage with a long lifetime, a large burst size, and high infection rate manages not to wipe out its grounds of existence still stands largely unanswered.

**Spatial heterogeneity and bacterial refuges.** The fact that we have seen that spatial heterogeneity clearly has a positive effect on coexistence of virulent phage and their bacterial hosts, led us to the idea of exploring the effect of bacterial refuges on coexistence. As mentioned earlier, many real phage-bacterial ecosystems are found in environments with a complex spatial structure, such as in soil, or wounds in animal and plant tissue. Furthermore, many bacterial species are capable of creating spatial structure themselves as Schrag and Mittler found when they observed that coexistence between virulent phage and bacteria is not possible in serial cultures, but is possible in a chemostat, due to biofilm refuge formation on the walls of the chemostat, [109]. Substantial evidence exists in the literature that conditions for phage can be more difficult inside a dense bacterial colony or biofilm - infection rates, burst sizes and diffusion are often lower, while degradation rates and latent times are higher. Reduced infection rates for cells that have reached stationary phase have been proposed in other model studies [142]. Reduction of the infection rate could arise, for example, because nutrient depletion and limitation effectively change the physiological condition of the cells. Also, bacterial cells tend to have fewer receptors for phage adsorption in a medium with low nutrients [20; 29]. Furthermore, murein, which forms the cell wall, becomes hyper-crosslinked and richer in covalently bound lipoprotein as cells approach stationary phase [93], which may alter the kinetics of phage infection. Reduced burst size and prolonged latent times have also been observed for cells with low growth rates or metabolic activity, as well as cells in stationary phase [115; 98; 8; 78; 90; 81]. Diffusivity inside a biofilm is significantly reduced locally due to the high density of exopolymers produced by bacteria [24]. Inside a biofilm, tight cell-to-cell binding, which may directly block phage receptors [102], could also reduce the phage infection rate. In addition biofilms often contain proteolytic enzymes as well as endoglycanases which can lead to phage inactivation [8].

**Refuges and edges in macro ecology.** Existing literature in macro ecology, argues that prey refuges may theoretically help stabilize predator-prey interactions [56; 22]. The formation of a spatial refuge invariably leads to the formation of a boundary zone or edge between two different environments and studies of natural macro-ecosystems have shown that there is an increased biodiversity on edges between different types of habitats (see, e.g., [51]). Refuges might thus be an important factor for coexistence of virulent phage and their bacterial hosts.

### 2.1.2 A map of this chapter

In this chapter we explore a more "bacteriocentric" way of enhancing coexistence than in the previous chapter where we focused on different phage strategies. Here we will explore the effect of having bacterial refuges on co-existence. In section 2.2 we describe two variants of the Basic model which have bacterial refuges – one where certain fixed grid sites are assigned different

phage efficiency parameter values, and the other where the phage parameters themselves dynamically change depending on the changing bacterial density. We also describe a model which adds an evolutionary timescale to the second variant over which parameters can evolve due to mutations in new phage and bacteria. In section 2.3.1 we discuss how having fixed refuges enhances coexistence, and in section 2.3.2 we show that bacterial density dependent mechanisms can cause such refuges to arise in a self-organized manner. Section 2.3.3 explores the robustness of this conclusion to changes in parameters as well as for many different variations of the model rules. Section 2.3.4 then explores the nature of the co-evolutionary arms race that can develop between one virulent phage species and one bacterial species in the presence of self-organized bacterial refuges. Sections 2.4 and 2.5 summarize our conclusions and discuss future directions for exploration.

## 2.2 Models

### 2.2.1 Fixed bacterial refuge model

The fixed bacterial refuge model is similar to the Basic model except here the grid is divided into two halves. Grid points in one half are assigned one set of $\delta$, $\alpha$, $\gamma$, $D$ values ($D$ is the diffusion constant of the phage), which make this half phage hostile – this is the bacterial refuge. We will call these values $\delta_{in}$, $\alpha_{in}$, $\gamma_{in}$, $D_{in}$, where the subscript "in" refers to being *in*-side the bacterial refuge. The other half is given another set of parameter values, $\delta_{out}$, $\alpha_{out}$, $\gamma_{out}$, $D_{out}$, which make it phage friendly (the subscript "out" refers to being *out*-side the bacterial refuge). This division is in contrast to the Basic model where $\delta$, $\alpha$, $\gamma$, $D$ values are the same all over the grid. Phage hostile and phage friendly parts of the plane can be created in many ways. The simplest is where only a single phage parameter is changed. For example $\delta_{in}$ could be high and $\delta_{out}$ could be low. Alternatively, some subset of the parameters could be chosen to be different in the two halves, while the rest remain the same in both halves. Bacterial parameters, such as their growth rate, are given the same value throughout the system.

### 2.2.2 Self-organized bacterial refuge model

In the self-organized bacterial refuge model we again allow $\alpha, \delta, \beta$ and $D$ to have different values for different grid points. However, unlike the Fixed refuge model, these values are not pre-assigned to each point. Instead they are determined dynamically during the course of simulation in a manner dependent on the density of bacteria. The rules which govern this were chosen to loosely mimic the formation of a biofilm within which phage efficiency is reduced. Each bacterium has a "density counter", which is an integer number that increments every time step that the bacterium spends with three neighbours or more, and decrements each time step

it spends with two neighbors or less (the counter stops increasing at a certain maximum value (100), and never goes below zero). New bacteria always start with a density counter of zero. These counters thus keep track of how long a bacterium has spent recently in high cell density, which we assume is correlated to its being within the biofilm protection. We explore different ways of making phage parameters at a site depend on the biofilm protection, i.e. on the value of the density counter of the bacteria that occupies that site: 1) we let one or more phage parameters, like for example $\delta$, be a step function of the density counter value, with end values, $\delta_{out}$ (for low density counter values) and $\delta_{in}$ (for high density counter values), and 2) by letting one or more phage parameters depend as a sigmoidal fashion on the density counter value, with hill factor 4 and end values $\delta_{out}$ (for density counter equal to zero) and $\delta_{in}$ (for density counter equal to its maximal value). In this model, $\delta_{in}$ and $\delta_{out}$ (and similarly for other parameters) are constants that are the same at all grid points and do not change with time in each simulation.

### 2.2.3 Self-organized bacterial refuge model with evolution

This model is very similar to the Self-organized refuge model except that the end-values, $\delta_{in}, \delta_{out}$ and $\alpha_{in}, \alpha_{out}$, of the functions which determine how $\delta$ and $\alpha$ depend on the density counter, are no longer the same over the entire grid. Instead, each individual phage has its own $(\delta_{out}, \alpha_{out})$ and each individual bacterium has its own value of $(\delta_{in}, \alpha_{in})$. Whenever a bacterium divides, the offspring get new values of $(\delta_{in}, \alpha_{in})$ drawn from a normal distribution[1] centered around the parent value and with the variance $\mu_{bacteria}$. Similarly, new phage offspring from a burst get new values of $(\delta_{out}, \alpha_{out})$ drawn from a normal distribution with a mean equal to the parent value and the variance $\mu_{phage}$. We also implemented a variant where mutants take values from a lognormal distribution whose peak is at the parent value.

[1]The normal distribution is of course truncated at zero so that no mutant can get negative values for any parameter.

## 2.3 Results

### 2.3.1 Fixed bacterial refuges enhance coexistence

In order to explore the influence of bacterial refuges on phage-bacteria coexistence, we first introduce a fixed spatial refuge into the Basic model. This is done in a very simple fashion: we divide the plane in two halves and allow phage efficiency to take on different values in the two halves (see details in section 2.3.1). As expected we find that when parameter values in either one of the half planes are chosen from within the coexistence region in figure 2.1 of the Basic model we get coexistence here too, whereas if parameters of both half-planes lie in the same non-coexistence region then we do not observe coexistence. A more interesting phenomenon is seen whenever parameters for one half are chosen from the right non-coexistence region of fig. 2.1 (where phage are too inefficient to survive in the Basic model), while parameters in the other half are chosen from the left non-coexistence region (where phage are so efficient that they drive bacteria, and then themselves, to extinction). In this case, we observe coexistence of phage and bacteria, which is stable for at least 1000 bacterial generations.

**Dynamics on the edge of a fixed bacteria refuge.** In the fixed bacteria refuge model the phage exist only in a zone around the edge between the two halves. The dynamics and width of this zone varies considerably, as seen in figure 2.2, which shows snapshots from three different simulations of the Fixed bacterial refuge model where only, $\delta$, the phage degradation rate, differs between the two half-planes. The same is observed when the phage infection rate, $\alpha$, is varied between the two half-planes, keeping all other parameters fixed, or when combinations of $\alpha$, $\delta$, $\gamma$ (intracellular phage production rate) and the phage diffusion constant are varied between the half-planes. It is interesting that it is thus possible to obtain long lived coexistence when the parameters in each half-plane in isolation would lead to extinction of phage or bacteria. The only condition required for coexistence in this case, is that one half-plane must be a bacterial refuge (i.e., the parameter values there make phage too inefficient to survive), while the other is phage-friendly. Thus, this stabilization of coexistence occurs for parameter values spanning many orders of magnitude; a vast set compared to the narrow band of parameters that allows coexistence in the Basic model.

### 2.3.2 Self-organized bacterial refuges also enhance coexistence

We also explored whether enhancement of coexistence is possible if bacterial refuges are not put in by hand, as in the Fixed refuge model, but instead form dynamically. In particular, we examined whether mechanisms that create phage unfriendly conditions in areas of high bacterial density are sufficient to produce robust coexistence. The version of the Basic model that we

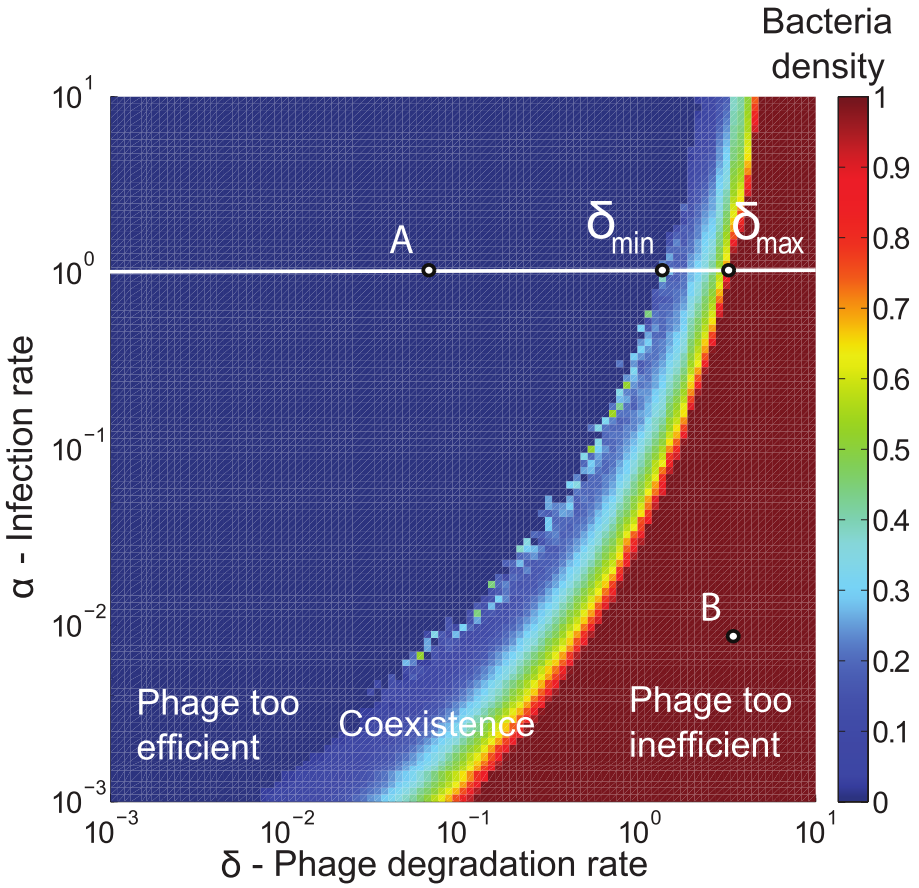


Figure 2.1: **Narrow coexistence region for the Basic model.** Colors shows average bacterial density for simulations after 1000 bacterial generations have passed as a function of phage infection rate $\alpha$ and degradation rate $\delta$, in units of $1/\Delta t$. Dark red is the maximal bacterial density of one, dark blue is zero – colors in between signify that bacteria and phage coexist. For each value of $\alpha$ there exists an interval $[\delta_{min}, \delta_{max}]$ outside which there will be no coexistence. Here these points are marked for $\alpha = 10^{-1} min^{-1} = 1/\Delta t$. Points $A$ and $B$ mark the parameters used for the simulation shown in fig 2.4. Grid size used in simulations was $100 \times 100$. Initial conditions consisted of 5% randomly chosen sites being occupied by healthy bacteria and 0.5% by infected bacteria.

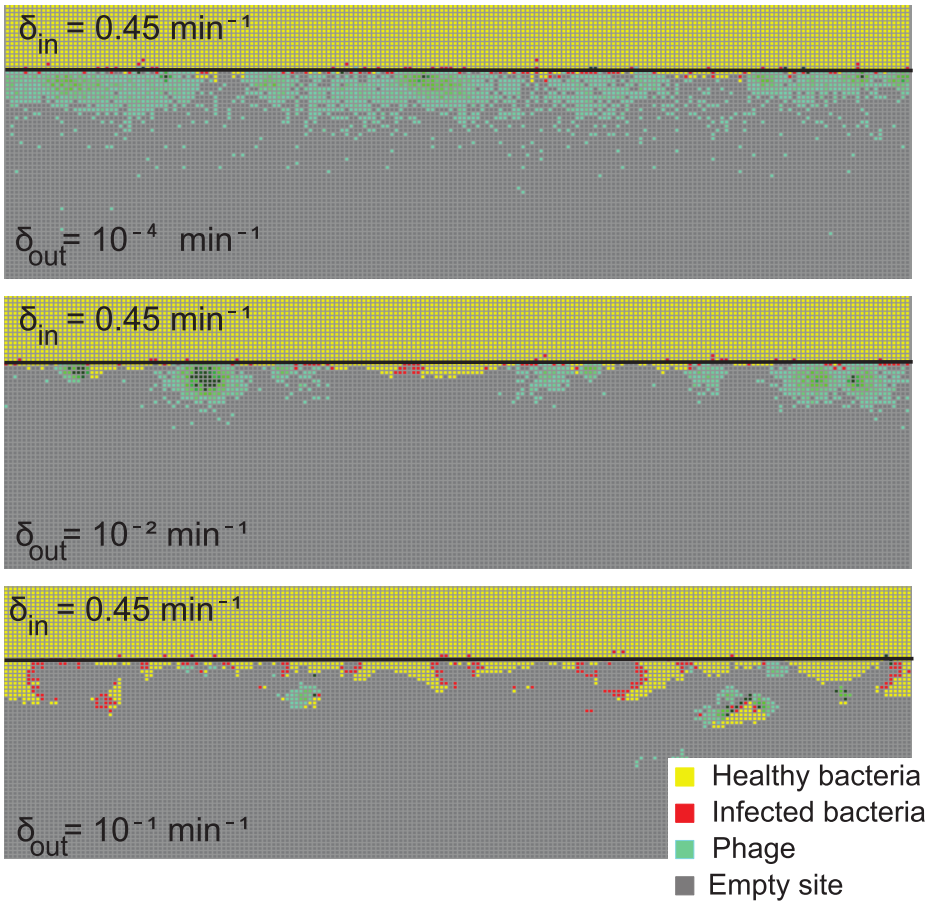


Figure 2.2: **Snapshots of fixed bacterial refuge simulations.** Yellow: healthy bacteria. Red: infected bacteria. Green: diffusing phage. Gray: empty space. The plane is divided into two halves. The upper part is a bacterial refuge where phage cannot sustain themselves for long because of a high phage degradation rate. The three snapshots show simulations with three different $\delta_{out}$ values in the lower part of the system. The $\delta_{in}$ value in the upper part of the system (the bacterial refuge) is kept constant at $\delta_{in} = 0.45 min^{-1}$. Grid size: $150 \times 150$ (the whole grid is not shown). Initial conditions: upper plane was filled with healthy bacteria and one line of infected bacteria was placed on the boundary between the two halves. **Top:** $\delta_{out} = 10^{-4} min^{-1}$. This very low phage degradation rate allows phage to diffuse long distances before they die. As a consequence of the high density of phages close to the boundary, almost all new bacteria get infected and bacteria cannot penetrate into the phage friendly half. **Middle:** $\delta_{out} = 10^{-2} min^{-1}$. At this higher phage degradation rate, phage attack becomes more localized which in turn allows for some bacterial excursions into the lower half plane. **Bottom:** $\delta_{out} = 10^{-1} min^{-1}$. The region where both bacteria and phage are found together further broadens as $\delta_{out}$ becomes so large that bacteria and phage can nearly coexist in the lower half-plane. One observes "plumes" of bacteria which migrate substantially deep into the lower half plane before they are eventually killed by phages.

constructed in order to test this effect is termed the Self-organized bacterial refuge model. Here parameters such as the infection rate and phage degradation rate can be different at different spatial locations. However, unlike in the Fixed bacterial refuge model, the values are not pre-specified at each point in space. Instead they depend on local bacterial density as it develops dynamically during the course of the simulation (see Self organized refuge model in section 2.2.2). We implemented the density dependent effect by assigning to each bacterium a "density counter". Each counter is an integer number that is incremented every time step that the bacterium spends with three or more neighbors and decremented otherwise. The value of these counters thus correlate with how long a bacterium has spent recently in high density. We then let the parameters of a specific site in the 2D grid depend on the density counter of the bacterium which occupies that site[2], such that when the bacteria are young or alone, and thus have a low density counter value, they are more susceptible to phage. Figure 2.3 shows schematically how this can be done by making the phage degradation rate an increasing function of the density counter value. Similarly phage infection rate or burst size or diffusion, or combinations of all of these, can be made a decreasing function of the density counter. As indicated by the dashed lines in figure 2.3 we tried out functions with different shapes. In all cases we found that bacterial refuges self-organized and the system developed an almost static pattern of bacterial islands, with phage proliferating on new bacteria produced on the edges of the islands, see fig. 2.4.

### 2.3.3 Self-organizing "life on the edge" is robust

The phenomenon of long-lasting coexistence on the edge of self-organized density-dependent refuges occurs for a huge range of parameter values and is also stable against many changes in the model rules. Figure 2.6 shows the duration of coexistence as a function of $\delta_{out}$ and $\delta_{in}$, for simulations where the only parameter that depends on the density counter is $\delta$ (recall that $\delta_{out}$ and $\delta_{in}$ are the phage degradation values used at sites with minimal and maximal density counter values respectively, see fig. 2.3). In the region where $\delta_{in} > \delta_{max}$ and $\delta_{out} < \delta_{min}$, we find that coexistence times rise steeply compared to the values outside this region. Thus, whenever $\delta_{in}$ is chosen from the dark red "phage too inefficient" region ($\delta_{in} > \delta_{max}$) of figure 2.1 and $\delta_{out}$ from the dark blue "phage too efficient" region ($\delta_{out} < \delta_{min}$), phage coexist with bacteria on the edges of the bacterial colonies for several hundreds or thousands of generations.

[2]It would perhaps be simpler to make the phage parameters depend directly on the bacterial density in some small region around each site, instead of on a density counter. However, we wanted to include the slight time delay that the density counter allows, with the idea that biofilm material would take some time to be produced when bacterial density is increasing, and would take some time to disappear in case bacterial density decreases sufficiently after having been high for some time.

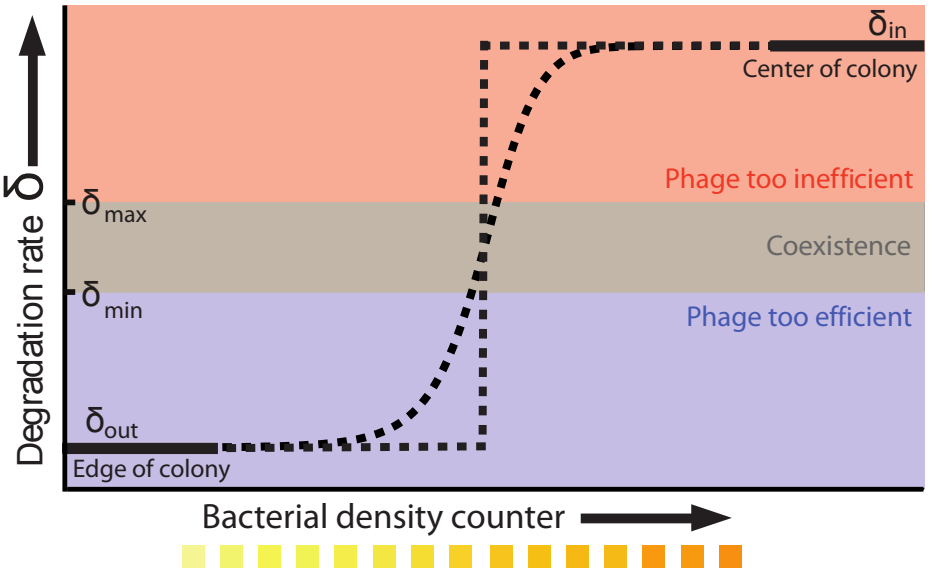


Figure 2.3: **Phage degradation rate dependence on bacterial density counter.** One way of implementing the Self organized bacterial refuge model is by making phage degradation rate an increasing function of the bacterial density counter. Thereby, bacteria that are young or alone occupy sites where the phage degradation rate is low, whereas bacteria that have spent some time at high density are at sites with high phage degradation rates. The plot above shows schematically how this may be done. The degradation rate at zero and maximal density counter values are denoted "out" and "in", respectively. Also shown schematically is the region between $\delta_{min}$ and $\delta_{max}$ where phage and bacteria would coexist in the Basic model. $\delta_{out}$ and $\delta_{in}$ can be chosen without restriction, but phage-bacteria coexistence is enhanced when they are chosen, as shown, with $\delta_{out} < \delta_{min}$ and $\delta_{in} > \delta_{max}$. The dotted lines signify that we have also tried smoother, sigmoidal, functions and this gives similar results.

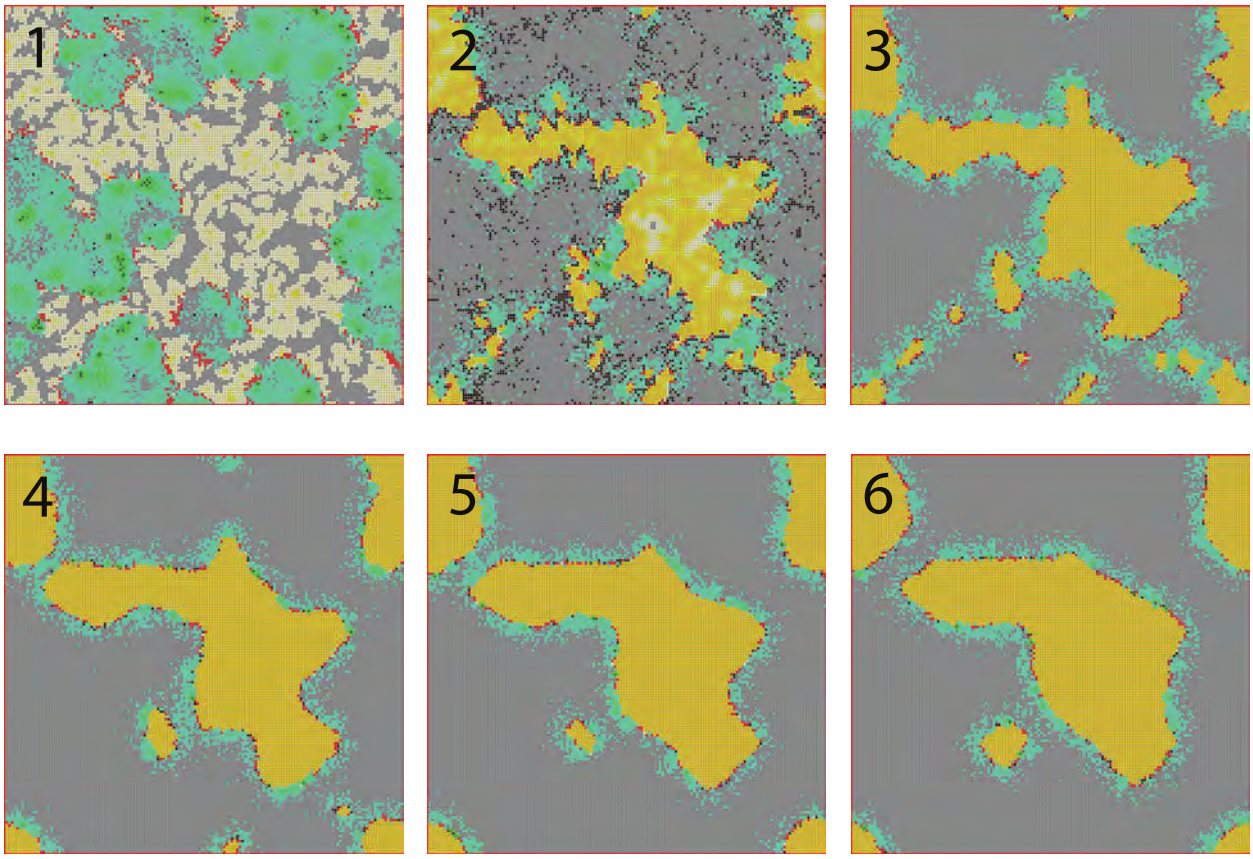


Figure 2.4: **Snapshots of simulations of the Self organized bacterial refuge model.** Yellow: healthy bacteria (bacteria with low density counters are light yellow and bacteria with increasingly higher density counters are colored darker shades of yellow). Red: infected bacteria. Green: diffusing phage. Gray: empty space. The initial condition consisted of randomly distributed bacteria with density counter equal to zero and a few infected with phage on a grid of size $200 \times 200$. After some time bacteria in the center of colonies reach the maximal density counter value and grid spots inside colonies become phage unfriendly. At the same time, new bacteria with density counter equal to zero are produced at the colony edges. Parameters were $(\delta_{out};\ \alpha_{out}) = (0.05 \cdot 10^{-1} min^{-1}; 1.0 \cdot 10^{-1} min^{-1})$ and $(\delta_{in};\ \alpha_{in}) = (5.0 \cdot 10^{-1} min^{-1}; 0.01 \cdot 10^{-1} min^{-1})$ marked by $A$ and $B$ respectively in Fig. 2.1. **(1)** snapshot taken 4 bacterial generations after $t = 0$. **(2)** after 8 bacterial generations. **(3)** after 70 bacterial generations. **(4)** after 500 bacterial generations. **(5)** after 1000 bacterial generations. **(6)** after 2000 bacterial generations.

In simulations done to produce the data shown in figure 2.6, the dependence on the density counter was a step function, but we find that long-lasting coexistence does not depend on the precise shape of the function (see fig. 2.7). If the increase in $\delta$ is a smoother, e.g. sigmoidal, function of the counter value we get a similar result as in fig. 2.6. Also, the precise threshold density counter value at which $\delta$ increases from $\delta_{out}$ to $\delta_{in}$ does not matter for the qualitative behavior, nor does the precise rate of change of the counters as a function of time or as a function of the number of neighbors. Further, if different, but fixed, values of other parameters such as $\alpha$ are chosen then, as expected, the values of $\delta_{min}$ and $\delta_{max}$ change but the above condition ($\delta_{in} > \delta_{max}$ and $\delta_{out} < \delta_{min}$) for long-lasting coexistence still holds. The same is true if instead of varying $\delta$, $\alpha$ is made a decreasing function of the density counter while $\delta$ kept fixed. In this case, as shown fig. 5.16 in Appendix 2, the requirement for self organized refuge formation is that $\alpha_{in} < \alpha_{min}$ and $\alpha_{out} > \alpha_{max}$ (where $\alpha_{max}$ and $\alpha_{min}$ are the upper and lower boundaries of the coexistence region in figure 2.1 for a fixed value of $\delta$). What is required for coexistence on the edge of bacterial refuges is thus merely that the bacteria in the center of the colony are so resilient that phage cannot sustain themselves in there, while newborn bacteria on the edge of the colonies are (possibly very) susceptible to phage infection.

**Making phage efficiency depend on the bacterial density counter.** In the Self organized refuge model we can thus make phage efficiency depend on the bacterial density counter in many different ways, but it is easiest both to implement and visualize the results when just one parameter (e.g. $\delta$) is varied at a time, which is why we have chosen to do this for many of the figures in this chapter. When we only vary one parameter we of course need to go to more extreme end values within that specific parameter range in order to get to opposite sides of the coexistence region in the Basic model, i.e. $\delta_{min}$ and $\delta_{max}$ will have to be relatively far apart for us to get coexistence, when only $\delta$ varies with the density counter. However as soon as we vary not just one parameter but several, e.g. infection rate $\alpha$, intracellular phage production rate, $\gamma$, phage diffusion constant, etc., the relative differences for "in" and "out" values required for coexistence become much smaller and more reasonable biologically (see fig. 2.5).

**Ecosystem dynamics in the selforganized refuge model.** Fig. 2.4 shows an example of how the dynamics of the model looks when the phage degradation rate is made an increasing function of the density counter, and the phage infection rate is made a decreasing function of the density counter while all other parameters are kept fixed everywhere in the system (using a combination of $\delta$ and $\alpha$ allows us to get coexistence with smaller differences between the values of these parameters at low and high density counter values). The system develops a static pattern of islands of self-constructed bacterial refuges, with phage proliferating on new bacteria

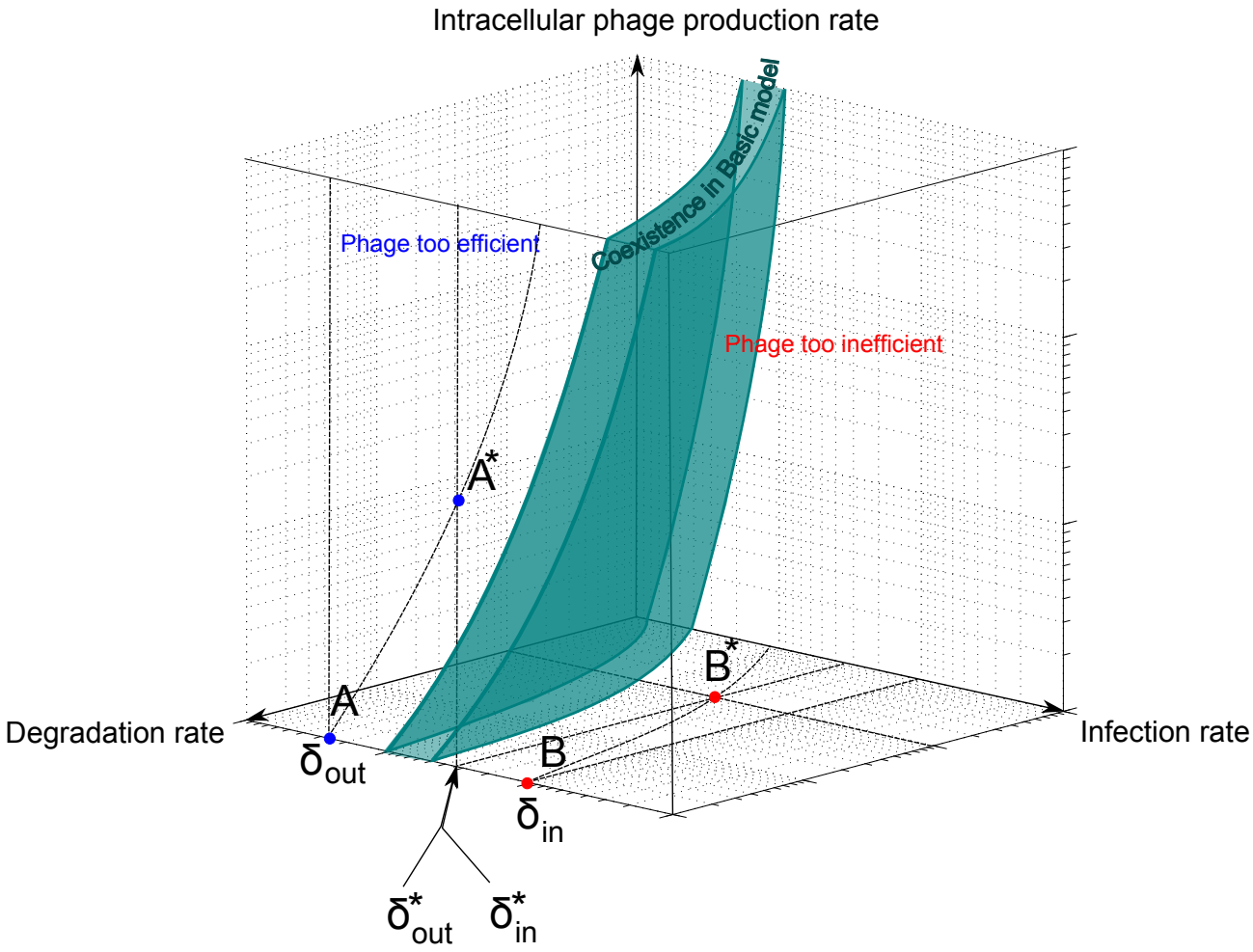


Figure 2.5: **Tweaking phage efficiency parameters in many dimensions.** Schematic figure showing possible coordinates for in-refuge (point $B$ and $B^*$) and out-of-refuge parameter values (point $A$ and $A^*$) which would provide self organized refuge formation and thus long lived coexistence. For points $A$ and $B$ only $\delta$ is varied and thus the difference between $\delta_{in}$ and $\delta_{out}$ needs to be relatively large to get coexistence. For points $A^*$ and $B^*$ two other parameters influencing phage efficiency are varied (here exemplified by infection rate and intracellular phage production rate). This allows $\delta^*_{in}$ and $\delta^*_{out}$ to have the same value although points $A^*$and $B^*$are as far from the coexistence region of the Basic model as points $A$ and $B$. This illustrates that when phage efficiency parameters are tweaked in a high dimensional space the relative difference between "in" and "out" values for one specific parameter need not be very large.

produced on the edges of the islands. The spreading infection fronts become almost stationary after around 10 bacterial generations, see fig. 2.9 and fig. 5.17 Appendix 2. On a longer timescale they tend to straighten from an initial rough interface into smoother boundaries, although this tendency is stronger for some parameters than for others (see fig. 2.8). The boundaries thus seem to act almost like there is an effective surface tension; the perimeters of the bacterial colonies decrease over time because sections with high curvature see a higher local density of phage, see figure 2.9. There also appears to be an effective nucleation threshold: very small colonies tend to die out in the beginning of the simulation while larger colonies stabilize and persist (see fig. 2.9).

### 2.3.4 Stabilization of bacterial refuges via evolution

The Self organized refuge model can be extended to allow both bacteria and phage to evolve the ability to form refuges and the ability to penetrate refuges, respectively. By doing this we can test whether phage and bacteria evolution contribute to the stability of the refuge formation we observed in the Self organized refuge model or whether it destabilizes it. We tried implementing evolution in a few different ways (see section 2.2.3). Figure 2.12 shows the results of one such implementation, where $\delta_{in}$ is a property that bacteria pass on to their offspring, and $\delta_{out}$ a property inherited by phage offspring from their parents, and both were allowed to mutate. The colored trajectories in figure 2.12 starting at different initial conditions each show, as time progresses, the changing values of $\delta_{in}$ and $\delta_{out}$, averaged over all phage and bacteria at that time. We see how the average parameters of the system are all pushed deeper into the blue shaded region, towards more long lived coexistence, by bacteria evolving to increase $\delta_{in}$ and phage evolving to decrease $\delta_{out}$. Notice that we chose the initial values of $\delta_{in}$ and $\delta_{out}$ in these simulations to be outside the coexistence region. Thus, in the absence of evolution, coexistence would have lasted a very brief time. A similar pattern is seen when we allow the infection rates, $\alpha_{in}$ and $\alpha_{out}$, to mutate instead (see fig. 5.19 in Appendix 2). Interestingly, this pattern is also maintained when the mean mutation step size of the phage is very different from that of the bacteria, i.e. there is asymmetry between the evolutionary rates of change of phage and bacteria. For example, we observe that evolution of $\delta_{in}$ and $\delta_{out}$, from the initial condition of $\delta_{in} = \delta_{out} = 10^{-1} min^{-1}$, is able to bring the system into the blue region of figure 2.12 both when $\mu_{phage}/\mu_{bacteria} = 0.1$ and when $\mu_{phage}/\mu_{bacteria} = 5.0$.

**Asymmetric mutation rates.** Irrespective of the particular values chosen for the mutation rates, the self-organized refuges result in an asymmetry in the evolutionary rates of phage and bacteria. Bacterial mutations occur more often at the edges of colonies because that is where new bacteria are formed, but these mutations are often quickly eliminated by phage infections.

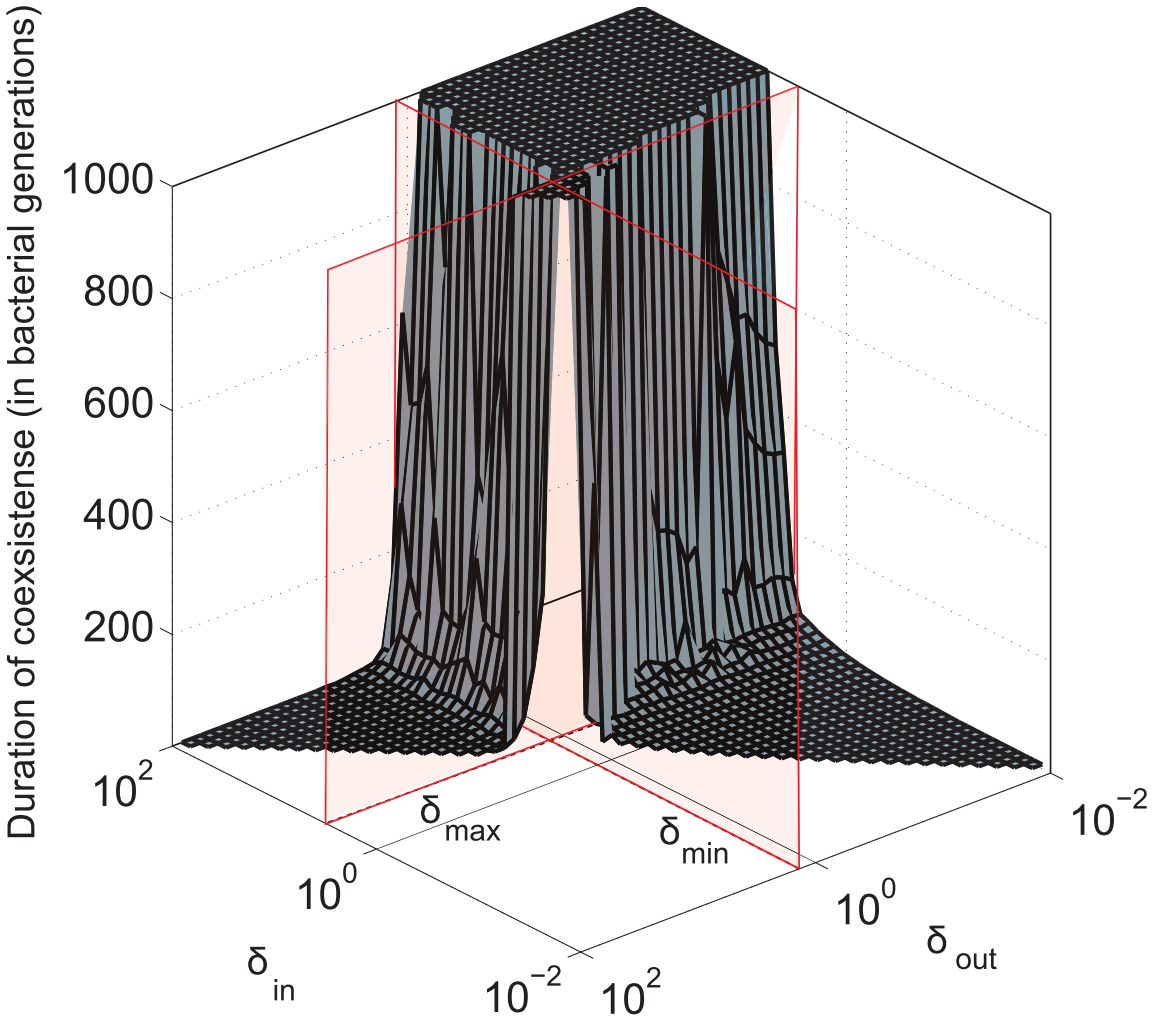


Figure 2.6: **Long lived coexistence for a broad range of $\delta_{in}$ and $\delta_{out}$.** Duration of coexistence as a function of $\delta_{in}$ and $\delta_{out}$ ($\alpha_{in} = \alpha_{out} = 10^{-1} min^{-1} = 1/\Delta t$ ). Red lines mark $\delta_{min}$ and $\delta_{max}$ for $\alpha = 1/\Delta t$ in the Basic model. If time reached 1000 bacterial generations while there was still coexistence (i.e. both phage and bacteria were present) then the simulation is stopped. Only parameter sets where $\delta_{out} \leq \delta_{in}$ were considered. Within the region where $\delta_{in} > \delta_{max}$ and $\delta_{out} < \delta_{min}$ the phage and bacteria coexisted for durations much longer than the bacterial generation time. In this region of parameter space, the average infection front speeds were also relatively low (see Appendix 5). When $\delta_{in} > \delta_{max}$ and $\delta_{out} > \delta_{min}$, the phage live only for a short time on the edge of the expanding bacterial colony before dying out. When $\delta_{in} < \delta_{max}$ and $\delta_{out} < \delta_{min}$ the phage infection fronts rapidly eat into the colonies and eventually wipe out the bacteria. In the small region where both $\delta_{in}$ and $\delta_{out}$ are within the narrow range of $[\delta_{min},\delta_{max}]$, there is stable coexistence but the infection fronts are far from stationary. Grid size: $100 \times 100$. Initial conditions: upper half plane filled with healthy bacteria and a single line of infected bacteria on the boundary between the upper part and the empty lower half plane.

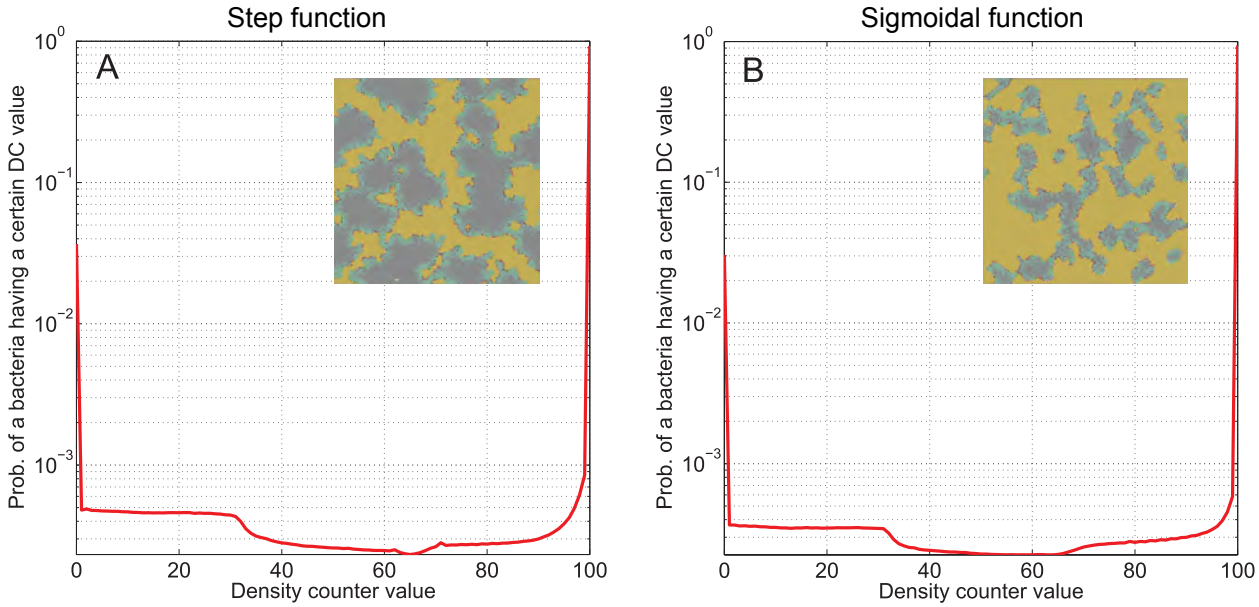


Figure 2.7: **Bimodal density counter value distribution for both step function and sigmoidal dependence of $\delta$ and $\alpha$ on the bacteria density counter.** The average distribution of density counter values found in a simulation of the Self organized bacterial refuge model with parameters: $\delta_{out} = 0.05 \cdot 10^{-1} min^{-1}$ , $\delta_{in} = 5.0 \cdot 10^{-1} min^{-1}$, $\alpha_{out} = 1.0 \cdot 10^{-1} min^{-1}$ , $\alpha_{in} = 0.01 \cdot 10^{-1} min^{-1}$ (same as the parameters in fig. 2.4). The average is over time starting after the system has reached close to a static pattern of bacterial colonies (see inserts). The overall appearance of the refuges look different for the step function and the sigmoidal function, but we see that the distribution of density counter values among the cells is very similar. The plots also show that, in both cases, the probability of finding a bacterium with either very low or very high density counter is much higher than finding a bacterium with an intermediate density counter value. For both plots we have grid size: $200 \times 200$. Initial conditions consisted, as usual, randomly scattered bacteria and bacteria infected with phage. **A:** The dependence of $\delta$ and $\alpha$ on the density counter is a step function. **B:** The dependence of $\delta$ and $\alpha$ on the density counter is a sigmoidal function with Hill factor 4.

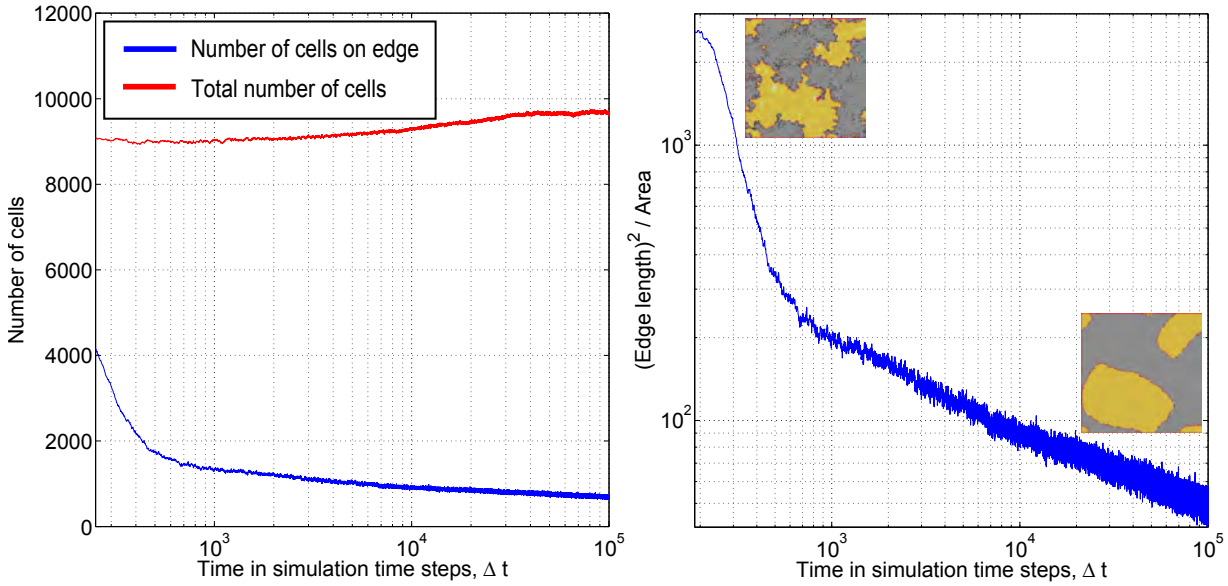


Figure 2.8: **Boundaries of refuges become smoother over time. Left:** The blue curve shows the number of bacterial cells on the edges of refuges as a function of time, and the red curve shows the total number of bacteria as a function of time. **Right:** The blue curve shows a crude measure of the roughness of the bacterial colony edges – the ratio of the square of the sum of edge lengths to the sum of areas of bacterial refuges in the system squared – as a function of time. Inserts show a simulation snapshot at an early and a late time point. Parameters used $(\delta_{out};\ \alpha_{out}) = (0.05 \cdot 10^{-1} min^{-1}; 1.0 \cdot 10^{-1} min^{-1})$ and $(\delta_{in};\ \alpha_{in}) = (5.0 \cdot 10^{-1} min^{-1}; 0.01 \cdot 10^{-1} min^{-1})$ marked by $A$ and $B$ respectively in Fig. 2.1, (same as for fig. 2.4). The phenomenon of refuge boundary smoothening is more pronounced for some parameters than for others. In general the effect is more pronounced when the parameter points lie deeper within the coexistence region (shown in fig. 2.10) and when more than just one parameter is tweaked (i.e. when in and out values differ for both, $\delta$ and $\alpha$ etc.).

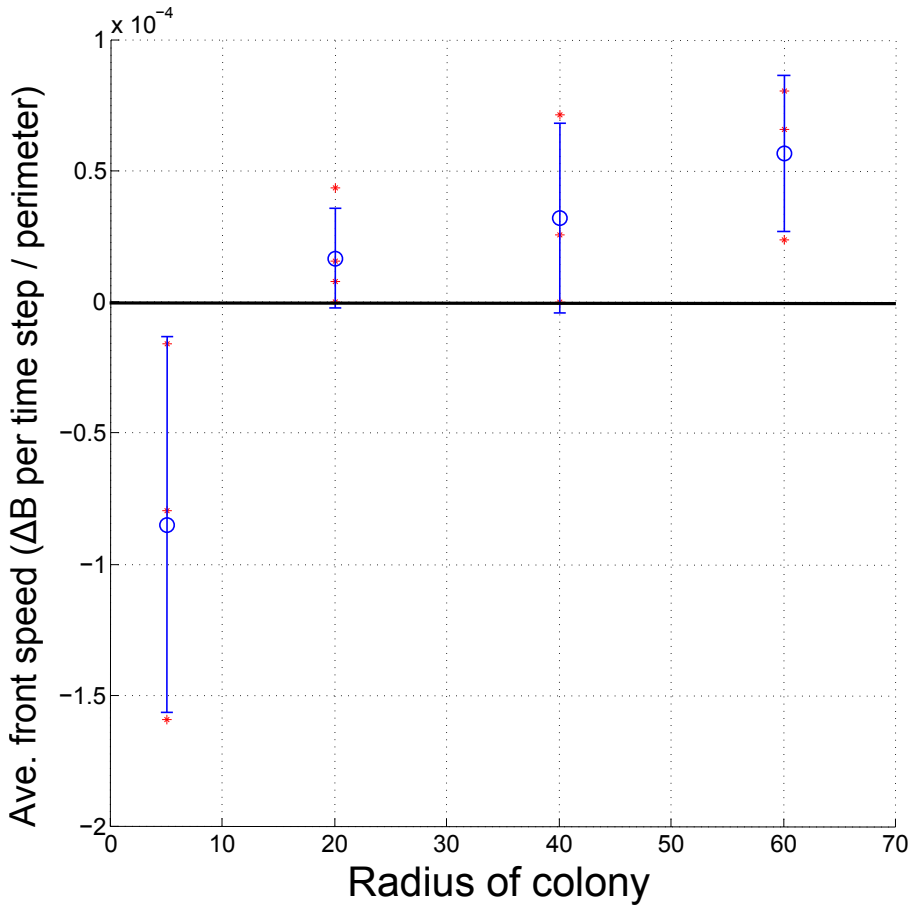


Figure 2.9: **Refuge front speed depends on local curvature.** Refuge edges are in general slow moving but not entirely stationary for parameters inside the coexistence region of the Self organized refuge model. The speed of a front depends on different factors, one being the curvature of the front. This is illustrated here by plotting the rate of change of the number of bacteria in a given colony divided by the perimeter length of the colony, for circular colonies initialized with different radii. We see that higher curvature (smaller radius) means colony shrinks slowly, while lower curvature (larger radius) results in a slowly growing colony. This is because phage density on the edge of colony increases on average as the the radius of the colony decreases. This dependence on radius also shows that there is an effective nucleation threshold: for this set of parameters colonies with a radius smaller than$\approx 15\mu m$ tend to shrink and disappear Parameters were: $(\delta_{in};\alpha_{in}) = (10.0 \cdot 10^{-1} min^{-1}; 1.0 \cdot 10^{-1} min^{-1})$ and $(\delta_{out};\alpha_{out}) = (0.01 \cdot 10^{-1} min^{-1}; 0.01 \cdot 10^{-1} min^{-1})$. Red points: average front speeds for three different simulations for each value of initial colony radius ($r = 5\mu m$, $r = 20\mu m$, $r = 40\mu m$ and $r = 60\mu m$). Blue: mean of the three simulations with error bars showing one standard deviation from the mean.

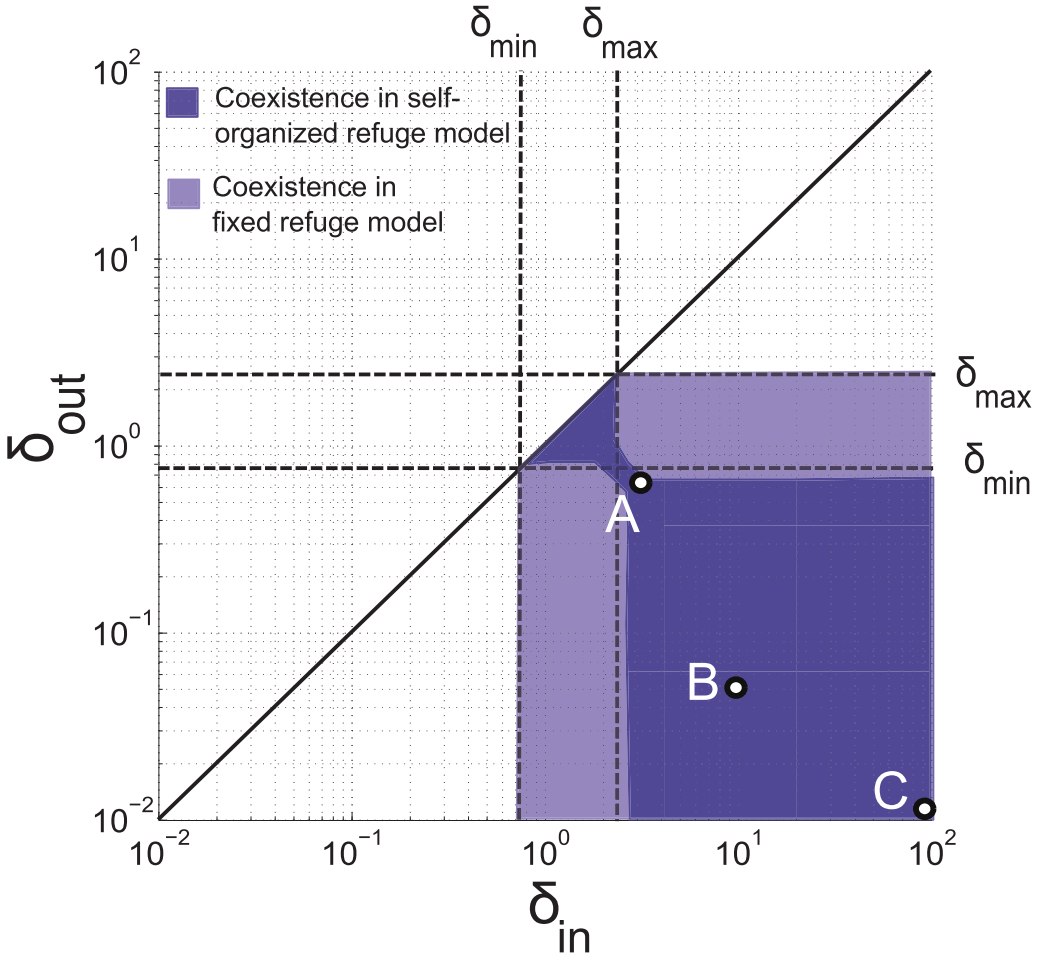


Figure 2.10: **Comparison between coexistence region in Fixed refuge model and Self organized refuge model.** Schematic figure showing the rough outline of the coexistence regions for the Fixed refuge model (light blue) and for the self organized refuge model (dark blue) in the parameter space of $\delta_{in}$ and $\delta_{out}$. Coexistence is defined as having both phage and bacteria present in the system for at least 1000 bacterial generations. A, B and C mark the parameter sets used for the simulation screen shots shown in fig. 2.11.

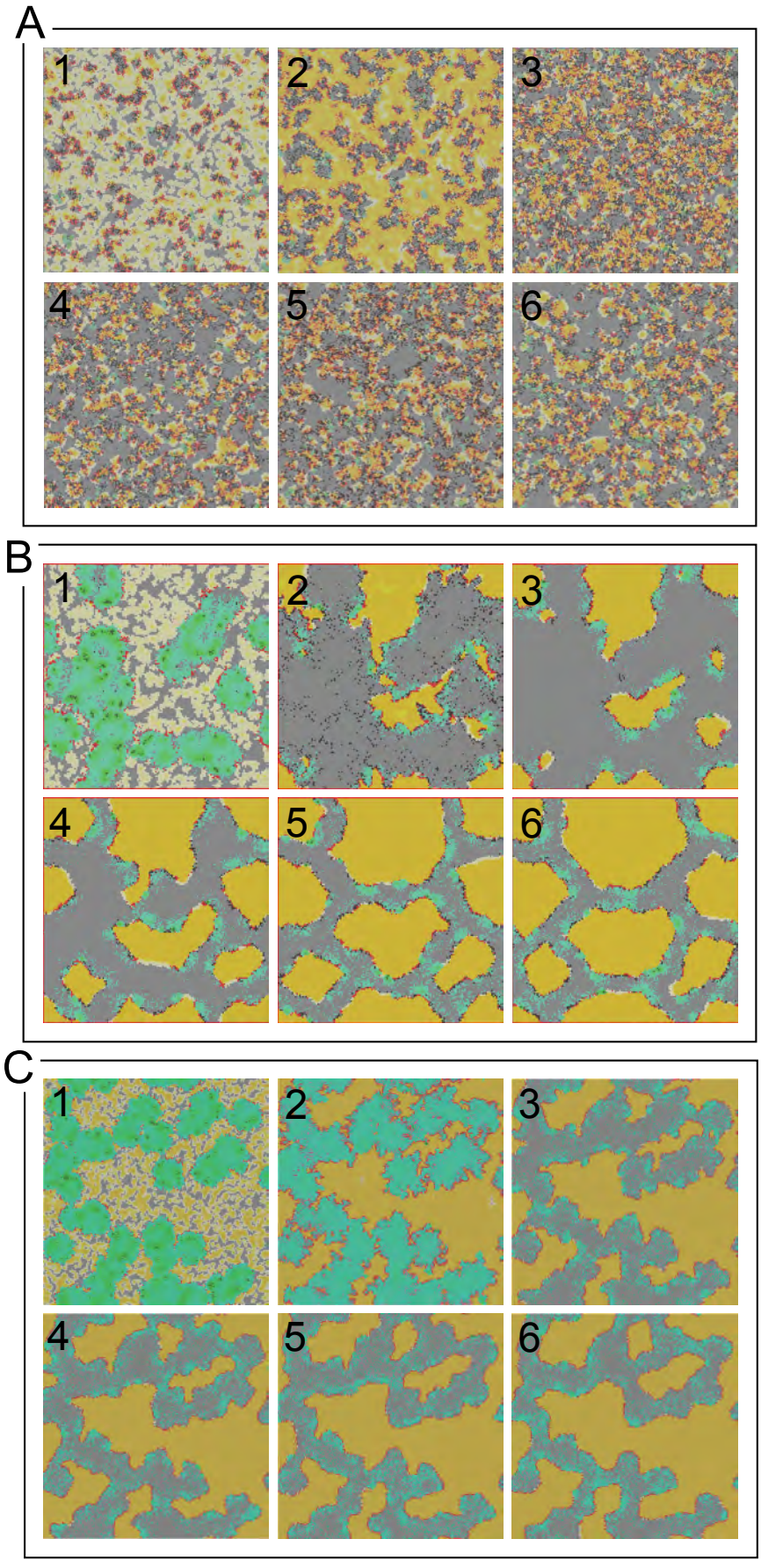


Figure 2.11: Figure caption on following page.

Figure 2.11: **Refuge formation in different parts of the $\delta_{in}-\delta_{out}$ plane.** Snapshots from simulations with parameters sets marked by points A, B and C in fig. 2.10. For all three simulations we have:$\alpha_{out} = \alpha_{in} = 10^{-1}min^{-1}$ and grid size $200 \times 200$. Initial conditions, as usual, consisted of randomly scattered healthy and infected bacteria. For all three simulations, the phage and bacteria manage to coexist for at least 3333 bacterial generations. **A:** (1) snapshot taken 4 generations after $t = 0$. (2) 8 generations after. (3) 33 generations after. (4) 66 generations after. (5) 533 generations after. (6) 1666 generations after. $\delta_{in} = 3.3 \cdot 10^{-1}min^{-1}$ and $\delta_{out} = 0.8 \cdot 10^{-1}min^{-1}$. Notice that the relative difference between the inside and outside degradation rates is just a factor 4; the $\delta_{in}$ and $\delta_{out}$ values lie very close to, but just above and below, $\delta_{max}$ and $\delta_{min}$ respectively. **B:** (1) snapshot taken 4 generations after $t = 0$. (2) 12 generations after. (3) 100 generations after. (4) 500 generations after. (5) 1666 generations after. (6) 3333 generations after. Here $\delta_{in} = 10 \cdot 10^{-1}min^{-1}$ and $\delta_{out} = 0.05 \cdot 10^{-1}min^{-1}$. Note how little change there is between (5) and (6) between which 1666 bacteria generations go by. **C:** (1) snapshot taken 4 generations after $t = 0$. (2) 8 generations after. (3) 133 generations after. (4) 400 generations after. (5) 800 generations after. (6) 1666 generations after.

On the other hand, phage mutations (which also occur mainly at the edges) can persist and spread through the population. This likely explains the shape of the evolutionary trajectories shown in fig. 2.12: changes in bacterial parameters typically occur early on when the refuges are still stabilizing, whereas later the trajectory moves mainly in the direction of changing phage parameters.

## 2.4 Discussion

In this chapter we explored bacterial refuges and their formation by density dependent mechanisms as a mechanism for enhancing phage-bacteria coexistence. We find that coexistence between a virulent phage and its bacterial host is remarkably stable and robust on boundaries between habitats within each of which coexistence is not possible – provided one habitat is a bacterial refuge where conditions are hostile to phage, while the other is phage friendly. We show that this enhancement of coexistence also stabilizes the long term co-evolution between phage and bacteria. Phage bacteria coexistence as an edge phenomenon is not as restrictive as it might sound. Even the smallest grain of sand can provide hugely varying conditions, for example associated to wetting with thin layers of water.

**Observations of phage and bacteria.** Spatial heterogeneity is a prominent feature of many real phage-bacteria ecosystems. This is reflected in the fact that soil or biofilms, and even ocean data, show high variability of the phage and bacteria density over small length scales [124]. In oceans, heterogeneity could be self-organized by cyanobacteria making colonies in the form of sheets and mats [117]. But perhaps even more important is the fact that bacteria at high density can create a heterogeneous and somewhat phage hostile environment by themselves. One such density dependent mechanism is the use of quorum sensing systems to trigger biofilm formation. Biofilm is not invincible to phage attack [24] but many factors contribute to make phage existence in biofilm harsher, as discussed earlier in 2.1.1. Costerton et al. [25] report that *E. coli* persist in the intestinal tract by adhering to tissue surfaces and food particles, where they live in encapsulated micro colonies akin to biofilms. Sternberg et al. [119] report that within biofilms cells typically form clusters (micro colonies) with the most metabolically active cells located on the periphery of each micro colony; a scenario which resembles the self organized bacterial clusters formed in our simulations. Corbin et al. [24] observe ongoing phage proliferation and sustained coexistence of bacteria and phage populations of T4 in *E. coli* glucose limited biofilm. They propose that such biofilms may act as natural reservoirs for virulent bacteriophage, which they also suggest multiply only in the part of the *E. coli* biofilm population where bacteria are *not* in stationary phase, much like in our simulations. Other studies have also reported that phage may alter biofilm morphology but that bacteria and virulent phage are able to coexist stably inside biofilm [8; 126].

### 2.4.1 Characteristics of phage-bacteria coexistence on edges of refuges

In our simulations, we found that density dependent, or quorum sensing, mechanisms are a robust way of forming self-organized bacterial refuges, and that having stable refuges is, in

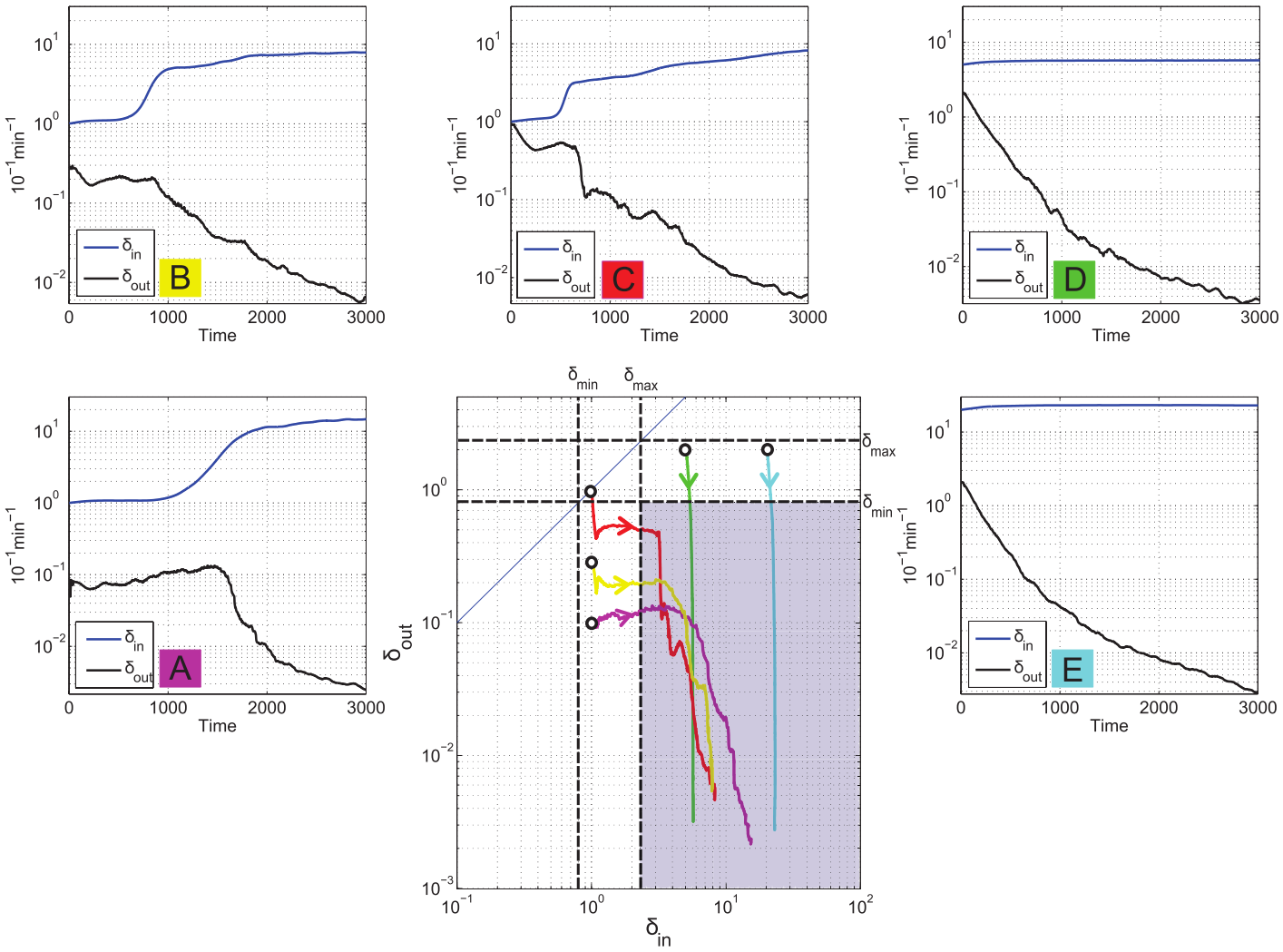


Figure 2.12: **Evolution pushes the self organized bacterial refuge system deeper into parameter region with long lived coexistence.** Trajectories show how the values of $\delta_{in}$ and $\delta_{out}$ averaged over all bacteria and phage, respectively, change with time during five different simulations of the Self organized bacterial refuge model when bacteria and phage are permitted to evolve (here $\mu_{phage} = 0.07$, $\mu_{bacteria} = 0.1$, see section 2.2.3 for details on implementation). Each simulation is for 3000 time steps. For these simulations the value of $\delta$ for each new phage and bacterium is drawn from a lognormal distribution whose peak is at the parent value. Note that when evolution takes logarithmic steps like this, the mean of any parameter value tends to increase if there is no selection pressure to go towards lower values. This explains why the red, yellow and purple curves in some parts (where susceptible bacteria happen to be plentiful and there is therefore not much selection pressure on the phage) have a slight tendency to drift towards higher $\delta_{out}$ values. However, once the selection pressure kicks in it tends to push $\delta_{in}$ (the parameter inherited by bacteria) to higher values and $\delta_{out}$ (the parameter inherited by phage) towards lower values. This drives the system deeper into the parameter region where $\delta_{in} > \delta_{max}$ and $\delta_{out} < \delta_{min}$ (the light blue region) where the phage and bacteria coexist for much longer than the bacterial generation time.

**A:** Purple start point: $(\delta_{in};\ \delta_{out}) = (10^{-1}min^{-1}; 0.1 \cdot 10^{-1}min^{-1})$. **B:** Yellow start point: $(\delta_{in};\ \delta_{out}) = (10^{-1}min^{-1}; 0.3 \cdot 10^{-1}min^{-1})$. **C:** Red start point: $(\delta_{in};\ \delta_{out}) = (10^{-1}min^{-1}; 10^{-1}min^{-1})$. **D:** Green start point: $(\delta_{in};\ \delta_{out}) = (5.0 \cdot 10^{-1}min^{-1}; 2.0 \cdot 10^{-1}min^{-1})$. **E:** Blue start point: $(\delta_{in};\ \delta_{out}) = (20.0 \cdot 10^{-1}min^{-1}; 2.0 \cdot 10^{-1}min^{-1})$.

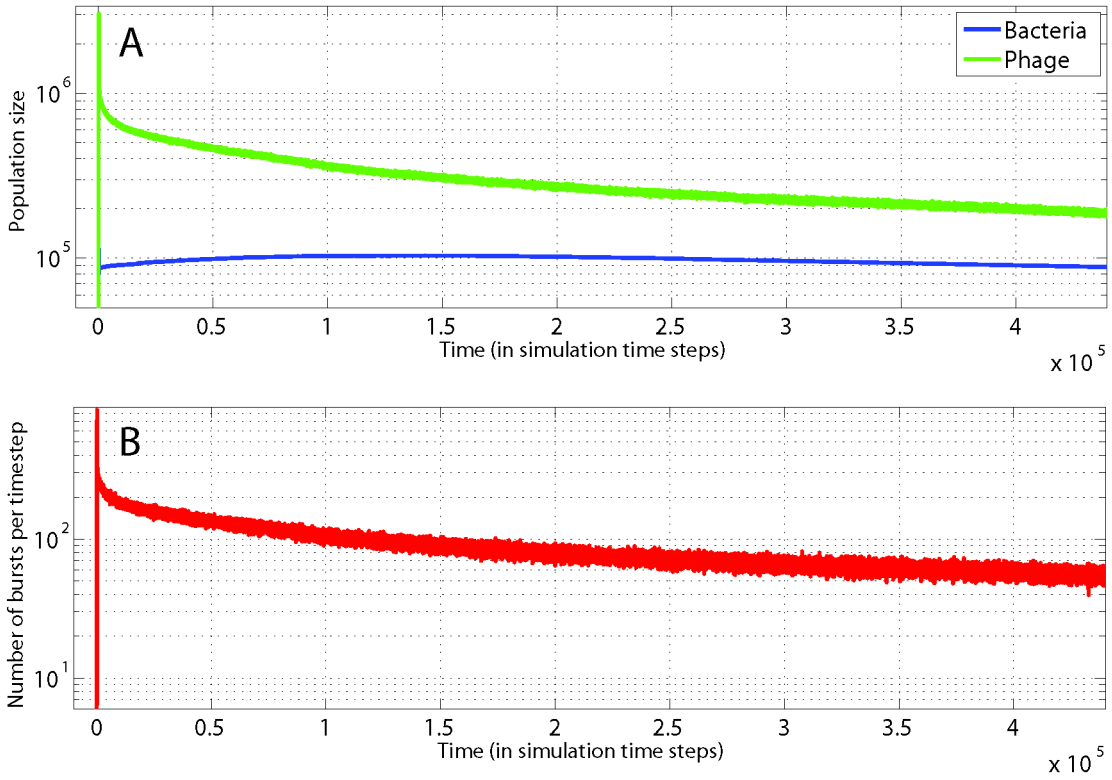


Figure 2.13: **Stable populations and large turn over rates for a long time span.** **A:** Bacteria and phage numbers as a function of time (in simulation time steps). **B:** Number of phage bursts per time step as a function of time (in simulation time steps). In this simulation we see that both phage and bacteria numbers eventually slowly decrease over time (note that for the first 300 generations the bacterial population grows slowly). If we assume that the bacteria numbers are decreasing linearly we would predict extinction of bacteria would happen after roughly 8000 bacterial generations. Note that since the front speed depends on the curvature of the front (see fig. 2.9) it would also be possible to have a simulation with the same parameters as the one shown here where bacteria numbers would steadily increase over time. Parameters are the same as the ones used in fig 2.4: $(\delta_{in}, \alpha_{in}) = (5.0 \cdot 10^{-1} min^{-1}, 0.01 \cdot 10^{-1} min^{-1})$ and $(\delta_{out}, \alpha_{out}) = (0.05 \cdot 10^{-1} min^{-1}, 1.0 \cdot 10^{-1} min^{-1})$. Grid size: $500 \times 500$. Initial conditions consisted of randomly scattered healthy and infected bacteria.

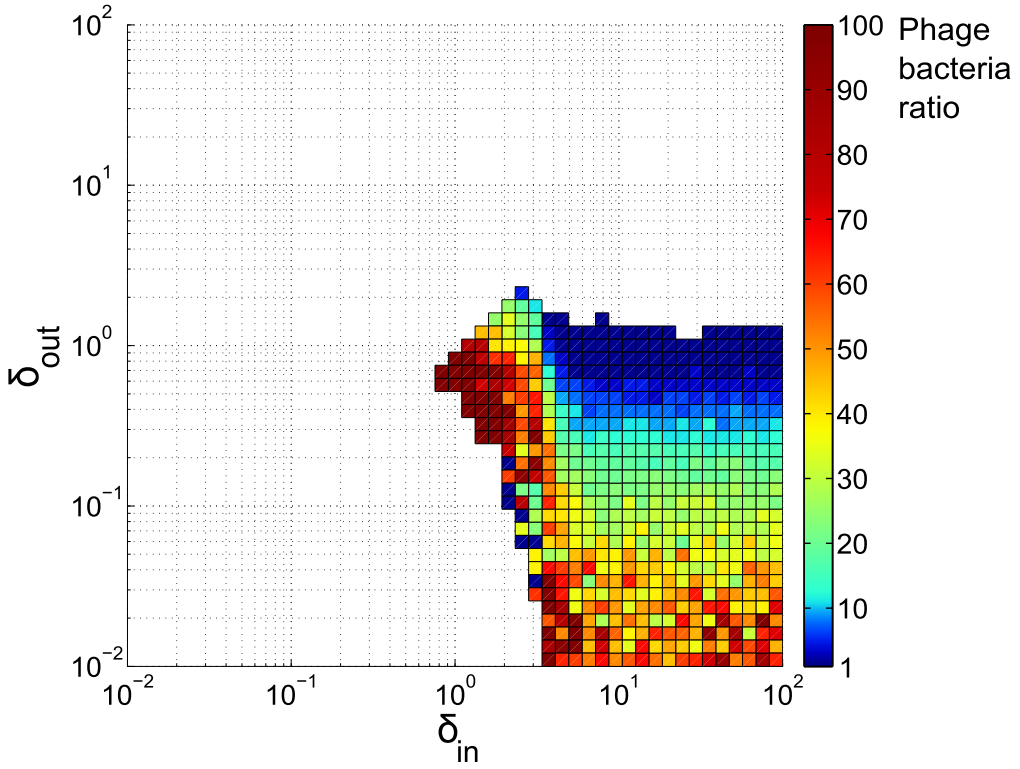


Figure 2.14: **High ratio of phage to bacteria in coexistence region of the Self organized refuge model.** Color map shows the average ratio of phage to bacteria after 20 bacterial generations as a function of $\delta_{in}$ and $\delta_{out}$ in simulations of the Self organized refuge model. Initial density of healthy bacteria was 0.08 and initial density of infected bacteria was 0.004, giving an initial ratio of $\approx \frac{0.004 \times 100}{0.08} = 5$ (because the burst size is 100). For the points with no color (white) either phage or bacteria had died out before 20 bacterial generations passed. Grid size: $200 \times 200$.

turn, a robust way to enhance phage bacteria coexistence. We found that coexistence, in these simulations, has the following characteristics: (i) phage and bacterial densities are quite high with phage being concentrated on the edges of dense bacterial colonies, (ii) phage can outnumber bacteria easily by an order of magnitude without destabilizing the system, (iii) there is a high turnover of the phage population, and also of the bacterial population at the edge of colonies (see fig. 2.13,2.14 and fig 5.21 in Appendix 2). And all this despite the phage being intrinsically very efficient predators, with a large burst size, long lifetimes and high infection rates outside the bacterial refuge. As discussed earlier in section 2.1.1 we could not achieve coexistence with all these characteristics in the Basic model without refuges. Data from soil [6] and marine [123] phage-bacteria ecosystems seem to match the characteristics of the refuge model better; the population densities of both phage and bacteria are observed to be relatively high and the phage:bacteria ratio is around 10:1. Moreover, stable population numbers and a high turnover rate of phage and bacteria are also observed: virulent phage are estimated to kill $\sim 20-40\%$ of the bacteria in the oceans on a daily basis [123].

**Parameters to measure.** Our results suggest that it would be particularly interesting to measure parameters that affect phage efficiency, such as phage lifetime, infection rate and diffusion constant, in natural ecosystems where such phage have been observed to coexist with bacteria. The half life of nine different virulent phage were measured in laboratory conditions with bacteria growing on LB[3], and found to be of the order of 10 days on average [28], but the corresponding numbers are not known in natural ecosystems in soil or oceans. If measured parameters are found to lie outside the coexistence region of the Basic model, that would strongly suggest that there must be additional mechanisms which allow coexistence. The specific mechanism of coexistence along the edge of refuges also predicts that the variance of these parameters should be large, even over very short length scales. It would, for example, be interesting to measure the variance of burst sizes in a biofilm instead of just the mean burst size which is the norm.

It is encouraging that the model behavior is robust to many alterations in the dynamical rules. In addition to the variants described above, we have also found qualitatively similar refuge formation and enhancement of coexistence in a three dimensional version of the Self organized refuge model (see fig. 2.15) and in a version with bacterial diffusion, and with hydrodynamic flow which make bacteria and phage drift in a specific direction (see fig. 2.16).

[3]LB: Lysogeny broth, a nutritionally rich medium used for growth of bacteria.

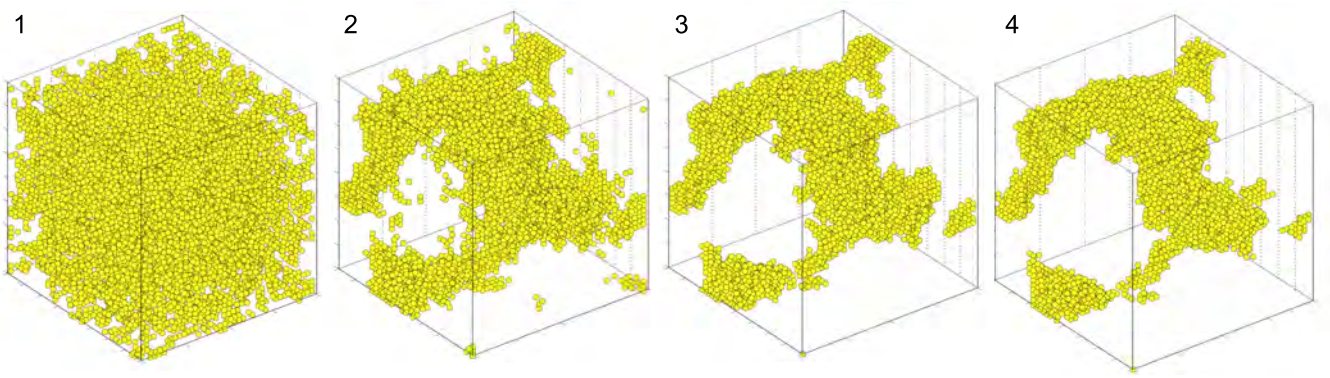


Figure 2.15: **3D model has dynamics similar to 2D model.** Yellow dots show sites occupied by healthy bacteria. For clarity, sites with infected bacteria and diffusing phage are not shown. Parameters were $(\delta_{out}, \alpha_{out}) = (0.05 \cdot 10^{-1} min^{-1}, 1.0 \cdot 10^{-1} min^{-1})$ and $(\delta_{in}, \alpha_{in}) = (5.0 \cdot 10^{-1} min^{-1}, 0.01 \cdot 10^{-1} min^{-1})$ (same as parameters of fig. 2.4). **(1)** snapshot taken 4 bacterial generations after $t = 0$. **(2)** after 6 bacterial generations. **(3)** after 70 bacterial generations. **(4)** after 140 bacterial generations. Grid size: $40 \times 40 \times 40$. Initial conditions consisted of randomly scattered healthy and infected bacteria.

### 2.4.2 Bacterial refuges and the co-evolutionary arms race

The bacterial refuges found in the Self organized refuge model alone may not be sufficient to ensure very long-term coexistence of virulent phage and bacteria. In real ecosystems, very long-term coexistence certainly involves bacteria evolving to become resistant to phage, and phage counter-evolving strategies to infect resistant bacteria. However, such a co-evolutionary arms race cannot be stable if at any time conditions arise where either the phage or bacteria could rapidly die out. Any non-evolutionary mechanisms which enhance coexistence could play a crucial role in allowing sufficient time for evolution to occur. Self-organized bacterial refuges are one of several such possible mechanisms. We have shown that, for a very broad region of parameter space, such refuges can slow down the rate of extinction immensely, while maintaining a high density of both phage and bacteria for time spans of at least a thousand times longer than the bacterial generation time. The evolutionary simulations we have done complete the second part of this argument. We found that even when the system starts with parameter values that do not allow coexistence for very long, evolution of the phage and bacteria pushes these parameter values into regions which do allow coexistence. Interestingly, this is true both when the phage mutated faster than the bacteria, and vice versa. In these evolutionary simulations the puzzling properties of real ecosystems, described earlier, are all maintained: highly efficient

phage living on the edge of almost static refuges, with a high turnover of both phage and bacterial populations, and there is continuous evolution of phage which are more efficient, and bacteria that create better refuges. Ironically, the defense mechanisms of bacteria, such as biofilm formation, may thus be crucial not only for the survival of the bacteria but also for the long term survival of their most vicious predators.

## 2.5 Future work

The models in this and the previous chapter clarify how spatial heterogeneity can play a major role in enhancing coexistence between virulent phage and bacteria. However, it is important to note that these are just the first steps towards understanding exactly how phage-bacteria ecosystems self-organize and co-evolve, because our models are highly simplified versions of real ecosystems. There are two broad aspects of real ecosystems that strike us as important to study in more realistic models:

1. The environment and geometry of the space in which real phage bacteria ecosystems exist is much more complex than a simple 2D plane. Not only can there be geographical barriers to growth, there will also often be hydrodynamic flows which add to the diffusion and drift of phage and bacteria.

2. Even more importantly, ecosystems outside laboratories are unlikely to consist of just a single bacterial species and a single phage species.

**Versions of the Self-organized refuge with non-stationary bacteria.** We have briefly experimented with versions of the Self-organized refuge model where the bacteria are themselves motile and diffuse around and can drift, along with phage, in specific directions due to hydrodynamic flow (see fig. 2.16). Interestingly, cell motility/diffusion and hydrodynamic flows seems to make coexistence more stable than in the version of the model where bacteria are stationary because it allows bacteria to, once in a while, escape an established refuge and start a new one in an empty part of the plane, thus eliminating the problem of slowly shrinking refuges. More cases need to be investigated to understand the limits of this effect.

**Multiple phage and bacteria species.** We have not investigated any models with multiple phage or bacteria species, but the first step in such a direction might be to study the network that determines which phage species can infect which bacteria, or which bacteria are immune to which phage. Bacterial defence mechanisms, other than biofilm production, could influence the structure of these immunity/infection networks. For example, CRISPR[4] defences against phage have been modeled mathematically in [41], and it would be interesting to examine how such

[4] Clustered Regularly Interspaced Short Palindromic Repeats

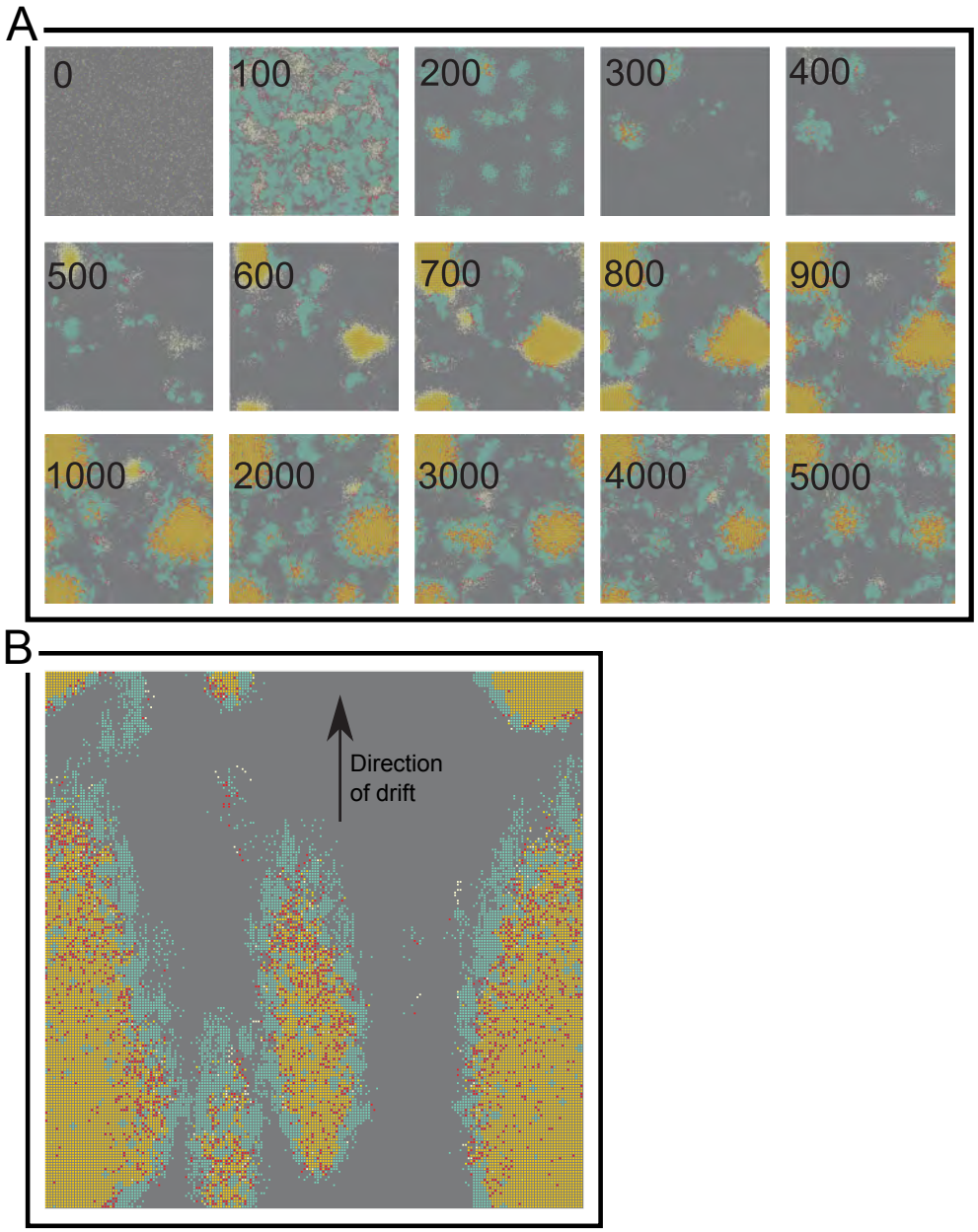


Figure 2.16: **High cell diffusion or drift does not stop refuges from forming. A:** Simulation of a version of the Self organizing refuge model where both bacteria and phage diffuse (each snapshot is numbered with the number of time steps that have passed). Phage diffusion constant was set to its default value as used in all earlier simulations. Bacterial diffusion constant was set to half of the phage diffusion constant. Diffusing bacteria were allowed to exchange places with neighbouring cells so there are no crowding effects preventing, for example, an infected cell from diffusing into a dense colony. Parameters: $\delta_{in} = 5 \cdot 10^{-1} min^{-1}$, $\delta_{out} = 0.1 \cdot 10^{-1} min^{-1}$, $\alpha_{in} = 0.001 \cdot 10^{-1} min^{-1}$ and $\alpha_{out} = 1 \cdot 10^{-1} min^{-1}$. Grid size was $200 \times 200$. **B:** Adding a constant drift, mimicking laminar hydrodynamic flow, does not stop refuge formation. Parameters: $\delta_{in} = 5 \cdot 10^{-1} min^{-1}$, $\delta_{out} = 0.1 \cdot 10^{-1} min^{-1}$, $\alpha_{in} = 0.001 \cdot 10^{-1} min^{-1}$ and $\alpha_{out} = 1 \cdot 10^{-1} min^{-1}$. Here the bacterial diffusion constant was set to 1/10 of the phage diffusion constant and both phage and bacteria experienced a drift in the upward direction (such that both bacteria and phage where 50% more likely to move upwards than in the other three directions). Grid size: $200 \times 200$.

defence mechanisms would spread and evolve in variants of our models. Another interesting question to ask is whether one can construct a model where virulent phage and temperate phage can both coexist together with bacteria. A well-mixed model of an ecosystem involving multiple bacterial species as well as multiple virulent and temperate phage species was studied in [104]. That model included a complex and evolving network of infection and immunity interactions between the species and the authors found that it was very hard to obtain coexistence between bacteria and both virulent and temperate phage; typically at least one of the categories went extinct. A suitable combination of the Rosvall model and our models could thus be constructed to investigate whether spatial heterogeneity and refuges plays a similar role in enhancing coexistence when there are multiple interacting species of bacteria and phage.

## 2.6 Take home messages

- In a system with bacterial refuges, i.e. regions where phage are rendered inefficient, there will be coexistence of phage and bacteria along the edge of the refuge especially if the phage are intrinsically so efficient that they would drive the bacteria to extinction outside the refuge.
- Such bacterial refuges can arise in a self-organized manner due to the action of bacterial density dependent mechanisms, such as biolfim production.
- The long term co-evolution of the phage and bacteria further stabilize the self-organized bacterial refuges, and in turn, the refuges stabilize the arms race by preventing sudden extinction events when phage efficiency improves or new bacterial defences arise due to mutations.
- Coexistence on the edges of bacterial refuges in our model share many characteristics with real ecosystem. They exhibit (i) highly efficient virulent phage with relatively long lifetimes, high infection rates and large burst sizes, (ii) large, stable and high density populations of phage and bacteria, (iii) a fast turnover of both phage and bacteria, and (iv) stability over evolutionary timescales despite imbalances in the rates of phage vs. bacterial evolution.

# Part II

# Cooperation and Communication

# Chapter 3

# Microbial strategies for dealing with common goods

## 3.1 Introduction

### 3.1.1 A map of this chapter

In this chapter, we will look at some of the important factors that could influence the behaviour of a microbe producing and excreting public or common goods, which are molecules which may improve its own fitness as well as those of its immediate neighbours. The phenomenon of a population of microbes producing and excreting a common good, is typically referred to as cooperation. Common good production is often regulated by quorum sensing (QS) systems, and this in turn is usually interpreted as bacterial communication. A common good producing, quorum sensing microbial community might thus constitute the simplest possible model system which can be used when asking questions of how an organism, capable of a cooperative behavior, can gain from making the behavior conditional. We will begin, in sections 3.1.2, 3.1.3 and 3.1.4, by providing some background on studies of cooperation, quorum sensing and common good production in bacteria. Then in section 3.2.1 we focus on exactly how the benefit gained from having a common good in the environment depends on the concentration of the common good, hereafter referred to as *the benefit function*. In section 3.2.3 we show analytically that the optimal bacterial strategy for turning on or off production of the common good depends crucially on qualitative features of the shape of the benefit function. In section 3.2.4 we further argue that the shape of the benefit function influences the need for quorum sensing regulation of that common good. Sections 3.2.5 and 3.2.6 then probe mechanisms that could influence the shape of the benefit function. One scenario we examine in more detail is that of an excreted exoenzyme that degrades polymers into more easily digestible pieces. Possible experiments that could be done to check these results will be presented in the next chapter, along with a study of how bacteria can deal with cheats that gain the benefit of the common good without paying the costs.

### 3.1.2 Cooperation

Understanding cooperative behavior is regarded as one of the greatest challenges in the field of evolutionary biology and ecology. In famous games like "Prisoner's dilemma" and the "Snowdrift game"[1] [10], which serve as allegories for real world cooperative scenarios, the optimal strategy is defection. "Defection[2]" is usually defined as a strategy which beats a cooperative strategy when played against such, but gets a lower payoff when played against another defector than that gained by two cooperators playing each other. Ever since games like the Prisoner's dilemma and the Snowdrift game were formulated, people have tried to explain in various ways why there are seemingly so many examples of cooperation all around, among us and inside us [10]. Hamilton [43], for example, introduced the notion of "inclusive fitness" of an individual, defined roughly as the sum of the number of its genes which are passed down to the next generation via its own offspring (the conventional "non-inclusive" fitness), and the number of its genes which it would propagate to the next generation by supporting relatives. He suggested that individuals are designed to maximize their inclusive, rather than their individual fitness and this indirect fitness favors cooperation. He also argued that robust cooperation within a population of cooperators and defectors/cheaters can be achieved when the public good is somewhat privatized either due to a "Green beard" mechanism, cooperators recognize other cooperators and preferentially distribute common good to them, [43], or due to mechanisms which provides spatial segregation of cheats and cooperators (e.g. [58; 136]). Cooperation has

[1] *Prisoner's dilemma:* Two criminals have been caught and are being kept in isolation cells. They each have two options/strategies: 1) cooperation (keep quiet), or 2) defection (rat on the other guy). If both prisoners keep quiet they each get a very short time in prison due to lack of evidence. If one defects and the other cooperates, the defector is set free as a reward for giving information to the police while the prisoner who kept quiet is given a harsh sentence. If both prisoners defect, both are given a harsh sentence. The strategy that gives the highest minimal payoff when all strategies are played against each other is defection and this strategy is thus always the logical choice for a single player who has no information about what the other prisoner will choose (even though the two prisoners as a group are obviously better off when both cooperate). *Snowdrift game:* (also known as "chicken" or "Hawk/dove"). Two drivers are stuck on a road due to a pile of snow. Each has a shovel in the back and the only way to get home is to get out of the car and remove the snow pile. The two possible strategies are again to 1) cooperate, i.e., get out of the warm car and shovel, or 2) stay inside and hope the other driver will get to work. If both cooperate the collective payoff for the group is highest like in the Prisoner's dilemma, because the snow is cleared faster. If both defect no one gets home, the worst case scenario. If one cooperates and the other defects both get a positive payoff (both get to go home) but the cooperator's payoff is smaller than the defector's because he payed the price of shoveling. Again, the strategy with the highest minimal payoff when all pairs are considered is defection. Note that the situation where a microbe is producing a common goods is more like the Snowdrift game than Prisoner's dilemma, because a cooperator cell will feel the benefit from the produced common good along with a neigbouring defector cell, just as the shoveling cooperator will get to go home after his hard work.

[2] We will use the terms "defector" or "cheater" interchangeably for an individual using the defection strategy.

been studied extensively (as summarized in [94]) and is widely documented in the macroscopic world, but only relatively recently has attention turned to social behavior in microbial systems. Cooperation in general becomes harder to explain when one deals with simple non-conscious organisms. Many animals can plan ahead, communicate and negotiate, and can therefore come up with more complex strategies that combine cooperation and defection based on what the opponent's strategy appears to be. For example tit-for-tat strategies (which try to cooperate but punish a defecting opponent by defecting themselves; defined more precisely in [39]) have been observed in sticklebacks [79] and humans [113]. But what strategies can a single celled organism like a bacterium employ?

### 3.1.3 Bacterial common goods and Quorum sensing: the mechanism and the debate

The simplest examples of phenomena in the biological world which could be termed cooperation is found among microbes. Here common goods are often diffusible molecules produced and excreted by single cells. These molecules act in the environment to improve conditions, and thereby fitness, for the cell which excreted them but also potentially for its neighbours. Microbes which produce extracellular molecules that can be thought of as common goods are ubiquitous. Examples of such products are:

- extracellular enzymes (often used for degrading large molecules into smaller bits which can then be transported over the cell membrane); examples of this are known in the plant pathogen *Erwinia carotovora* [92] and in *Pseudomonas aeruginosa* [105].

- exopolysaccharides (these are used in biofilms [135], and have a variety of other uses also, reviewed in [140]).

- surfactants aiding motility (reviewed in [57]; a neat experiment involving these is described in [147]).

- antibiotics for fighting other microbes [5; 75; 82; 83].

- virulence factors for fighting a host organism's immune system, or for exploitation of host resources (examples are discussed in [105; 61; 150])

- siderophores (reviewed in [87]; an experimental demonstration can be found in [44]; a neat experiment and a model involving these are described in [63]).

Many excreted bacterial common goods have been found to be under quorum sensing regulation[3]. In for example *Pseudomonas aeruginosa* the most represented functional class in the list of quorum sensing regulated gene products are excreted compounds, like toxins and extracellular enzymes [110]; a fact which is usually explained by a relatively loose verbal argument about how cooperative activities are only beneficial if the population is above a certain critical density (e.g. [31; 139]). Quorum sensing (QS) is a bacterial behaviour ubiquitously present in the microbial world and most bacteria possess at least one quorum-sensing system, [80; 37; 107]. This term covers all types of behaviour where bacteria produce, excrete, and subsequently respond to diffusible signal molecules. Typically, the signal molecules are small and relatively cheap to produce; often a peptide, a boron derivative of ribose, or an acyl homoserine lactone [37].

**The how and why of quorum sensing.** QS has been a well known phenomenon and has been investigated scientifically for almost half a century. By now a lot is known about the "how" of QS: the different mechanisms, molecules, genes, receptors, feedback loops and regulation involved (see, e.g., [88; 71]). In comparison very little is known about the "why" of QS. Although the term "quorum sensing" comes from the initial interpretation that the mechanism exists to sense population density, precisely what the mechanism is for is still debated in the scientific QS community. One faction (by far the most prominent one) claims that QS is about sensing the density/number of the colony (e.g. [139; 80]) while another smaller faction claims that the population sensing of QS is merely a side effect of what is really diffusion sensing: one cell gauging the diffusive properties of the outside environment, e.g. [101; 114]. Recently, a third alternative position arose, which reconciles the two camps by claiming that QS should be renamed "efficiency sensing" [48] because the function is both about sensing some combination of the density, the population number and the diffusive properties of the environment together. This position received support from a recent computational study [77] where, using a 2D model, they argue that cells cannot distinguish between changes in diffusion constant and population size using one QS mechanism. Sam Brown (University of Edinburgh) recently proposed that the different QS systems of *Pseudomonas aeruginosa* (which have signal molecules with different decay rates and diffusion constants) might each be for probing either the social or diffusive properties of the environment (presented at a conference in Nov. 2011, but not published, see [120]).

[3]Most genes which are QS regulated are believed to also be influenced by other factors than the concentration of the QS signal, such as the metabolic state of the cell, [110]

### 3.1.4 Factors influencing production and excretion of a common good

It is worthwhile to examine the exact conditions under which a bacterial population will benefit from producing a common good and thereby establish when this production would benefit from being under QS regulation. The factors which one can imagine may influence whether excreting molecules is advantageous for a single cell, or a cell population, are:

- The benefit gained (positive contribution to fitness) by having a certain concentration of the common good in the outside environment.

- The rate of production per cell and the associated cost (negative contribution to fitness) [13; 63].

- The cell density, inhomogeneity of the distribution of cells in space and the geometry of the environment (a nifty experiment dealing with these issues is described in [23]; a relevant modeling study is [77]).

- The total number, as opposed to the density, of common good producing cells present in the system (see the experiments in [23]).

- The molecular durability of the common good (i.e., the extent to which it can be reused multiple times), which is influenced by the rate at which the excreted common good is removed from the environment by degradation, diffusion and/or advection [63; 15].

- The presence of cheats/defectors which may get a fitness advantage compared to cooperators because they avoid the costs of production (cheats have been studied in models in e.g. [77; 86; 85; 26; 146], and experimentally in e.g. [105; 147; 31; 64]).

Others have (see references above) studied, experimentally and theoretically, how a quorum sensing mechanism may condition the expression of a public good to several of the environmental and other factors, listed above. However, to our knowledge no-one has investigated how the functional form of the benefit gained by having different amounts of common good in the environment influences the need (or lack of same) for QS regulation.

## 3.2 Results and Discussion

### 3.2.1 Benefit function for a common good

Typically the net fitness associated with production of a common good is quantified as the net increase in growth rate [4] of the community consisting of common good producers[5]. There will usually be both a negative contribution (cost) and a positive contribution (benefit) to the net fitness associated with the production of a common good. The change in growth rate, $\Delta g$, due to common good production will thus be given by:

$$\Delta g = \text{benefit} - \text{cost} \tag{3.1}$$

$$= B(E) - \sigma_E p_{cost} \tag{3.2}$$

Of course, $\Delta g$ can be a function of time, as well as various other variables and parameters such as the number of cells, their density, the diffusion constant and lifetime of the common good, etc. We make the assumption that the negative contribution from common good production, the cost, is linearly proportional to the rate of production $\sigma_E$ of the common good with the proportionality constant denoted $p_{cost}$. We further assume that the benefit is some function $B(E)$ of the outside concentration, $E$, of the excreted common good[6] – all dependence on time, number of cells, diffusion constant etc. will be through the dependence of $E$ on these factors. Henceforth, we will refer to $B(E)$ as the *benefit function*. The exact shape of the benefit function potentially depends on many details of the specific situation and of the nature of the common good at hand, however, we can assume some reasonable constraints, such as continuity of the function. At zero concentration there must, of course, be no benefit, $B(0) = 0$, and when approaching infinitely high concentration we expect the benefit function to saturate to some finite value. As the concentration $E$ increases from zero, we can imagine three general cases: 1) the benefit immediately decelerates with increasing concentration of common good forming

[4] Alternative ways of quantifying bacteria fitness by e.g. the ability to form biofilm, survival in water and resistance to drying are described in ref. [95].

[5] If the number of cells in a population is denoted $N(t)$, then the growth rate $g(t)$ describes how the cell number changes with time: $dN(t)/dt = g(t)N(t)$. When common good production starts, let the growth rate change to $g'(t)$. Then the cell number will grow following $dN'/dt = g'(t)N'(t)$. The change in growth rate due to common good production, $\Delta g(t) \equiv g'(t) - g(t)$, then describes the change in the ratio, $R \equiv N'/N$, of the number of cells in the common good producing population to the number of cells in a non-producing population: $dR(t)/dt = \Delta g(t).R(t)$. Even if we are not in a well-mixed situation, similar equations will hold, with growth rate and cell number being functions of position as well as time, and with additional terms that account for diffusion or motion of cells in space.

[6] Note that we will use $E$ to refer both to the common good molecule and the concentration of the common good - hopefully it will be obvious from the context which is meant where. This is stylistic choice done in order to avoid the more cumbersome notation of $[E]$ for the concentration.

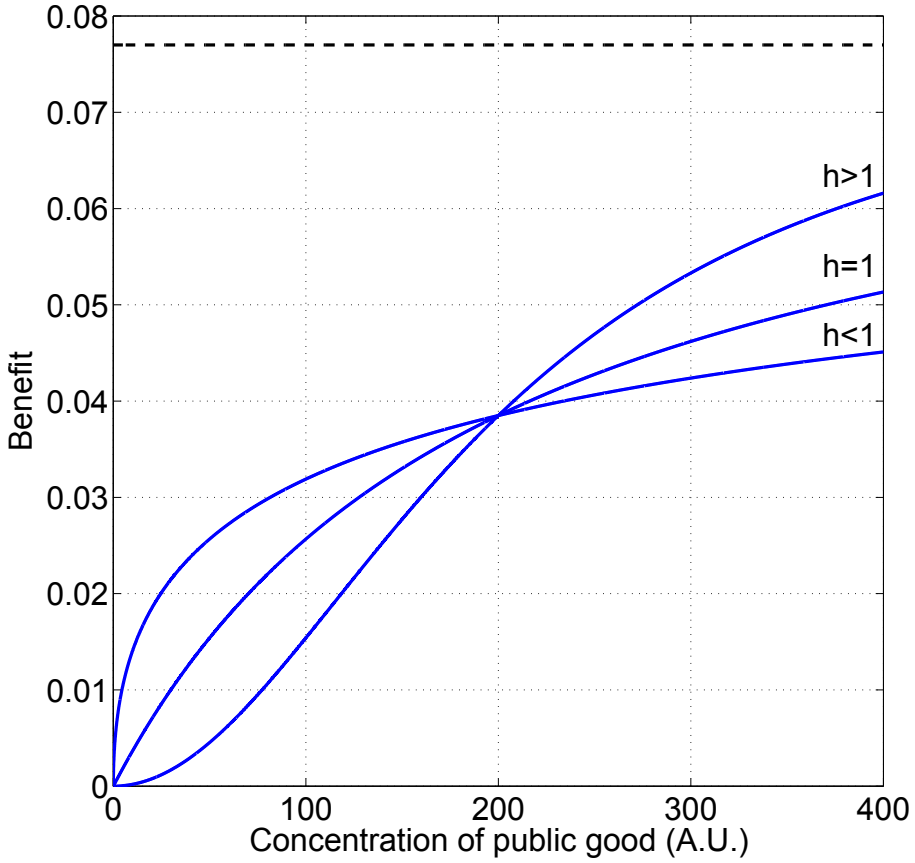


Figure 3.1: **Benefit functions:** Blue curves show the benefit described by eq. 3.3 in units of $min^{-1}$, for three different values of the benefit function Hill-factor $h \in [0.5, 1.0, 2.0]$. Black dashed line marks $B_{max}$. Parameters used were: $B_{max} = 0.077\ min^{-1}$, $K = 200$ (arbitrary units).

a *convex* curve, 2) the benefit initially accelerates forming a *concave* curve before decelerating later to reach the saturation value, and 3) the benefit is initially exactly proportional to the concentration of common good forming a straight line before decelerating later to saturate (see fig. 3.1). These characteristics can be captured by a benefit function of the general form:

$$B(E) = B_{max}\frac{E^h}{E^h + K^h} \tag{3.3}$$

Here the Hill-factor $h$ determines whether the initial response to small doses of common good, $E$, in the environment is concave ($h < 1$), convex ($h > 1$) or linear ($h = 1$) (later when the function approaches saturation all three curves of course become concave). $B_{max}$ is the level of benefit at which the function saturates for very high concentrations of common good and $K$ is the concentration of common good where the benefit is half its maximum value: $B(K) = \frac{1}{2}B_{max}$. Assuming that the benefit function has Hill-factor 1 (see, e.g. [55]) is a decent first order assumption, but there are cases where this is not true (more on this later).

The interesting question is now whether the initial concavity/convexity of the benefit function influences when it is prudent for a cell to produce the common good.

### 3.2.2 Modeling the dynamics of the common good concentration

We begin by formulating some simple models that determine the concentration of the common good when there are one or more cells producing it. Consider first a single cell excreting a common good molecule $E$ at a constant rate $\sigma_E$. The change of $E$ in time at a point $\mathbf{r} = (x, y, z)$ at the time $t$ can be described by the partial differential equation:

$$\frac{\partial E}{\partial t} = D\frac{\partial^2 E}{\partial \mathbf{r}^2} - \gamma_E E(\mathbf{r}, t) + \delta(\mathbf{r} - \mathbf{r}_0)\sigma_E \tag{3.4}$$

The first term on the right hand side models diffusion of $E$ with a diffusion constant $D$. The second term represents the degradation of $E$, with $\gamma_E$ being the degradation rate. The third term models a point source of $E$ at position $\mathbf{r}_0$ where the single cell is located. In most cases we can reasonably assume that the time scales of cell division and cell movement are far slower than that of diffusion and degradation of the common good molecules. This means that, for now, finding the steady state solution, $E_{ss}(x)$, will suffice. [7] We can thus set $\frac{\partial E}{\partial t} = 0$ and solve the ordinary differential equation:

$$D\frac{d^2 E_{ss}}{dx^2} = \gamma_E E_{ss}(x) - \delta(x - x_0)\sigma_E \tag{3.5}$$

The solution of eq. 5.36, with boundary conditions $E(x) \to 0$, for $x \to \pm\infty$, (see derivation in Appendix 6):

$$E_{ss}(x) = \frac{\sigma_E}{2\sqrt{D\gamma_E}} \exp\left(-\sqrt{\frac{\gamma_E}{D}}|x - x_0|\right) \tag{3.6}$$

is shown in figure 3.2. We now wish to know the concentration of common good felt by a cell, in the steady state, when other (identical) producing cells are placed at distances $\pm ka$ from it (where $k$ takes values over a finite range of positive integers). We can obtain this from eq. 5.45 by calculating the sum $E_{middle} = \sum_{x_0} E_{ss}(0)$ where $x_0$ runs over the positions of the cells. For a line of $C$ cells, where $C$ is an odd number, the middle cell will feel a concentration given by:

$$E_{middle}(C, D) = \begin{cases} \frac{\sigma_E}{2\sqrt{D\gamma_E}} & \text{for } C = 1 \\ \frac{\sigma_E}{2\sqrt{D\gamma_E}}\left(1 + 2\sum_{k=1}^{\frac{C-1}{2}} \exp\left(-\sqrt{\frac{\gamma_E}{D}}ka\right)\right) & \text{for } C \geq 3 \end{cases} \tag{3.7}$$

$$= \frac{\sigma_E}{2\sqrt{D\gamma_E}}\left(1 + 2\left(\frac{1 - \exp\left(-\sqrt{\frac{\gamma_E}{D}}\frac{a}{2}(C-1)\right)}{\exp\left(\sqrt{\frac{\gamma_E}{D}}a\right) - 1}\right)\right), \text{ for } C \geq 1 \tag{3.8}$$

[7] For simplicity, we will find the solution for the 1 dimensional case. For 2 dimensions the solution is a Bessel function and thus not so easy to manipulate analytically later on.

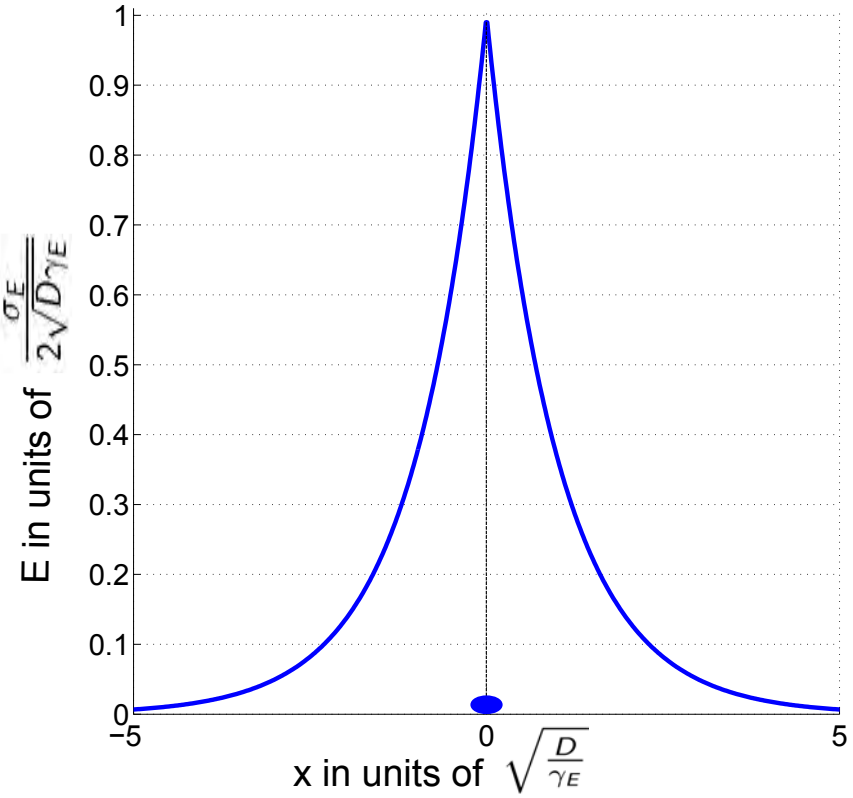


Figure 3.2: **Steady state concentration of common good with a single point source.** The steady state concentration eq. 5.45 of common good concentration around a single cell at $x_0 = 0$ (marked by the blue ellipse) continuously producing the good at the rate $\sigma_E$. Distance from the producing cell, $x$, is shown in units of $\sqrt{\frac{D}{\gamma_E}}$, which is roughly the mean length a common good molecule will diffuse before decaying. Concentration of the common good is shown in units of $\frac{\sigma_E}{2\sqrt{D\gamma_E}}$.

Similarly, a cell on the edge of the colony will feel: $E_{edge}(C,D) = \frac{\sigma_E}{2\sqrt{D\gamma_E}}\left(1+\left(\frac{1-\exp\left(-\sqrt{\frac{\gamma_E}{D}}\frac{a}{2}(C-1)\right)}{\exp\left(\sqrt{\frac{\gamma_E}{D}}a\right)-1}\right)\right)$, exactly the same expression as eq. 3.8 but without the factor 2 inside the parentheses[8]. Of course, $E_{middle}$ is a function of $\sigma_E, \gamma_E, a$ also, but we have emphasized its dependence on $C$ and $D$ because this dependence is what we will investigate further (recall that the debate in the QS community was whether QS systems measure quorum or diffusion.) In fig. 3.3 A and B we have plotted eq. 3.8 as a function of $C$ and $D$ respectively. When the average length a common good molecules diffuses before decaying, $\sqrt{\gamma_E/D}$, is much longer than size of the system $\left(\sqrt{\frac{\gamma_E}{D}}Ca \ll 1\right)$, we see that $E_{middle}(C,D)$ (and similarly $E_{edge}$) is approximately linear in $C$:

$$E_{middle}(C,D) \approx \frac{\sigma_E}{2\sqrt{D\gamma_E}}C \tag{3.9}$$

Note that this maps exactly onto the solution for a well-mixed/non-spatial system. For the well-mixed case, we would have the differential equation:

$$\frac{dE}{dt} = \tilde{\sigma}_E C - \gamma_E E \Rightarrow \tag{3.10}$$

$$E_{ss}(C) = \frac{\tilde{\sigma}_E}{\gamma_E}C \tag{3.11}$$

so we will refer to the limit where $\sqrt{\frac{\gamma_E}{D}}Ca \ll 1$ as the "well-mixed" case. Note that in both the general 1D case, and the well-mixed limit, the steady-state concentration of the common good is linearly proportional to the production rate $\sigma_E$. We will use this fact in the next section.

### 3.2.3 The optimal production rate for the common good

We now investigate whether there exists an optimal production rate (which may be a function of time) that maximizes the growth rate of this 1 dimensional colony of cells. If such an optimal strategy exists it would be interesting to determine how it is influenced by the initial convexity/concavity of the benefit function. To do this we must make some assumptions about how the 1D colony grows. We will assume: (i) cells divide on a time scale much slower than the production, diffusion and degradation of the common good, so the common good concentration is in steady-state at all times: $E(x,t) = E_{ss}(x)$; (ii) new cells expand the total length of the colony but at all times the cells arrange themselves to occupy positions $x = ka$, where $k$ ranges from 1 to $(C-1)/2$ when $C$ is odd, and 1/2 to $(C-1)/2$ when $C$ is even; (iii) the growth

[8]When $C$ is an even number, we still get the same answer as long as $E_{middle}$ refers to the concentration exactly at the middle of the line, between the middle two cells. Therefore, from now on, we will not restrict $C$ to odd numbers.

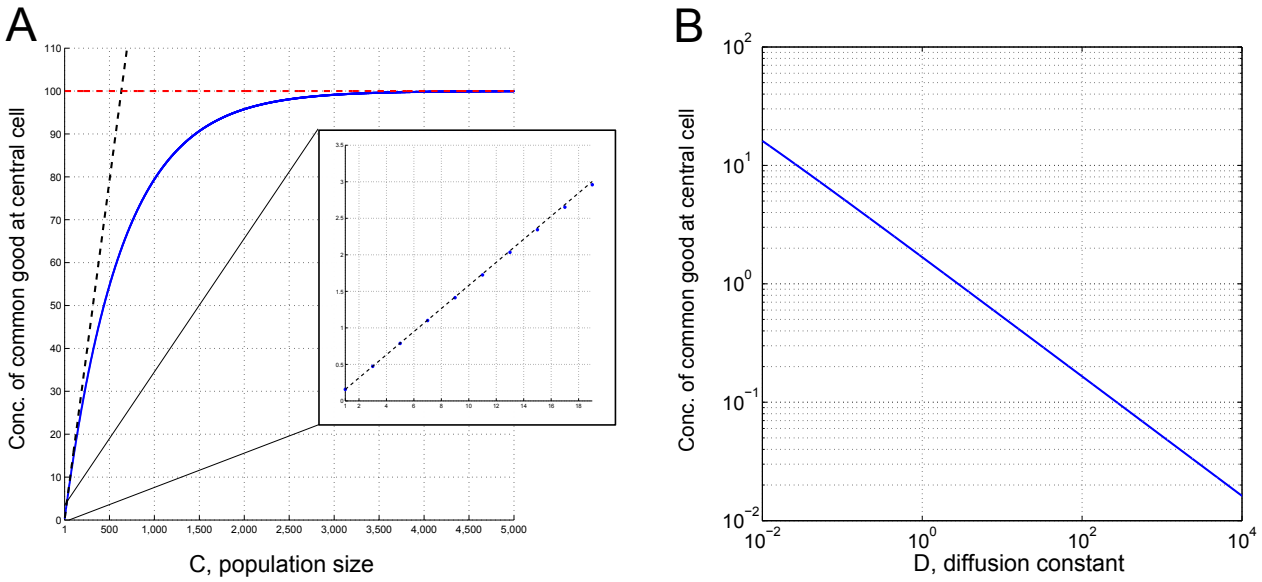


Figure 3.3: **Concentration of common good felt by middle cell as a function of the total number of cells and the diffusion constant.** **A:** Blue points show eq. 3.8, the steady state concentration of common good felt by the middle cell in a line of cells, as a function of the total number of cells $C$. Black dashed line shows eq. 3.9, red dashed line shows the maximum value of common good concentration $\sigma_E \left( \frac{1}{\gamma_E a} + \frac{1}{2\sqrt{D\gamma_E}} \right)$ (derived in Appendix 3, section 5.8.3). Insert shows that eq. 3.9 is a good approximation to eq. 3.8, for relatively small $C$. Other parameters were: $D = 100\,(\textit{unit length})^2/(\textit{unit time})$, $\gamma_E = 0.1\,(\textit{unit time})^{-1}$, $\sigma_E = 1\,(\textit{unit time})^{-1}$, $a = 0.1\,(\textit{unit length})$. **B:** Blue curve shows eq. 3.8, the steady state concentration of common good felt by the middle cell in a line of cells, as a function of the diffusion constant, $D$, of the common good. Other parameters were: $\gamma_E = 8\,(\textit{unit time})^{-1}$; $\sigma_E = 1\,(\textit{unit time})^{-1}$; $a = 0.001\,(\textit{unit length})$, $C = 10$.

rate of the cells is fixed by the net benefit that would go to a cell in the middle[9] of the line, i.e. $dC/dt = \Delta g\,(E_{middle})\,C$. As mentioned earlier we take the net change in the growth rate, $\Delta g$, due to common good production at the rate $\sigma_E$, to be:

$$\begin{aligned}
\Delta g(C, D, \sigma_E) &= \text{benefit} - \text{cost} && (3.12)\\
&= B(E) - \sigma_E p_{cost} && (3.13)\\
&= B_{max}\frac{E^h}{E^h + K^h} - \sigma_E p_{cost} && (3.14)\\
&= B_{max}\frac{(\sigma_E f(C, D))^h}{(\sigma_E f(C, D))^h + K^h} - \sigma_E p_{cost} && (3.15)
\end{aligned}$$

In the last line we have taken advantage of the fact that the steady-state concentration, $E_{middle}$, scales linearly with the production rate per cell so that we may simply express it as $\sigma_E$ multiplied by a function, $f(C, D)$, of the number of cells in the system, the diffusion constant, and other parameters which we hide for clarity, because we will hold all other parameters fixed. We now want to determine whether there exists an "optimal strategy" of common good production at different times, $\sigma_E^{opt}(t)$, which would maximize the size of the colony at any given time. Evidently, a strategy that maximized $\Delta g$, for each possible value of $C$ and $D$, would be unbeatable. That is, we need to find a function $\sigma_E = \sigma_E^{opt}(C, D)$ that, for all values of $C$ and $D$, maximizes $\Delta g(C, D, \sigma_E)$ (the separation of timescales – cells divide at a rate much slower than the dynamics of $E$ – allows this simplification of the calculation). Local maxima of $\Delta g$ must satisfy:

$$\left.\frac{\partial \Delta g(C, D, \sigma_E)}{\partial \sigma_E}\right|_{\sigma_E = \sigma_E^{opt}} = 0, \qquad (3.16)$$

and

$$\left.\frac{\partial^2 \Delta g(C, D, \sigma_E)}{\partial \sigma_E^2}\right|_{\sigma_E = \sigma_E^{opt}} < 0 \qquad (3.17)$$

It turns out that, for the sigmoidal functional forms we use for the benefit function (see eq. 3.3) and the forms of $f(C, D)$ we get from eq. 3.8 or 3.9, there is at most one local maximum. However, for some values of $C$ and $D$ it can happen that this local maximum has a negative value for $\Delta g$. In that case, and in the case where there is no local maximum, the real maximum

[9] This choice was made just for convenience. Perhaps a more realistic assumption would be to use the edge benefit with the idea that new cells arise only at the edges, or to use some sort of weighted sum of benefits all along the line. However, the results would be identical in all important respects because the functional dependence of the benefit function on the production rate $\sigma_E$ is very similar at the middle, the edges and at any point on the line. In fact, our main results from this 1D calculation, concerning the influence of the benefit function Hill-factor on the optimal production strategy, also hold for the 2D case as will be evident in the next chapter which examines simulations of a 2D model of common good producing bacterial colonies.

is at $\sigma_E^{opt}(C,D) = 0$ because that gives $\Delta g = 0$. Thus, the optimal strategy is to attempt to satisfy equations 3.16 and 3.17, as well as:

$$\Delta g(C, D, \sigma_E^{opt}) > 0. \tag{3.18}$$

If for some $C$ and $D$ values these three conditions cannot be satisfied then, for those values, $\sigma_E^{opt}(C,D) = 0$. We can expand out the three conditions above by using equation 3.15 and then substituting for $f(C,D)$ from equations 3.9 or 3.8 depending on whether we are interested in the well-mixed case or the more general spatial case. This is done in Appendix 3, section 5.8.2.

**Optimal production rate of the common good in the case where the benefit function hill factor is one.** When the benefit function hill factor is equal to one, $h = 1$, we can actually put everything in closed form:

$$\left.\frac{\partial \Delta g(C,D,\sigma_E)}{\partial \sigma_E}\right|_{\sigma_E=\sigma_E^{opt}} = 0 \Rightarrow \tag{3.19}$$

$$\left(\frac{B_{max}K}{p_{cost}}\right)\frac{\sigma_E^{opt} f(C,D)}{\left(\sigma_E^{opt} f(C,D) + K\right)^2} = \sigma_E^{opt} \Rightarrow \tag{3.20}$$

$$(\sigma_E^{opt})^2 f(C,D) + 2K\sigma_E^{opt} + \frac{K^2}{f(C,D)} - \left(\frac{B_{max}K}{p_{cost}}\right) = 0 \Rightarrow \tag{3.21}$$

$$\sigma_{E,h=1}^{opt}(C,D) = \sqrt{\frac{B_{max}K}{f(C,D)p_{cost}}} - \frac{K}{f(C,D)} \tag{3.22}$$

In the well mixed limit (where $f \equiv f_{wm}(C,D) = \frac{1}{2\sqrt{D\gamma_E}}C$), the optimal production rate for $h = 1$ is thus:

$$\sigma_{E,h=1}^{opt}(C,D) = \sqrt{\frac{2\sqrt{D\gamma_E}B_{max}K}{p_{cost}C}} - 2\frac{K}{C}\sqrt{D\gamma_E} \tag{3.23}$$

We note that eq. 3.23 approaches 0 for large $C$, and small $D$. In the general case (henceforth referred to as the "spatial case") corresponding to equation 3.8 $f \equiv f_{sp}(C,D)$ where:

$$f_{sp}(C,D) = \frac{1}{2\sqrt{D\gamma_E}}\left(1 + 2\left(\frac{1 - \exp\left(\sqrt{\frac{\gamma_E}{D}}\frac{a}{2}(1-C)\right)}{\exp\left(\sqrt{\frac{\gamma_E}{D}}a\right) - 1}\right)\right), \text{ for } C \geq 1, \tag{3.24}$$

$\sigma_{E,h=1}^{opt}$ approaches a constant for large $C$ and small $D$ (see appendix 3, section 5.8.4 for derivation of these limits). Keeping $D$ constant, we see that $\sigma_E^{opt,h=1} = 0$ for $C$ less than a critical population size $C_{c,h=1}$, and above this critical value $\sigma_E^{opt,h=1} > 0$. That is, for $h = 1$, there exists a critical population size at which common good production should be initiated.

This critical value can be calculated as follows:

$$\sigma^{opt}_{E,h=1} = 0 \Rightarrow \tag{3.25}$$

$$\sqrt{\frac{1}{q(C)}}\sqrt{\frac{B_{max}K}{p_{cost}}} = \frac{K}{q(C)} \Rightarrow \tag{3.26}$$

$$C_{c,h=1} = q^{-1}\left(\frac{Kp_{cost}}{B_{max}}\right) \tag{3.27}$$

where $q(C) \equiv f(C,D)$. Thus, in the well mixed limit, we would substitute $q^{-1}$ with:

$$q^{-1}_{wm}(x) = 2x\sqrt{D\gamma_E} \tag{3.28}$$

and in the general spatial case with:

$$q^{-1}_{sp}(x) = 1 - \frac{2}{a}\sqrt{\frac{D}{\gamma_E}}\log\left[1 - \frac{1}{2}\left(\exp\left(\sqrt{\frac{\gamma_E}{D}}a\right) - 1\right)\left(2x\sqrt{D\gamma_E} - 1\right)\right] \tag{3.29}$$

In the well mixed limit we thus have,

$$C_{c,h=1} = 2\frac{\sqrt{D\gamma_E}Kp_{cost}}{B_{max}} \tag{3.30}$$

We see from this expression that, as expected, a higher cost, $p_{cost}$, will result in a later optimal turn on point and a higher maximal benefit, $B_{max}$, will result in an earlier turn on point. Furthermore, high diffusion or degradation, corresponding to a higher loss rate of the excreted common good, will result in a later turn on point. In the general spatial case:

$$C_{c,h=1} = 1 - \frac{2}{a}\sqrt{\frac{D}{\gamma_E}}\log\left[1 - \frac{1}{2}\left(\exp\left(\sqrt{\frac{\gamma_E}{D}}a\right) - 1\right)\left(2\frac{\sqrt{D\gamma_E}Kp_{cost}}{B_{max}} - 1\right)\right] \tag{3.31}$$

$$\left(\text{and } \frac{1}{2\sqrt{D\gamma_E}} < \frac{Kp_{cost}}{B_{max}} < \left(\frac{1}{\exp\left(\sqrt{\frac{\gamma_E}{D}}a\right) - 1} + 1\right)\frac{1}{\sqrt{D\gamma_E}}\right) \tag{3.32}$$

we see that a smaller distance between the cells, $a$, will result in a earlier turn on. (For $\frac{1}{2\sqrt{D\gamma_E}} > \frac{Kp_{cost}}{B_{max}}$ we have $C_{c,h=1} < 1$ which means that here it is beneficial to turn on common good production even for a single cell. For $\frac{Kp_{cost}}{B_{max}} > \left(\frac{1}{\exp\left(\sqrt{\frac{\gamma_E}{D}}a\right)-1} + 1\right)\frac{1}{\sqrt{D\gamma_E}}$, there exists no production rate which will make turn on beneficial at any population number). In the same manner we can find an expression for the critical diffusion rate $D_{c,h=1}$ above which common good production is no longer beneficial in the well mixed limit:

$$D_{c,h=1} = \left(\frac{B_{max}C}{2Kp_{cost}\sqrt{\gamma_E}}\right)^2 \tag{3.33}$$

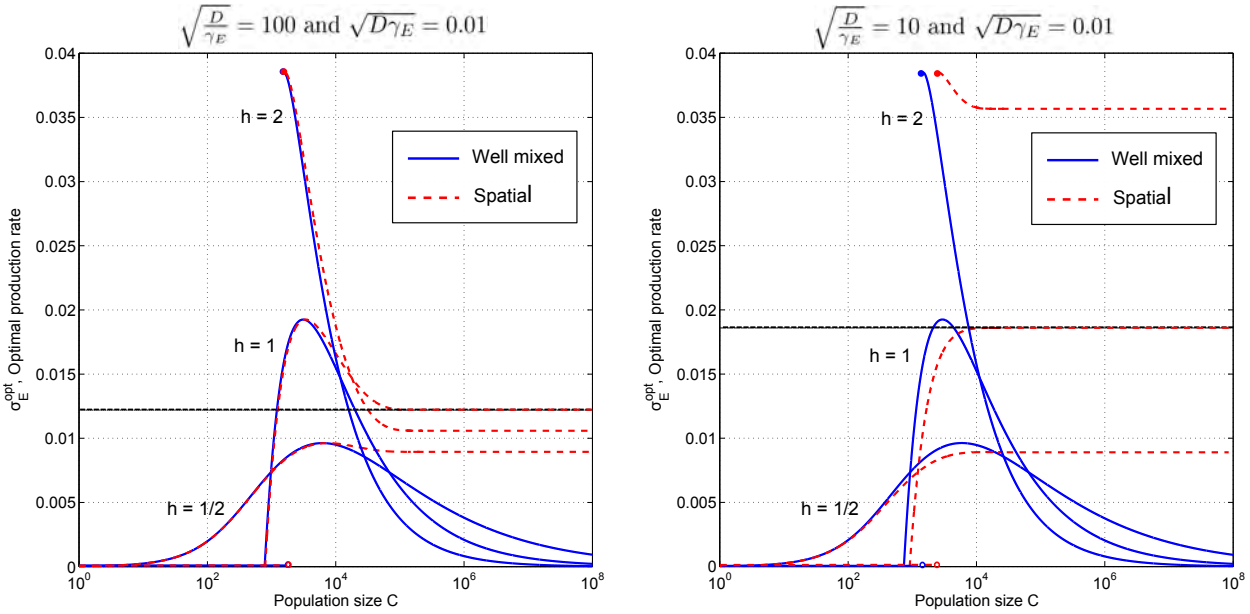


Figure 3.4: **Optimal production curves, as a function of $C$, for benefit functions with $h < 1$, $h = 1$ and $h > 1$.** Blue solid curves: the solution $\sigma_E^{opt}(C)$ to equations 3.16, 3.17 and 3.18 when $f \equiv f_{wm}(C) = \frac{1}{2\sqrt{D\gamma_E}}C$, plotted for $h = \frac{1}{2}$, $h = 1$ and $h = 2$. Red dashed curves: the solution to equations 3.16, 3.17 and 3.18 when $f \equiv f_{sp}(C) = \frac{1}{2\sqrt{D\gamma_E}}\left(1 + 2\left(\frac{1-\exp\left(\sqrt{\frac{\gamma_E}{D}}\frac{a}{2}(1-C)\right)}{\exp\left(\sqrt{\frac{\gamma_E}{D}}a\right)-1}\right)\right)$, (for $C \geq 1$), plotted for $h = \frac{1}{2}$, $h = 1$ and $h = 2$. The thin black line marks the constant (eq. in Appendix 3, section 5.8.4 which $\sigma_E^{opt}(C)$ approaches for large $C$, when $h = 1$. **Left side:** Parameters used were such that $\sqrt{\frac{D}{\gamma_E}} = 100\,(\textit{unit length})$ and $\sqrt{D\gamma_E} = 0.01\,(\textit{unit length})/(\textit{unit time})$, $(D = 10\,(\textit{unit length})^2/(\textit{unit time})$, $a = 0.01\,(\textit{unit length})$, $\gamma_E = 0.001(\textit{unit time})^{-1}$, $B_{max} = 0.077$, $p_{cost} = 1.0$ and $K = 300)$. **Right side:** Parameters used were: $\sqrt{\frac{D}{\gamma_E}} = 10\,(\textit{unit length})$ and $\sqrt{D\gamma_E} = 0.01\,(\textit{unit length})/(\textit{unit time})$, $(D = 1\,(\textit{unit length})^2/(\textit{unit time})$, $a = 0.01\,(\textit{unit length})$, $\gamma_E = 0.01(\textit{unit time})^{-1}$, $B_{max} = 0.077$, $p_{cost} = 1.0$ and $K = 300)$.

Here we see (again as expected) that a higher production cost, $p_{cost}$, and degradation rate, $\gamma_E$, will result in a lower diffusion constant turn off point while increasingly higher $B_{max}$ and larger population sizes, $C$, will make common good production beneficial in environments with higher diffusion constants. A similar calculation can be done for the general spatial case but it is not possible to write out $D_{c,h=1}$ in closed form because $D$ cannot be isolated from $f_{sp}(C, D)$.

**Comparing optimal production rates for different shapes of the benefit function.** When $h \neq 1$, $\sigma_E^{opt}$ has to be determined from equations 3.16, 3.17 and 3.18 numerically. In fig. 3.4 and 3.5 we have plotted $\sigma_E^{opt}(C, D)$ as a function of $C$ and $D$, respectively, for three different values of the benefit function Hill factor, $h$, corresponding to benefit functions that are (for low $E$) concave, linear and convex. Looking at these figures it becomes apparent that for $h \geq 1$

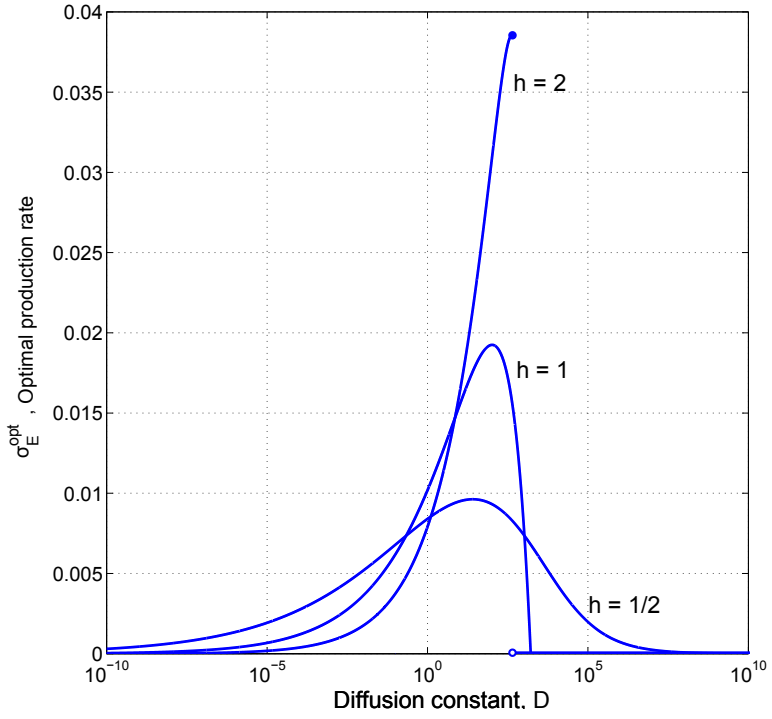


Figure 3.5: **Optimal production curves, as a function of $D$, for benefit functions with $h < 1$, $h = 1$ and $h > 1$.** Optimal production rate $\sigma_E^{opt}$ as a function of the Diffusion constant, $D$, for three different values of the benefit function hill factor $h \in [0.5, 1, 2]$ in the well mixed limit. Note that these optimal curves are mirror images of the curves in fig. 3.4. This is no coincidence. Because $f_{wm}(C, D) = \frac{1}{2\sqrt{D\gamma_E}}C$, if we plot $\sigma_E^{opt}$ as a function of $\frac{1}{\sqrt{D}}$ we will get the exact same curve as when it is plotted as a function of $C$. Parameters used: $C = 10$, $\gamma_E = 0.01(unit\ time)^{-1}$, $B_{max} = 0.077$, $p_{cost} = 1.0$ and $K = 300$.

optimal common good production requires that you only produce when the population number is larger than a critical value $C_c$ (which depends on $D$ and other parameters) or when the diffusion constant is smaller than a critical value $D_c$ (which depends on $C$ and other parameters). We also note that for $h > 1$ (convex benefit functions) the optimal production curve becomes discontinuous at $C_c$ and $D_c$ (for $h = 1$ only the first derivative becomes discontinuous).

The main difference between the well-mixed and the general spatial cases seems to be that in the spatial case the optimal production rate does not approach zero for high $C$ or low $D$ (as expected, when $\sqrt{\gamma_E/D}Ca \ll 1$, i.e. low $C$ or high $D$, the well-mixed limit and general spatial cases are identical.) The fact that $\sigma_E^{opt}(C, D)$, in the well mixed limit, goes to zero for high $C$ and low $D$ is due to the fact that all common good produced in the system will be felt by all cells. Therefore, for example, larger and larger colonies require less and less common good to be produced per cell to reach a level that provides a substantial benefit. Real systems

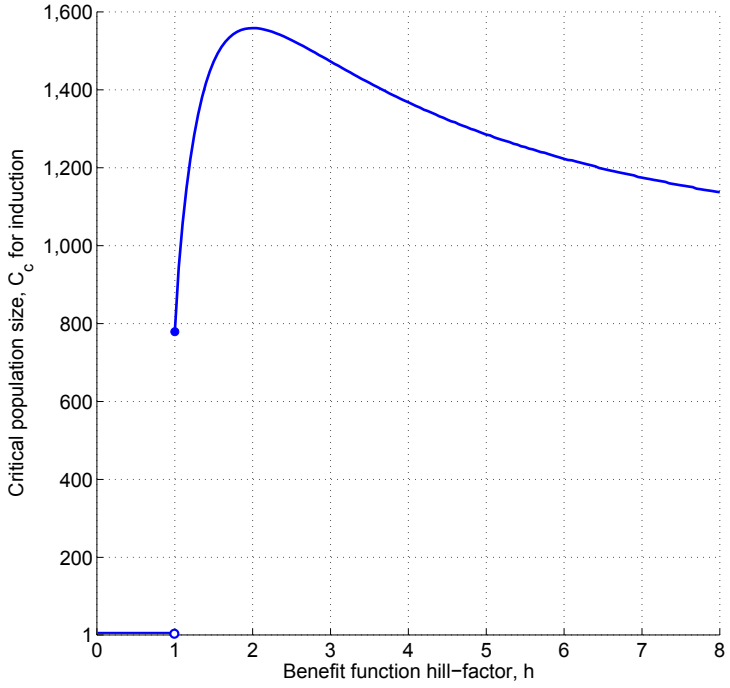


Figure 3.6: **Critical population size where common good production should start.** $C_c$, as a function of benefit function Hill-factor $h$, for the well mixed limit. Filled blue circle shows $C_{c,h=1} = \frac{K\sqrt{D\gamma_E}p_{cost}}{B_{max}}$. For $h \to \infty$, $C_c$ approaches the same value $\frac{K\sqrt{D\gamma_E}p_{cost}}{B_{max}}$ Parameters used were: $D = 1\,(unit\ length)^2/(unit\ time)$, $\gamma_E = 0.01(unit\ time)^{-1}$, $B_{max} = 0.077$, $p_{cost} = 1.0$ and $K = 300$ (same as in fig. 3.4 left side).

are much more likely to be like the spatial case where there is a characteristic length scale the common good molecule can travel in its lifetime and, therefore, the well-mixed assumption, that common goods produced at one end of the system can be felt by the cells at the other end, becomes increasingly bad.

### 3.2.4 Producing the common good at rates other than the optimal is detrimental when benefit functions is convex

Now that we know how the optimal common good production rate looks as a function of population size and the diffusion constant, it is interesting to investigate how much deviations from this optimum affect growth rates for different $h$. In figure 3.7 and 3.8 we see the change in growth rate, $\Delta g$, plotted for a colony following the optimal strategy and producing common good at exactly the rate $\sigma_E^{opt}(C)$, but also the $\Delta g$ of colonies deviating from the optimal by producing either consistently too little or too much enzyme compared to the optimum level.

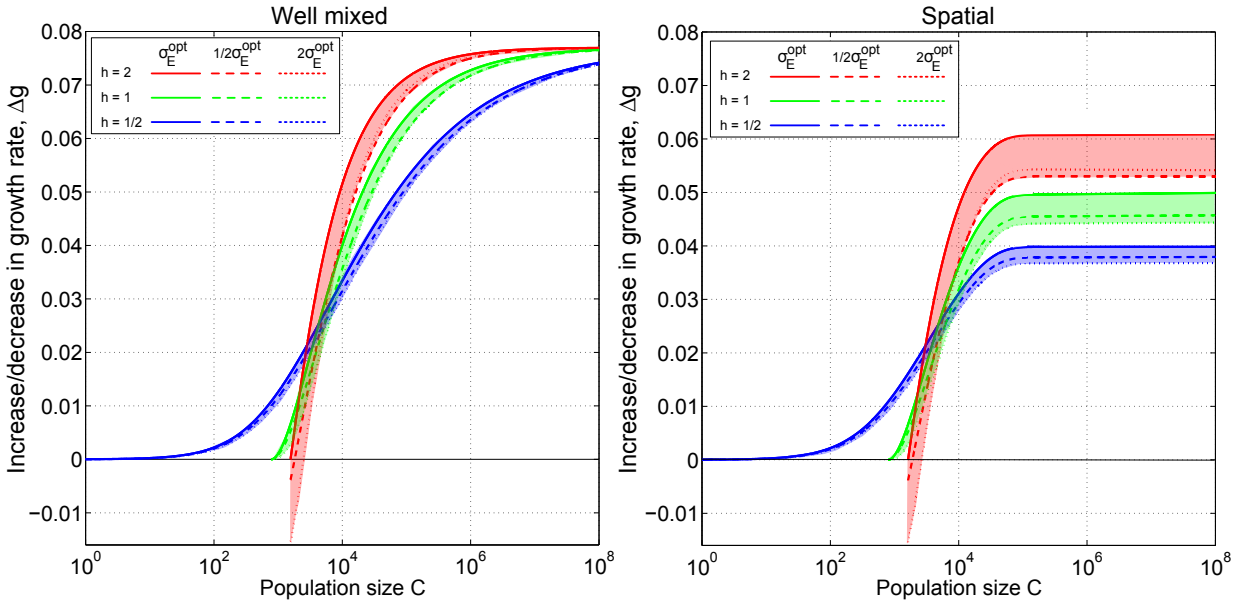


Figure 3.7: **Cost of not producing at the optimal rate decreases with population size for a well mixed system but not for a spatial system**. Solid lines: maximum possible increase in growth rate $\Delta g$, as a function of population size $C$, when enzyme production is exactly $\sigma_E^{opt}(C)$ (blue: $h = 1/2$, green: $h = 1$, red: $h = 2$). Dashed lines: change in growth rate when enzyme production is lower than optimal ($0.5\sigma_E^{opt}(C)$). Dotted lines: change in growth rate when enzyme production is higher than optimal ($2.0h_E^{opt}(C)$). Parameters used were: $D = 1\,(unit\ length)^2/(unit\ time)$, $a = .01(unit\ length)^2$, $\gamma_E = 0.01(unit\ time)^{-1}$, $B_{max} = 0.077$, $p_{cost} = 1.0$ and $K = 300$ (same as in fig. 3.4 left side).

It is clearly seen that producing less or more than the optimal rate comes at a higher cost for higher values of $h$. Note, in particular, how being away, in either direction, from the optimal growth rate for $h > 1$ can even lead to a net reduction in the growth rate, i.e. $\Delta g$ can become negative. For some parameter values this is also possible for $h \leq 1$, but never when you produce at less than the optimal rate.

Elaborating on this point, we examine how well an enzyme production strategy does compared to the optimal strategy, when there is a non-zero basal growth rate, $g_{basal}$, even when no common good is being produced. Then the actual growth rate of a colony is $g = g_{basal} + \Delta g$, and $\nu(\sigma_E) \equiv (g_{basal} + \Delta g(\sigma_E(C, D)))/(g_{basal} + \Delta g(\sigma_E^{opt}(C, D)))$ is a measure of how well the strategy $\sigma_E$ does compared to the optimal strategy $\sigma_E^{opt}$ (the lower the value of $\nu$, the worse it is doing). In figure 3.9 and 3.10 we plot $\nu\left(\eta\sigma_E^{opt}\right)$, for $\eta = 1/2$ and $\eta = 2$, as a function of population size, $C$ and diffusion rate, $D$. Note how deviating from the optimal strategy comes at a great cost right at the point where common good production should be initiated/terminated (at $C_c$ and $D_c$), particularly for $h > 1$. For all values of $h$ we see that the

cost of deviating from optimality decreases for increasing $C$ in the well mixed limit, but not in the spatial case.

**Suboptimal production is not detrimental when benefit function is concave.** Note that when the benefit function is concave ($h \leq 1$), $\Delta g$ can only become negative when the production rate is higher than the optimal rate (i.e., $\eta > 1$). Suboptimal production is thus not too detrimental when the benefit function is concave ($h \leq 1$), while when the benefit function is convex ($h > 1$), both sub and super optimal production rates can potentially result in negative $\Delta g$, (precisely at $C_c$ or $D_c$, $\Delta g$ will be negative for $\eta \neq 1$ and $h > 1$). With a concave benefit function ($h \leq 1$) one could thus "play it safe", produce a little less than the optimal rate and still get a net growth increase compared to when not producing. Whereas with a convex benefit function ($h > 1$), both producing too little and too much can be worse than not producing the common good at all. We also see that $\Delta g$ rises/falls more steeply around $C_c$ or $D_c$ for $h > 1$ than for $h \leq 1$, which means that the potential loss from *not* producing at the optimal rate is also higher here. All in all, these results show that differences in population number and diffusion rate have a far greater impact on growth rate when a common good benefit function has Hill-factor $h > 1$, which suggests that having a system that carefully regulates the production rate of a common good could be very important for a convex benefit function, and not as important for a concave benefit function. This regulatory mechanism would at least need to be able to detect when some combination of $C$, $D$ and $\gamma_E$ crosses a critical threshold[10]. Perhaps that is the role of QS regulation of common good production. We will pursue this thought in the next chapter.

### 3.2.5 What does a typical common good benefit function look like?

From the results above, we can conclude that the initial convexity/concavity of the benefit function of the common good can have a huge influence on the optimal production strategy. But what is the Hill-factor of a typical benefit function?

**Virulence factors.** It has been proposed that when virulent bacteria delay production of a virulence factor, via QS regulation, it is because a low concentration of the virulence factor would alert the host immune system, while at the same time not do much harm to the host. Instead, delaying production of the virulence factor until a sufficiently high bacterial density had been reached could lead to more positive outcomes (from the bacterial point of view): either

[10] In the limit $\sqrt{\gamma_E/D}Ca \ll 1$, the optimal production rate becomes non-zero only when the combination $C/\sqrt{D\gamma_E}$ crosses a threshold value (because in this limit the steady-state value of $E$ only depends on this combination; see equations 3.9 and 3.23). For the more general spatial case it may be a more complex combination that cannot be easily written in a closed form.

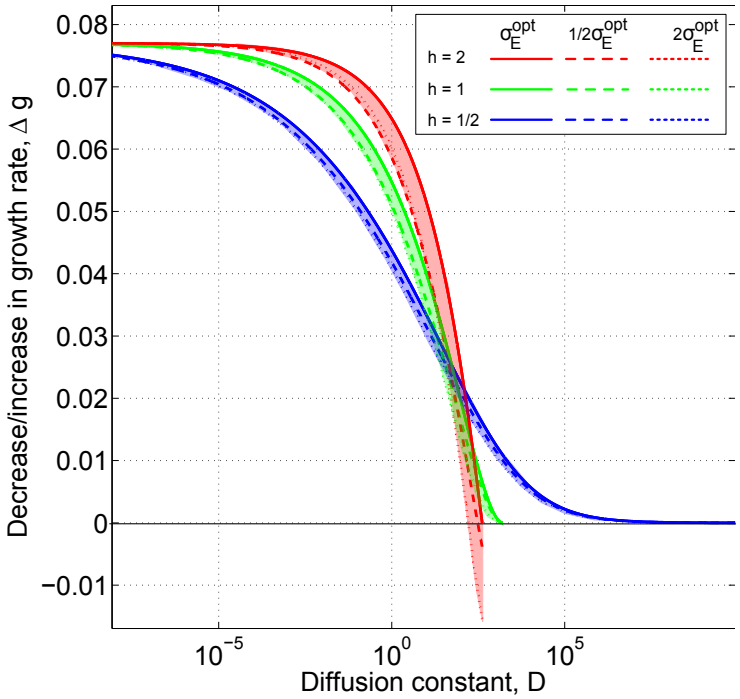


Figure 3.8: Solid lines: maximum possible increase in growth rate $\Delta g$ as a function of the diffusion constant $D$, when enzyme production is exactly $\sigma_E^{opt}(C)$ (blue: $h = 1/2$, green: $h = 1$, red: $h = 2$). Dashed lines: change in growth rate when enzyme production is lower than optimal ($0.5\sigma_E^{opt}(C)$). Dotted lines: change in growth rate when enzyme production is higher than optimal ($2.0h_E^{opt}(C)$). Parameters used were: $C = 10$, $\gamma_E = 0.01(\mathit{unit\ time})^{-1}$, $B_{max} = 0.077$, $p_{cost} = 1.0$ and $K = 300$ (same as in fig. 3.5). $\Delta g$ can go negative for $\eta < 1$ when $h > 1$, but not for $h \leq 1$ (because of the discontinuity of the $\sigma_E^{opt}$ curve). This makes the deviating from the optimal strategy potentially more harmful for $h > 1$ than for $h \leq 1$, especially around $D_C$.

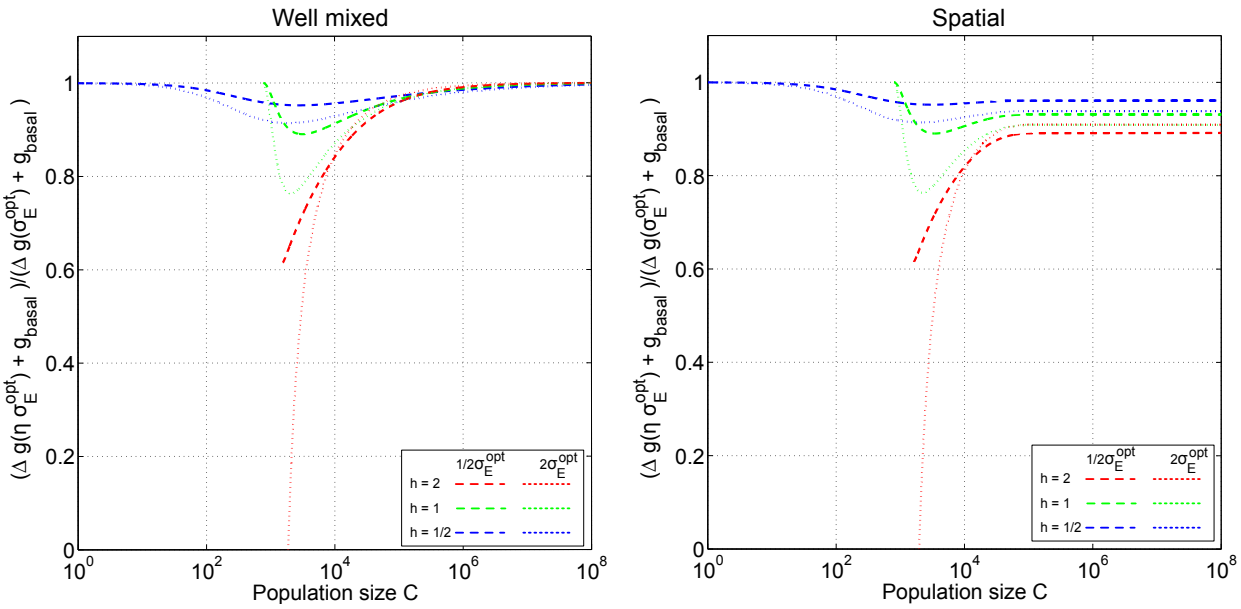


Figure 3.9: **Not producing the common good at the optimal rate comes at a more severe cost for $h > 1$ around $C_c$.** Fractional deviation from optimal growth, $\frac{\Delta g(\eta\sigma_E^{opt}(C))+g_{basal}}{\Delta g(\sigma_E^{opt}(C))+g_{basal}}$, for $\eta = 0.5$ and 2.0, as a function of population number $C$. (Blue: $h = 1/2$, green: $h = 1$, red: $h = 2$ ), when we assume that cells which are not producing the common good are growing at the basal rate $g_{basal} = 0.01\,(unit\ time)^{-1}$. (This basal rate is chosen to be relatively low for this plot, i.e., of the same order of magnitude as $\Delta g$, so that not producing at the optimal rate has a big impact. If $g_{basal} \gg \Delta g$ then, of course, not producing at the optimum rate becomes much less important, but in that case there is anyway not much benefit to be gained from the common good even if cells are producing it at the optimal rate). Parameters used were: $D = 1\,(unit\ length)^2/(unit\ time)$, $a = .01(unit\ length)$, $\gamma_E = 0.01(unit\ time)^{-1}$, $B_{max} = 0.077$, $p_{cost} = 1.0$ and $K = 300$ (same as in fig. 3.4 left side).

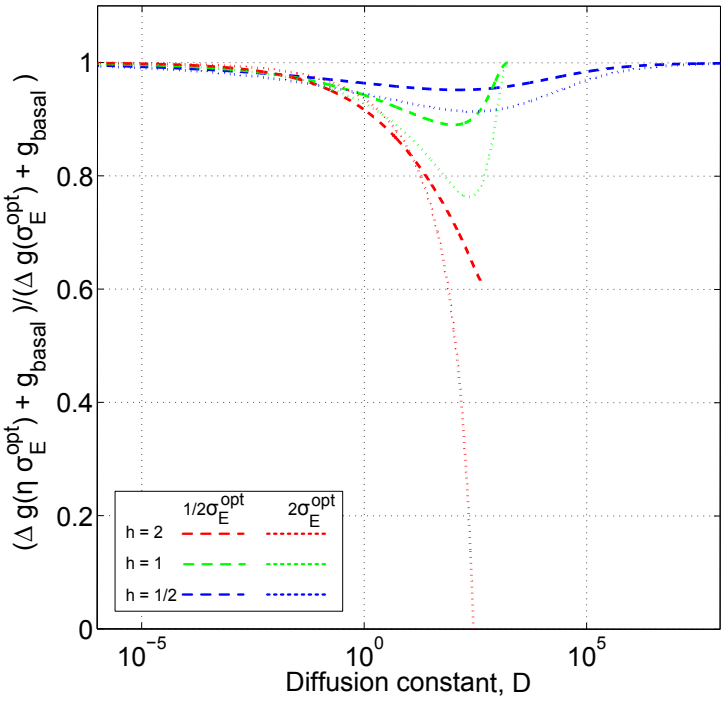


Figure 3.10: **Not producing the common good at the optimal rate comes at a more severe cost for $h > 1$ around $D_c$.** Fractional deviation from optimal growth, $\frac{\Delta g(\eta \sigma_E^{opt}(C)) + g_{basal}}{\Delta g(\sigma_E^{opt}(C)) + g_{basal}}$, for $\eta = 0.5$ and 2.0, as a function of diffusion constant $D$. (Blue: $h = 1/2$, green: $h = 1$, red: $h = 2$ ), when we assume that cells which are not producing the common good are growing at the basal rate $g_{basal} = 0.01\,(unit\ time)^{-1}$. (This basal rate is chosen to be relatively low for this plot, i.e., of the same order of magnitude as $\Delta g$, so that not producing at the optimal rate has a big impact. If $g_{basal} \gg \Delta g$ then, of course, not producing at the optimum rate becomes much less important, but in that case there is anyway not much benefit to be gained from the common good even if cells are producing it at the optimal rate). Parameters used were: $C = 10$, $\gamma_E = 0.01\,(unit\ time)^{-1}$, $B_{max} = 0.077$, $p_{cost} = 1.0$ and $K = 300$ (same as in fig. 3.5).

1) death of the host organism on a faster time scale than the immune system could detect and launch a counter attack, or 2) enough time for the bacteria to produce means of protection (e.g. biofilm) from the immune system before producing virulence factors. This idea is sometimes refereed to as the "sneak attack" hypothesis (e.g. in [145]) for obvious reasons. If this theory it is right, it is a good example of a situation where the benefit function of a common good (the virulence factor) would be highly convex. Note that in this scenario, as small amounts of virulence factor would provoke an attack from an otherwise indifferent immune system, the benefit could actually be negative for small concentrations of virulence factor.

**Antimicrobials.** Another typical common good is an antibiotic produced to kill or harm other species of bacteria living in the same habitat as the common good producer. Its has been shown experimentally that the "killing curve" - the rate of death of the bacteria which is sensitive to the antibiotics vs. the concentration of the antibiotics – is often sigmoidal with a hill factor of $2-4$, [84; 70]. This thus constitutes another example of a situation where the benefit function is convex. The source of the convexity of the killing-curve is not well-established. For toxins which damage parts of the target cell which are monitored by specific repair mechanisms, the convexity could be related to the time scale over which the cell-repair mechanisms act. Small doses of toxin may allow time for the repair mechanisms to "keep up" and continuously repair the damage done by the toxin between each new damage event, while at higher concentrations of toxin the damage would start to accumulate and become fatal. Another factor, acting on an evolutionary time scale, is that small sub-lethal doses of antibiotics would allow an enemy-bacteria to slowly adapt and become resistant to the toxin over time.
On a more hypothetical note we can mention that an excreted common good molecule which acted in a cooperative manner outside the cell (as is the case for many proteins acting inside the cell), would also result in a convex benefit function, although we do not currently know of any common goods where this has been demonstrated.

**Siderophores.** An example of a common good which might have a benefit function with Hill-factor 1 is siderophores: small molecules which diffuse from the cell and bind to specific metals (like e.g. iron) which the cell's survival depends on, but which are not sources of metabolic energy; without siderophores the cells are unable to transport the metals across the cell membrane, but the siderophore-metal complexes can be imported into the cells and the metals extracted from them [87; 44]. This could probably even be a scenario where the Hill factor would be lower than 1 (decelerating benefits) since the small amount of, e.g., iron a cell could get from having just a few siderophores in the environment would give a comparatively

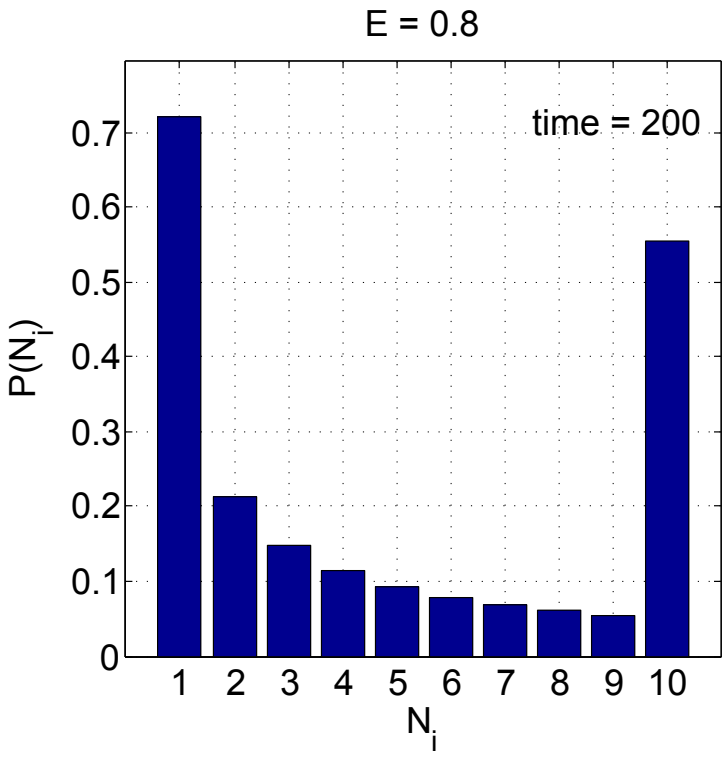


Figure 3.11: **Steady state polymer length distribution.** Example of the steady state distribution of polymer of different lengths (determined numerically) when parameters are: $N_i(t=0)=0$, $E=0.8$, $n=10$, $p=\delta=1\,(time\ unit)^{-1}$. (At time $t=200$ the distribution is stationary for these parameters).

large benefit relative to the iron molecules gained later at higher siderophore concentrations when siderophore-iron complexes where plentiful and thus not as precious/valuable to the cell.

**Extracellular enzymes.** One last large group of typical common goods are extracellular enzymes which degrade large molecules, e.g. long organic polymers, in the environment thus providing metabolizable nutrients to nearby cells. A well studied example is *Pseudomonas aeruginosa* which can excrete multiple proteases[11] capable of degrading, e.g., casein[14] into casamino acids by breaking the polymer peptide bonds [60; 128; 49]. In this situation, it is not intuitively obvious what the shape of the benefit function would be. In the next section, we formulate a simple model for the action of such an exoenzyme to try and assess the shape of the benefit function.

[11] LasAB and AprA, the major secreted proteases by *Pseudomonas aeruginosa*, *[128; 49]*. LasA preferentially cleaves peptide bonds subsequent to Gly-Gly pairs [60].

### 3.2.6 A simple model for polymers degraded by an excreted enzyme

Consider the example of *Pseudomonas aeruginosa* excreting enzymes that can cut long polymers, like casein, into digestible bits. Let us assume that the specific sites where the enzymes can break the polymers are distributed randomly along the length of the polymer[12]. We will assume that the fitness increase is proportional to the number of pieces of polymer present which are small enough for transport over the cell membrane. Thus, what we need to determine is the steady state distribution of polymers of different lengths, and specifically the concentration of polymers of the "edible length", as a function of the concentration of excreted enzyme. We set this "edible length" (the maximal length that still allows transport over the cell membrane), to one, we assume a constant external source of polymers of length $n$, and a constant degradation rate $\delta$ which is the same for polymers of all lengths. Finally, we model all this in a well-mixed setting.

The concentration of a polymer of length $i$ is denoted $N_i$. The longest polymers are the ones supplied by an external source, i.e. the ones with length $n$, which produces these polymers at a rate $p$. Concentration of enzyme (common good) is denoted $E$. The equations describing the change in concentration of polymers of each possible length are, thus, as follows:

$$\frac{dN_n}{dt} = p - N_n(E+\delta) \tag{3.34}$$

$$\vdots$$

$$\frac{dN_i}{dt} = 2E\sum_{j=i}^{n-1}\frac{N_{j+1}}{j} - N_i(E+\delta) \tag{3.35}$$

$$\vdots$$

$$\frac{dN_1}{dt} = 2E\sum_{j=1}^{n-1}\frac{N_{j+1}}{j} - N_1\delta \tag{3.36}$$

where $i = 1, 2, \ldots, n$

Note that the rate of cleavage of polymers per enzyme molecule is set to 1. This can always be done by choosing the units of $E$ appropriately. The first term on the right hand side of the equations for $N_i\,(i < n)$ come from counting the number of ways one can get a polymer of length $i$ by randomly cutting a larger polymer. The terms have the form $2EN_{j+1}/j$ basically because a $j+1$ size polymer can be cut in $j$ places, and two out of $j$ ways will produce a polymer of size $N_i$. In the specific case of $j+1 = 2i$ then there is one place to cut which will result

[12] The proteases LasB and AprA secreted by *Pseudomonas aeruginosa* are "endoproteases", which means they cut the protein next to specific residues. Endoenzymes are generally more common among QS-regulated secreted enzymes than enzymes which cleave molecules from the one or both ends (Brook Peterson, U. Washington, personal communication).

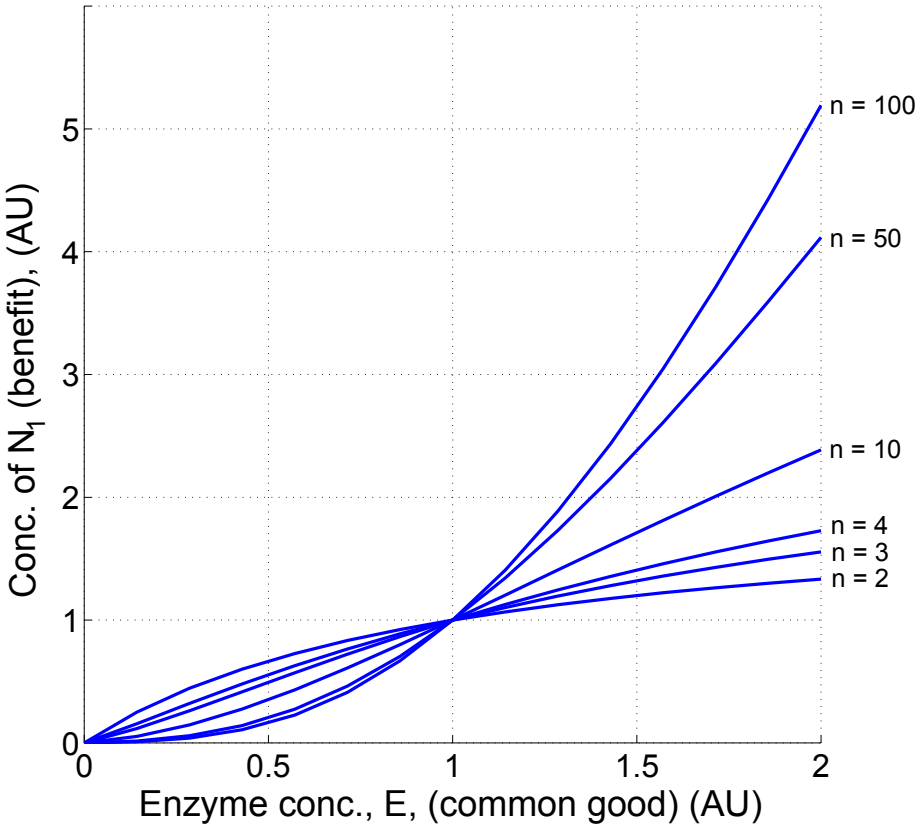


Figure 3.12: **Benefit function becomes increasingly convex as length of longest polymer in system increases.** Steady state concentration of $N_1$ as a function of enzyme concentration $E$, for systems with maximum polymer length of $n \in [2, 3, 4, 10, 50, 100]$.

in two polymers of length $N_i$, so the form of the term remains the same. The steady state concentrations, $N_n^*, \ldots, N_i^*, \ldots, N_1^*$ can be found by setting $\dot{N}_n = \cdots = \dot{N}_i = \cdots = \dot{N}_1 = 0$. See fig. 3.11 for an example of how the distribution looks for a certain choice of $E$ and $n$. The main quantity of interest is $N_1$, the concentration of digestible polymers. For $n = 2$, the steady state concentration of $N_1$ will be:

$$N_{1,n=2}^* = 2\frac{Ep}{\delta(\delta + E)} \tag{3.37}$$

and for $n > 2$, the steady state concentration of $N_1$ is given by:

$$N_{1,n>2}^* = \frac{2}{n-1}\frac{Ep}{\delta(\delta+E)}\left[1 + \left(\frac{2}{n-2} + \sum_{k=2}^{n-2}\frac{1}{k-1}\prod_{j=k}^{n-2}\left(1 + \frac{2}{j}\frac{E}{\delta+E}\right)\right)\frac{E}{\delta+E}\right] \tag{3.38}$$

(see section 5.8.5 in Appendix 3 for derivation). Eq. 3.37 and 3.38 are plotted in figure 3.12. In fig. 3.13 we plot a measure for the convexity of eq. 3.38, as a function of the length of the longest polymers in the system. We see that it is only for a system with a maximal polymer length of $n = 2$ that the benefit function is *not* convex. (The second derivative of eq. 3.37 is negative while the second derivatives of eq. 3.38 are increasingly more positive for increasing $n$). This means that, in general, benefits will accelerate with increasing concentration of enzyme if the polymers provided by the external source have a length of more than two edible units.

## 3.3 Future work: Non-linear cost of producing a common good

Above we focused on finding the optimal common good production rate when the cost of producing the common good was proportional to the production rate, while the benefit was a non-linear function. However if the cost vs. production rate did have an initial concavity/convexity, e.g., if:

$$\Delta g = \text{benefit} - \text{cost} \tag{3.39}$$

$$= B_{max}\frac{(f(C,D)\sigma_E)^h}{(f(C,D)\sigma_E)^h + K^h} - p_{cost}\sigma_E^H \tag{3.40}$$

and $H \neq 1$, then things, of course, depend on the exponent $H$ of the cost curve as well as on the benefit function Hill factor, $h$. A convex cost curve ($H > 1$) could arise, for example, if there is a start up cost associated with the production of a certain common good. Due to time constraints, we have not yet examined how non-linearity of the cost curves influence the results obtained above, but we plan to pursue this in the near future and expect to find similar results where concavity of the cost curve ($H < 1$) would favor QS regulation.

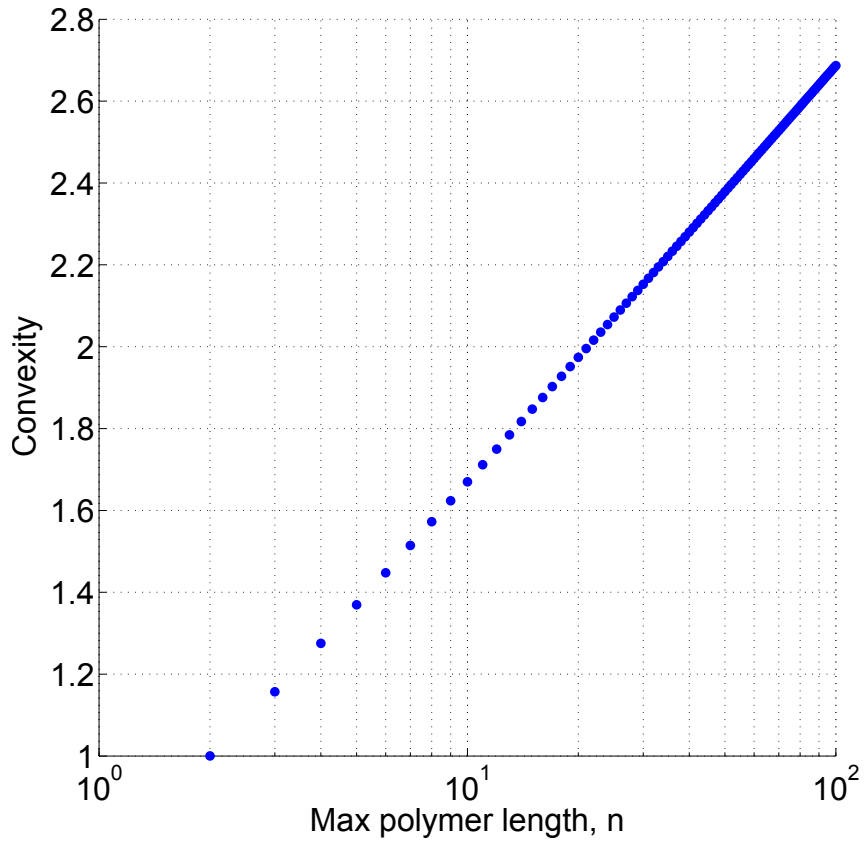


Figure 3.13: **'Convexity' as a function of increasing $n$ (maximum polymer length)**. For each value of $n$ the $N_1$ vs $E$ curve was fitted to a sigmoid (even though this is actually not a sigmoidal function) and the 'convexity' on the y-axis is simply the Hill-factor of this fit. The convexity, defined in this way, forms an almost perfect straight line in a semi log coordinate system indicating that the functional form is probably $convexity = c_1 \log(c_2 n)$. Note that it is only for $n = 2$ that the Hill factor of the benefit function is equal to one. For $n > 2$ , the Hill-factor is greater than one and the benefit function thus convex.

## 3.4 Take home messages

- The Hill-factor $h$ of the benefit function of a bacterial common good influences the nature of the optimal production strategy.
- For $h \geq 1$ there exists a critical population number $C_C$ *below* which common good production will not be advantageous, and a critical diffusion constant $D_C$ *above* which common good production will not be advantageous.
- When the benefit function of a common good is convex ($h > 1$), having a production strategy which differs from the optimal one comes at a greater cost than when it is concave ($h \leq 1$). This suggests that QS regulation of a common good might be more crucial when the benefit function is convex than when it is concave.
- An excreted enzyme which acts in the environment by degrading polymers into smaller "edible" pieces will have a convex benefit function if the polymers provided by the environment are at least twice the edible size.

# Chapter 4

# Spatial model of quorum sensing cooperators

## 4.1 Introduction

In the previous chapter, we found that microbes producing common goods with a convex benefit function can potentially gain a lot from producing the good, but that doing so at the wrong time and at the wrong rate could be quite detrimental (see section 3.2.4). The optimal times and rates of production depend on the population number and the diffusive properties of the common good, and the medium that the bacteria inhabit. All of these are factors which could change rapidly in the wild, even over time scales on the order of a bacterial generation. This implies that relying on mutation and adaptation to slowly change a population's cooperative strategy as the environment changes is probably not very efficient. Ideally, each cell would use continuous information about the social and diffusive properties of its environment in order to take an informed decision about whether or not to commit to common good production. This is presumably exactly the type of information which could be gained from quorum sensing (QS) systems, and indeed many bacterial common goods are under QS regulation, as discussed in section 3.1.3.

**A 2D model of quorum sensing cooperators.** In this chapter, we want to investigate whether a quorum sensing mechanism, for different benefit function shapes, is in fact a prudent way to regulate the expression of a common good in a more complex setting, and consequently verify whether the results we obtained are valid beyond the 1D model of the previous chapter. To do this we developed a simple individual-based stochastic 2D model of quorum sensing cells capable of excreting a common good. This spatial model has the additional advantage that it allows us to investigate how the presence of a non-producer, a cheat, influences the optimal behavior.

**Different types of cooperators.** In addition, the model allows us to compare different types of cooperators, for example, "constitutive cooperators" (which produce common goods regardless of what the external situation is like) vs. "conditional cooperators" (which produce common goods only when they receive a large QS signal from other cooperators). Two interesting parameters to study here, besides the benefit function hill factor, are the common good production rate, $\sigma_E$, and QS signal threshold that triggers common good production, $t_E$. Moving around the $\sigma_E$ and $t_E$ parameter space we get more or less cooperative types, and more or less conditional or communicative types. For example, $t_E = 0$ describes a bacterium that produces the common good as soon as it senses any non-zero amount of QS signal, i.e. it will effectively be a "constitutive cooperator". In contrast, a bacterium with a higher threshold would be a "conditional cooperator", that is, it only cooperates when it receives a sufficiently high QS signal from other cooperators.

### 4.1.1 A map of this chapter

In section 4.2 we introduce the model, briefly describe the simulations done and define measures for the fitness of the cooperators in the various simulation types.
In section 4.3.1, 4.3.2, 4.3.3 and 4.3.4 we examine exactly how the QS mechanism in the model allows common good production to be conditioned by the number of cooperators and discuss some of the problems which may be associated with obtaining information from a QS system.
In section 4.3.5 we describe the dynamics we observe when cooperators and cheats compete on a growing front for different parameter choices. In section 4.3.6 we assess the optimal $(t_E, \sigma_E)$-strategy for situations with convex and concave benefit functions, with and without cheats. The optima found show that QS regulation is advantageous when the benefit function is convex but not necessarily that important when it is concave and thus agrees nicely with the results obtained in chapter 3. In section 4.3.7 we discuss how the fact that QS regulation can ensure cooperation turn off, when cheats are threatening to take over, may be beneficial in different contexts.
In sections 4.4.1, 4.4.2, 4.4.3 and 4.4.4 we propose ideas for future developments of this model and in section 4.4.5 we outline experiments which we plan to conduct in order to test some of the hypotheses generated by the models presented in chapters 3 and 4.

## 4.2 Methods

### 4.2.1 Model

In our model, bacteria inhabit a 2D square lattice (most simulations were done with a grid size of $200 \times 200$). Each site in the grid can be either empty or harboring a micro-colony of $10^4$ cells. We assume the area of such a colony is roughly $100\mu m^2$, making the lattice step size $\Delta x = 10^{-4} m^2$. Time is incremented in discrete steps of constant size ($\Delta t = 1\, min$), and in each time step these micro-colonies have a chance to expand into one of the four nearest neighbors sites (the von Neumann neighborhood), with a growth rate of $g$ (meaning that the probability that a micro-colony will expand into an empty site in one time step is: $\frac{\#\text{empty neighbor sites}}{4} \exp(-g\Delta t)$.) Even though the numbers used in the simulation (diffusion constants, growth rates etc.) are based on the assumption that each site holds $10^4$ identical cells and not one - it is simpler to explain as if it were a model where there is just one cell per site, so from here on we will refer to the micro colonies of $10^4$ cells in each filled site in the grid as simply the "cells" of the model[1].

**Inducer and common good production.** Each cell/microcolony in the system has certain traits: it can produce a common good (henceforth referred to as the "enzyme", $E$) as well as a signal molecule used by the QS system (henceforth referred to interchangeably as the "signal" or "inducer", $I$). Both can diffuse to other micro-colonies, with diffusion constants $D_E = 0.01\frac{\Delta x^2}{\Delta t}$ and $D_I = 0.1\frac{\Delta x^2}{\Delta t}$ (i.e., inducer diffuses faster than enzyme), respectively, and both decay at a rate $\gamma_I = \gamma_E = 0.001\frac{1}{\Delta t}$. There exists a threshold $t_E$ such that when the inducer level is below $t_E$, the common good is not produced, and when the inducer level is above it, the common good is produced at the fixed rate $\sigma_E$ (see fig. 4.1). We also implement auto-induction of the QS signal molecule a feature which has been observed in all QS systems that have been studied [107]. Auto-induction works as follows in our model: when inducer level is below a threshold value $t_I$, the inducer is produced at a low basal rate $\sigma_{I,basal}$; when inducer level is above $t_I$, the production rate is $\min[\sigma_{I,basal} + \alpha(I - t_I), \sigma_{I,max}]$, i.e. it grows linearly with $I$ until it hits a maximum value of $\sigma_{I,max}$ (see fig. 4.1; see section 4.3.2 for an explanation of this choice). We add the additional rule that production rate of both inducer and enzyme are set to zero for any cell that has no empty neighbouring sites, based on the assumption that cells which are

[1] The reason for choosing the parameters such that each site holds 10,000 cells was that we wished to have have a total system size which would be visible on a macroscopic scale (here total system size is $1cm \times 1cm$ for a grid size of $100 \times 100$), so that it would later be easier to design agar plate experiments to test the predictions of the model. However, doing simulations of a $10000 \times 10000$ cell grid was not feasible timewise. Thus, we constructed this coarse-grained model, where each microcolony of 10,000 cells can be considered a little well-mixed unit of the system.

fully surrounded have zero nutrients and are thus deep into stationary phase where they do not produce enzyme or inducer (Brook Peterson, U. Washington, personal communication).
All the above thresholds and other parameters are the same for all cells in the system.

**Growth rate.** In the absence of common goods, the cells replicate at a growth rate of $g_{basal} = 0.0077\Delta t^{-1}$. With the chosen time-step size, this gives a generation time of $\sim 1h$ assuming exponential growth. When the common good concentration $E$ at a given lattice site is larger than zero, the growth rate $g$ of a cell at that site is given by

$$g = g_{basal} - p_{cost}P_E(I) - p_{I,cost}P_I(I) + B(E) \tag{4.1}$$

where $I$ is the inducer concentration at that site, $P_E(I)$ is the inducer-dependent production rate of the enzyme (a step function that jumps from 0 to $\sigma_E$ at $I = t_I$; see fig. 4.1), $p_{cost}P_E(I)$ is the cost of common good production, $P_I(I)$ is the auto-induced inducer production rate (the piecewise linear function described earlier and in fig. 4.1), $p_{I,cost}P_I$ is the cost of inducer production, and $B(E)$ is the benefit function. We will assume that the cost of signal molecule production is negligible compared to the cost of common good production and thus set $p_{I,cost} = 0$, (Brook Peterson, personal communication). Thus:

$$\begin{aligned} g &= g_{basal} - p_{cost}P_E(I) + B(E) && (4.2)\\ &= g_{basal} - p_{cost}P_E(I) + B_{max}\frac{[E]^h}{[E]^h + K^h} && (4.3) \end{aligned}$$

(whenever $g$ becomes negative when calculated from eq. 4.3, it is set to zero.) Only cells on the edge of a growing colony have empty neighbouring sites to grow into, so effectively all cells which are fully surrounded have a growth rate of zero. Space in this model is thus equivalent to a resource, and the carrying capacity of one site is one cell.

### 4.2.2 Simulations

**Growing alone.** Initial conditions for simulation of cooperators growing alone was one single cell placed in the middle of a grid of size $200 \times 200$ and with $I = 0$ and $E = 0$ everywhere. Simulations where terminated at time $T_{end} = 13000\Delta t$ (this was chosen to provide enough time for cooperators in most simulations to turn on, i.e. start producing the common good, and subsequently grow for a while in the presence of the common good). One simulation was done for each combination of $t_E \in [10^0, 10^{2.5}]$ and $\sigma_E \in [10^{-2}, 10^2]$ with $h = 0.5$, and each combination of $t_E \in [10^0, 10^{2.5}]$ and $\sigma_E \in [10^{-3}, 10^1]$ with $h = 2.0$. For all simulations, $t_I$ is chosen to be $\max[0,\ t_E - 50\sigma_{I,basal}\Delta t]$. We made this somewhat arbitrary choice in order to reduce the number of independent parameters.

**Growing with a cheat.** In these simulations the "cheats" are identical to cooperators in all aspects except they do not ever produce the common good or the QS signal molecule. The initial condition in the simulations with cheats present was a single line of cells stretching across the grid, with a repeating pattern of 5 cheats adjacent to 1 cooperator, and with $I = 0$ and $E = 0$ everywhere. The grid size used was $100 \times 100$. This choice was made in order to test whether cooperation with a given $(\sigma_E, t_E)$ strategy was advantageous even for low starting density and when surrounded by cheats. (We did runs with more random initial conditions but the outcomes of such simulations vary greatly, so a completely ordered initial condition was chosen to lessen the noise on the outcome). Simulations with cheats were run for the same parameters as used in the simulations with only cooperators, but for each set of parameters the results were averaged over 6 independent runs.

### 4.2.3 A measure for the fitness of a cooperator alone and with a cheat present

We wish to make statements about which $(\sigma_E, t_E)$-strategy is optimal in our simulations. In order to do this we need to define a fitness of the cooperators so that we can compare simulations with differing values of $(\sigma_E, t_E)$, where all other parameters and conditions are constant. For the simulations with cooperators growing alone, a good measure for fitness is simply the number of cooperators present at $T_{end}$, because this number is effectively like integrating over the growth rate from $t = 0$ to $T_{end}$.

**Fitness when growing together with a cheat.** For the simulations where cooperators are growing in the presence of cheats, this is not sufficient because another important factor is the number of cooperators present on the growing front at $T_{end}$ since only these cells can give rise to future progeny. We therefore decided to measure fitness of a cooperator in the presence of a cheat by a weighted sum of the total number of cooperators and the number present on the growing front at $T_{end}$ (giving the total number of cooperators double weighage). This way, both the integrated growth rate during $t = 0$ to $t = T_{end}$, as well as the future growth prospects are considered.

**Fitness depends on length of simulations.** For both growth alone and with a cheat we chose to evaluate fitness at $T_{end}$. This specific choice of simulation length was made since we wanted all cooperator types with $t_I < t_{max}$ to turn on in the course of one simulation, and grow for a decent while after turn on. In fig. 4.7 with $h = 0.5$ and growth alone we see fitness go down slightly with increasing $t_E$. This is due to the fact that a benefit is to be had by turning on even at one cell, so optimal turn on threshold is $t_E = 0$, however the longer the simulation the less the initial growth period, with the low rate of $g = g_{basal}$ before turn on,

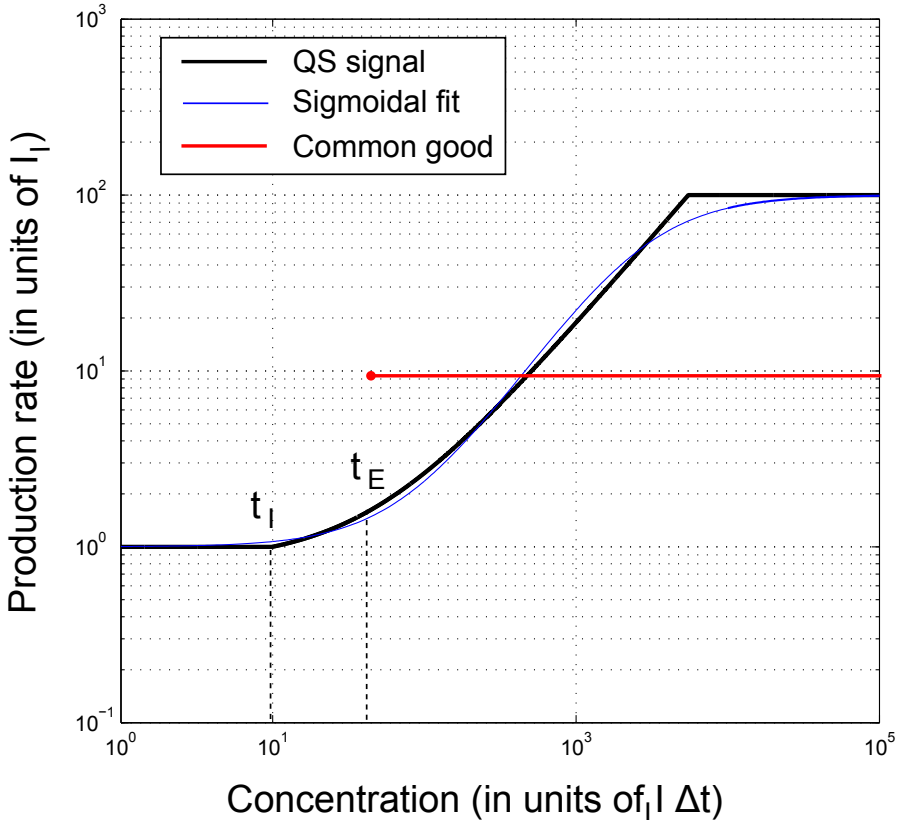


Figure 4.1: **QS signal and common good production curves.** Production rate of QS signal (black) and common good (red) by a cell as a function of the QS signal concentration at that grid site. Blue curve is the best sigmoidal fit to the black curve, and has a Hill factor of $h = 1.288$. This is consistent with real inducer expression data from experiments done with the two different QS systems of *P. aeruginosa*, which when fitted to sigmoidal functions, gave Hill-factors of $\approx 1.2$ and $\approx 1.3$, respectively (see fig. 5.23 Appendix 4). $t_I$ is the threshold at which the QS signal starts positive feedback on itself (auto-induction), and $t_E$ is the threshold where common good production is initiated at the constant rate $\sigma_E$. We use different values of $t_E$ and $\sigma_E$ in different simulations, but the difference between $t_E$ and $t_I$ is kept constant, ($t_E - t_I = 50\sigma_{I,basal}\Delta t$). See section 4.2.1 for details of other parameter values.

matters, because much more time is spend in the phase with high growth rate after turn on, making the short time before turn almost negligible for our choice of $T_{end}$. The fitness of a $(\sigma_E, t_E)$ strategy when compared with others thus depends on the choice of $T_{end}$; if we had chosen a much smaller time span we would see a larger difference in fitness between $t_E$ high and low, but also have that types with high thresholds would not have turned on at all during our simulations.

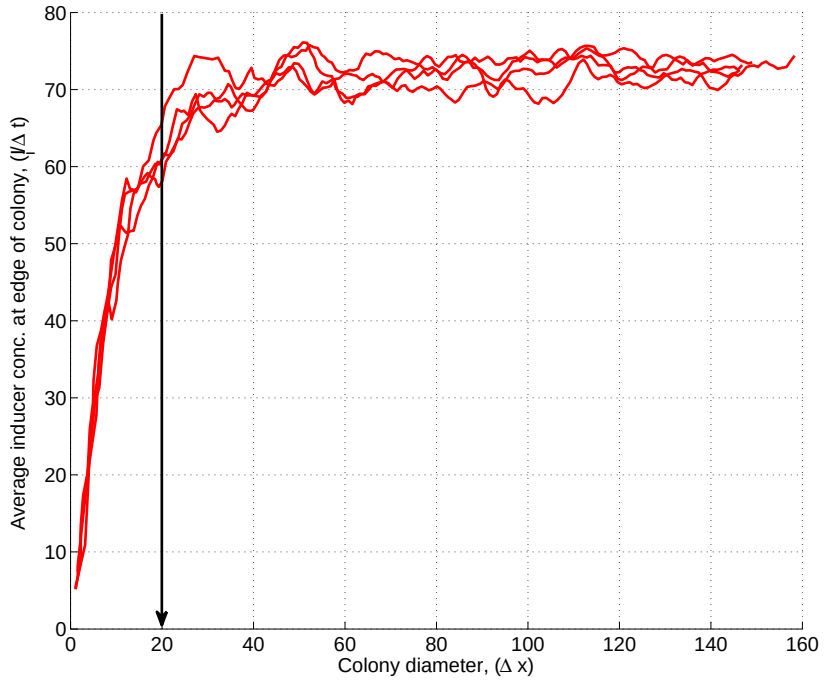


Figure 4.2: **Average QS signal felt on growing edge saturates with increasing colony size.** Average signal concentration at the edge of a growing colony as a function of colony diameter, when cells on the edge produce signal at the basal rate $\sigma_{I,basal}$ (i.e., there is no auto-induction). The four different red lines are from four different runs. Inducer concentration saturates soon after the diameter has reached the length $l^I_\infty = 2\sqrt{\frac{D_I}{\gamma_I}} = 2\sqrt{\frac{0.1\frac{\Delta x^2}{\Delta t}}{0.001\Delta t^{-1}}} = 20\Delta x$, marked with a black arrow. See section 4.2.1 for parameter values used.

## 4.3 Results and Discussion

### 4.3.1 Quorum sensing can ensure turn on at a specific colony size

As a circular colony grows while excreting inducer molecules at a constant rate, the concentration of inducer that a cell on the growing edge feels increases with time. When the size of the colony is such that the length of the diameter is much longer than the average distance an inducer molecule before decaying, $l^I_\infty = 2\sqrt{\frac{D_I}{\gamma_I}}$, then for an edge cell the growing front is effectively like an infinitely long line and the inducer concentration stops growing with the colony size (see fig. 4.2). For the parameters we use $l^I_\infty = 20\Delta x$. This saturating level of inducer of course depends on the production rate of the inducer. We denote by $t_{max}$ the saturating level of inducer achieved when the inducer production rate is $\sigma_{I,basal}$. Clearly, if the threshold

$t_I$ for auto-inducer feedback (the point where inducer production rate starts to increase linearly with inducer concentration) is above this level, $t_{max}$, then the system will never auto-induce and never start enzyme production, because $t_E > t_I$. All cooperator types with $\sigma_E = 0$ and/or induction threshold $t_I > t_{max}$ will thus have the same fitness as cheats.

**Enzyme production turn on.** If the threshold value $t_I$ is lower than $t_{max}$, then at some colony size the edge cells will auto-induce (the QS signal positive feedback will start) and the inducer concentration will start rising beyond $t_I$. For the parameter values we examine, the inducer concentration typically crosses $t_E$ very soon after the auto-induction starts. Thus, any threshold $t_E$ roughly corresponds to a specific colony size (or more accurately an approximate colony edge length – assuming that the edge is relatively smooth) at which common good production will commence. In practice, the exact population number at which turn on, i.e. the start of common good production, happens can vary since the roughness of the growing front does matter for the concentration which the edge cells feel, but usually once the auto-induction starts in one spot on the edge it quickly spreads and insures that all cells in the vicinity turn on at roughly the same time (this is to be expected when positive feedback is combined with diffusion of the inducer).

### 4.3.2 Hysteresis due to the positive feedback in quorum sensing

When the size of a colony is reduced the cells will turn off, i.e. stop producing the common good, at some specific size (unless $t_E$ is very low) but this size/length will be smaller than the size/length for turn on, for the parameters we examine. This hysteretic effect is also due to the positive feedback of the QS signal on itself; the steeper the inducer production curve (see fig. 4.1), the more the hysteresis ([45] also speak about QS hysteretic response to population size). A very shallow slope will, on the other hand, make the cells turn on in a much less collective manner, which in some situations could be perceived as disadvantageous because it would allow mutants with a slightly higher turn on threshold to transiently cheat on earlier starters. Assuming that neither strong hysteresis with respect to changes in colony size nor very non-collective turn on behavior is desirable, we have a trade off situation that makes an intermediate slope of the production curve optimal. The Hill factor of real production curves are usually around one [67; 129; 151]. We chose to follow the experiments by Brook Peterson, U. Washington, shown in Appendix 4, which yielded a sigmoidal production curve with Hill factors of 1.2 and 1.3. For simplicity, we approximated such a sigmoid with a piecewise linear function (see fig. 4.1). The slope of the linear increase of inducer production, above the threshold $t_I$, of this function falls nicely between the extremes of strong hysteresis and a non-collective turn on behavior.

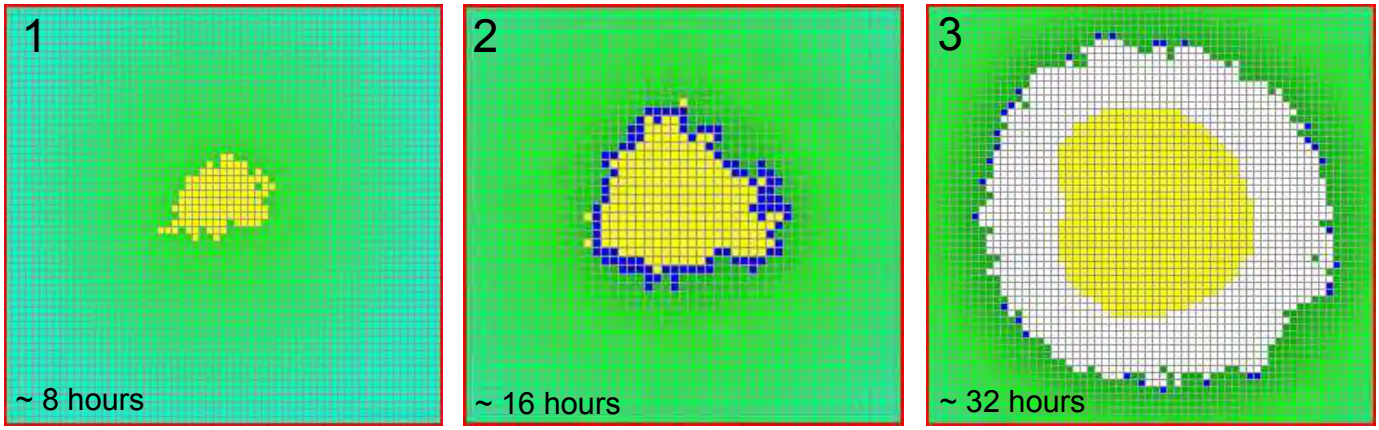


Figure 4.3: **Screen shots of common good producer growing alone.** Yellow indicates sites with cooperating bacteria. Red indicate sites with cheats. Shades of green signify concentration of inducer in empty grid sites with darker shades corresponding to higher concentration. Blue shows bacteria that have turned on, i.e. are producing the common good. White shows grid sites that contain bacteria and where the concentration of the common good is above $K$ (the concentration where the benefit function is half of its maximum). **1:** Colony is growing with the basal rate, $g_{basal}$; QS signal is being produced at the basal rate, $\sigma_{I,basal}$, and is slowly building up. **2:** Shortly after auto-induction has commenced; most edge cells have started common good production, but the level of the common good in the environment is still relatively low. **3:** Colony is growing at highest possible rate; all edge cells are committed to producing the common good and its concentration at the edge has reached a high level.

### 4.3.3 Signal molecule properties and sensitivity range

As explained earlier, the inducer concentration vs. colony size will be a saturating function (both with or without auto-induction). Above a certain colony size, therefore, the inducer concentration will change very little, i.e., the cells will no longer be sensitive to changes in colony size. The range over which the QS mechanism is sensitive to changes in colony size is thus dependent on characteristic length of inducer diffusion $l_\infty^I = 2\sqrt{\frac{D_I}{\gamma_I}}$. Smaller $D_I$, or larger $\gamma_I$, results in a smaller sensitive range. It has been suggested that one reason for inducer excretion is "testing the waters": assessing the concentration of an excreted product using cheap expendable molecules, before deciding to produce the, presumably more expensive, common good [101]. If the sole purpose of the inducer was to serve as a dummy for a specific common good molecule, then it seems the most appropriate choice would be an inducer with roughly the same diffusion constant and degradation rate as that molecule (although it might be argued that it would be hard to produce something as large as the average extracellular enzyme cheaply). A quorum sensing mechanism is however usually regulating hundreds of different genes, all with different products, many of which have different sizes and different turn-on thresholds (which is the case for e.g. *Pseudomonas aeruginosa* see [111]). Assuming that these genes need to be turned on over a wide range of different population densities, it would make most sense to have an inducer with high diffusion constant and low degradation rate in order to have a mechanism which was sensitive over a wide range of colony sizes. This, it turns out, is exactly what we see for most QS systems: small inducer molecules with long lifetimes.

### 4.3.4 Difficulties getting information with a system that has positive feedback

It seems that if a bacterium is using the inducer molecule to assess the cell density/colony size, the correspondence between the inducer concentration and the colony size should be relatively independent of other factors, like for example the growth rate of the bacteria. However, when we run simulations where bacteria grow with a constant rate, and there is no common good production, but the inducer is produced with auto-induction possible, then we find that the inducer concentration vs. colony size function depends a lot on the value of the growth rate of the cells (see fig. 4.4). These differences for different growth rates are due to the fact that the inducer concentration will not reach (quasi-)equilibrium at intermediate colony sizes if the timescales of diffusion and decay of the inducer are not much faster than the growth rate (at a very low growth rate the system would reach equilibrium after each new cell was added). Specifically, the differences for different growth rates are greatest in the parts of the curve where the system feels positive feedback. In this feedback regime, it is therefore difficult for a cell to extract reliable information about the colony size just from the inducer

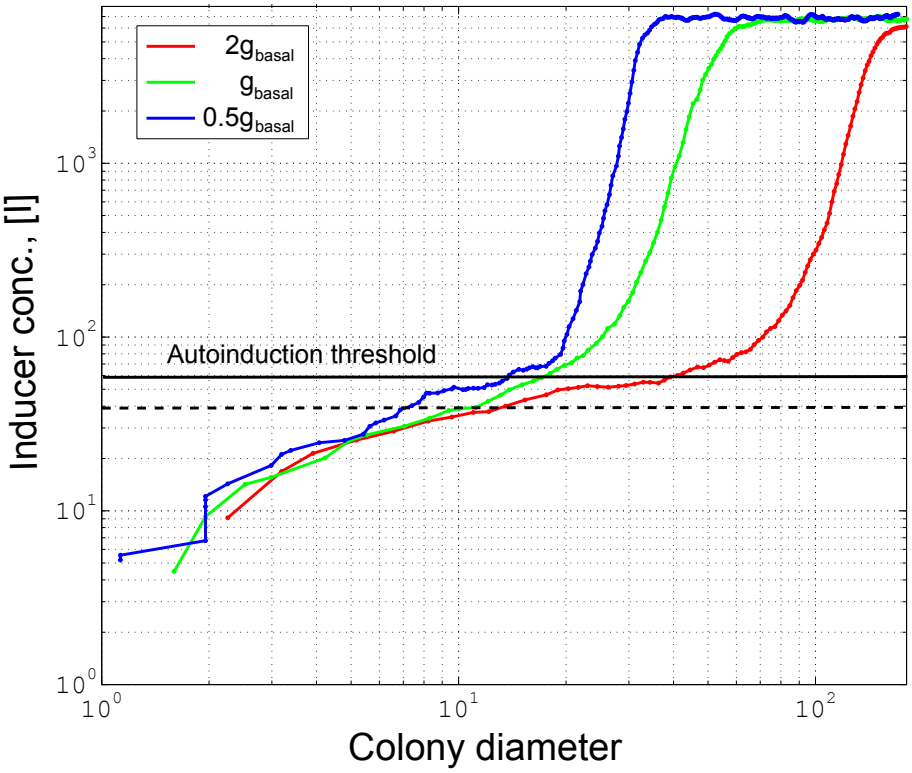


Figure 4.4: **Inducer concentration as a function of colony diameter varies with growth rate.** Average inducer concentration felt by a cell on the growing edge of a colony for three different constant growth rates $g' \in [0.5g_{basal}, g_{basal}, 2.0g_{basal}]$. Autoinduction threshold $t_I$ is marked by a full black line. We see that before autoinduction starts a certain colony diameter corresponds roughly to a certain inducer conc. even for different growth rates while after the autoinduction start a certain colony diameter corresponds to quite different inducer concentrations for the three different growth rates.

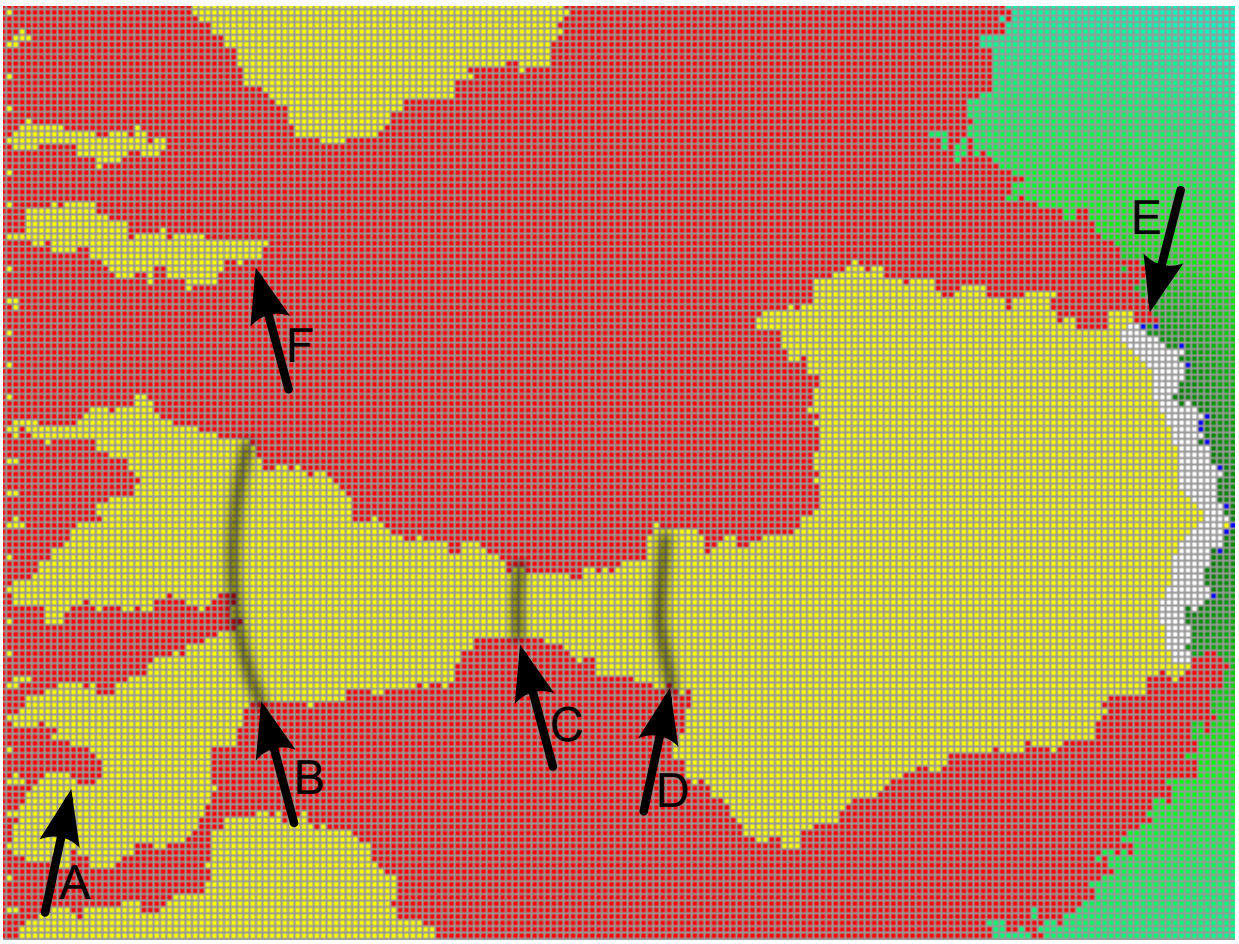


Figure 4.5: Figure caption on following page.

Figure 4.5: **Examples of cooperator and cheat dynamics on a growing front.** Yellow indicates sites with bacteria. Red indicate sites with cheats. Shades of green signify concentration of inducer in empty grid sites with darker shades corresponding to higher concentration. Blue shows bacteria that have turned on, i.e. are producing the common good. White shows grid sites that contain bacteria and where the concentration of the common good above $K$ (the concentration where the benefit function is half of its maximum). Parameters: ($\sigma_E = 3.0$, $t_E = 80$, $h = 0.5$). This simulation started with a vertical line of cooperators and cheats (as described in section 4.2.1) on the left edge of the grid, and all other sites empty. As time progresses the growing cell fronts move mainly from left to right, and the snapshot shown is at a late time when the fronts have almost reached the right edge of the grid. **A:** Example of two cooperator segments joining and cutting of a segment of cheats (this happened before common good production had been initiated and was thus a random event; see section 4.3.5). **B:** Two cooperator segments join cutting off a cheat segment. The top segment had already reached critical segment length and started common good production - the lower segment joins in and starts production (see section 4.3.5). **C:** Cheats are feeling the benefit from the common good and are growing slightly faster than the cooperators, thus reducing the cooperator segment length. Around the marked line the cooperators stop common good production because they have reached a sufficiently low segment length that the QS signal level falls below the threshold, $t_E$ (see section 4.3.5). **D:** After C: competition between the cooperators and the surrounding cheats is completely neutral. Random movement of the points where cooperator and cheat segments meet bring the cooperators above the critical length where common good production starts again. When common good production starts it is at first only in the middle of the cooperator segment and thus the cheats will not initially feel any benefit and the cooperator segment starts to "bulge out" and grow sideways with respect to the general direction of growth thus cutting off cheats and causing the cooperator segment to increase in size (see section 4.3.5). **E:** After a while the cheats start to feel the benefit from the common good and they once, more, start to reduce the cooperator segment length (see section 4.3.5). **F:** Here a cooperator segment was cut off before common good production was initiated due to the random movement of the points where cooperator and cheat segments meet.

concentration. It is thus a bit of a puzzle why real QS systems, whose purpose is supposedly to gauge information about colony size/density, contain such positive feedback loops. This suggests that QS systems provide reliable information about colony sizes only during the initial buildup of inducer concentration due to the near constant basal production rate of inducer (variations in growth rate at this stage do not affect the inducer concentration vs. colony size function as drastically), while the feedback loop that sets in at higher concentrations is just there to finalize the decision and force all other cells to synchronize the timing of their turning on, avoiding situations where cells with slightly higher thresholds can transiently cheat on cells with slightly lower thresholds.

### 4.3.5 Cooperators and cheats competing on a growing front

When cooperators and cheats (which produce neither the QS signal nor the common good) are growing next to each other on a 2D plane the actual competition takes place at the domain boundaries on a one dimensional expanding front (see fig. 4.5). Here, stochastic events can have dramatic effects because a sequence of random events that result in one cell type outgrowing and blocking just a few cells of the other type at an early stage will keep the latter from ever producing progeny. This process repeated many times produces segregated domains each containing only one type of cells (this kind of front growth dynamics has been studied in depth for cell types that have equal fitness in [42]). When the segments of a growth front containing cooperators reaches sufficient length for auto induction to set in and common good production to start, the cooperators can gain a growth advantage and their segments of the front will advance faster and start to "pucker out". However, after a little while, the common good will start to spill over and aid the growth of defectors in the neighboring sector. Defectors on the very edge of a cooperator segment can potentially get full benefit from the common good while paying no cost, which gives them an even higher growth rate than the cooperators. The victor of this race is decided by subtle factors like exactly how much common good spills over the edge to the defector (decided by the diffusion constant of the common good and the production rate $\sigma_E$) and the cost of common good production compared to the benefit.

**A high quorum sensing threshold can ensure increased privatization of the common good.** The turn-on threshold matters for how accessible the common good is to the cheat; for a very high threshold often only cells in the middle of the cooperator segment turn on, meaning that where the cooperator segment meets the cheat segment, not much common good will be present. This shows that a high threshold can ensure a higher degree of privatization of the common good by facilitating production only at central regions of the cooperator front that are away from cheats (see fig. 4.6).

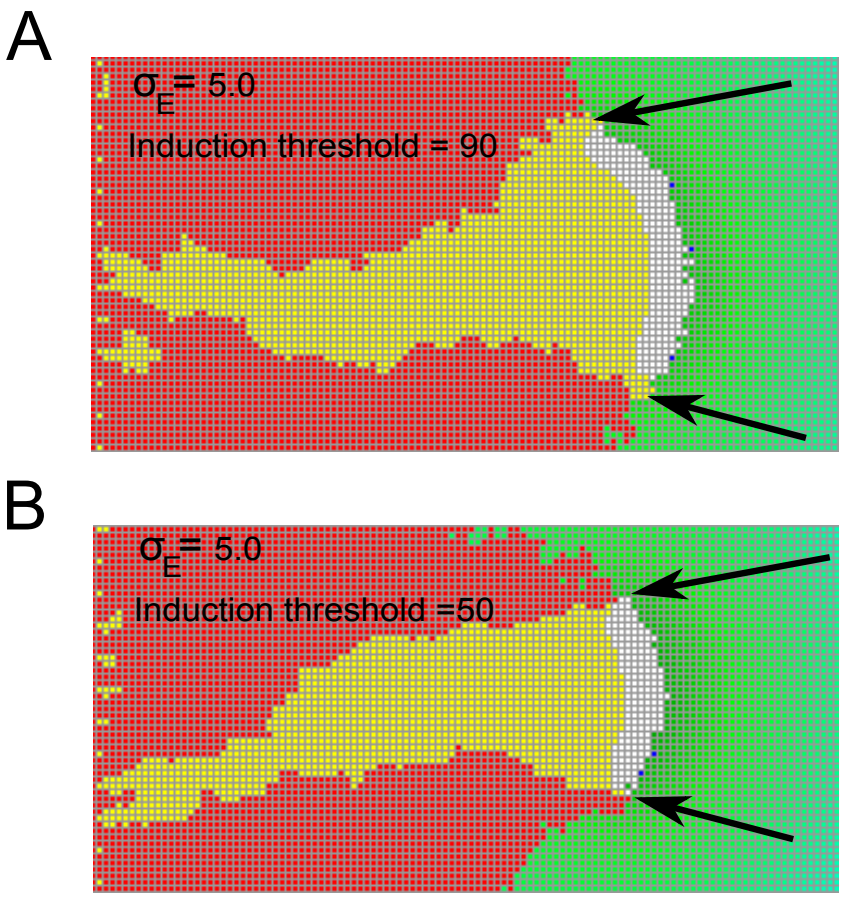


Figure 4.6: **A high QS threshold can ensure privatization of the common good by facilitating production only at central cells on a cooperator front segment.** Yellow indicates sites with bacteria. Red indicate sites with cheats. Shades of green signify concentration of inducer in empty grid sites with darker shades corresponding to higher concentration. Blue shows bacteria that have turned on, i.e. are producing the common good. White shows grid sites that contain bacteria and where the concentration of the common good above $K$ (the concentration where the benefit function is half of its maximum). **A:** Parameters used: $h = 2.0$, $t_E = 90$, $\sigma_E = 5.0$. The high threshold ensures that common good is not produced where cooperator segments meets cheat segments. **B:** Parameters used: $h = 2.0$, $t_E = 50$, $\sigma_E = 5.0$. For this lower threshold, common good production extends all the way to the end of the cooperator segment and as a result nearby cheats get a share of the benefit. (See section 4.3.5).

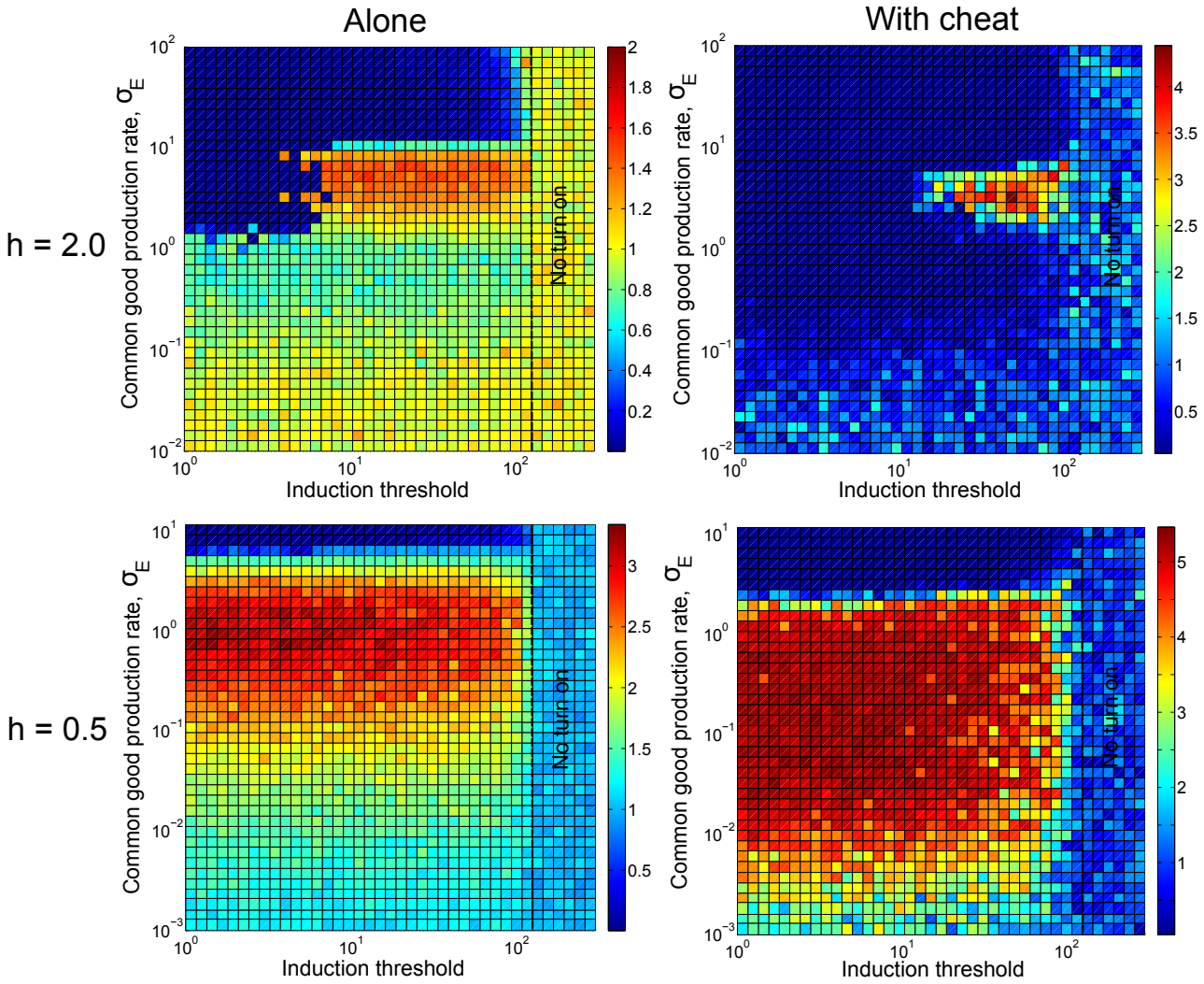


Figure 4.7: **Performance of $(\sigma_E, t_E)$-strategies for convex and concave benefit functions, with and without cheats present:** Fitness as a function of the production rate of common good $\sigma_E$ and the induction threshold $t_E$, for benefit functions with hill factor $h = 0.5$ and $h = 2.0$, and for growth alone and in the presence of a cheat. In each plot fitness has been normalized with respect to the average performance of a cooperator from simulations that are completely identical to these simulations, except that the cooperator growth rate is fixed to $g_{basal}$, i.e. a "non-producer". Note that the y-axis of the $h = 0.5$ plots show the range $\sigma_E \in [10^{-3}, 10^{1}]$ while the y-axis of the $h = 2.0$ plots shows the range $\sigma_E \in [10^{-2}, 10^{2}]$. For both Hill factor $h = 0.5$ and $h = 2.0$ the potential for performing better than neutral (normalized fitness $> 1$) is greater in the presence of a cheat. The optimal production rate, $\sigma_E^{opt}$, is much greater for $h = 2.0$ than for $h = 0.5$ both with and without the cheat. Both for $h = 2.0$ and $h = 0.5$ the optimal production rate, $\sigma_E^{opt}$, appears to be a little lower when a cheat is present than when alone. For $h = 2.0$, having too low an induction threshold can come at a great cost, while for $h = 0.5$ the fitness appears to be almost independent of the threshold. For $h = 0.5$ producing common good at very low rates still gives a better performance than neutral, while for $h = 2.0$ there is a range of low production rates which will make performance worse than neutral. These observations are all consistent with the analytical results found in section 3.2.3.

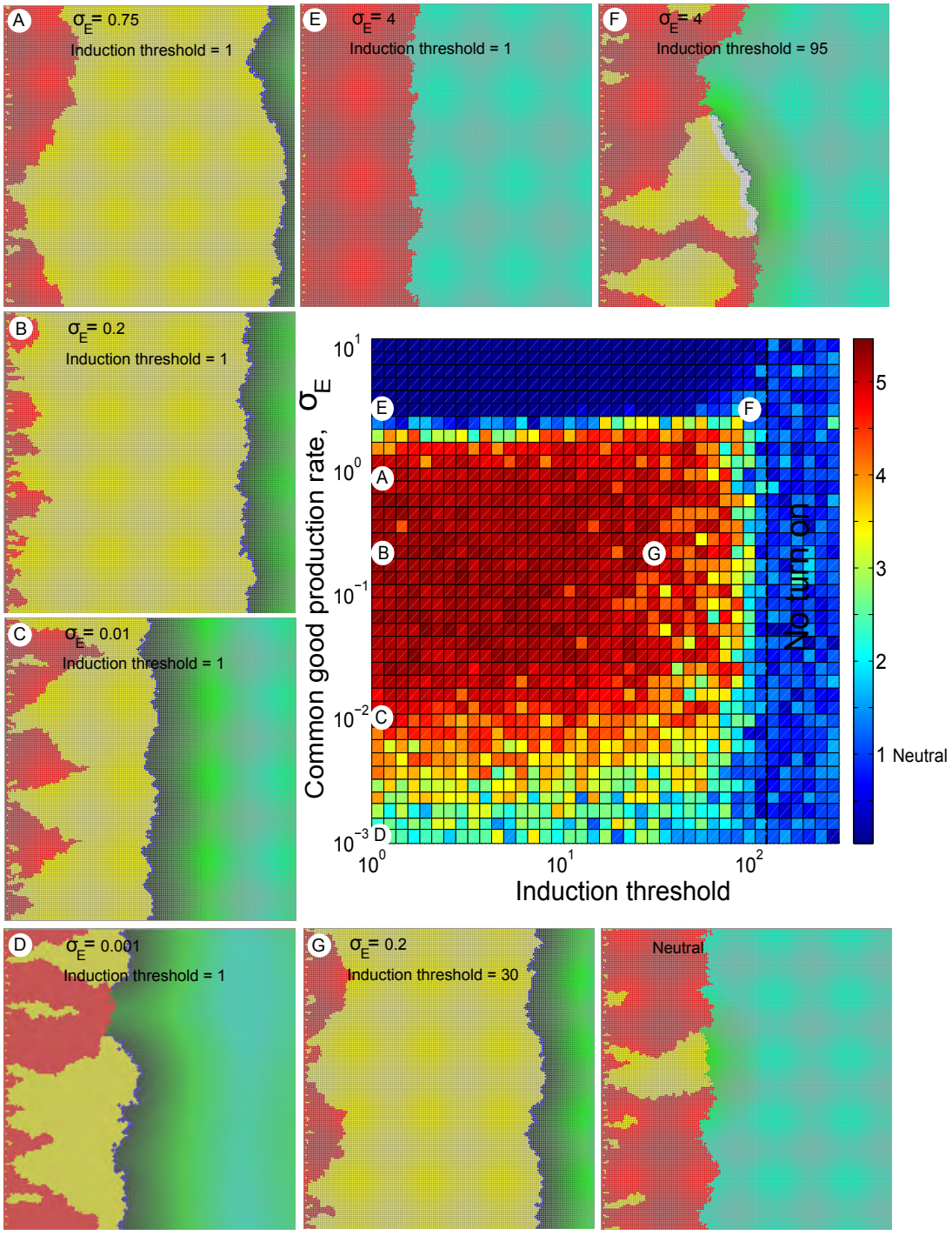


Figure 4.8: **Dealing with a cheat when the benefit function is concave ($h < 1$) does *not* require QS regulation of common good.** Yellow indicates sites with bacteria. Red indicate sites with cheats. Shades of green signify concentration of inducer in empty grid sites with darker shades corresponding to higher concentration. Blue shows bacteria that have turned on, i.e. are producing the common good. White shows grid sites that contain bacteria and where the concentration of the common good above $K$ (the concentration where the benefit function is half of its maximum). Color map shows the fitness at $t = T_{end}$, as a function of $t_E$ and $\sigma_E$. Initial conditions were a single line of cells on the left edge of the grid, arranged in a repeating pattern of 5 cheats, 1 cooperator, as described in section 4.2.1. **A - G**: Screen shots from simulations with different $(\sigma_E, t_E)$ parameters (these are typical outcomes but note that individual simulation can vary a great deal), taken at $t = 15000\Delta t$. Because very small thresholds $t_E$ give the same fitness benefit to cooperators as large thresholds, QS regulation is not really required in this case to deal with cheats.

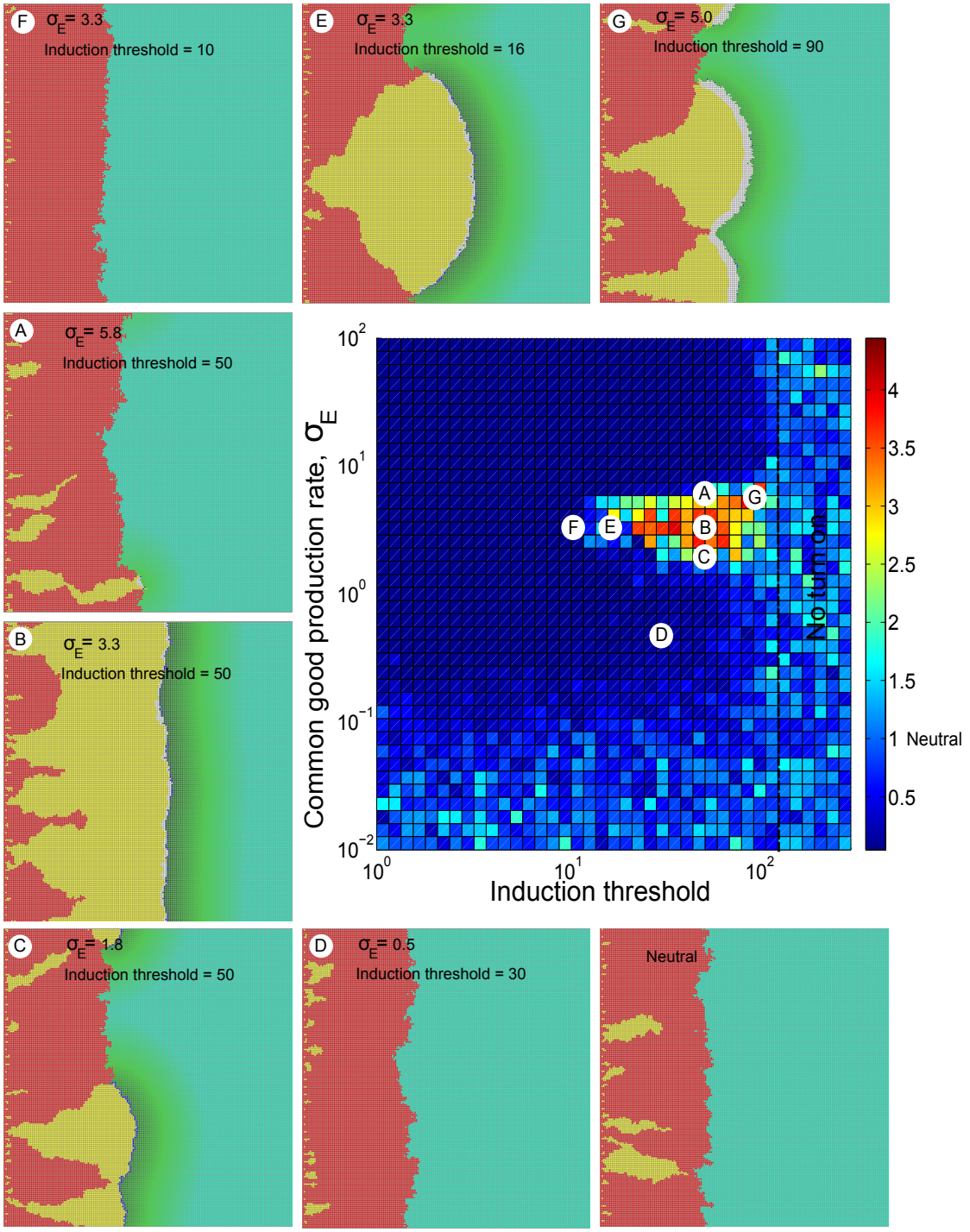


Figure 4.9: **Dealing with a cheat when the benefit function is convex ($h > 1$) does require QS regulation of common good:** Yellow indicates sites with bacteria. Red indicate sites with cheats. Shades of green signify concentration of inducer in empty grid sites with darker shades corresponding to higher concentration. Blue shows bacteria that have turned on, i.e. are producing the common good. White shows grid sites that contain bacteria and where the concentration of the common good above $K$ (the concentration where the benefit function is half of its maximum). Color map shows the fitness at $t = T_{end}$, as a function of $t_E$ and $\sigma_E$. Initial conditions were a single line of cells on the left edge of the grid, arranged in a repeating pattern of 5 cheats, 1 cooperator, as described in section 4.2.1. **A - G**: Screen shots from simulations with different ($\sigma_E, t_E$) parameters (these are typical outcomes but note that individual simulation can vary a great deal), taken at $t = 15000\Delta t$. In this case, a range of high $t_E$ values (along with a specific range of $\sigma_E$ values) does provide a much bigger fitness benefit to cooperators than having a low threshold $t_E$. Thus, compared to the case of the concave benefit function in the previous figure, here QS regulation can play an important role in competition with cheats.

### 4.3.6 The optimal strategy for common good production depends crucially on the shape of the benefit function

Perhaps the most dramatic feature that hits the eye when looking at figure 4.7 is how radically different the various $(\sigma_E, t_E)$ strategies perform when all things are kept equal except the benefit function Hill-factor. Turn-on at low thresholds comes with an advantage when $h = 0.5$ and at a great disadvantage when $h = 2.0$, and the optimal rate of production is much higher for $h = 2.0$ than for $h = 0.5$. We also note that when $h = 0.5$, producing at less than the optimal rate comes with an advantage compared to not producing at all, whereas when $h = 2.0$ it can be worse to produce a little less than at the optimal rate than to not produce the common good at all. These observations are consistent with the analytical results derived in the last chapter from the simple 1D model.
The region in the $\sigma_E - t_E$ space where cooperators have the highest fitness extends all they way down to vanishing low thresholds (actually the fitness is highest for $t_E = 0$; this is true both for simulations with and without cheats). Thus, there seems to be no reason in this situation to have a relatively costly QS mechanism regulating the expression of the common good. Perhaps it is not even fitting to call this type of common good excretion cooperation because it clearly benefits even single cells to produce the common good even when surrounded by cheats. For $h = 2.0$, on the other hand, having a QS system seems to be extremely advantageous, because here it seems the fine tuning of the optimal production rate and the exact timing of turn-on matters profoundly, both with and without cheats present.

### 4.3.7 Coexistence of cooperators and cheats: Quorum sensing as an emergency brake

In real ecosystems, coexistence of cooperators and cheats is often observed [144; 105] and it is debated in the ecology literature [32] what mechanism allows such coexistence to happen. It is even argued in some instances that the presence of a (closely related) cheat could be an advantage to a cooperator [73]. Figure 4.13 shows that, in our model with for $h = 0.5$, there is only a small region of parameter space (approximately at $t_E \in [30, 80]$ and $\sigma_E \in [2, 3]$) where both cheats and cooperators are present at the growing front at time $T_{end}$, and the total number of cooperators plus cheats summed over the entire grid is relatively high.

**Emergency brake.** In this region, the cooperators are producing common good at a rate higher than the optimal rate for growth alone ($\sigma^{opt}_{E,alone} = 0.7 \pm 0.04$), which makes them grow faster than the cheats but not as fast as is possible for them at lower production rates. At the same time, because the cooperators are producing at a relatively high rate, enough common good reaches the cheats by diffusion to significantly boost their growth rate. This causes the

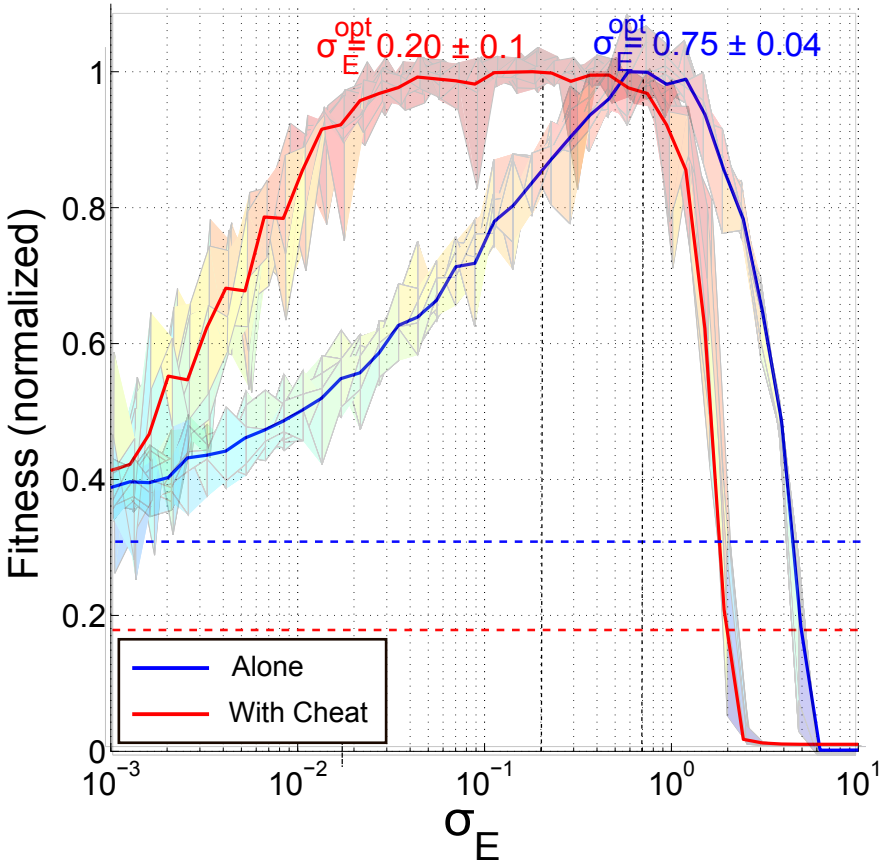


Figure 4.10: **Optimal common good production rate when cheats are present and when growing alone for** $h = 0.5$**.** Full curves show average fitness (normalized with respect to the maximum), as a function of $\sigma_E$, for growth alone (blue) and growth together with a cheat (red), for simulations with benefit function having hill factor $h = 0.5$. The curves are averages of cross sections (faded curves in the background) of the surfaces shown in fig.4.7 between induction threshold, $t_E$, 1 and 10. This interval was chosen because between these values the fitness seems to be more or less independent of the induction threshold for both growth with and without a cheat. Dashed blue and red lines show fitness of a non-producer for reference. We see that the profile of the normalized fitness as a function of the production rate is very different for the two situations. E.g. the optimal production rate when growing among cheats ($\sigma^{opt}_{E,cheats} = 0.20 \pm 0.1$) is more than three times smaller than the optimal production rate when growing alone ($\sigma^{opt}_{E,alone} = 0.75 \pm 0.04$), and the peak of the distribution is much broader with cheats present than without. We also see that the fitness peak is roughly five times higher than the neutral level for the simulations with cheats compared to simulations with cooperators growing alone, for which the peak is only roughly three times larger than the neutral level.

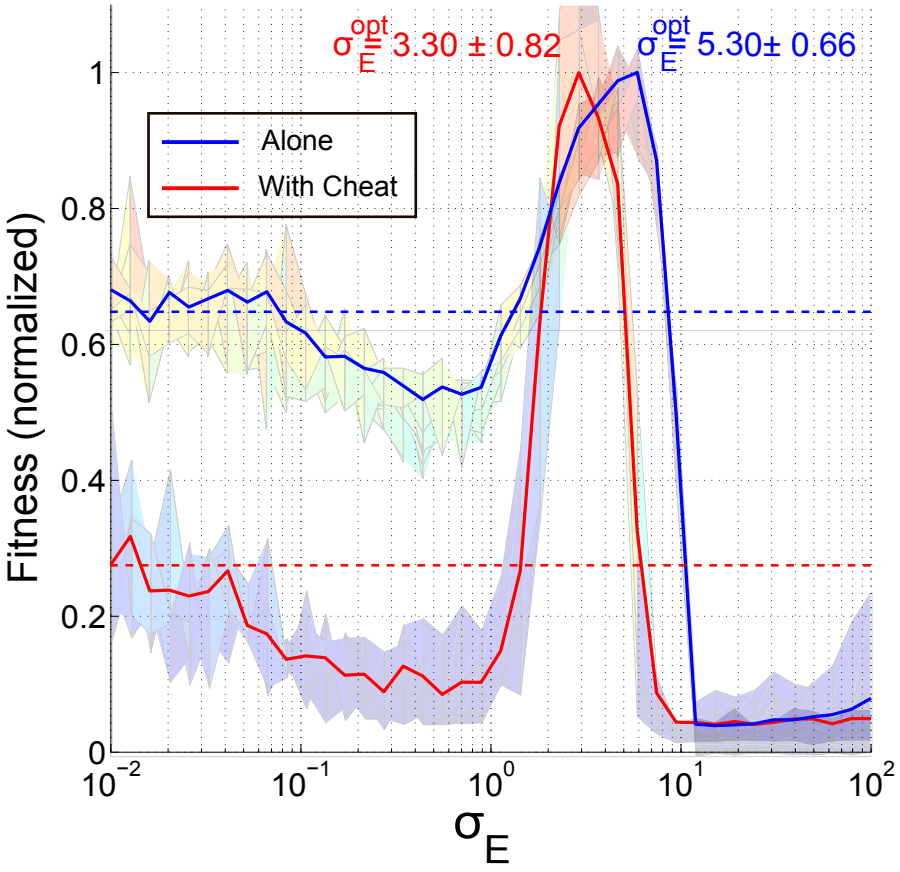


Figure 4.11: **Optimal common good production rate when cheats are present and when growing alone for** $h = 2.0$**.** Full curves show average fitness (normalized with respect to the maximum), as a function of $\sigma_E$, for growth alone (blue) and growth together with a cheat (red) for simulations with benefit function having hill factor $h = 2.0$. The curves are averages of cross sections (faded curves in the background) of the surfaces shown in fig. 4.7 between induction threshold, $t_E$, 10 and 80 for growth alone, and, 30 and 80 for growth with a cheat. These intervals were chosen because between these values the fitness seems to be more or less independent of the induction threshold. Dashed blue and red lines show fitness of a non-producer for reference. In this case, the optimal production rate when growing among cheats ($\sigma^{opt}_{E,cheats} = 3.30 \pm 0.82$) is slightly smaller than the optimal production rate when growing alone ($\sigma^{opt}_{E,alone} = 5.30 \pm 0.66$), and the peak of the distribution is only slightly broader for growth alone than with cheats present. We also see that the fitness peak is roughly three times higher than the neutral level for the simulations with cheats, and only roughly two times larger than the neutral level for simulations with cooperators growing alone.

cheats to grow even faster than the cooperators at the parts of the front where cooperator and cheat segments meet, making them "bulge out" which then cuts off the cooperators and reduces the length of their segment on the front. When that segment length becomes smaller than a critical value, the cooperators will shut off common good production thereby neutralizing the competition with the cheats. For the cooperators to have a good chance of avoiding extinction, this critical segment length needs to be relatively large, i.e. the threshold $t_E$ needs to be relatively high – in our simulations larger than around $30\sigma_{I,basal}\Delta t$. Here, the QS system plays the role of an "emergency brake"[2] which stops common good production when the cooperator population on the growth front is reducing [3]. At sufficiently high production rates ($\sigma_E > 3\sigma_{I,basal}\Delta t$) even this emergency brake is not enough to save the cooperators from extinction because there is so much common good still present and reaching the cheats at the point of turn-off that they grow too fast and usually manage to completely cut off the cooperators.

**Stability of cooperator and cheat coexistence.** While in our model there thus do exist parameter values where cheats and cooperators can coexist, if one is looking over evolutionary timescales our model with $h = 0.5$ does not provide any reason for the system to remain with the set of parameters that allow coexistence. As our model provides no incentive for the cooperator to keep the cheat around, nothing stops a cooperator from evolving to a lower production rate for the common good or eliminating QS regulation of common good production, because with $h = 0.5$ production of common good right from the very start (i.e. $t_E = 0$) is the best strategy for the cooperators (see section 4.3.6 and fig. 4.7). However, when $h = 2.0$, the parameter sets which allow coexistence of cheats and cooperators may be evolutionarily stable, because lowering $t_E$ or $\sigma_E$ too much will drastically reduce the fitness of the cooperator (see section 4.3.6 and fig. 4.7).

[2] Ref. [77] shows that such an emergency brake mechanism can work in a well-mixed system also.

[3] Note that once the emergency brake kicks in and common good production stops, cooperators and cheats have equal growth rates. Therefore, whether the cooperator segment then shrinks further or starts growing instead is random which is possibly why very different outcomes are seen in the insert of fig. 4.13. The chance of avoiding extinction of the cooperators is evidently higher the larger the critical segment length at which the emergency brake kicks in, which means it would be better for a cooperator to have higher $t_E$. However, at sufficiently large $t_E$ cooperators never turn on, so we are back to the case where cooperators and cheats have equal fitness and the growth dynamics is random. In that case, in the long run for a finite system one or the other cell type will eventually go extinct [42].

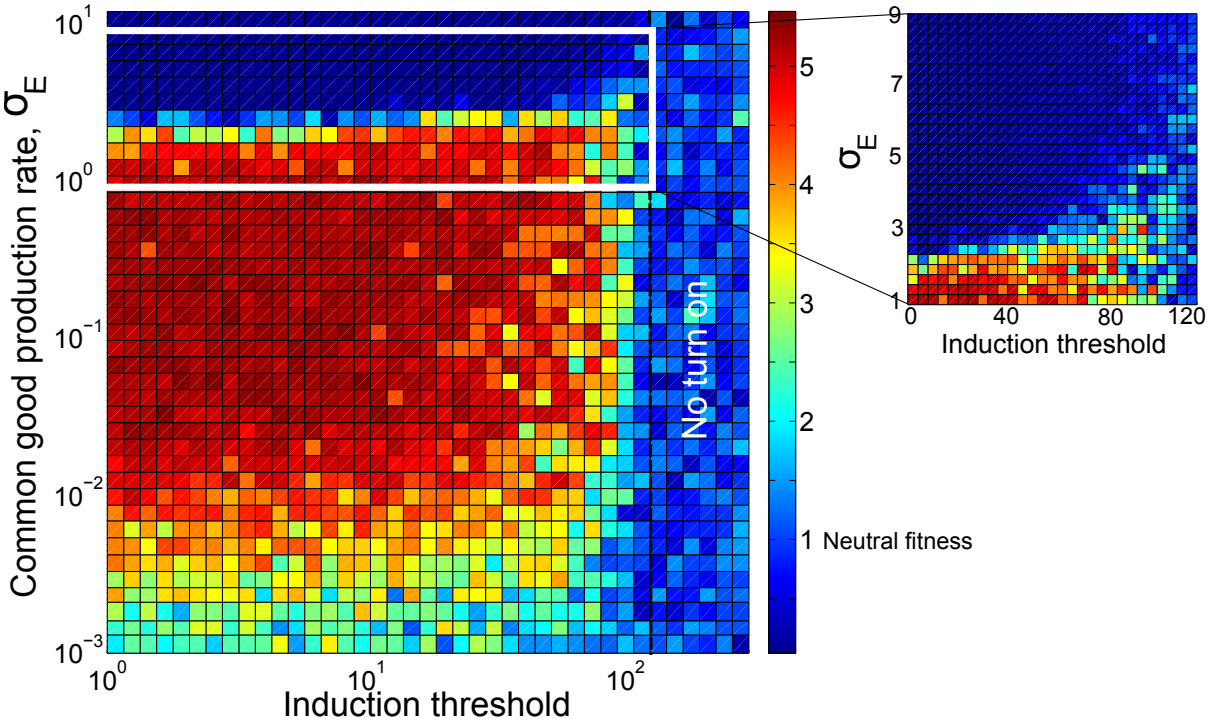


Figure 4.12: **Growth with a cheat when h = 0.5.** Large plot is the same as in fig. 4.7, bottom right panel. The zoom-in shows the range: $t_E \in [0, 120]$ and $\sigma_E \in [1, 9]$, on linear axes. The plot shows that there is a slight tendency for the cooperators to do better for relatively higher production rates when the threshold is higher. This is due to the fact that at these thresholds a cooperator will turn off common good production when its segment on the growing front is reduced below a critical length. Once common good is turned off, competition with the advancing cheat becomes completely neutral and the cooperators then have a chance of randomly reaching a larger segment length again. In contrast, if they had kept on producing they would have faced a high risk of extinction.

## 4.4 Future work

### 4.4.1 2D model with a constant number of cells

Our analytical results suggest that cells should turn-on at a critical diffusion constant, $D_c$, particularly when $h > 1$. We would like to test this in 2D simulations. For this, we would need to modify the simulation to allow us to keep cell number constant while varying the diffusion constant. This could be done by letting the cells grow but at the same time removing cells from the system at the same rate as they appear.

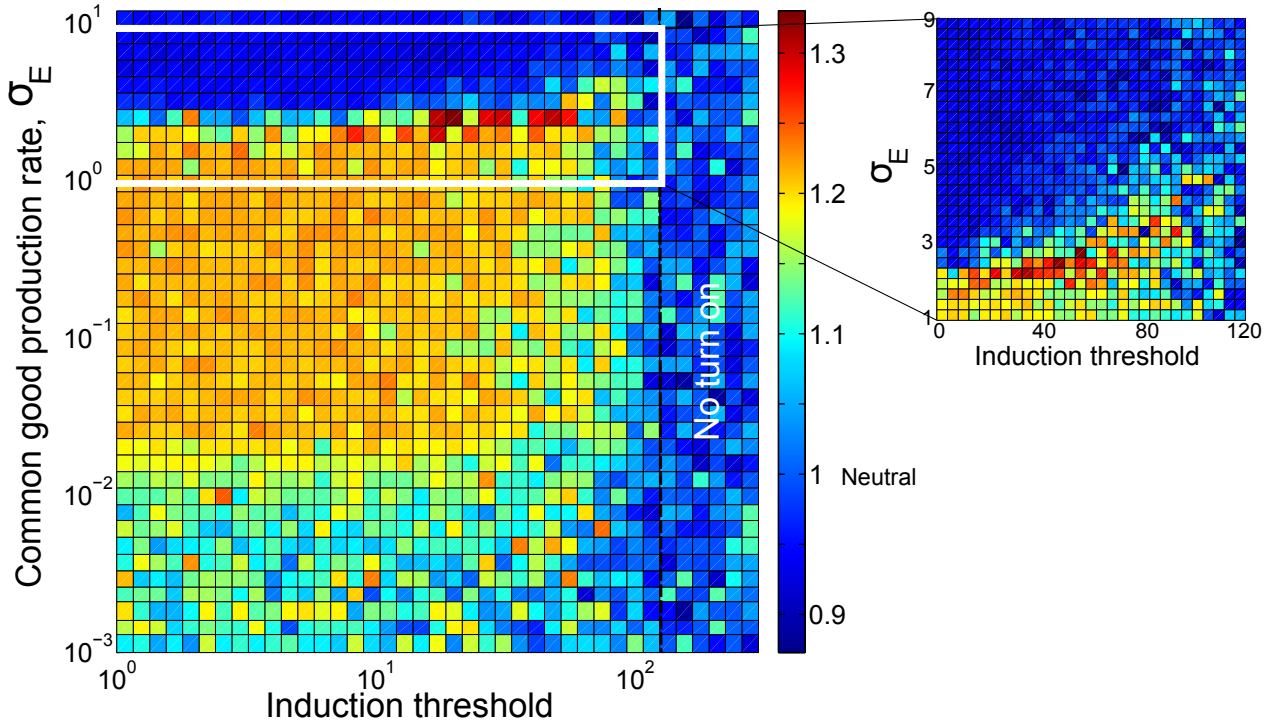


Figure 4.13: **Cooperators and cheats coexisting while at the same time reaching high numbers requires a turn-off threshold and non-privatization of the common good.** In this plot colors depict the value of a quantity, $A$, averaged over six simulations for each choice of $(\sigma_E, t_E)$. Here $A$ is determined by first calculating (1/3)(fraction of simulations where both cooperators and cheats are still present at the growing front at $T_{end}$)+(2/3)(total number of cheats + cooperators at $T_{end}$, normalized by its maximum value), and then normalizing by the value obtained by the same calculation for simulations where cooperators grow at a fixed rate of $g_{basal}$ (i.e. they are non-producers). The plot shows that only when $\sigma_E$ and $t_E$ are sufficiently high (the parameter region shown in the zoomed-in inset) can the value of $A$ become relatively large, i.e dark red. That is, only for these parameters can you get coexistence of cheats and cooperators on the front along with a relatively large total (i.e., summing over the entire grid) population of cells. In section 4.3.7 we explain that the high $t_E$ is required so that the cooperators turn-off common good production before their numbers on the growth front get too small, and the high $\sigma_E$ is required to allow cheats to get the benefit of the common good at least some of the time. The somewhat arbitrary looking weighted sum in the calculation of $A$ was chosen simply to obtain a quantity that clearly distinguishes the zoomed-in region, where cheats and cooperators coexist with a large total population, from the region with a low common good production rate ($\sigma_E \in [10^{-3}, 10^{-2}]$) where cheats and cooperators coexist but the total cell population is quite low at $T_{end}$.

### 4.4.2 Cooperator vs. cooperators

Here we have concentrated on investigating how different $(\sigma_E, t_E)$ strategies did, alone and in the presence of cheats (i.e. a cell type that produces neither common good nor QS signal). It would be interesting to examine how two different $(\sigma_E, t_E)$ strategies would perform in each other's presence. If we assumed that both types produced and responded to the same type of QS signal, we would get a situation where one type with a high threshold could entice another low threshold type to produce common good even when at too low a density. It has been proposed that the strong feedback which the inducer has on its own production serves exactly to avoid exploitation of this kind. The argument is that, once the feedback sets in, the concentration of inducer will rise so fast in the system that the exact threshold value will not matter much for the timing of common good production initiation. If this holds, one QS type will only be able to cheat another, by delaying production, if their respective thresholds are very different. An important parameter would thus be the slope of the inducer production curve as a function of inducer concentration (see fig. 4.1). A lower slope would make this kind of "slightly higher threshold cheating" more effective.

### 4.4.3 Other kinds of cheats

The only kind of cheat we have studied so far is one which produces neither the common good nor the QS signal. It is possible to construct a mutant bacterium which produces and responds to the QS signal, but does not produce one of the common goods under QS regulation (for example by mutating the promoter of that specific gene). Such a "lying cheat" could potentially fool cooperators into turning on common good production earlier than they would in the absence of the cheat. Another type of cheat can be created by knocking out the QS signal receptors. Such "signal blind" cheats, as well as the above "lying cheats", do occur in real microbial systems [105]. Interestingly, "signal blind" cheats appear to do better than other cheats in pairwise competition with cooperators (based on the experiments of Sarah Hammerlund with *P. aeruginosa*, Ben Kerr lab, U. Washington; personal communication). In the case of the "lying cheat", this is probably because it turns on many other potentially costly QS regulated genes, whereas the "signal blind" mutant will not turn on any of the QS regulated genes (in *P. aeruginosa* 6% of the entire genome is QS regulated [54; 105]). Our model can easily be extended to include these and other varieties of cheats.

### 4.4.4 Varying initial ratio of cooperators to cheats

We have only looked at one fixed initial ratio of cheats to cooperators but obviously it would be interesting to determine optimal $(\sigma_E, t_E)$-strategies when averaged over simulations with dif-

ferent starting ratios. It is possible that we would find an effect like Simpson's paradox [116; 4] when averaging over different initial ratios. That is, it could be that even when cooperator numbers decrease because they are outcompeted by cheats present in the same colony/simulation as them, the total number of cooperators averaged over a large ensemble of systems (with different initial cooperator/cheat ratios) could still go up globally and outperform cheats, provided cooperator+cheat colonies perform better on average than cheat-alone colonies.

### 4.4.5 Experiments

**Quorum sensing regulated common good production in *Pseudomonas aeruginosa*.** An experimental collaborator, Brook Peterson (Matthew Parsek's lab at U. Washington), has engineered a set of *Pseudomonas aeruginosa* strains and mutants which will be used to test the results we obtained above.

*Pseudomonas aeruginosa* are found in diverse terrestrial and aquatic environments, but has the ability to transition from its environmental habitats and become an opportunistic pathogen in humans. It causes severe infections by forming thick biofilms in the lungs of in immunocompromised individuals and patients with cystic fibrosis. About 6% of *P. aeruginosa* genes are QS regulated [54; 105] and among these are genes which code for virulence factors such as extracellular enzymes (e.g. the protease *LasB*, see fig. 4.14 for a schematic figure of one of the two QS systems in *P. aeruginosa*) that provide nutrients for the bacteria by degrading host lung tissue [106]. Due to the QS regulation, virulence factor production is "turned on" only when the bacteria have reached a sufficiently high density to successfully overcome the patient's immune system [106]. Wild type *P. aeruginosa* is thus an example of a QS regulated cooperator, or what we called a "conditional cooperator" in section 4.1. Mutations which knock out production of either QS receptor molecules or common goods will transform a wild type conditional cooperator into a cheat. Different kinds of cheats who benefit from the common goods (e.g. LasB) without incurring the cost of production have been observed to arise in natural systems, for example in isolates from the lungs of cystic fibrosis patients. A higher frequency of cheats has been shown to result in a less severe infection for the patient [105; 106]. These properties, and the fact that knowledge of cooperator/cheat dynamics of this bacteria might be medically relevant, make *P. aeruginosa* an ideal and interesting organism for studying cooperation and communication in microbes.

***P. aeruginosa* mutants.** Brook Peterson has enginered mutants which in an experimental setting could play the roles of a signal-blind cheat and constitutive cooperator, respectively, see fig. 4.15. The signal blind cheat has a mutation in both signal-receptor genes ($\Delta$*lasRrhlR*), and the constitutive cooperator is a $\Delta$*lasBaprA* knock-out with an additional gene *lasB* put

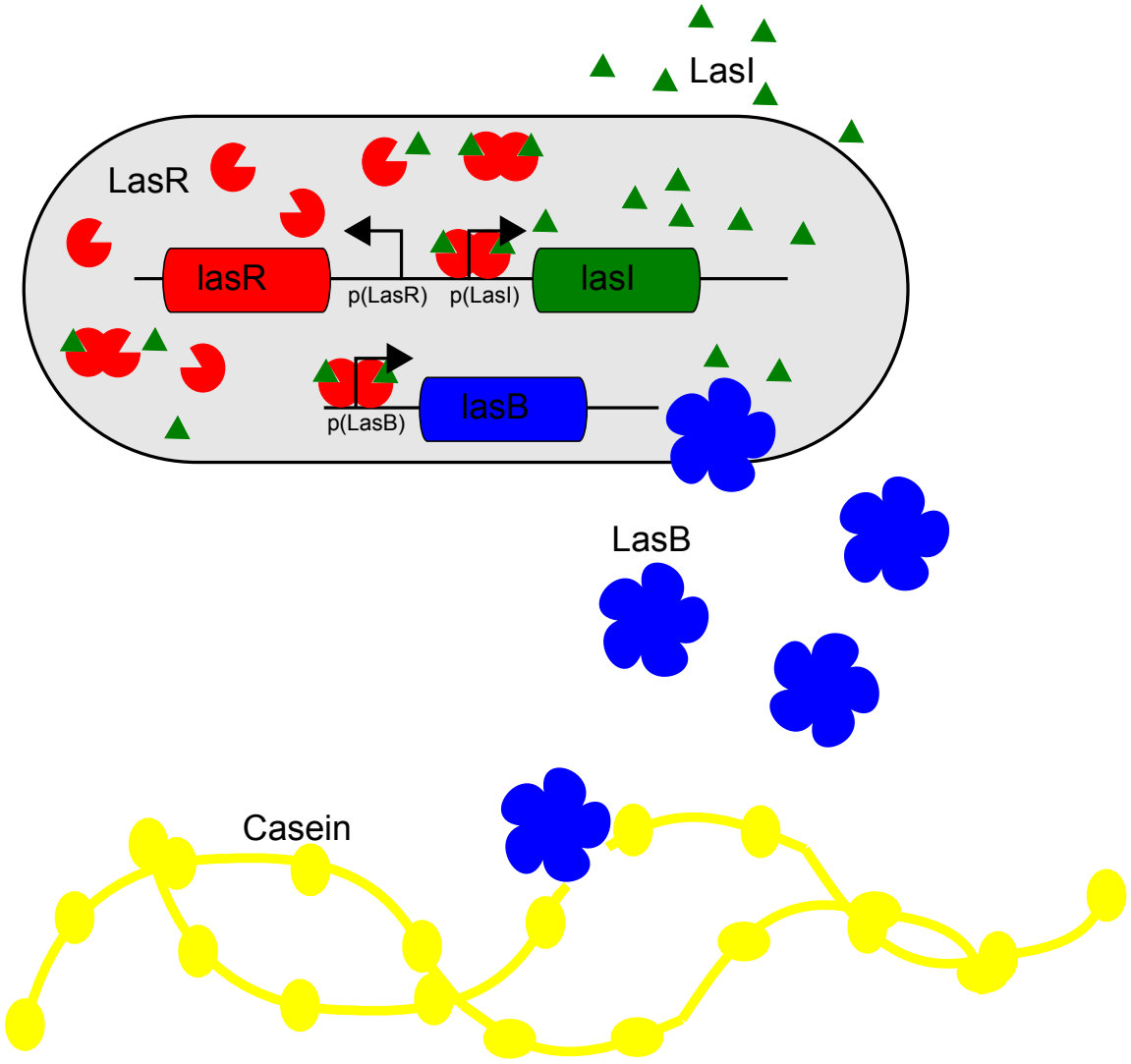


Figure 4.14: **Schematic of one of then two quorum sensing system in wild type *P. aeruginosa*** Signal molecules (green triangles) are encoded by the *lasI* gene, and receptor molecules (red 'pac-man' shapes) by the *lasR* gene. The signal-receptor complex, dimerized, acts as a transcription factor that promotes expression of the *lasB* gene, which encodes for a protease (blue flower shapes). The proteases break down polymers (yellow) which can be imported and metabolized by the cell when sufficiently degraded.

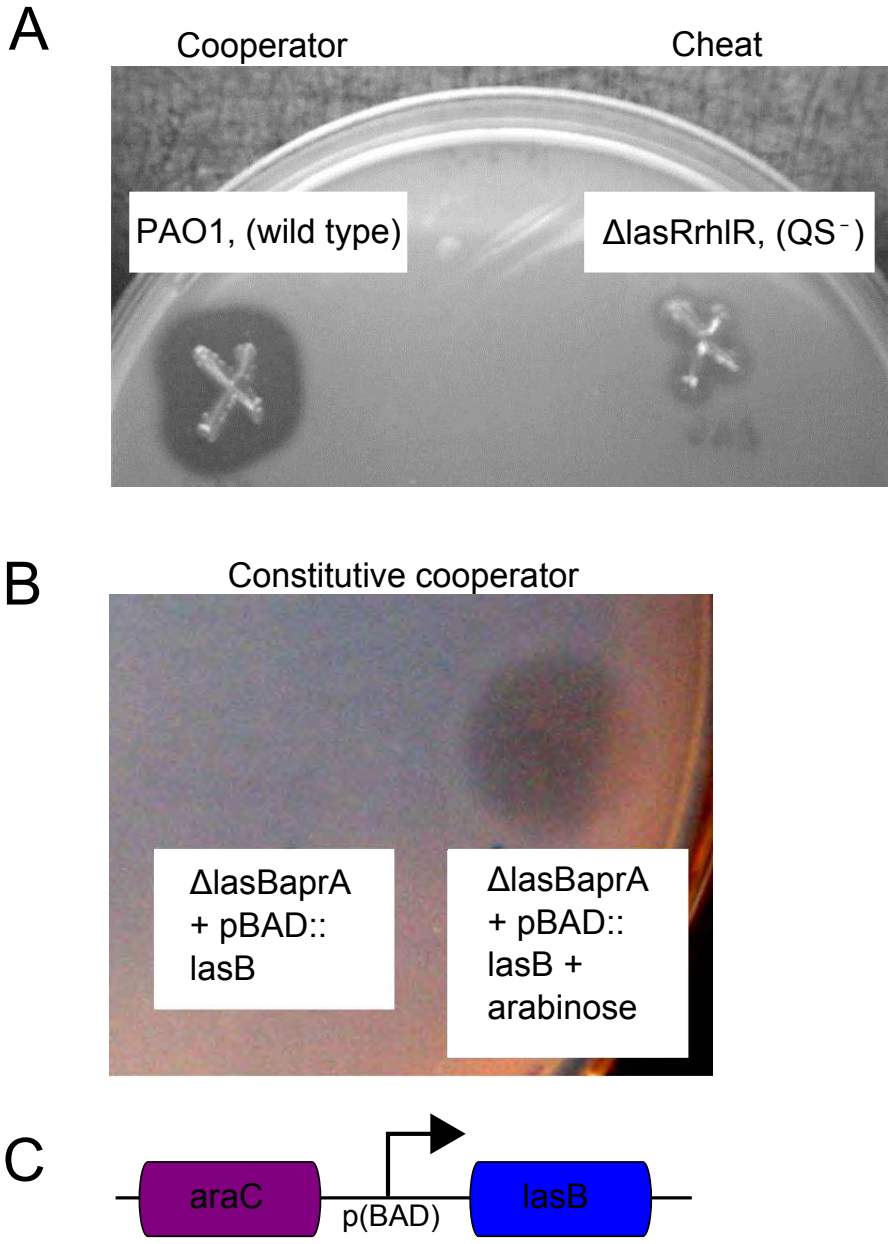


Figure 4.15: ***P. aeruginosa* mutants. A:** Photo of the cooperator (*P. aeruginosa* wild type) (left) and signal-blind cheat (Δ*lasRrhlR* QS mutant) (right) plated on skim milk agar. The wild type produces protease that dissolves the milk protein (giving a large halo around the X-shaped colony), while the cheater lacks production of QS-dependent proteases (the small halo is due to low baseline protease production). **B:** Constitutive cooperator: a *P. aeruginosa* Δ*lasBaprA* knock-out with an additional *lasB* gene put under regulation of the arabinose-inducible *araBAD* promoter (see C). Picture shows the constitutive cooperator plated on skim milk agar with (right) and without (left) arabinose added. When arabinose is present the constitutive cooperator expresses *lasB* regardless of whether QS signal is high or low. **C:** In the constitutive cooperator, *lasB* is placed under regulation of the arabinose-inducible *araBAD* promoter *p*(*BAD*). Photos and *P. aeruginosa* mutants engineered by Brook Peterson at Matthew Parsek's lab, U. Washington, Seattle.

under regulation of an arabinose-inducible *araBAD* promoter. The latter strain thus produces the common good *LasB* at a constant rate independent of QS signals, and we can control that rate by controlling the arabinose level. Other types of cheats were also constructed but experiments done by my collaborator Sarah Hammerlund (Ben Kerr's lab at U. Washington) showed that the mutant lacking function of both signal-receptor ($\Delta$*lasRrhlR*) genes was the most efficient cheat, therefore initial experiments will focus on this signal-blind cheat.

**Measuring the shape of the benefit function.** The benefit function for *LasB* can be quantified by measuring the growth rates of signal-blind cheats (the $\Delta$*lasRrhlR* mutants) in a chemostat, as a function of the concentration of externally added *LasB*.
It would be interesting to automate this type of measurement so that it could be done for a wide range of different molecules from different bacteria species, which are thought to be common goods. The shape/convexity of the measured benefit functions could then be compared with already known information about whether the molecules are QS regulated or not, to determine whether convex benefit functions are typical for QS regulated common goods.

**Manipulating the shape of the benefit function.** The way *LasB* works provides a way for us to manipulate the convexity of its benefit function. When provided solely with a diet of casein polymers, *P. aeruginosa* growth depends on the production of *LasB* (and similar proteases) that degrade the casein polymers into smaller "edible" bits, which can be transported over the cell membrane and metabolized. This is what inspired our calculation, in section 3.2.6, which showed that the benefit function becomes convex if the maximum length of the polymers in the environment is greater than 2 "edible units"[4]. That calculation suggests that one way of experimentally tweaking the benefit function would thus be to pre-digest casein polymers to varying degrees before providing them to *P. aeruginosa*. We will implement this, first to test our prediction from section 3.2.6 that, even if the exact shape of the benefit function is not sigmoidal, media with undigested casein would result in a more convex benefit function than media with pre-digested casein. If that is true, then mutants grown along with wild-type *P. aeruginosa* in these media will be used to test our results in sections 4.3.6 regarding the importance of the convexity of the benefit function for QS regulation.

[4]One "edible unit" is defined as the maximum polymer length which can be transported over the cell membrane.

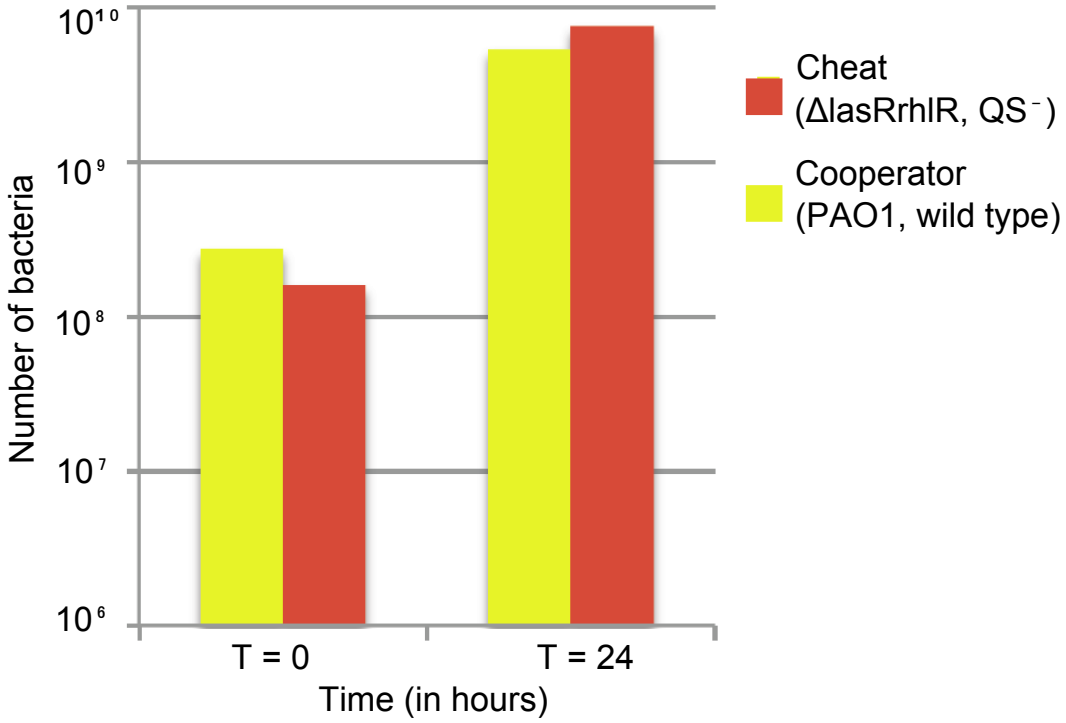


Figure 4.16: **Results of a competition between cooperator and cheat in an unstructured environment.** Here, the cooperator was *PAO*1 (*P. aeruginosa* wild type) and the cheat was the Δ*lasRrhlR* "signal blind" QS mutant. In the experiment, the cheat started out at a lower population size than the cooperator, but after 24 hours it ended up with a higher population. The average fitness of the cheat relative to the cooperator (i.e., the ratio of growth rates) was 1.28. Other kinds of cheats can be engineered, e.g. by knocking out genes of either *lasRrhlR* (receptor genes), *lasIrhlI* (inducer genes) or *lasBaprA* (protease genes), but experiments by Sarah Hammerlund (Ben Kerr lab, U. Washington) showed that the mutant lacking both signal-receptor (Δ*lasRrhlR*) genes was the strongest cheat.

### 4.4.6 Experimental plan

The first experiments we plan are:

- Grow signal-blind cheat in chemostat with undigested casein as the only food source, and different amounts of externally added *LasB*, in order to measure the benefit function.
- Repeat the same experiment with casein polymers predigested to different levels, in order to measure the change in convexity of the benefit function.
- Grow wild type *P. aeruginosa* in well-mixed flasks and petri dishes with varying agar concentrations, to compare with our results for (conditional) cooperators growing alone. The varying agar concentration effectively varies the degree of spatial structure present because it will, for example, affect the diffusion constant of the common good *LasB*.
- Repeat the same experiment with the constitutive cooperator mutant, with different levels of arabinose, in order to set a baseline for normalization of measurements, and to compare with our results for non-producers growing alone.
- Repeat the above experiments with the signal-blind cheat grown in competition with wild-type conditional cooperators, to compare with our results on cooperator+cheat populations. We will try to generate initial conditions similar to those used in the simulations by inoculating the bacteria on a line using a razor edge (as in [42]), but we can also easily redo our simulations using whatever other initial conditions we find easy to set up experimentally.

Further in the future, we think it would be neat to engineer fluorescent versions of the three types of *P. aeruginosa* mentioned above and visually monitor competition and growing front dynamics with an experimental setup like the one used in [42], in order to determine if it resembles the dynamics observed in the simulations.

**Main predictions.** Fig. 4.17 show the expected outcomes of different experiments where spatial structure, benefit function convexity, QS properties and the presence/absence of a cheat is being varied. The most important prediction is that the wild-type cooperator will do better than the constitutive cooperator when grown on undigested casein (both with and without cheat), while a constitutive cooperator will do just as well or better than a conditional cooperator when grown alone on predigested casein. Another important prediction is that a more spatially structured environment (i.e., less diffusion due to higher agar concentration) will make it harder to cheat on a constitutive or wild-type cooperator.

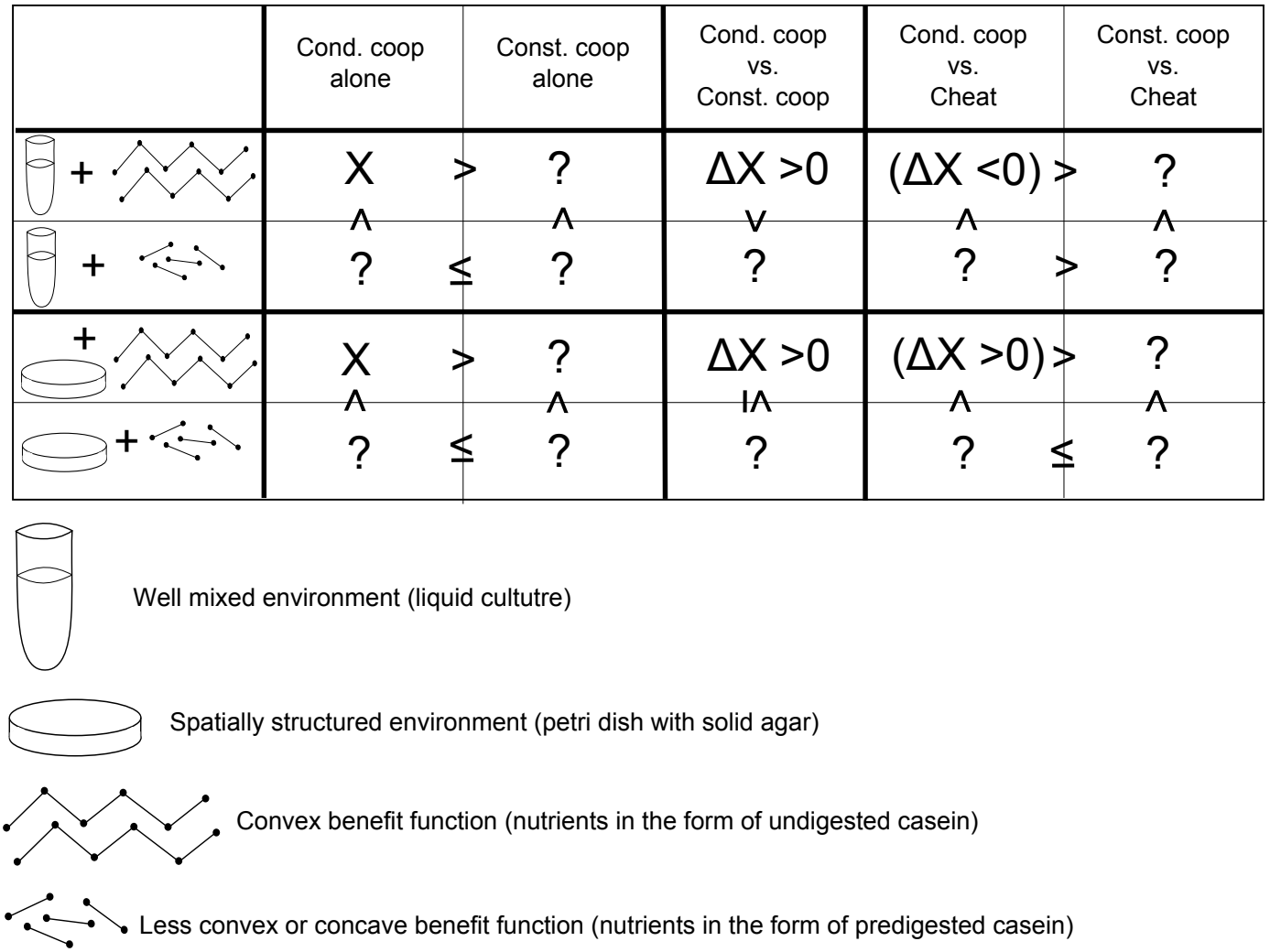


Figure 4.17: **Predictions of experimental outcomes based on results from analytical calculations and simulations of the 2D model.** $X$ denotes the fitness of the conditional cooperator (*PAO*1, wild type *P. aeruginosa*) growing alone in media with undigested casein. The $>$ and $<$ signs denote whether the fitness of a type growing alone in a certain experimental setup is predicted to be more or less than $X$. $\Delta X$ denotes the relative fitness of the conditional cooperator (*PAO*1, wild type *P. aeruginosa*) with respect to the other type present (constitutive cooperator or cheat) in media with undigested casein. A positive $\Delta X > 0$ means that the conditional cooperator ended up with the highest population of the two types present. The $>$ and $<$ signs denote whether the relative fitness of the cooperator (conditional or constitutive) is predicted to be more or less than $\Delta X$, for other competition assays. Two important predictions are that the conditional cooperator should do better than the constitutive cooperator when grown on undigested casein, both with and without a cheat, and that a structured environment will make it harder to cheat on a constitutive or conditional cooperator. (In all experimental setups with a constitutive cooperator, we assume that arabinose is present and therefore the protease is produced constitutively).

## 4.5 Take home messages

- When benefit function is concave, *constitutive* cooperators with relatively low production rates of common good have highest fitness both when grown alone and together with a cheat. Producing less than at the optimal rate is, in this case, always better than not producing.
- When benefit function is convex, *conditional* cooperators with relatively high production rates of common good have highest fitness both when grown alone and together with a cheat. Producing less than at the optimal rate can in this case be worse than not producing. When a cheat is present the parameter values, which ensure an advantage compared to not producing common good, are confined to a very small region of parameter space.
- When the benefit function is convex, a QS mechanism can ensure that cooperation commences only after the population has reached a sufficient size to make benefits outweigh costs.
- QS can facilitate privatization of common goods in a spatial setting by confining cooperation cells that are not near the edge, where cheats might reside.
- QS can act as an emergency brake for cooperation and lower the risk of cooperators getting driven to extinction when cheat numbers are rising. This effect can help ensure coexistence of cooperators and cheats at a relatively high yield.

# Chapter 5

# Quorum sensing and common goods in bacterial warfare

## 5.1 Introduction

Antimicrobials are a very typical example of compounds produced and excreted by bacteria which could be perceived as common goods. In particular, bacteria found in soil often produce molecules which either kill or inhibit the growth of other bacterial species found in the same environment. Although it has been proposed that the antimicrobial activity of these compounds is merely a side effect and that the primary function is signaling [27; 148], another likely possibility is that these compounds are toxins and that they are primarily means to gain a competitive advantage in a multi-species environment [82; 83; 75].

**A convex killing curve.** The killing rate of many toxins produced by bacteria, as a function of the concentration of the toxin, has been found, experimentally, to be non-linear, often best described using a sigmoidal curve with a Hill-factor of 2-4 [70; 84]. The cause of the convexity of the killing-curve is not well established, but could perhaps be related to the time scales on which cell-repair mechanisms act. While small doses of toxin may allow enough time for cell repair mechanisms to keep pace and continuously repair the damage between each new damage event, the damage could start to accumulate and become fatal at higher concentrations of toxin. There is another important factor that acts on an evolutionary time scale, which could make production of small doses of toxin detrimental; small sub lethal doses of antibiotics could allow an enemy bacteria to slowly adapt and become resistant over time.
The sigmoidal *killing-curves* make antimicrobials a prime example of a common good which has a highly convex benefit function, because the benefit felt from the presence of common good in the environment here comes from a reduction of the competitive pressure from an enemy

species. Based on the conclusions drawn in the previous chapter, it seems that it could be important to gauge population density before committing to antimicrobial production.

**Eavesdropping.** This fits well with the observation that most antimicrobials produced by bacteria living in soil are under QS regulation [76; 9; 62; 38; 100; 34]. Another factor which one would think is important for whether or not toxin production is worth the effort or not, is of course the density of the enemy species. If the antagonizing species happens also to produce QS signals, then information about enemy density is literally floating around in the environment. Many bacteria living in soil have been found to respond to not only to their own QS signal but also to those of other species, due to promiscuous signal receptors [3; 35; 50; 91; 103; 118; 131]. It has been proposed that such signal receptor promiscuity is akin to "eavesdropping", in that it allows a species to "listen in" on enemy communication and make their toxin production depend not only on their own density, but also on that of their enemy. It has, however, not yet been shown experimentally or via modeling whether having a promiscuous signal receptor can provide any advantage compared to having a more signal specific receptor.

### 5.1.1 A map of this chapter

We begin, in section 5.2, by summarizing the experimental findings from a model experimental system constructed in order to study the role of eavesdropping in bacterial warfare. In section 5.3, we introduce a coupled differential equation model inspired by the experimental system. In sections 5.4.1, 5.4.2 and 5.4.3 we examine the dynamics of the model and determine the parameter ranges for which eavesdropping provides an advantage and the ranges for which it does not. Then in section 5.4.4, we introduce a simpler model, similar to the full model but without eavesdropping which can be solved analytically, and find that in this system there exists an optimal QS induction threshold which cannot be beaten. In section 5.4.4, we explore how this optimal threshold depends on different parameters of the model. Finally, in section 5.5 we speculate about how this work could be extended to include situations where different eavesdropping strategies are played against each other.

## 5.2 Experimental model system

QS has been experimentally investigated very thoroughly in the context of bacteria producing virulence factors (e.g. *P. aeruginosa* [105] and *Vibrio cholerae* [150]), but only a few studies have addressed its importance for inter-species toxin warfare [5; 75; 82; 83], and so far no one has investigated the effects of having a promiscuous QS signal receptor. To remedy this, my experimental collaborators Josephine Chandler and Pete Greenberg (University of Washington, Seattle) constructed and experimented with a model system consisting of the two species *Burkholderia thailandensis* and *Chromobacterium violaceum*. Both species are found in the soil of rice fields and both species have been found to produce QS-controlled broad spectrum antimicrobials during stationary phase [76; 34]. Furthermore, *C. violaceum*'s signal receptor (CviR) has been shown to be promiscuous and respond to not just the acylated homoserine lactone (AHL) produced by *C. violaceum* itself (C6-HSL) but also to a number of other AHL signals [76; 125]. In a nutshell, experiments done with this model system by Chandler and Greenberg [19] demonstrate that:

- Both *B. thailandensis* and *C. violaceum* produce QS sensing regulated antimicrobials that inhibit growth of or kill the other species.
- Both species can get a fitness advantage, in the presence of the other species, by producing their respective antimicrobial compound.
- When grown in co-culture, the model system exhibits bistable dynamics (where one or the other species ends up dominating the other, depending on the initial populations size of the two species).
- Even though the QS signals used by the two species are different, *C. violaceum* will respond not just to its own signal (C6-HSL) but also one (or more) of *B. thailandensis*'s signals (C8-HSL, 3OHC8-HSL and 3OHC10-HSL), see fig. 5.1. In contrast, *B. thailandensis* responds only to its own signals.
- *C. violaceum*'s ability to "eavesdrop" on *B. thailandensis*'s signal can provide it with a fitness advantage in co-culture, see fig. 5.2.

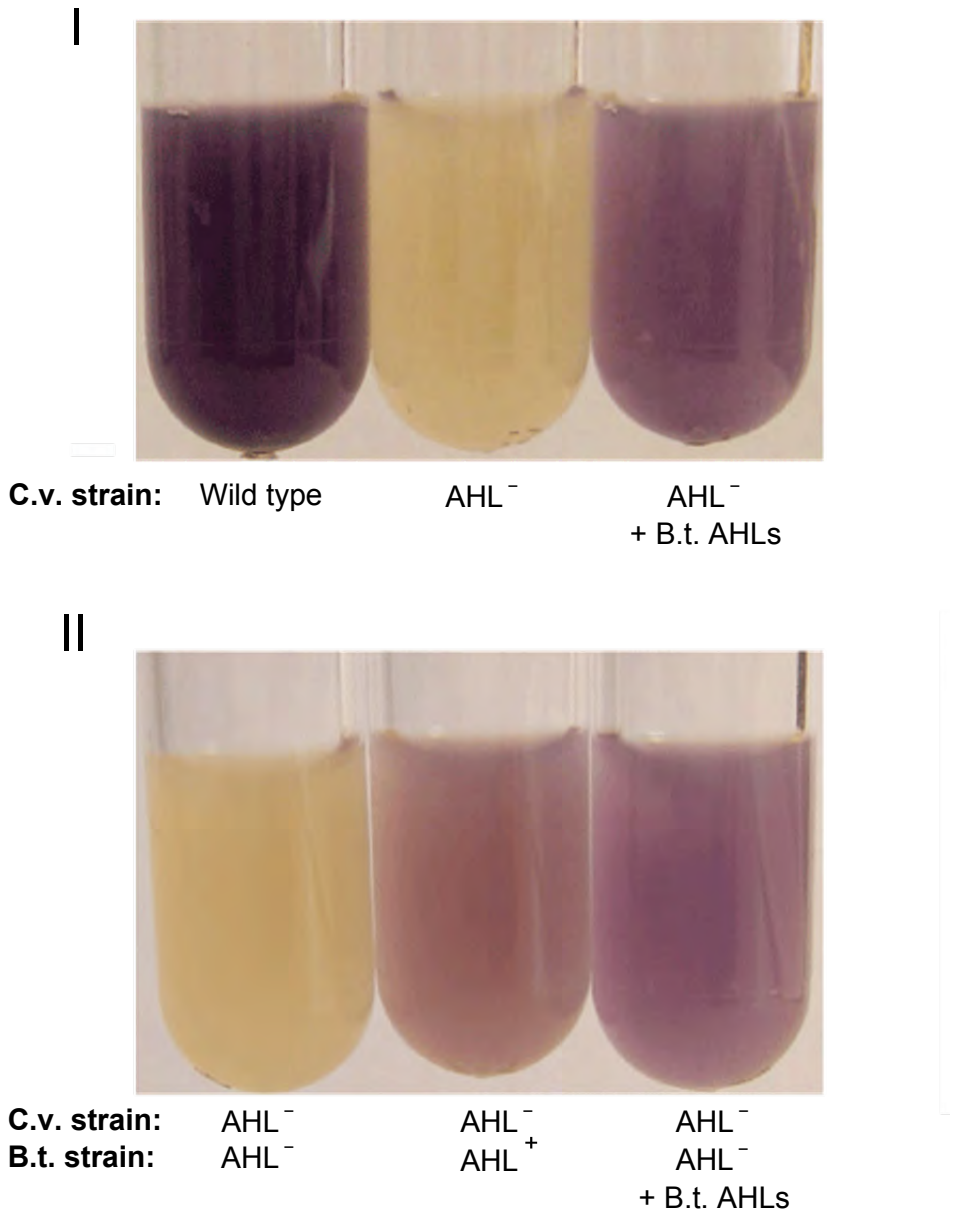


Figure 5.1: ***C. violaceum* quorum sensing is activated by *B. thailandensis* AHLs.** Quorum sensing activation can be monitored in *C. violaceum* due to the quorum sensing-dependent production of a purple pigment, violacein. **I:** Left: *C. violaceum* wild-type growing alone. Middle: *C. violaceum AHL*$^-$ mutant growing alone. Right: *C. violaceum AHL*$^-$ mutant growing alone with with fluid added from a stationary phase culture of *B. thailandensis* BD20 (a bactobolin mutant, which does not produce toxin) which contains the AHLs. **II:** Left: Co-culture of *C. violaceum AHL*$^-$ mutant and *B. thailandensis AHL*$^-$, *bactobolin*$^-$ double mutant. Middle Left: Co-culture of *C. violaceum AHL*$^-$ mutant and *B. thailandensis bactobolin*$^-$ mutant. Right: Co-culture of *C. violaceum AHL*$^-$ mutant and *B. thailandensis AHL*$^-$, *bactobolin*$^-$ double mutant plus added *AHL*s extracted from the stationary phase culture fluid of *B. thailandensis* BD20.

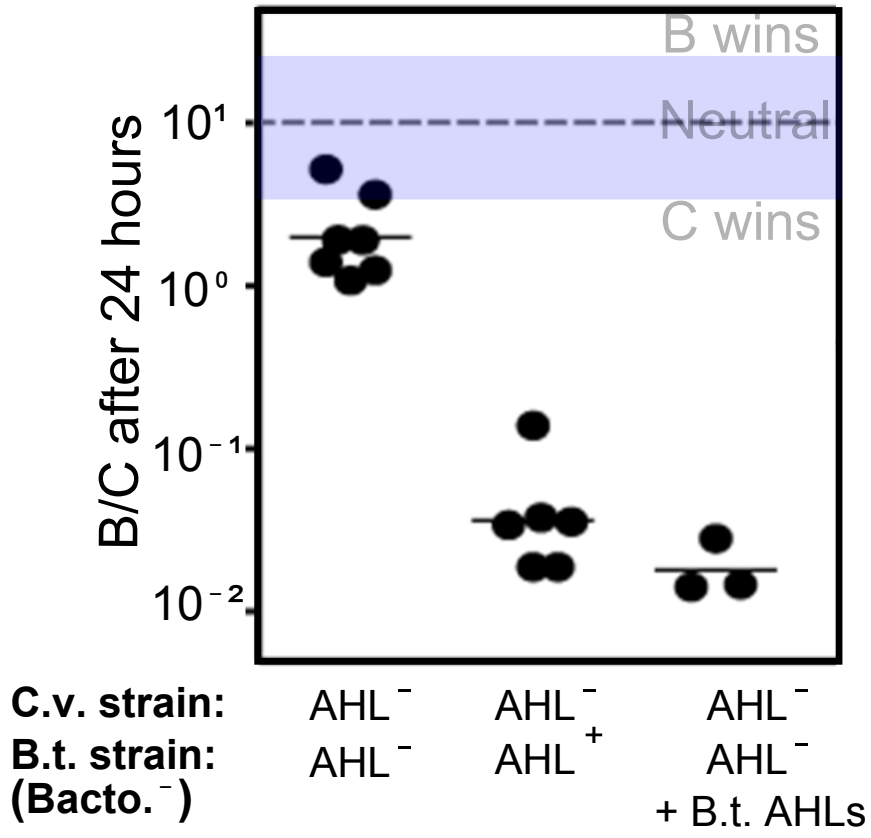


Figure 5.2: **Eavesdropping promotes *C. violaceum* competitiveness in co-culture.** After 24 h of co-culture growth, the ratio of *B. thailandensis* to C. *violaceum* was determined. The dashed line indicates the initial ratio of *B. thailandensis* to *C. violaceum*. Co-cultures were grown in 20 ml volumes; each black dot represents the result of one experiment. Solid black lines are the mean of each set of experiments. Added *AHL*s were extracted from the stationary-phase culture fluid of *B. thailandensis* BD20 (a bactobolin mutant, which does not produce toxin). The final experiment which would have to be done in order to prove that eavesdropping provides *C. violaceum* with a fitness advantage, would of course be to compare a non-eavesdropping mutant version of *C. violaceum* with the wild type. However, at this point it is not obvious how to construct such a mutant. For now, therefore, the best we can do is show the evidence in this figure: a mutant version of *C. violaceum* which has lost the ability to produce its own signal (an $AHL^-$ mutant) performs better against an enemy that produces signal, than against one that does not produce signal.

## 5.3 Mathematical model of two competing bacterial species with eavesdropping

Chandler and Greenberg's experimental setup inspired the construction of a coupled differential equation model of two quorum sensing bacterial species each producing antimicrobials to target the other, opponent, species. Using this model we wished to address the question of whether a bacterial species having a promiscuous signal receptor could gain a competitive advantage when up against another species exactly alike in all aspects except for having a strictly specific signal receptor.

When experimenting with different ways of modeling the system we found that toxin concentration in all relevant cases[1] was very close to being proportional to inducer[2] concentration for both species, so in the final model we chose to use the QS signal for a species as a proxy for the toxin concentration of that species. This allowed us to model the system using just four equations instead of six, and did not make a difference for the results shown further below.

**Equations.** In the equations below, $B$ denotes concentration of *B. thailandensis*, $C$ denotes concentration of *C. violaceum*, $I_X$ is concentration of inducer/toxin of species $X$:

$$\frac{dB}{dt} = B\left(1 - r\left(\frac{I_B^h}{I_B^h + K^h}\right)\right)(1 - B - C) - k\left(\frac{I_C^H}{I_C^H + K_T^H}\right)B \tag{5.1}$$

$$\frac{dC}{dt} = C\left(1 - r\left(\frac{(I_C + \epsilon I_B)^h}{(I_C + \epsilon I_B)^h + K^h}\right)\right)(1 - B - C) - k\left(\frac{I_B^H}{I_B^H + K_T^H}\right)C \tag{5.2}$$

$$\frac{dI_B}{dt} = \alpha B\left(\frac{I_B^h}{I_B^h + K^h}\right) + \beta B - \delta I_B \tag{5.3}$$

$$\frac{dI_C}{dt} = \alpha C\left(\frac{(I_C + \epsilon I_B)^h}{(I_C + \epsilon I_B)^h + K^h}\right) + \beta C - \delta I_C \tag{5.4}$$

The first terms on the right hand side of equations 5.1 and 5.2 model the logistic growth [132] of the bacterial species, reduced by the cost of toxin production. The cost is assumed to be proportional to the production rate of the toxin and $r$ sets the maximal reduction of growth

[1] The main difference between the equations for toxin and inducer production is that the basal rate of inducer production is non-zero, though small, while the basal rate of toxin production is zero. Thus, (only) at very low inducer concentrations is it a bad approximation to assume that toxin concentration is proportional to inducer concentration; here the toxin concentration should really be zero since QS has not yet been turned on and thus no toxin is being produced. However, we always choose the threshold concentration, at which toxin starts significantly killing opponent cells, to be much larger than the maximal inducer level when it is only produced at the basal rate. Therefore, in this parameter regime, assuming that the toxin level is is proportional to the inducer level, rather than zero, is not of much consequence because at this low level it will not affect the dynamics of the cell density much. See caption of fig. 5.5 for more discussion of this point.

[2] We interchangeably use the terms "inducer" and "signal" for the quorum sensing signal molecules.

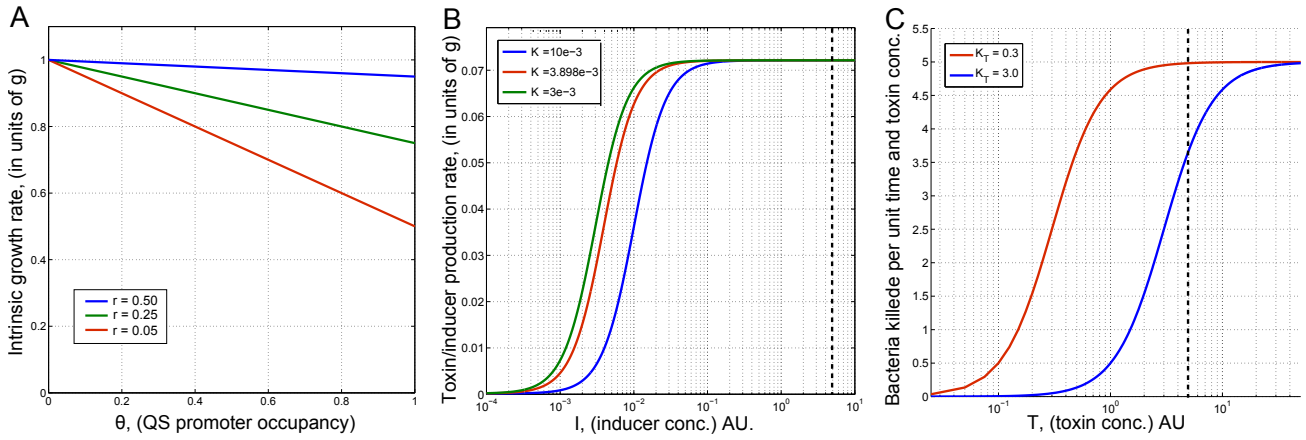


Figure 5.3: **Toxin cost curves, inducer production curves and toxin potency curves. A:** Effective intrinsic growth rate $1-r\left(\frac{I_B^h}{I_B^h+K^h}\right)=1-r\theta$ as a function of QS promoter occupancy $\theta\equiv\left(\frac{I_B^h}{I_B^h+K^h}\right)$, for three different cost parameters $r$ (note that we thus assume that cost is linearly proportional to production rate). **B:** Inducer/toxin production per capita $\alpha\left(\frac{I_B^h}{I_B^h+K^h}\right)+\beta$ as a function of inducer/toxin concentration $I_B$ for three different values of $K$. The black dashed line marks the maximum inducer/toxin concentration possible for either species at steady state, $(\alpha+\beta)/\delta\approx 5$. **C:** Toxin kill rate $k\left(\frac{I_B^H}{I_B^H+K_T^H}\right)$ as a function of toxin/inducer concentration $I_B$, for two different "kill thresholds" $K_T$. The black dashed line marks the maximum inducer/toxin concentration either species can reach at steady state.

rate due to the toxin production (see fig. 5.3A). For $B$, which only senses its own signal the toxin production rate is a function only of its own signal level, whereas for $C$ which senses both signals the toxin production rate is a function of the weighted sum of the two signals. The parameter, $\epsilon$ is thus the "eavesdropping sensitivity", i.e., how much weight $C$ gives to the opponent's signal compared to its own. The second (negative) terms on the right hand side of equations 5.1 and 5.2 model the death of bacteria due to the toxin produced by the opponent species, at a rate that is given by a Michaelis-Menten like sigmoidal term, where $H$ is the steepness of the sigmoid and $K_T$ is the "threshold" toxin concentration (at which the death rate is half its maximum value, $k$; see fig. 5.3C). The next two equations model the dynamics of the concentrations of inducer/toxin for both species. The negative terms correspond to the degradation of the inducer/toxin that is proportional to its concentration. The production rate is the sum of a basal rate of production by each cell $\beta$ and an auto-induced rate of production $\alpha$. The latter is modeled as a Michaelis-Menten like sigmoidal term, where $h$ is the steepness of the sigmoid and $K$ is the "threshold" inducer/toxin concentration (at which the auto-induced production rate is half its maximum value; see fig. 5.3B). Again, because $C$ senses both its own and $B$s signal, the auto-induced production rate of $C$s inducer/toxin is proportional to the weighted sum of the two inducer/toxin concentrations. In order to eliminate two parameters, the units for concentration and time have been chosen such that the carrying capacity of the

system is set to one (i.e. $B + C$ cannot grow larger than 1), and basal growth rate of both species is set to 1. That is why the growth rates of the bacteria have the mathematical form $B(1 - B - C)(1 - cost)$. In the experiments, the carrying capacity was $N_{max} = 10^9 cells/ml$, and the doubling time of both species was close to 1 hour, so the unit of time is $1/g \approx 1.4h$. Table 5.1 lists all the parameters and the value assigned to them, or the range of values we have explored.

**$\Delta g$ - a relative fitness measure.** The way to determine which species wins in this model with eavesdropping, for a given set of parameters and initial conditions, is by determining the relative fitness at a given time point $T_{end}$ (well after stationary phase had been reached):

$$\Delta g(T_{end}) \equiv g_C(T_{end}) - g_B(T_{end}) \tag{5.5}$$

where:

$$g_C(T_{end}) \equiv \frac{\log\left(\frac{C(T_{end})}{C_0}\right)}{T_{end}} \tag{5.6}$$

and

$$g_B(T_{end}) \equiv \frac{\log\left(\frac{B(T_{end})}{B_0}\right)}{T_{end}} \tag{5.7}$$

are the average growth rates of $C$ and $B$ respectively during the time span between $t = 0$ and $t = T_{end}$. Whenever $C$ wins (has highest concentration at end time $T_{end}$) then $\Delta g > 0$, else $\Delta g \leq 0$. Thus the sign of $\Delta g$ tells us whether $C$ or $B$ wins and the absolute value measures how big the victory/loss was.

Table 5.1: List of parameters of the model and the (range of) values assigned to them.

| Parameter: | Explanation: | Value or range used in dimensionless model | Value or range used in real units |
|---|---|---|---|
| $N_{max}$ | Carrying capacity | set to 1 | $10^9 cells \cdot ml^{-1}$ (from experiment) |
| $B_0$ | Initial density of $B$ | $10^{-3}$ | $10^6 cells \cdot ml^{-1}$ (from experiment) |
| $C_0$ | Initial density of $C$ | $[0.9 - 1.1] \cdot 10^{-3}$ | $[0.9-1.1]\cdot 10^6 cells \cdot ml^{-1}$ (from experiment) |
| $g$ | Intrinsic growth rate of $B$ and $C$ | set to 1 | $\approx 0.7 h^{-1}$ (based on doubling time $1h$ from experiment) |
| $k$ | Maximum kill rate for both species | 5 | $3.4655 h^{-1}$ |
| $\alpha$ | Maximum inducer production rate for both species | $7.20 \cdot 10^{-2}$ | $0.0500 h^{-1}$ |
| $\beta$ | Basal inducer production rate for both species | $1.44 \cdot 10^{-4}$ | $6.9310 \cdot 10^{-4} h^{-1}$ (set to be 1/500 times $\alpha$) |
| $\delta$ | Degradation rate of inducer for both species | $1.44 \cdot 10^{-2}$ | $0.0100 h^{-1}$ [108; 138] |
| $K$ | Inducer conc. where $B$ and $C$s QS promoter activity is 50% of max | $[10, 3.898, 3] \cdot 10^{-3}$ | $[10, 3.898, 3] \cdot 10^6 ml^{-1}$ |
| $K_T$ | Toxin conc. where killing rate is 50% of max. | $[0.3, 3]$ | $[0.3, 3] \cdot 10^9 ml^{-1}$ |
| $h$ | Hill factor of inducer activation of QS genes for both $B$ and $C$ | 1.3 | 1.3 (unitless) [67; 129; 151] |
| $H$ | Hill factor of toxin potency increase for both $B$ and $C$ | 2 | 2 (unitless) ([70], [84]) |
| $r$ | Max. cost of QS gene expression. | $[0.05, 0.25, 0.5]$ | (unit less, unknown) |
| $\epsilon$ | Eavesdropping sensitivity. | $0 - 10$ | (unit less, unknown) |
| $T_{end}$ | End time for determining relative fitness | 100 | $\sim 6 days$ $(144.27 hours)$ |

## 5.4 Results

### 5.4.1 Eavesdropping model exhibits bistability

The model with eavesdropping has bistable dynamics just like the experimental model system constructed by Chandler and Greenberg. In the long run either $B$ or $C$ takes over completely (even though for some parameters the take over of one species over the other happens so slowly that the fitness difference between the two species at time $T_{end}$ is negligible) and which one wins depends on the initial condition (see fig. 5.4).

### 5.4.2 Eavesdropping can be advantageous

For high $K$, neither species will induce (this is shown in fig. 5.5 for the case where $B_0/C_0 = 1$, though it is true for other initial ratios also), unless $\epsilon$ is enormously high which is biologically unreasonable, and therefore competition is neutral. For high $K_T > (\alpha + \beta)/\delta$, neither species can reach a toxin concentration sufficiently high to have a major impact on the opponent species, so here too competition becomes neutral (this is shown in fig. 5.5 for the case where $B_0/C_0 = 1$, though it is true for other initial ratios also). We see in fig. 5.4 that there are parameters for which eavesdropping (having a non zero $\epsilon$) will provide $C$ with a substantial advantage when the starting ratio is $B_0/C_0 = 1$, and from fig. 5.6 it becomes apparent that this advantage can enable $C$ to beat $B$ even when starting out at a slightly lower density.

### 5.4.3 Eavesdropping can also be disadvantageous

However we also note from fig. 5.4 that for all the different choices of parameters $K_T$ and $r$, there exists a value of $K = K'$ (marked with a white dashed line) below which eavesdropping is downright disadvantageous at almost any non zero sensitivity level ($\epsilon \neq 0$). It seems that the effect of eavesdropping in this model is that it effectively lowers the QS threshold of $C$, and that when $K < K'$, it is no longer advantageous for $C$ to be induced early due to eavesdropping.

### 5.4.4 Simple model without eavesdropping

**Equations of the simple model.** The model with eavesdropping is nonlinear and thus hard to deal with analytically. It turns out to be instructive to study a much simpler model which shares some of its main characteristics. In the full model it seemed that the advantage provided by eavesdropping was related to earlier QS induction and thus in this simplified model we will ignore eavesdropping and just allow $B$ and $C$ different induction thresholds $K_B$ and $K_C$. In addition, we model both the quorum sensing induced toxin production curve and the toxin efficiency curve as step functions instead of sigmoids, and ignore degradation or decay of the

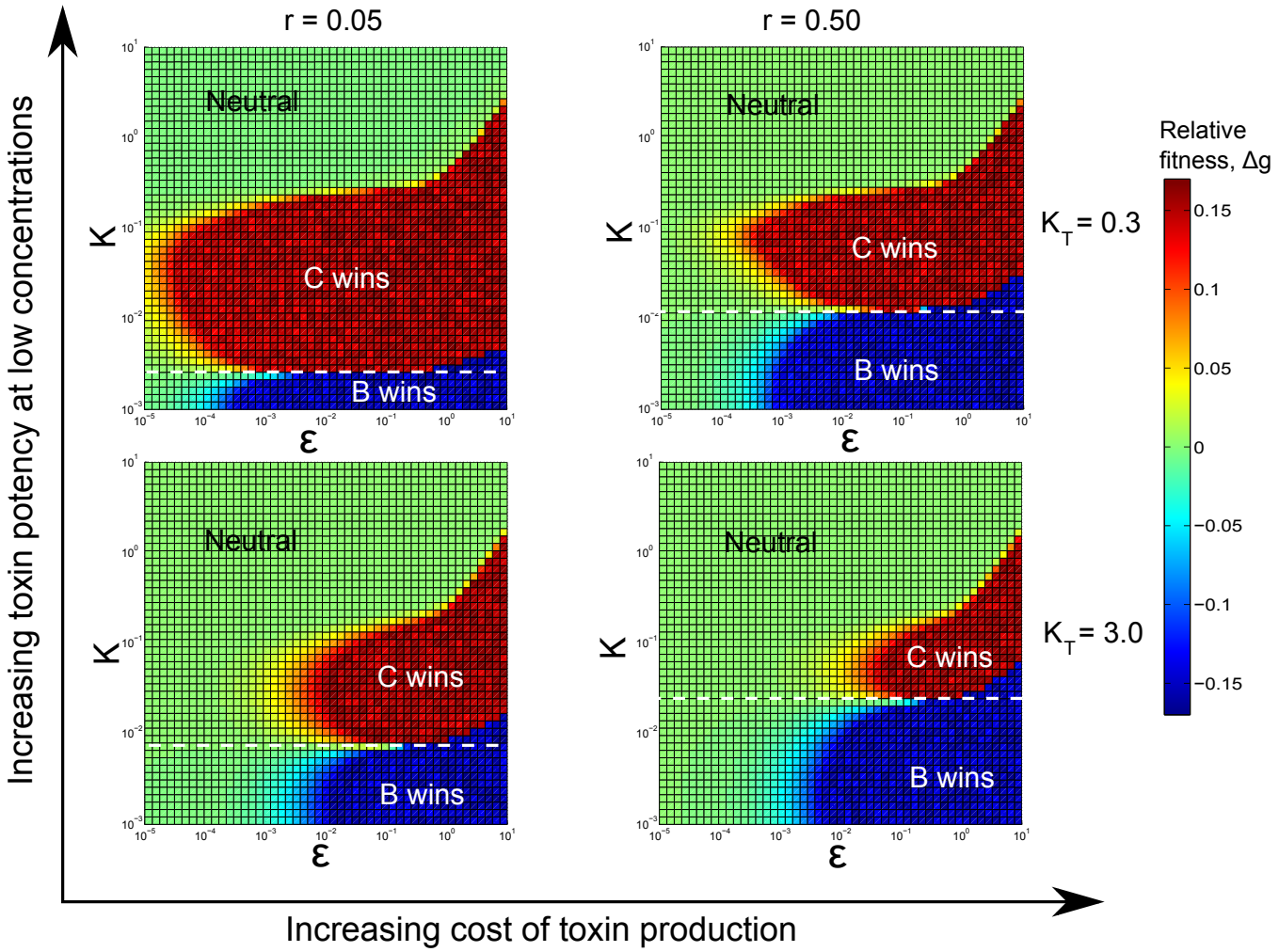


Figure 5.4: **The success of an eavesdropping strategy $\epsilon$ depends on K, $K_T$ and r:** Plots show relative fitness $\Delta g$ as a function of the eavesdropping sensitivity of $C$, $\epsilon$, and $K$ for four different sets of $(r, K_T)$-values: $r \in [0.05, 0.5]$, $K \in [0.3, 3.0]$. In all cases, initial conditions were $C(0) = B(0) = 0.001$ and $I_B(0) = I_C(0) = 0$. We see that for each set of $(r, K_T)$-values there exists a tongue shaped region in the $\epsilon - K$ space where eavesdropping provides an advantage for $C$. However, also note that for each plot there is a value of $K = K'$ (marked by a white dashed line) below which eavesdropping is never beneficial. This value, $K'$, appears to increase with increasing $r$ and decrease with decreasing $K_T$. We also see that the region where eavesdropping can provide an advantage becomes bigger for decreasing $K_T$ (decreasing $K_T$ increases the toxin potency for both species at low toxin concentrations) and decreasing $r$ (lower $r$ means lower cost of toxin production for both species).

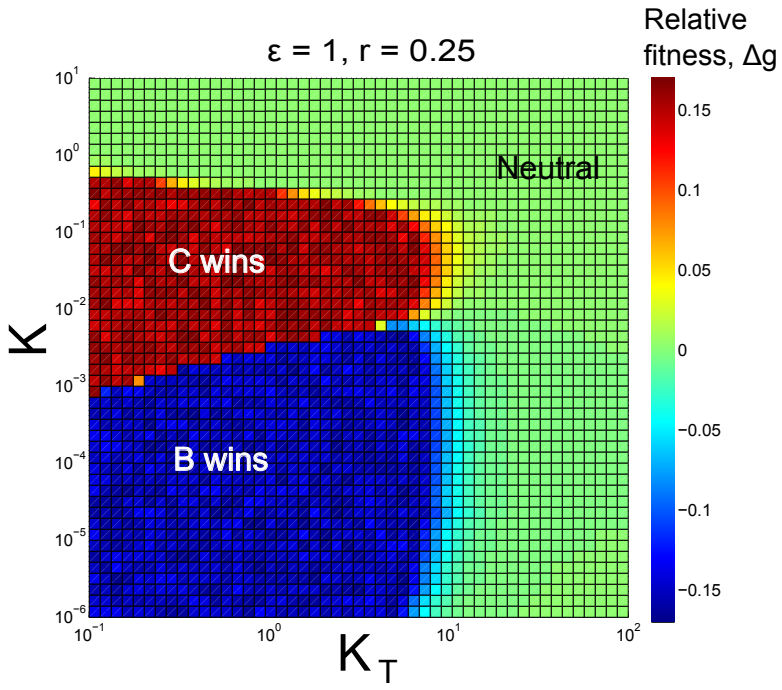


Figure 5.5: **For high $K_T$ and high K, competition becomes neutral.** Relative fitness, $\Delta g(T)$, from simulations starting with $B_0 = C_0 = 0.001$, as a function of $K_T$ and $K$, for eavesdropping sensitivity $\epsilon = 1$ and toxin production cost of $r = 0.25$. The eavesdropping ability effectively gives $C$ a slightly lower QS threshold than that of $B$. (Note that for $\epsilon = 0$ , $\Delta g(T_{end}) = 0$ everywhere, because here $B$ and $C$ are exactly alike). For values of $K_T$ higher than the maximum inducer/toxin concentration possible for either species at steady state, $(\alpha + \beta)/\delta \approx 5$, competition becomes neutral ($\Delta g(T) \approx 0$). For high $K$ (above $K \approx 0.5$) neither $B$ nor $C$ induces and toxin is never produced at a high rate. We do not plot $\Delta g$ for very low $K_T$ since for $K_T \lesssim \frac{\beta}{\delta} = 10^{-2}$, the assumption of toxin concentration being proportional to inducer concentration causes problems: If the steady state level of toxin/inducer is already at a level where the toxin is potent when the bacteria are only producing at the low basal rate $\beta$, then there is no need to turn on QS and incur the cost of further toxin production. This means that our simplified model wrongly predicts that for very low $K_T < \frac{\beta}{\delta}$ early QS turn on due to eavesdropping is not advantageous, while a more detailed model with separate equations for the toxin concentration (in particular, equations that account for the zero basal production rate of toxin) would show that for low $K_T$, early turn on does give an advantage. Because very low $K_T$ is not biologically realistic and would effectively constitute a situation where the benefit function of the common good is not convex, we are anyway not interested in this parameter range and thus deemed it acceptable that the model is not valid here.

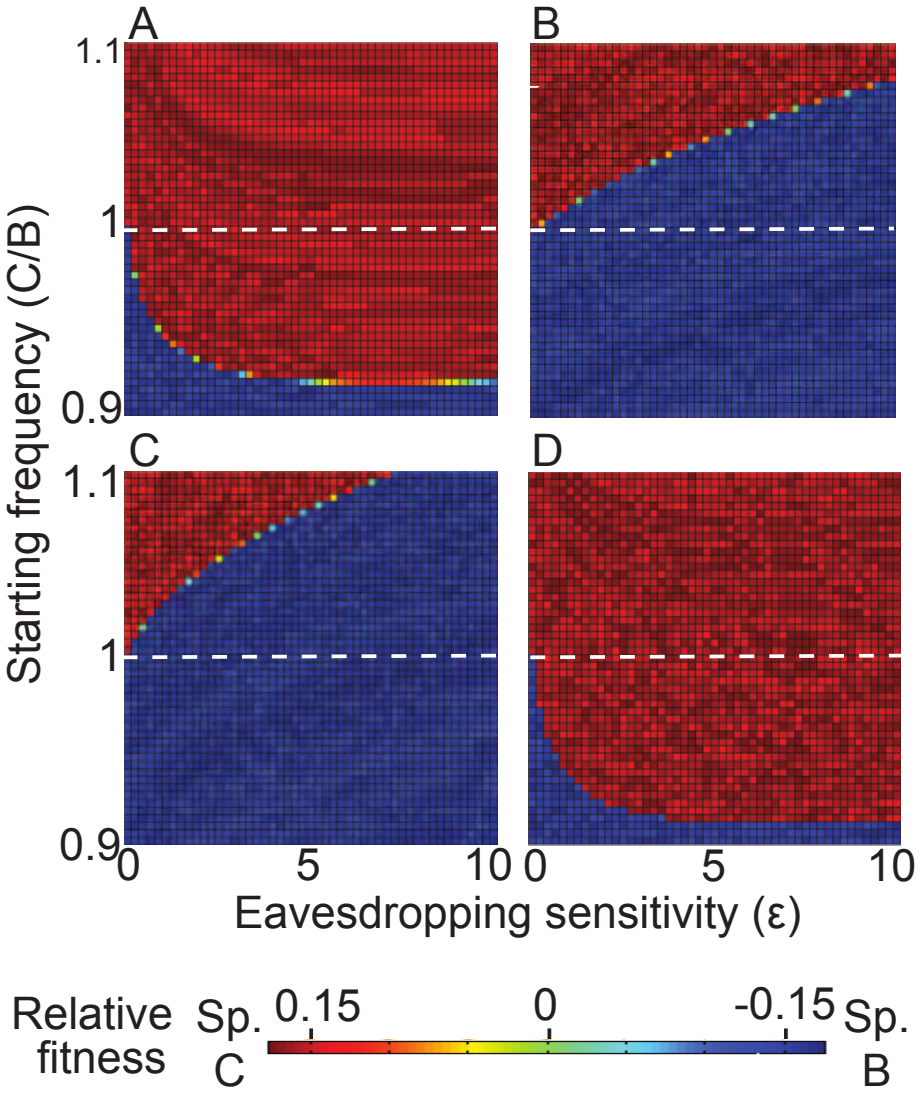


Figure 5.6: **Eavesdropping can either provide an advantage or a disadvantage depending on K and $K_T$.** Plots show relative fitness $\Delta g$ as a function of the initial ratio ($C(0)/B(0)$) and the eavesdropping sensitivity $\epsilon$ of $C$, for different values of $K$ and $K_T$. ($K_T = 3.0$ for A, B and C and $K_T = 0.3$ for D). **A:** The QS activation threshold for production of the antibiotic is relatively high for both species, ($K = 0.01$). **B:** The QS activation threshold is lower ($K = 0.003898$). This value corresponds to the optimal threshold value $K'$ that is the best value of $K$ for each species to have when there is no eavesdropping (see section 5.4.4). **C:** Both species have an activation threshold ($K = 0.003$) lower than the optimal threshold. **D:** The same parameters were used as in C, except that $K_T$ was reduced tenfold. This changes the optimal activation threshold to $K' = 0.001113$, which is below the activation threshold value used ($K = 0.003$).

inducer/toxin. Finally, in order to make the growth rates linear functions of the cell densities, we no longer impose a carrying capacity on the system. The equations of the simple model are thus:

$$\frac{dB}{dt} = \begin{cases} B & \text{if } I_B < K_B \\ B(1-r) & \text{if } K_B < I_B < K_T \\ B(1-r-k) & \text{if } I_B > K_B \text{ and } I_C > K_T \end{cases} \quad (5.8)$$

$$\frac{dC}{dt} = \begin{cases} C & \text{if } I_C < K_C \\ C(1-r) & \text{if } K_C < I_C < K_T \\ C(1-r-k) & \text{if } I_C > K_B \text{ and } I_B > K_T \end{cases} \quad (5.9)$$

$$\frac{dI_X}{dt} = \begin{cases} X(t)\beta & \text{if } I_X < K_X \\ X(t)\alpha & \text{if } I_X > K_X \end{cases} \text{, where } X \text{ is an index } C \text{ or } B, \text{ and } \beta \ll \alpha \quad (5.10)$$

**Behaviour of the simple model and comparison with the full model.** In this model the only property that makes $B$ different from $C$ is the induction threshold (apart from this, because there is no eavesdropping, the equations are exactly symmetric in $B$ and $C$). Thus, $B$ and $C$ can be in one of four states:

1. Growing exponentially at the rate 1. In this state the bacteria are not affected by the presence of the other species at all.

2. Growing exponentially at the rate $1-r$, where $0 < r < 1$. In this state the bacteria are producing toxin and thus paying a cost for toxin production, but the enemy's toxin is not high enough to affect the growth rate.

3. Growing exponentially at the rate $1-r-k$. The bacteria are producing toxin and thus paying a cost, and the enemy's toxin has crossed the critical concentration $K_T$ so the bacteria are also dying at a rate $k$.

4. Growing/decaying exponentially at the rate $1-k$. The bacteria have not yet started toxin production but the enemy's toxin has crossed the critical concentration $K_T$.[3]

[3]This last option is not listed in eq. 5.8 and 5.9 because it requires $K_B$ and $K_C$ to be very different and/or roughly the same magnitude as $K_T$. We are only interested in the case where they are relatively close to each other and much smaller than $K_T$. Since $I_X$ plays the role of both the signal and the toxin in this model, it is biologically unrealistic to put the "kill threshold" $K_T$ at the same level as the thresholds for quorum sensing induction.

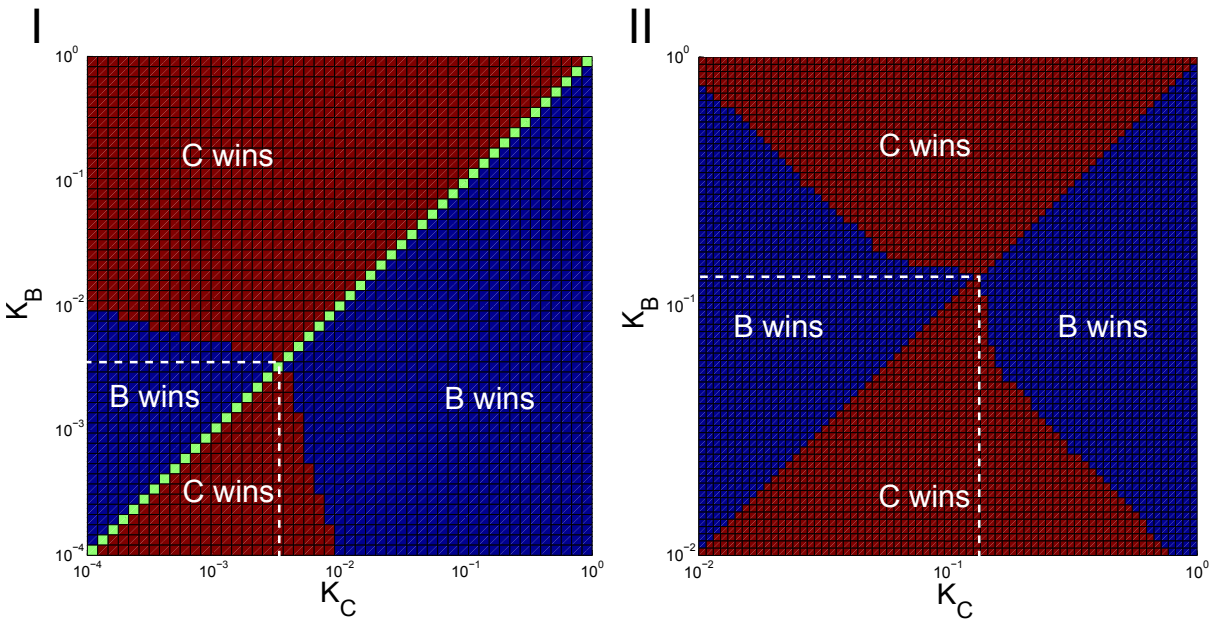


Figure 5.7: **Competition outcome of simple and full models, without eavesdropping, as a function of the QS inductions thresholds $K_B$ and $K_C$.** Although quantitatively the two models have very different outcomes we see that the overall qualitative behavior is very similar. For both models we see that whenever $K_B$ is at a certain value ($K'$ - marked by white dashed lines) it cannot be beat by any other threshold. Below $K'$, $K_B$ can only be beaten by a threshold higher than itself, and above this value it can only be beaten by a lower threshold than itself (and vice versa when we look at things from $C$'s perspective). It is this value $K'$ below which eavesdropping gives no advantage in the full model for $K \equiv K_B = K_C$. **I:** Full model with no eavesdropping ($\epsilon = 0$), and with different QS thresholds ($K_B$, $K_C$) for $B$ and $C$. In red regions $C$ wins and in blue regions $B$ wins at time $T_{end}$. On the boundaries between red and blue regions, $B$ and $C$ do equally well. Parameters and initial conditions used were: $C_0 = B_0 = 0.001$, $r = 0.25$, $K_T = 3$ (other parameters were as in Table 5.1). **II:** Simple model without eavesdropping. In red regions $C$ wins and in blue regions $B$ wins at time $T_{end}$. On the boundaries between red and blue regions, $B$ and $C$ do equally well. Parameters and initial conditions used where: $C_0 = B_0 = 1, \alpha = 1, \beta = (1/100), r = 0.5, k = 0.7, K_T = 5$.

In fig. 5.7 the competitive outcomes of the simple model without eavesdropping and the full model with ($\epsilon = 0$) and with different QS thresholds ($K_C, K_B$) are plotted side by side for comparison. We see here that although quantitatively the two models are different, the overall qualitative behavior is very similar. For both models, whenever $K_B$ or $K_C$ is below a value ($K'$) it can only be beat by a threshold higher than itself. Consistent with this, is the fact that in the full model where $K \equiv K_B = K_C$, when $K < K'$, eavesdropping gives no advantage (see fig. 5.6).

**An optimal quorum sensing threshold.** We can thus conclude that for a system with two quorum sensing toxin producing bacteria where there is *no* eavesdropping going on, there exists an optimal threshold (equal to $K'$) which cannot be beaten by any other threshold higher or lower. The existence of such an optimum comes from the fact that in both models, the toxin only becomes efficient above a certain concentration and that production of toxin comes at a cost. Thus, a species with $K_C < K^{'}$ up against a species with $K_B = K^{'}$ will lose because it is paying the costs of producing toxin but, because the kill threshold $K_T$ is much larger, not producing enough toxin to gain the benefit of killing its competitor. Conversely, bacteria with a threshold $K_C > K^{'}$ up against a species with $K_B = K^{'}$ will lose because it does not start toxin production early enough. $K = K^{'}$ is the best compromise between not paying a cost too early and not starting toxin production too late. In a "game" where two players ($B$ and $C$) each have to pick a QS induction threshold, $K'$ would thus be the evolutionary stable strategy, and therefore also the Nash equilibrium [74], because at this threshold, no other competing species with a threshold higher or lower can beat it.

**Analytical solution of the simple model.** We solve the simple model analytically in the limit where $K_B, K_C \ll K_T$ and $K_B$ and $K_C$ are not too different. This allows us to investigate deeper how the optimum, $K'$ depends on other parameters of the model, like $K_T$, $r$ and $k$. The solutions to the system in eq. 5.8, 5.9 and 5.10 when the initial conditions are $C(0) = C_0$, $B(0) = B_0$ are:

$$C(t) = \begin{cases} C_0 \exp(t) & \text{for } 0 < t < t_1^C \\ C_0 \exp\left(t_1^C r\right) \exp((1-r)t) & \text{for } t_1^C < t < t_2^B \\ C_0 \exp\left(t_1^C r + k t_2^B\right) \exp((1-r-k)t) & \text{for } t_2^B < t \end{cases} \tag{5.11}$$

$$B(t) = \begin{cases} B_0 \exp(t) & \text{for } 0 < t < t_1^B \\ B_0 \exp\left(t_1^B r\right) \exp((1-r)t) & \text{for } t_1^B < t < t_2^C \\ B_0 \exp\left(t_1^B r + k t_2^C\right) \exp((1-r-k)t) & \text{for } t_2^C < t \end{cases} \tag{5.12}$$

$$I_X(t) = \begin{cases} \beta x_0 \left(\exp(t) - 1\right) & \text{for } \quad 0 < t < t_1^X \\ K_X + \frac{\alpha}{1-r} X_0 \mu_X \left[\exp((1-r)t) \mu_X^{-(1-r)} - 1\right] & \text{for } \quad t_1^X < t < t_2^Y \\ K_X + \frac{\alpha}{1-r} X_0 \mu_X \left[\left(\frac{K_T - K_Y}{\frac{\alpha}{1-r} Y_0 \mu_Y} + 1\right) \left(\frac{\mu_Y}{\mu_X}\right)^{1-r} - 1\right] + \ldots & \\ \ldots + \frac{\alpha}{1-r-k} \left(X_0 \mu_X^r \left(\frac{K_T - K_Y}{\frac{\alpha}{1-r} Y_0 \mu_Y} + 1\right) \mu_Y^{1-r}\right) \ldots & \text{for } \quad t_2^Y < t \\ \ldots \times \left[\exp((1-r-k)t) \left(\left(\left(\frac{K_T - K_Y}{\frac{\alpha}{1-r} Y_0 \mu_Y} + 1\right) \mu_Y^{1-r}\right)^{\frac{-(1-r-k)}{1-r}}\right) - 1\right] & \end{cases} \tag{5.13}$$

where $X$ is an index that goes over the values "$B$" and "$C$", and $Y$ takes the "opposite" value meaning that when $X = B$ then $Y = C$, and vice versa. $\mu_X \equiv 1 + \frac{K_X}{\beta X_0}$. $t_1^X$ is the time where then concentration of the signal/toxin of bacteria type $X$ reaches the induction threshold $K_X$ (here the toxin/signal production rate jumps from $\beta$ to the much higher $\alpha$, and the growth rate drops from 1 to $1 - r$). $t_2^X$ is the time where signal/toxin of bacteria type $X$ reaches the critical concentration $K_T$ where it is potent enough to kill the enemy type. When $K_B \simeq K_C$ and $K_B, K_C \ll K_T$ the order of events is always such that $t_1^B, t_1^C < t_2^B, t_2^C$, (see fig. 5.8). Depending on parameters, either $t_2^B < t_2^C$ or vice versa – we will denote whichever is the smaller of the two times as $t_{2,first}^Y$ and the larger of the two as $t_{2,last}^X$.

**Determining the optimal induction threshold.** The time point at which it becomes apparent which species will dominate in the simple model is the moment where the toxin concentration of the second bacteria species reaches $K_T$; the species which has the largest population at this point is the winner. The battle between the two before this point is all about reaching the critical toxin concentration $K_T$ fast while at the same time having a large population size when the opponent's toxin concentration reaches $K_T$. Waiting a long time before induction (having

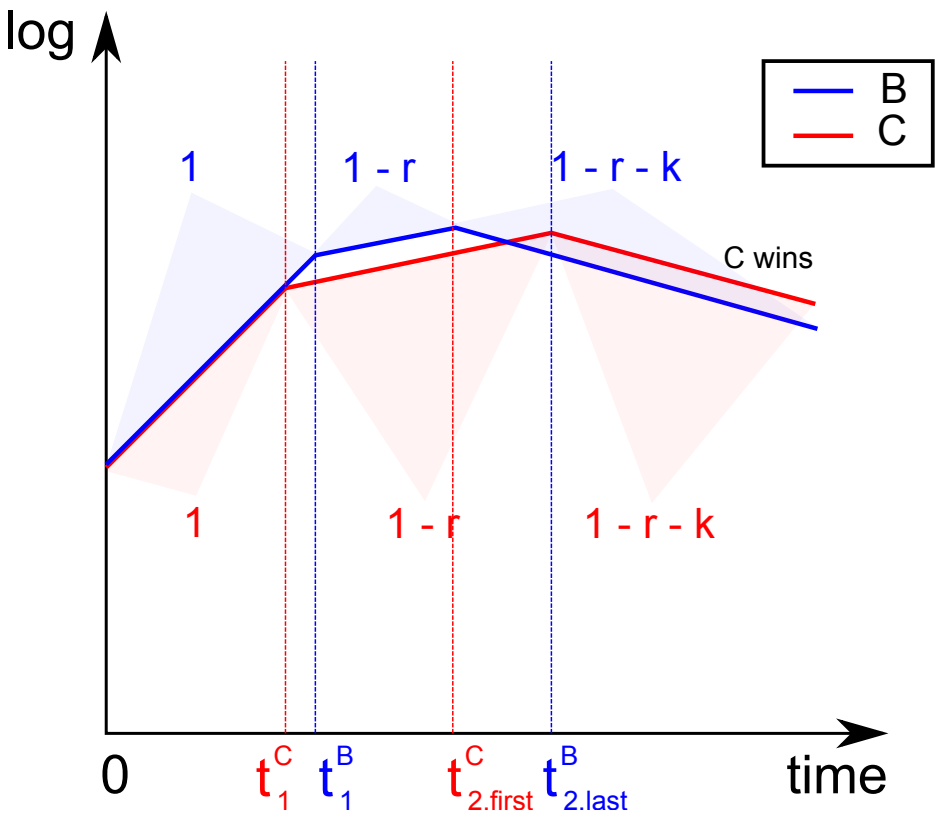


Figure 5.8: **Population dynamics in simple model without eavesdropping.** Schematic figure showing an example of how populations of $B$ and $C$ can develop over time in the simple model without eavesdropping. $t_1^C$ is the time where inducer/toxin of $C$ reaches a concentration of $K_C$, $(I_C(t_1^C) = K_C)$. $t_1^B$ is the time where inducer/toxin of $B$ reaches a concentration of $K_B$, $(I_B(t_1^B) = K_B)$. $t_2^C$ is the time where inducer/toxin of $C$ reaches a concentration of $K_T$, $(I_C(t_2^C) = K_T)$. $t_2^B$ is the time where inducer/toxin of $B$ reaches a concentration of $K_B$, $(I_B(t_2^B) = K_T)$. In this plot $K_C < K_B$ ($C$ induces first), and $C$ is also the first to reach a toxin concentration of $K_T$. Even though $B$ heads the race for a while after $t_1^C$, $C$ manages to catch up by $t_2^B$ and ultimately wins. The plot also indicates the rate of exponential growth/decay of the species at different times.

a high induction threshold $K_X$) gives a long time span with exponential growth at the highest possible rate, 1, and thus allows for quick population growth, while early induction (having a low induction threshold $K_X$) results in earlier toxin production at the high rate $\alpha$ and thus allows for quicker toxin build up. There thus exists a trade off between getting a high population and producing toxins fast and the optimal induction threshold, $K'$, puts the turn-on time at an optimal point somewhere between early and late turn on. In order to determine the optimal threshold value we need to know the time at which the toxin of the second species will reach the concentration $K_T$. We can use the fact that (by definition) $I_X(t_1^X) = K_X$ and $I_X(t_2^X) = K_T$ to find expressions for $t_1^X$, $t_{2,first}^Y$ and $t_{2,last}^X$:

$$I_X(t_1^X) = K_X \Rightarrow \tag{5.14}$$

$$t_1^X = \log(\mu_X) \tag{5.15}$$

(recall that $\mu_X \equiv 1 + \frac{K_X}{\beta X_0}$).

In the case where species $X$ reaches $K_T$ before species $Y$, $t_1^Y < t_1^X$ (and $1 - r \neq k$), we have:

$$I_Y(t_{2,first}^Y) = K_T \Rightarrow \tag{5.16}$$

$$t_{2,first}^Y = \frac{1}{1-r} \log\left[\left(\frac{K_T - K_Y}{\frac{\alpha}{1-r} Y_0 \mu_Y} + 1\right) \mu_Y^{1-r}\right] \tag{5.17}$$

and

$$I_X(t_{2,last}^X) = K_T \Rightarrow \tag{5.18}$$

$$t_{2,last}^X = t_{2,first}^Y + \frac{1}{1-r-k} \log\left[\frac{1-r-k}{\alpha X_0 \mu_X^r \left(\frac{K_T - K_Y}{\frac{\alpha}{1-r} Y_0 \left(1 + \frac{Y}{\beta Y_0}\right)} + 1\right) \mu_Y^{1-r}} \times \ldots\right.$$

$$\left. \ldots\left(K_T - \left(K_X + \frac{\alpha}{1-r} X_0 \mu_X \left[\left(\frac{K_T - K_Y}{\frac{\alpha}{1-r} Y_0 \mu_Y} + 1\right)\left(\frac{\mu_Y}{\mu_X}\right)^{1-r} - 1\right]\right)\right) + 1\right] \tag{5.19}$$

Note that expression (5.19) is only valid when species $Y$ is first to induce ($K_Y < K_X$) and species $X$ reaches $K_T$ last (that is we have $t_1^Y < t_1^X < t_2^Y < t_2^X$ ). When species $X$ is first to induce but reaches $K_T$ last ( $t_1^X < t_1^Y < t_2^Y < t_2^X$ ), $Y$ always wins, so we know that if $K_X < K_Y$ and $t_{2,first}^Y < t_{2,last}^X$ then $Y$ has already won. For the cases where $t_1^Y < t_1^X < t_2^Y < t_2^X$ (and either species could win) we can determine the winner by finding the ratio $f \equiv \frac{X(t_{2,last}^X)}{Y(t_{2,last}^X)}$ (i.e., $f > 1$ whenever species $X$ is the winner). When $K_B = K_C$ and thus $t_1^B = t_1^C$, and $t_2^B = t_2^C$, $f$ is of course 1. However, it turns out there is also another way of getting $f = 1$ while having $K_B \neq K_C$. When we express $K_C = K_B + \Delta$, and plot the ratio $f$ as a function of $K_C$ and $\Delta$ we see that there are in general two solutions $\Delta_0 = 0$ and $\Delta_1$ to the equations $f = 1$, for a given $K_C$ (see fig. 5.9). The value of $K_C$ where these two solutions intersect, $\Delta_0 = \Delta_1(K_C) = 0$, is the optimal induction threshold $K'$.

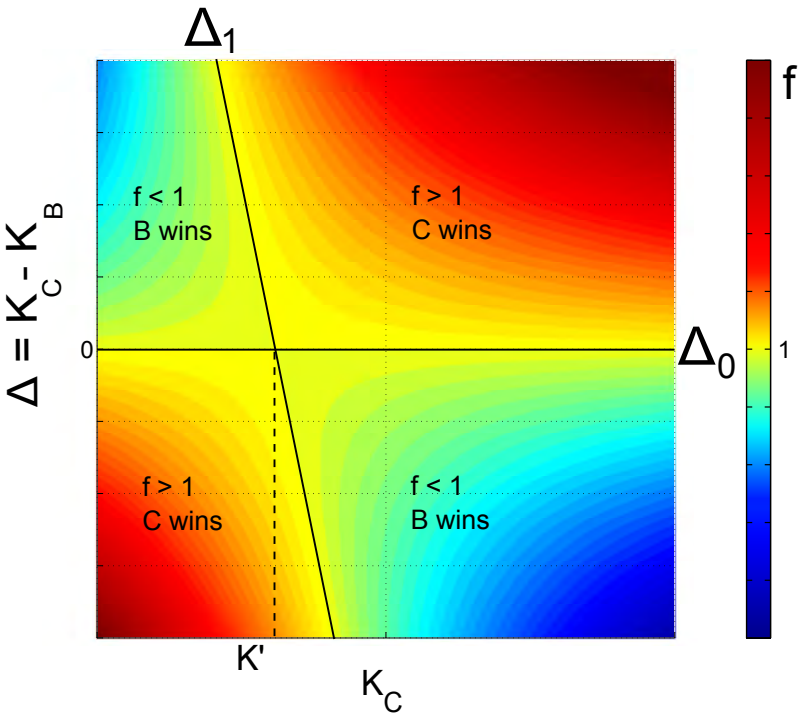


Figure 5.9: **Determining the optimal QS threshold K′.** Schematic figure showing $f = \frac{C(t^X_{2,last})}{B(t^X_{2,last})}$, (where $X$ is an index that takes values "$C$" or "$B$") plotted as a function of $K_C$ and $\Delta = K_C - K_B$. The equation $f = 1$ has two solutions: one trivial, $\Delta_0 = 0$, and one nontrivial, $\Delta_1(K_C)$. The optimal turn on threshold $K'$ is found where the two solutions intersect.

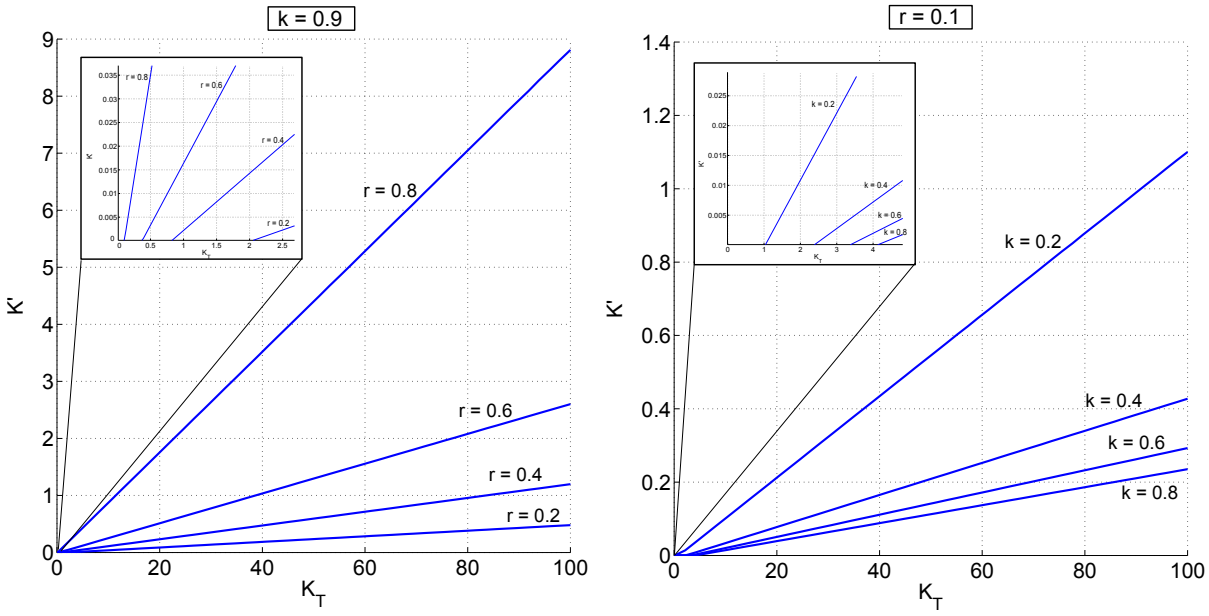


Figure 5.10: **Optimal QS threshold as a function of $K_T$.** Blue lines: Value of $K'$, as a function of $K_T$, found numerically by determining the intersection of $\Delta_0$ and $\Delta_1(K_C)$ for different $r$ and $k$ values. Parameters used were: $C_0 = B_0 = 1, \alpha = 1, \beta = (1/100)$.

**Dependence of the optimal induction threshold on various parameters.** In fig. 5.10 we have plotted the value of $K'$ (found numerically by determining the intersection of $\Delta_0$ and $\Delta_1(K_C)$ ) as a function of $K_T$ for different values of the toxin cost parameter, $r$, and the toxin potency, $k$ (which are the same for both species). We see that the optimal QS induction threshold $K'$ is proportional to $K_T$ and that a high cost of toxin raises the threshold while a high toxin potency lowers the threshold. For very low values of $K_T$ (when the common good benefit function is effectively no longer convex) the optimal threshold goes to zero, and thus here there would be no need for QS regulation of the toxin production. In fig. 5.11 we see $K'$ plotted as a function of $r$ and $k$ (for fixed $K_T$). We see that when toxin potency, $k$, becomes very low then the optimal threshold diverges, i.e. when toxin is not very efficient compared to the cost of production it is best not to turn on production at all. Similarly when cost of production becomes very large compared to the basal growth rate ($g = 1$), we see $K'$ become very large. For deceasing costs we see that $K'$ will go to zero rapidly at a non-zero value of $r$. Increasing toxin potency will also cause $K'$ to decrease but in this case more and more slowly for higher values of $k$,[4], this means that even though the toxin might be infinitely potent once $K_T$ is reached, this still does not mean that constitutive toxin production is a good idea. Only

[4]In fig. 5.11 left, $k$ only goes to 1, but we checked much much higher values of $k$ and observed that $K'$ still does not go fully to zero.

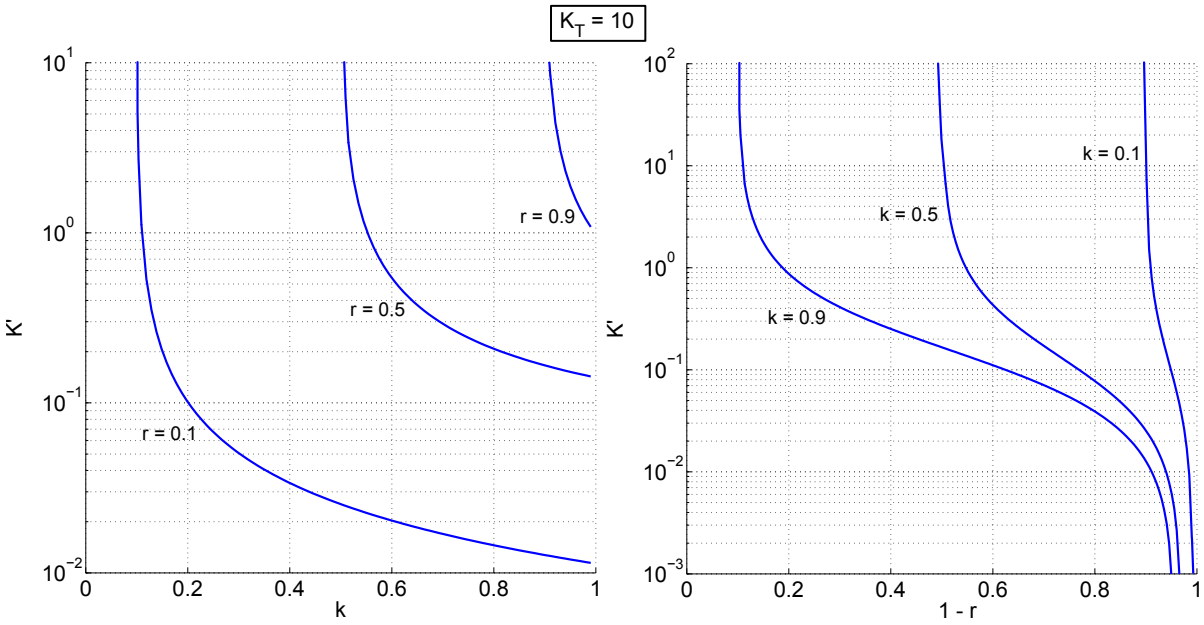


Figure 5.11: **Optimal QS threshold as a function of k and r.** Blue lines: Values of $K'$ found numerically by determining the intersection of $\Delta_0$ and $\Delta_1(K_C)$ for different $r$ and $k$ values. Parameters used were: $C_0 = B_0 = 1, \alpha = 1, \beta = (1/100), K_T = 10.0$.

when cost, $r$, is very low and $K_T$ is also very low will the optimal induction threshold truly approach zero.

## 5.5 Discussion and future work

### 5.5.1 Eavesdropper versus eavesdropper

The biological system that inspired the modeling above consisted of two species out of which only one used the eavesdropping strategy. However, once this scenario has been considered one invariably ends up wondering: How would an eavesdropper do when competing with another eavesdropper? What is the Nash equilibrium, if any, in the game where both players are toxin producers with independent induction thresholds $K$ *and* eavesdropping sensitivities $\epsilon$? When two eavesdroppers are up against each other things get a bit complicated: Crudely speaking, from the behaviour of the full model described above, we would expect that a certain $(K_C, \epsilon_C)$-pair will result in a specific turn on behavior which will resemble that of a "pure" non-eavesdropping strategy $(K_{C,eff}, 0)$, and that this effective threshold $K_{C,eff}$ will depend on $K_C$, $\epsilon_C$, on the enemy $(K_B, \epsilon_B)$-strategy, and also on the starting ratio $(B_0/C_0)$.

**Difficulties determining the optimal $(K, \epsilon)$-strategy.** We have tried determining the optimal $(K, \epsilon)$-strategy when the initial ratio is $B_0/C_0 = 1$, using the minimax algorithm [133]: we first choose a $(K_B, \epsilon_B)$ strategy, play this against a large number of $(K_C, \epsilon_C)$ strategies and determine which of these maximizes the fitness (or "payoff" in the language of game theory) for $C$. We then repeat this for a large number of $(K_B, \epsilon_B)$ choices. Figure 5.12 shows the resulting maximum payoff for $C$ as a function of $(K_B, \epsilon_B)$ as well as the $(K_C, \epsilon_C)$ strategies that yield this maximum payoff, obtained by solving the differential equations in section 5.3 using a 5th order Runge-Kutta scheme [96]. The strategy (or strategies) that minimizes this maximum payoff is the optimal strategy, and may also be a Nash equilibrium. The exact result in this particular case however turns out unfortunately to depend in a highly sensitive manner on, for example, the choice of ODE solver. It seems that because the the system is bistable and both species grow exponentially, the simulations are highly sensitive to small numerical errors, which tend to amplify and then cause different ODE solvers to reach different "solutions". So, while the overall qualitative trends seen in fig. 5.12 are consistent across ODE solvers and therefore trustworthy, the quantitative details should be approached with caution. Another source of quantitative error is that so far we have sampled the $(K, \epsilon)$-strategy space at a set of points lying on a regular lattice. Even here we find that small shifts in the $K_B$ or $\epsilon_B$ values can result in large changes in the $(K_C, \epsilon_C)$ strategy that maximizes payoff for $C$. Thus, by sampling on a regular grid we might miss the real optimal strategies which lie off-grid. An alternative approach would be to use a minimization/maximization algorithm like for example Steepest descent [96], but this will unfortunately have to be left to future work due to time constraints.

**A line of strategies which are hard to beat.** From the simulations done so far we can only conclude that for $B_0/C_0 = 1$ there appears to be a line in $(K_B, \epsilon_B)$-space where the maximal payoff is lowest, and very close to zero. This line has its end point at $(K_B = K', \epsilon = 0)$ as expected (see the discussion of optimal thresholds when there is no eavesdropping in section 5.4.4), and has increasingly higher $K$ for higher values of $\epsilon$ (see fig. 5.12I). The $(K_C, \epsilon_C)$-strategies which appear to be beating, by a nose hair, the strategies on this nearly unbeatable line, are strategies which themselves are also somewhere on the line (see fig. 5.13). Also, it looks like in the close vicinity of this "hard to beat"-line very small changes in $K_B$ or $\epsilon_B$ will radically change the strategy of $(K_C, \epsilon_C)$ which is best at beating that $B$ strategy. For example, we see in fig. 5.12III that the $C$ strategies, which beat $B$ best, abruptly shift from having low to high $\epsilon$s when moving from just left of the "hard to beat" line to just right of it. All in all, with the knowledge we have from the simulations so far, we cannot yet distinguish between the following scenarios:

1. There is more than one Nash equilibrium, i.e. the entire line of "hard to beat"-strategies in $(K, \epsilon)$-space (or portions of it) consist of Nash equilibria.

2. There is just one Nash equilibrium somewhere on the "hard-to-beat"-line for a finite $\epsilon$.

3. The true "Nash equilibrium" is at $\epsilon \to \infty$, (in which case there effectively is no Nash equilibrium, but here evolution would tend to push values of $\epsilon$ higher and higher).

4. There is no Nash equilibrium and there exists rock-paper-scissor like cycles of different $(K, \epsilon)$-strategies on the "hard-to-beat"-line which can cyclically beat each other.

Even though we do not yet know the true nature of the strategies on the "hard to beat"-line in $(K, \epsilon)$-space, we do know that in any real world scenario the starting ratio will of course never be exactly one, and that there would be plenty of environmental sources of noise influencing the population levels of both species. Therefore, biologically speaking, it might not matter much whether the line really consists of true Nash equilibria or not, because no real world scenario could ever be precise enough to hit the exact values needed. Our best bet so far is that all strategies along the line are effectively equal in any realistic scenario with noise. This conclusion would imply that there is not any strong reason to pick an eavesdropping strategy from somewhere on the line over the non-eavesdropping strategy of $(K', \epsilon = 0)$, when the starting ratio is $B_0/C_0 = 1$ or close to it.

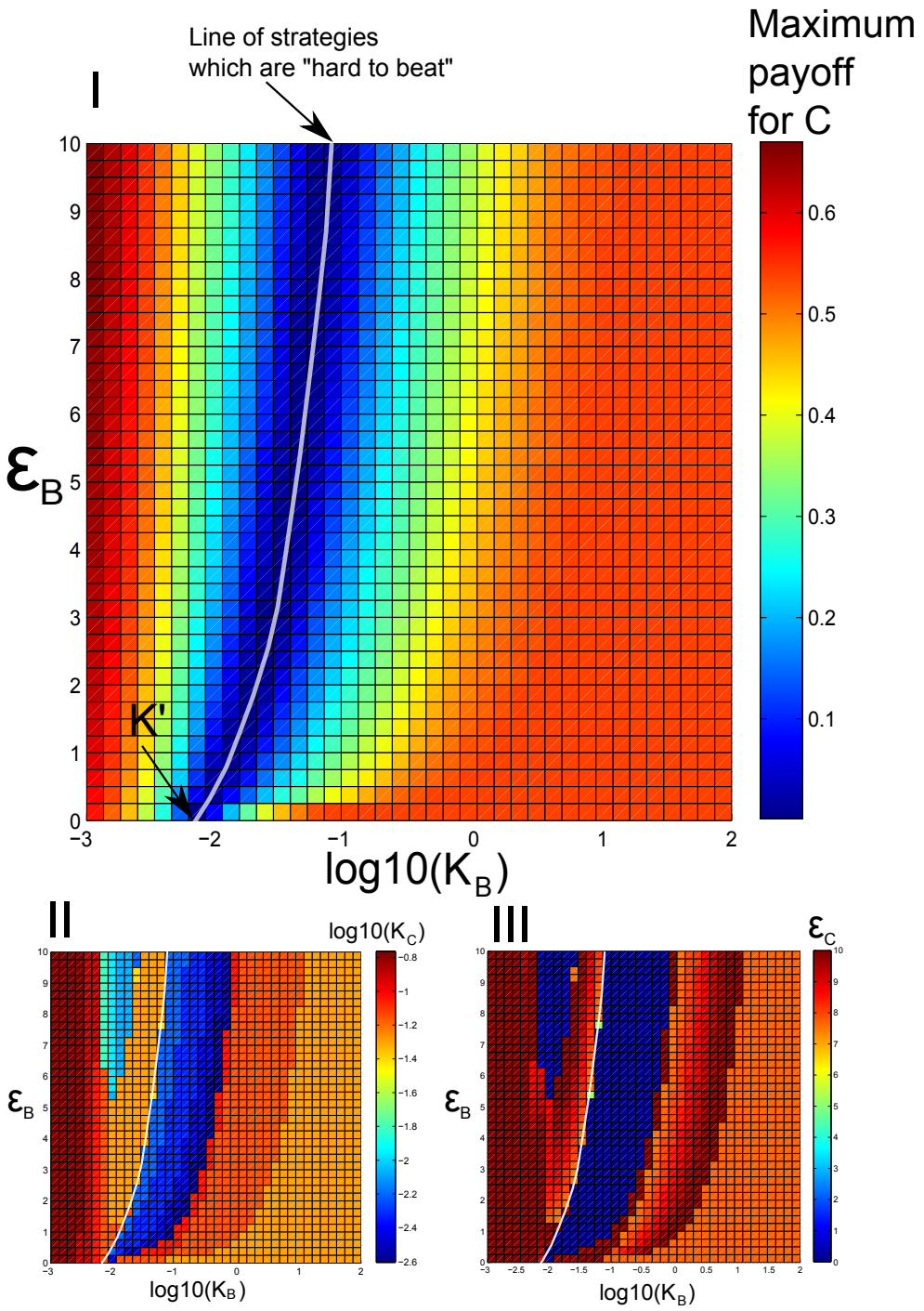


Figure 5.12: **Maximum payoff for C as a function of $K_B$ and $\epsilon_B$ in the game of $(K_B, \epsilon_B)$ vs. $(K_C, \epsilon_C)$ when initial ratio is** $B_0/C_0 = 1$. **I:** Maximum payoff ($\Delta g$) which $C$ can achieve as a function of the enemy threshold, $K_B$, and the enemy eavesdropping sensitivity $\epsilon_B$ which $C$ is playing against. We see that there is a line of strategies (marked by a white line) which have payoffs very close to zero, and that this line starts at $(K_B = K', \epsilon_B = 0)$. **II:** The threshold value, $K_C$, used by $C$ to beat the $(K_B, \epsilon_B)$-strategy and get the payoff shown in I. **III:** The eavesdropping sensitivity, $\epsilon_C$, used by $C$ to beat the $(K_B, \epsilon_B)$-strategy and get the payoff shown in I.

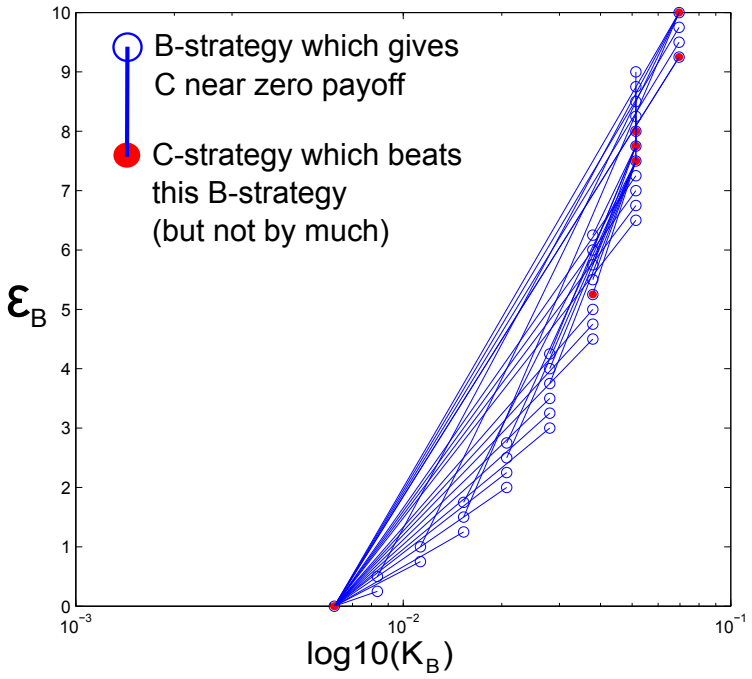


Figure 5.13: **Who is beating whom?** Blue circles show $(K_B, \epsilon_B)$-strategies on the "hard to beat"-line (in other words the $B$-strategies which give $C$, at best, a very small but positive payoff - see fig. 5.12l). Red dots show the $C$-strategies which beat the $B$-strategies on the "hard to beat"-line by a tiny amount. There is a blue line connecting each $B$-strategy to the $C$-strategy which beat it (thus there can be several lines going from a red dot, but only one line leading from a blue circle). We see that the $C$ strategies which beat the $B$-strategies on the "hard to beat"-line are themselves also somewhere on this line.

### 5.5.2 Varying the initial ratio of population densities

So far we have focused on determining the optimal strategy in the situation where initial ratio ($B_0/C_0$) of the populations of the two potentially eavesdropping enemies was 1. When the starting ratio is not one, we see that the line of lowest maximal payoffs for $C$ in $(K_B, \epsilon_B)$-space is slightly different than the line obtained for $B_0/C_0 = 1$ (see fig. 5.14).
For future work, it would be interesting to look more at which $(K, \epsilon)$-strategy is optimal when averaging over a range of different starting ratios. Consider for instance a situation where one non-eavesdropping species (let's say $B$) has a far higher starting density than the other. Here it could be that the the optimal threshold for $B$ would be higher than for a starting ratio of one. Being at a far higher starting density than the enemy starts to resemble the situation where you are growing alone with no enemy present and in this situation it is optimal to postpone the costly toxin production as long as possible because it is not needed. For the opposite situation - starting at a lower density than the enemy - it is not intuitively very clear what will happen to the optimal $(K, \epsilon)$ strategy. The results seen in fig. 5.6A and D suggest that when the one species starts out with a higher density, then its enemy can gain from starting toxin production slightly earlier to compensate for low numbers, and that this early induction can be implemented either by simply lowering $K$ or by eavesdropping on the enemy signal (i.e. having non-zero $\epsilon$). On the other hand, one could imagine that having a very large $\epsilon$, when starting out at a lower density than the enemy, would result in induction at a lower density than desired. In fig. 5.14 right panel, where $B$ is at a disadvantage initially, it looks like optimal strategies in general lie at higher $K$ values when $\epsilon$ is high, whereas the optimal strategies at low $\epsilon$ values do not shift. This fits the interpretation that high $\epsilon$ makes you vulnerable to being forcibly induced when enemy density is high.
It seems that the optimal $(K, \epsilon)$-strategy depends very sensitively on many factors including the starting ratio ($B_0/C_0$). Because real world scenarios would probably entail a range of different situations where a species is either alone or together with enemies at various different densities, it seems that a truly optimal $(K, \epsilon)$-strategy should optimize performance averaged over a range of different situations. How the terms in this average should be weighted is completely unknown, but one starting assumption could be to set $B_0 + C_0 \equiv X$, and $B_0 = fX$ and $C_0 = (1 - f)X$, and iterate through $f \in [0, 1]$, (see fig. 5.14 for the results of two sample simulations where the maximum payoff for $C$ is plotted for $f = 0.6$ and $f = 0.4$).

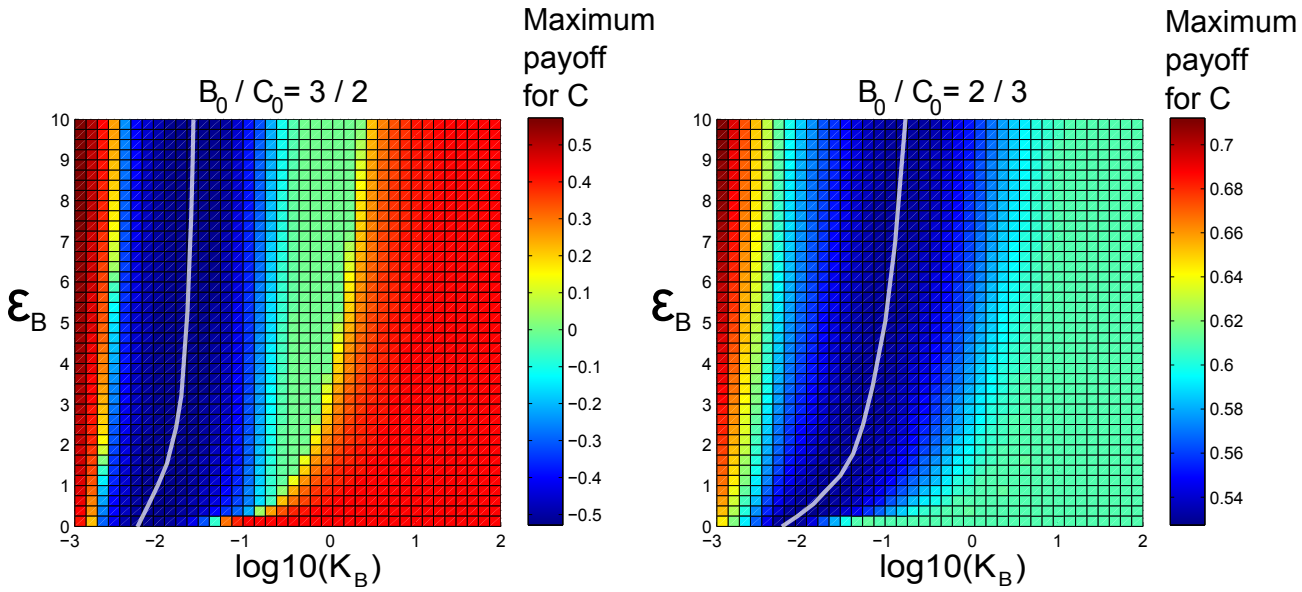


Figure 5.14: **Initial ratio different from one.** Maximum payoff ($\Delta g$) which $C$ can achieve as a function of the enemy threshold, $K_B$, and the enemy eavesdropping sensitivity $\epsilon_B$ which $C$ is playing against for starting ratios of $B_0/C_0 = 3/2$ (left panel) and $B_0/C_0 = 2/3$ (right panel). The line of strategies where $C$ has lowest maximum payoffs is marked by a white line. We see that when $B$ starts at a disadvantage (right) then the line of best strategies for $B$ (marked by a white line) is slightly different than when $B$ starts with an advantage (left).

**Eavesdropping - providing a differentiated response for different environments?** If we imagine a species which often experiences growth both alone and in the presence of enemies, then this would correspond to a situation where when we determine the optimal strategy we should average over different starting density ratios (some of which should have no enemy present at all). When growing alone, it is undoubtedly best to delay induction indefinitely, i.e., it is best to have a very high $K$, whereas when growing with an enemy, the optimal induction threshold, $K$, should have an intermediate value. Because eavesdropping provides a way of effectively lowering the induction threshold only when enemies are around, it could be argued that eavesdropping could provide the necessary differentiated response for a species often faced with the two different situations:

1. growth with an enemy
2. growth alone

Eavesdropping could thus perhaps be an adaptive response to existence in varying environments. Having a high $\epsilon$ would results in very different effective thresholds in situation 1 and 2, and thus a very differentiated response. Having a low $\epsilon$ on the other hand would mean being less sensitive to varying conditions – enemy or no enemy present, turn on would happen at roughly the same cell density. However, having a very high $\epsilon$ could also mean that you risk being sometimes forcibly induced by enemy signal in situations where toxin production is not beneficial. Choosing an optimal $\epsilon$ for existence in changing environments would depend, it seems, on *when* costs are greatest and which types of situations you encounter more often. If, for example, the Hill-factor of the toxin potency-curve $H$ is high and you often encounter situations where enemy density is higher than your own, then it could be disadvantageous to have a very high $\epsilon$. Put simply, in that scenario it would be more important to "listen" to your own signal than to the signal of the enemy. If, on the other hand, the cost of toxin production is high (high $r$), but toxin is also very potent even at low concentration (low $H$ and low $K_T$) then having a very differentiated response could become more important and the risk of induction at too low a density from listening to enemy signal would be negligible; in the most extreme case it seems that the optimal strategy would be to only induce due to enemy signal, and not respond to one's own signal at all – this would result in a very differentiated response pattern for different environments.

### 5.5.3 Eavesdropping mutant invading a non-eavesdropping population

It is worth thinking about how a mutant eavesdropper would be able to arise and invade a non eavesdropping population. When two similar species grow together, mutant $E$ and recent ancestor $C$, which both produce the same toxin (and thus will not harm each other, but only compete through the carrying capacity), then it is the one which induces first (let's say it is $E$) and thus pays the greatest cost who will lose ($E$ will have a lower fitness than $C$). When a third enemy species ($B$) is present, this is still the case. Because $E$ and $C$ produce the same toxin and both are sensitive to the toxin of $B$, both will feel equal benefit from the toxin produced regardless of where it came from, i.e. the one with the higher threshold ($C$) will thus effectively act as a cheat. If a mutant ($E$) thus only evolves to get a receptor with relaxed specificity (i.e. $\epsilon > 0$), but still has the same $K$ as the wild type ($C$) then this mutant would not be able to invade, because the eavesdropping would effectively lower the QS threshold whenever enemy $B$ was around. Only if the mutant first evolved to get a higher threshold and then a more relaxed receptor specificity, would it be able to invade. The two types of alterations, higher QS threshold and relaxed receptor specificity might however often come hand in hand, possibly via the same mutation: A receptor that mutates to become capable of binding other types of AHLs might very well also bind the original inducer molecule less efficiently, and thus effectively give the mutant a higher $K$. Thus, evolution from a "pure" non-eavesdropping strategy ($K = K'$, $\epsilon = 0$) towards strategies with ($K > K', \epsilon \neq 0$) could perhaps be partly driven by this phenomenon of "cheating your ancestor" which would happen when the mutant threshold was raised. The acquisition of a relaxed receptor and thus the ability to eavesdrop on enemy signals would then be merely a byproduct of this cheating strategy, which might later give an advantage when dealing with a toxin producing enemy $B$.

## 5.6 Take home messages

- Our experimental model system shows that *C. violaceum*'s ability to "eavesdrop" on *B. thailandensis*'s signal can provide it with a fitness advantage when grown in co-culture.

- A simple mathematical model without eavesdropping shows that there exists one optimal QS threshold $K'$ which cannot be beaten. This optimum arises because of a tradeoff between having a high growth rate and suppressing the growth rate of the enemy.

- When both species have the same QS threshold it is always an advantage to eavesdrop when that threshold is above the optimal value $K'$, but it is a disadvantage when the threshold is below $K'$.

- When two eavesdroppers are up against each other, we find that there exist many strategies that are hard to beat, with a range of different eavesdropping sensitivities.
- The optimal strategies, i.e. optimal induction thresholds, are different when bacteria grow alone and when the grow in the presence of an enemy. Eavesdropping provides a mechanism for effectively lowering the induction threshold only when enemies are around and thus it could be hypothesized that eavesdropping is an adaptive response to existence in varying environments.

# Concluding remarks

## Thoughts on modeling

A simple model is a tool for generating and exploring ideas about a system. It can, for example, take the form of a short list of well defined interaction rules between agents, or a set of simple equations. When thinking about a model gets confusing or when equations turn out be analytically intractable, a computer is helpful.

A good simple model is one with just the appropriate amount of information necessary to capture the dynamics in which we are interested. The level of detail included in the model needs to be in the "Goldilocks zone"[5] – not too much and not too little. If we put in too little we are unable to capture the features of the real system in which we are interested. If, on the other hand, we include too much, then we risk ending up with another complex system that we also do not understand.

In the model construction phase, theoreticians and experimentalists need to work very closely together and good interdisciplinary communications skills are crucial. A theory person needs to listen acutely and attentively to the vast stream of knowledge/information about a target organism that the collaborating microbiologists possesses and try and negotiate which details matter for the specific problem at hand, and weed out those that do not.

Simple qualitative models have the advantage that they often allow us to capture general dynamics common to many different species, ecologies, and settings. Throughout this thesis, my models are usually constructed with one particular organism in mind, but I have tried to keep them in such general terms that they may apply to many other species that could have similar interaction patterns as the original organism(s).

[5] "This porridge is too hot," Goldilocks exclaimed. So she tasted the porridge from the second bowl. "This porridge is too cold." So she tasted the last bowl of porridge. "Ahhh, this porridge is just right!" she said happily. And she ate it all up. - Children story by Robert Southey, 1837.

Above, I have outlined my ideals for modeling, but I am still learning, and the models I have constructed in this thesis are far from perfect. Often after a project is more or less finished and the article submitted, I get a strong suspicion that it would probably be a good idea to start all over and construct a new and improved model from scratch. Simple models are tools that we often design when we are still fumbling in the dark and they therefore often end up having flaws and peculiarity when looked at in hind sight. There is of course also a time and place for highly detailed modeling: for example when recreating experimental findings quantitatively down to every decimal number, for designing large scale integrated circuits and predicting the weather. But I personally prefer fumbling in the dark with a simple bacteria model anytime.

## Acknowledgments

I would like to thank Kim Sneppen, my supervisor, not only for his enthusiasm and acuity, but also for his ability to withdraw, allowing me plenty of time and space to explore my own ideas. Many thanks both to Kim Sneppen and (the Yin for his Yang) Mogens Høgh Jensen for giving me the opportunity to do a PhD degree at CMOL and for creating and maintaining a delightful and scientifically fruitful atmosphere in the K-building of NBI (a.k.a. home away from home). It will be a tearful goodbye to the CMOL table soccer table and the many fantastic people who have played with and against me around it.

Throughout my PhD studies Namiko Miterai has always had an open door and been ready to help with scientific problems of all sizes and sorts, providing me inspiration and consolation when needed. For this I am very grateful.

I would like to express my deep gratitude to Ben Kerr, who was my supervisor during my stay abroad at the University of Washington (UW) in Seattle. His sharp mind, lucid communication skills and an uncommon ability to bridge theory and experiment have both impressed and inspired me. I thoroughly enjoyed my time at UW and learned a lot from interacting with him and his delightful postdocs and students. At UW, I also found several formidable experimental collaborators: Sarah Hammarlund, Brook Peterson, Josephine Chandler, John Mittler and Pete Greenberg, whom I hope to continue working with in the near future.

The final month of writing this thesis was spent at the National Center for Biological Sciences (NCBS) in Bangalore, India, where zero distractions, a warm climate, delicious canteen food and a swimming pool made the writing process nearly bearable. This writing retreat was made possible by my perceptive and diligent NCBS collaborator Sandeep Krishna, whom I would like to thank deeply for his hospitality, valuable feedback, and supreme ideas.

Last but not least, thanks to my dear family: mom, dad, farmor, Lise, Janne, Gudbrandur, Sigrun, Sif, Hannah, Herdis, Clara and wonderful friends: Kirsten, Mikala, Pernille, Tatu and Kristoffer for putting up with my mental and physical absence, and for being interested and supportive, whenever I ranted about modeling bacteria.

I particularly want to thank two of my sisters, Sigrun and Hannah, for providing the beautiful cover picture and graphical design for the cover.

# Part III

# Appendix

# Appendix 1: Supplementary information for Chapter 1

### 5.6.1 Rates and probabilities

In the simulations time is incremented in constant steps of size $\Delta t \equiv 1$. In *each* time step *all* the sites in the grid have their state updated synchronously. Because of the constant time step used in the simulations, the constant rates for the Poissonian processes of phage infection, phage decay and phage diffusion, ($\alpha$, $\delta$ and $\lambda$), have to be reinterpreted in terms of probabilities that an event will happen in each time step $\Delta t$. The probability for one phage to decay during an infinitesimal time step $dt$ is: $\delta dt$. The macroscopic time step used in the simulations can be written as $\Delta t \equiv Mdt$. Thus the probability for a phage *not* to decay during a time span $\Delta t$ is:

$$1 - p_\delta = (1 - \delta dt)^M = \left(1 - \delta \frac{\Delta t}{M}\right)^M. \tag{5.20}$$

In the limit of $M \to \infty$, i.e. $dt \to 0$, this becomes:

$$1 - p_\delta = \lim_{M \to \infty} \left[\left(1 - \delta \frac{\Delta t}{M}\right)^M\right] = e^{-\delta \Delta t}. \tag{5.21}$$

which means that the probability to decay within the a time step $\Delta t$ is:

$$p_\delta = 1 - e^{-\delta \Delta t}. \tag{5.22}$$

Using the same argumentation as above, the probability for one phage to jump to a neighbor lattice site during a time step, can be expressed as:

$$p_\lambda = 1 - e^{-\lambda \Delta t}. \tag{5.23}$$

Note that this expression just gives the probability that a phage will jump at least once during a time step $\Delta t$. For large $\Delta t$ and large $\lambda$ it quickly becomes very probable that a phage jumps more than once in one time step. In the simulations, however, we do not allow phages to jump twice within one time step. Since the $\Delta t$ used is relatively large this is a crude approximation

but effectively it just results in a slightly smaller phage diffusion constant. The effective diffusion constant becomes $D \simeq 0.23\frac{\mu m^2}{min}$ instead of $D = \frac{1}{4}\frac{\mu m^2}{min}$ which $\lambda = 1$ would have given had the simulation time steps been infinitesimal (see [46]). Since phage can both decay and infect during a time step, $\Delta t$, the probability for a bacterium to get infected, $p_\alpha$, within a time step depends both on the number of phages, $N_0$, present in the site with the bacterium at the start of the time step, the infection rate per phage per bacterium, $\alpha$, and the degradation rate, $\delta$. Large numbers of phage and high infection rate increases the infection probability, while a high decay rate lowers it, since phages then have a high risk of decaying before they get to infect. We assume that the effect of phages who diffuse to neighboring sites during one time step and thereby miss the chance of infecting is negligible; the loss of phages in one time step due to diffusion will be somewhat balanced by flow in from neighboring sites. We consider the situation where one bacterium spends a time span of $\Delta t$ with a number of phage that infect with the rate $\alpha$, and decay with the rate $\delta$. The number of phage present at the beginning of the time step is $N_0$. The probability $1 - p_\alpha$ that no infection will happen in $M$ time steps of size $dt = \frac{\Delta t}{M}$ is approximately:

$$1 - p_\alpha = (1 - \alpha dt)^{N_0 e^{-\delta dt}}(1 - \alpha dt)^{N_0 e^{-2\delta dt}} \times \cdots \times (1 - \alpha dt)^{N_0 e^{-M\delta dt}}. \tag{5.24}$$

The exponents of the form $N_0 e^{-n\delta dt}$ stem from the fact that as time passes there are fewer and fewer phages left due to phage decay. The expression eq. 5.24 can be rewritten:

$$\left(1 - \alpha\frac{\Delta t}{M}\right)^{N_0 e^{-\delta\frac{\Delta t}{M}}}\left(1 - \alpha\frac{\Delta t}{M}\right)^{N_0 e^{-2\delta\frac{\Delta t}{M}}} \times \quad \cdots \quad \times\left(1 - \alpha\frac{\Delta t}{M}\right)^{N_0 e^{-M\delta\frac{\Delta t}{M}}} = \left(1 - \alpha\frac{\Delta t}{M}\right)^{N_0\sum_{i=0}^{M} e^{-i\delta\Delta t}} \tag{5.25}$$

$$= \quad \left(1 - \alpha\frac{\Delta t}{M}\right)^{N_0\frac{1-\exp\left(-\left(\frac{M+1}{M}\right)\delta\Delta t\right)}{1-\exp(-\delta\Delta t/M)}}. \tag{5.26}$$

When $M$ is large, the exponent of eq. 5.26 can be approximated by:

$$N_0\frac{1 - \exp\left(-\left(\frac{M+1}{M}\right)\delta\Delta t\right)}{1 - \exp\left(-\delta\Delta t/M\right)} \simeq N_0 M\frac{1 - \exp\left(-\delta\Delta t\right)}{\delta\Delta t} \tag{5.27}$$

(here we use the Taylor expansion of $(1 - e^x) \simeq x$ for $x \ll 1$, and the fact that $\frac{M+1}{M} \simeq 1$ for large $M$). When $M \to \infty$ a good approximation for the probability that an infection will happen in a time period $\Delta t$ is:

$$p_\alpha \simeq 1 - \left(1 - \alpha\frac{\Delta t}{M}\right)^{MN_0\frac{1-\exp(-\delta\Delta t)}{\delta\Delta t}} \tag{5.28}$$

$$\simeq 1 - \exp\left(-N_0\alpha\left(\frac{1 - \exp(-\delta\Delta t)}{\delta}\right)\right). \tag{5.29}$$

Here we use $\left((1 - \frac{x}{n})^k\right)^n \simeq (1 - k\frac{x}{n})^n$ for small $\frac{x}{n}$ and $\lim_{n\to\infty}\left((1 - k\frac{x}{n})^n\right) = \exp(-kx)$. It is expression eq. 5.29 which is used in the program to determine whether or not a bacterium

will become infected in one time step of size $\Delta t$ when there are $N_0$ phages in the same site as the bacterium at the beginning of the time step, and the phages decay with rate $\delta$ and infect with rate $\alpha$. In each time step of the simulation, the phages, at a site where there is also a bacterium, are first given the chance to infect with probability $p_\alpha$. If the bacterium gets infected, one phage is removed from the site and then the remaining phages risk decaying with probability $p_\delta$.

## 5.7 Right boundary of the co-existence region in the $\delta$-$\alpha$ plane

An analytical expression for the right boundary of the co-existence region in the $\alpha$–$\delta$ plane can be derived. Since the phages are very ineffective on the right boundary we can assume that the bacterial density is high ($B \simeq 1$) and that a bursting bacterium, on average, will have four healthy bacteria as nearest neighbors. The number of phages, originating from a burst, that will reach and infect one of the surrounding healthy bacteria in a single time step $\Delta t$ is, in this situation, given by:

$$\beta e^{-\delta \Delta t}(1 - e^{-\lambda \Delta t})(1 - e^{-\alpha_{eff} \Delta t}), \tag{5.30}$$

where $e^{-\delta \Delta t}$, $(1 - e^{-\lambda \Delta t})$ and $(1 - e^{-\alpha_{eff} \Delta t})$ are the respective probabilities to not decay, jump to a neighbor site, and infect a bacterium. The effective infection rate $\alpha_{eff} = \alpha(\frac{1-\exp(-\delta \Delta t)}{\delta})$ comes from the expression eq. 5.29 and accounts for the fact that the phage also need to survive for a while, after they have jumped to a neighbor site with a susceptible bacterium, before infecting it. To sustain the population, at the very least one phage needs to succeed in reaching and infecting a neighboring bacterium. That is, if a burst in a bacterial population of density $B \simeq 1$ will not result in at least one new infection on average, then the phage will die out. The right boundary, between co-existence and phage-extinction, for the Spatial model should thus lie at:

$$\beta \left(1 - e^{-\lambda \Delta t}\right) e^{-\delta \Delta t} \left(1 - e^{-\alpha_{eff} \Delta t}\right) = 1 \tag{5.31}$$

$$\Rightarrow \alpha = -\left(\frac{\delta}{1 - \exp(-\delta \Delta t)}\right) \log\left(1 - \frac{1}{\beta(1 - \exp(-\lambda \Delta t)) \exp(-\delta \Delta t)}\right). \tag{5.32}$$

In eq. 5.32 we assume that all phages either decay, or infect within the first two time steps after the burst. This is a fair approximation, as $B \simeq 1$ and $\Delta t(\alpha + \delta) \geq 1$. The expression in eq. 5.32 goes to infinity when

$$\beta(1 - \exp(-\lambda \Delta t)) \exp(-\delta \Delta t) = 1, \tag{5.33}$$

since $-\log(x) \to \infty$ for $x \to 0$. This means that there exists a maximal value for the degradation rate above which there can be no co-existence:

$$\delta_{max} = \log\left(\beta\left(1 - \exp\left(-\lambda \Delta t\right)\right)\right) \frac{1}{\Delta t}. \tag{5.34}$$

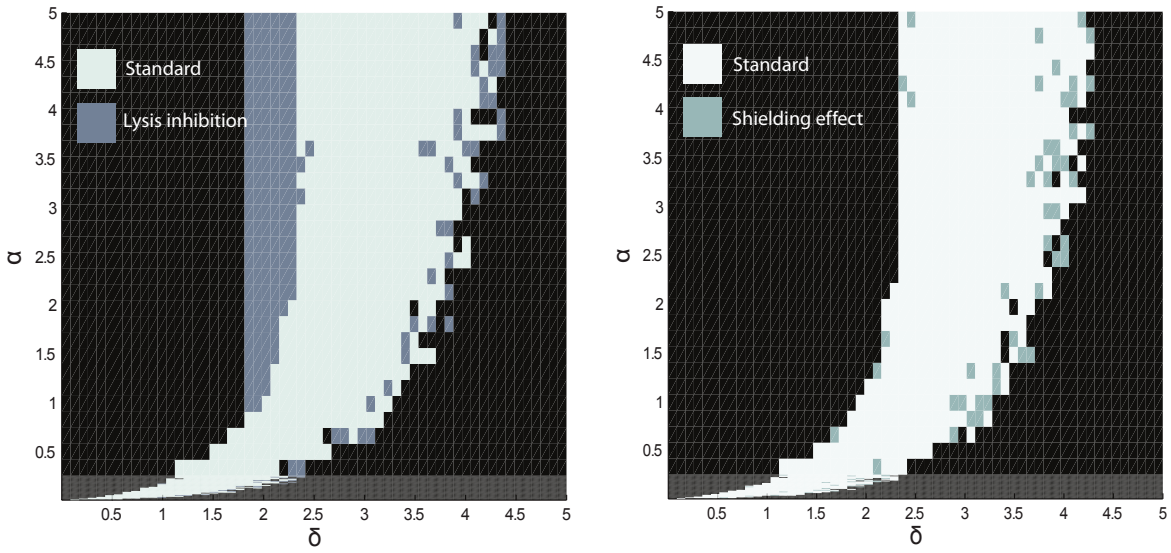


Figure 5.15: **Left panel:** The coexistence region of the Well-mixed model with and without the effect of lysis inhibition. **Right panel:** The coexistence region of the Well-mixed model with and without the effect of having dead and infected bacteria act as sinks for phage.

## 5.8 Effect of shielding and lysis inhibition in the Well-mixed model

We observe enhancement of coexistence in the Well-mixed model when lysis inhibition is implemented (see figure 5.15 left panel). The enhancement in this case occurs because the strategy of delaying lysis desynchronizes burst events and therefore dampens population oscillations. As seen in figure 5.15 right panel, there is no significant effect of letting the dead and infected act as sinks for phage in the Well-mixed model for the degradation rate of dead bacteria, $\delta_B = 0.01$, used in our simulation. The $\delta_B$ would have to be much lower, i.e. the dead bacteria would have to remain in the system for much longer, for any effect to be visible.

# Appendix 2: Supplementary information for Chapter 2

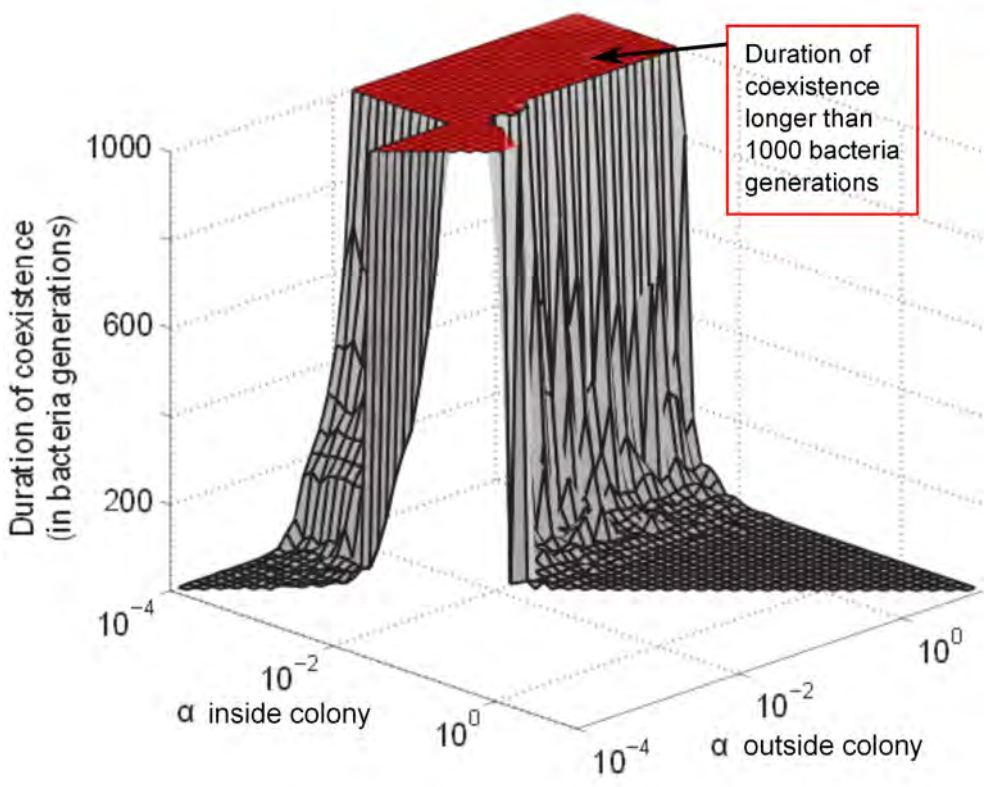


Figure 5.16: **Long lived coexistence for a broad rage of $\alpha_{in}$ and $\alpha_{out}$.** Surface shows length of coexistence for different sets of $\alpha_{in}$ and $\alpha_{out}$, if coexistence lasted longer than an upper cut off value of a 1000 bacteria generations the simulation was stopped. Note that the $\alpha$-axis runs in opposite direction of the $\delta$-axis in fig. 2.6 in chapter 2. Grid size: $100 \times 100$ Initial conditions for simulations where phage infected bacteria placed on a straight colony edge of healthy bacteria, were bacteria had max density counter value from $t = 0$.

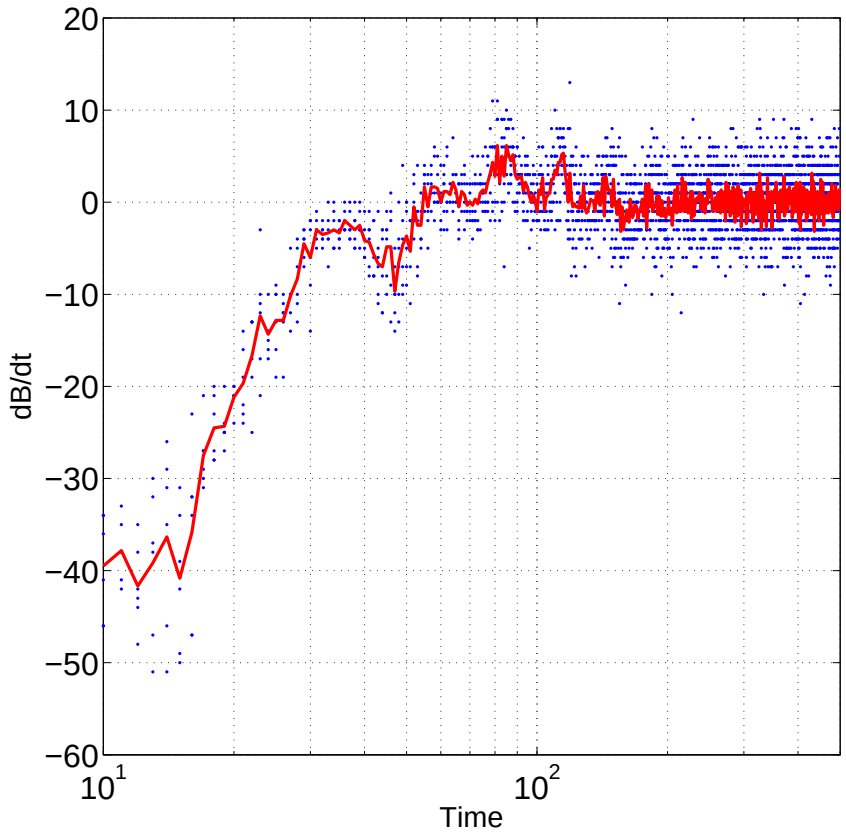


Figure 5.17: **Infection front speed slow down over time.** Blue dots show $dB/dt$ as a function of time (in units of simulation time steps) for six different simulations with same parameters as in fig. 2.4 in chapter 2, $(\delta_{out}; \alpha_{out}) = (0.05 \cdot 10^{-1} min^{-1}; 1.0 \cdot 10^{-1} min^{-1})$ and $(\delta_{in}; \alpha_{in}) = (5.0 \cdot 10^{-1} min^{-1}; 0.01 \cdot 10^{-1} min^{-1})$, red line show average value. Grid size: $200 \times 200$. Initial condition was phage placed on the edge of a straight colony edge. The bacteria in the colony had all density counters set to zero at $t = 0$. In the beginning before bacteria reach a high density counter values phage infection front eat rapidly through the colony. After roughly 2 bacteria generations the bacteria have reached higher density counter numbers and the advancing infection fronts slow down and become almost stationary.

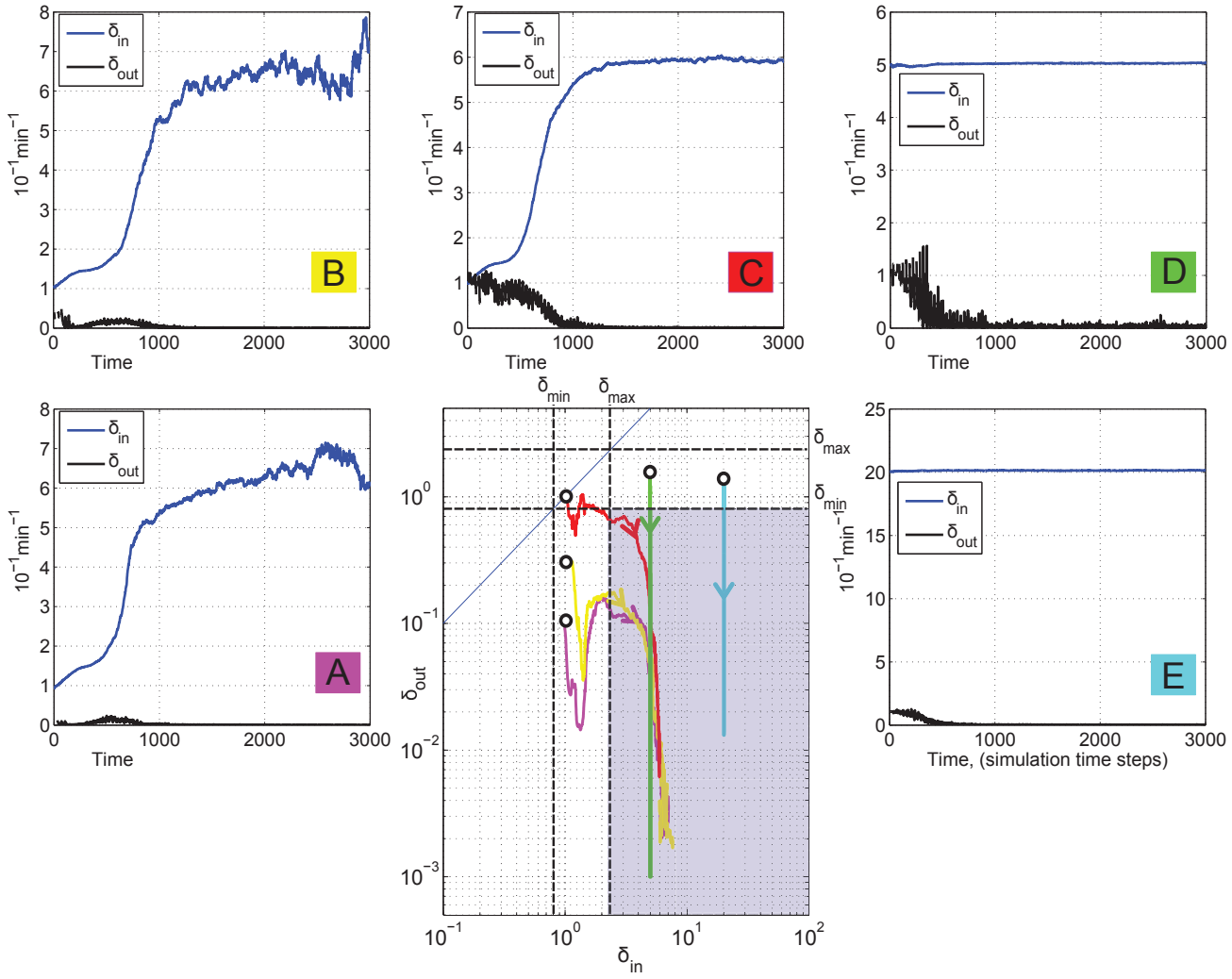


Figure 5.18: **Degradation rate evolution with normal steps.** $\alpha_{in} = \alpha_{out} = 1.0 \cdot 10^{-1} min^{-1}$ at all times. Offspring values for these parameters was allowed to take normal distributed steps away from the parent value with mean $\mu_{phage} = 0.05$ for $\delta_{out}$ and $\alpha_{out}$ and $\mu_{bacteria} = 0.5$ for $\delta_{in}$ and $\alpha_{in}$ respectively, (but not to go below zero). A: Initial condition $(\delta_{in}, \delta_{out}) = (1.0 \cdot 10^{-1} min^{-1}, 0.1 \cdot 10^{-1} min^{-1})$. B: Initial condition $(\delta_{in}, \delta_{out}) = (1.0 \cdot 10^{-1} min^{-1}, 0.3 \cdot 10^{-1} min^{-1})$. C: Initial condition $(\delta_{in}, \delta_{out}) = (1.0 \cdot 10^{-1} min^{-1}, 1.0 \cdot 10^{-1} min^{-1})$. D: Initial condition $(\delta_{in}, \delta_{out}) = (5.0 \cdot 10^{-1} min^{-1}, 3.0 \cdot 10^{-1} min^{-1})$. E: Initial condition $(\delta_{in}, \delta_{out}) = (20.0 \cdot 10^{-1} min^{-1}, 2.0 \cdot 10^{-1} min^{-1})$. Trajectories show how the system averages of $\delta_{in}$ and $\delta_{out}$ change during a simulation which lasts 3000 time steps. Grid size: 80×80.

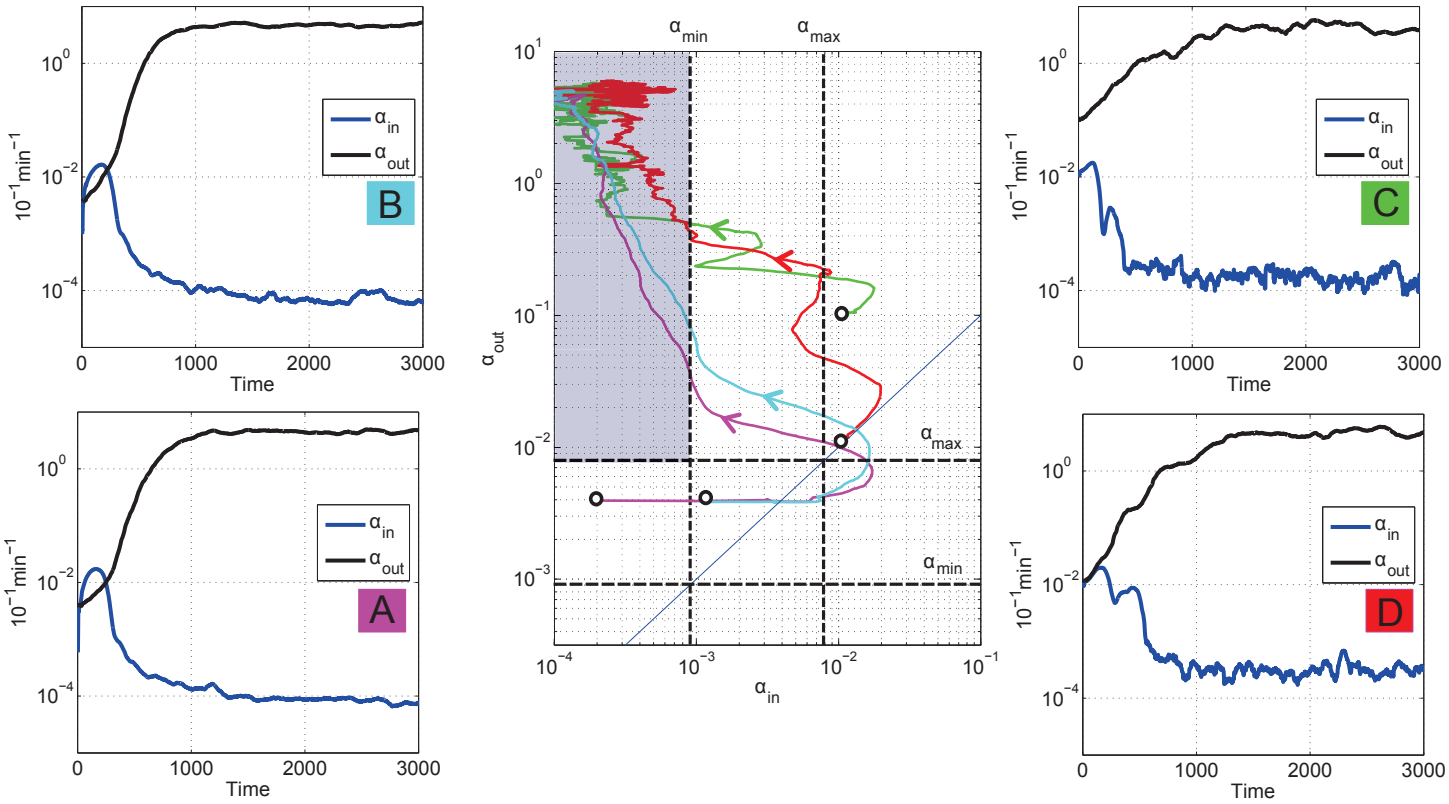


Figure 5.19: **Infection rate evolution with normal steps.** $\delta_{in} = \delta_{out} = 0.1 \cdot 10^{-1} min^{-1}$ at all times. Offspring values for these parameters was allowed to take normal distributed steps away from the parent value with mean $\mu_{phage} = 0.025$ for $\delta_{out}$ and $\alpha_{out}$ and $\mu_{bacteria} = 0.025$ for $\delta_{in}$ and $\alpha_{in}$ respectively, but not to go below zero. A (purple): initial values $\alpha_{in} = 0.0002 \cdot 10^{-1} min^{-1}$,$\alpha_{out} = 0.004 \cdot 10^{-1} min^{-1}$. B (light blue): initial values $\alpha_{in} = 0.001 \cdot 10^{-1} min^{-1}$,$\alpha_{out} = 0.004 \cdot 10^{-1} min^{-1}$. C (green): initial values $\alpha_{in} = 0.01 \cdot 10^{-1} min^{-1}$,$\alpha_{out} = 0.1 \cdot 10^{-1} min^{-1}$. D (red): initial values $\alpha_{in} = 0.01 \cdot 10^{-1} min^{-1}$,$\alpha_{out} = 0.01 \cdot 10^{-1} min^{-1}$. Trajectories show how the system averages of $\alpha_{in}$ and $\alpha_{out}$ change during a simulation which lasts 3000 time steps. Note that in the beginning of each simulation selection pressure on $\alpha_{in}$ is low since there are few phage and bacteria and they are relatively far apart in the random initial condition. Since we do not allow $\alpha_{in}$ to take on negative values the average tend to drift up when there is no strong selection, which is the reason why all trajectories initially go to higher $\alpha_{in}$ values, before moving in to the blue region. Grid size 40×40 grid. Random Initial conditions.

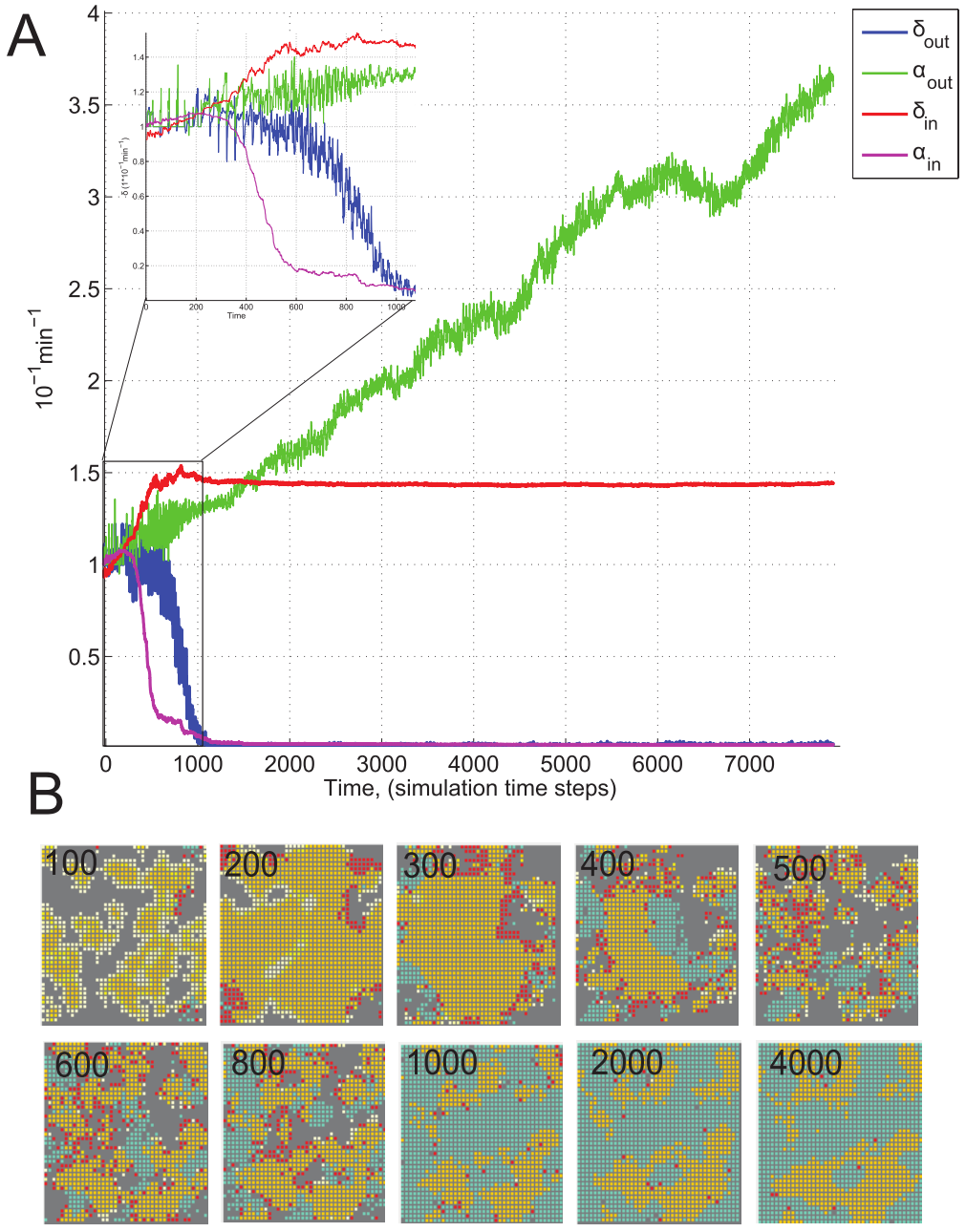


Figure 5.20: **Evolution pushes selforganizing bacteria refuge system into parameter region with stable coexistence. A:** System averages of $\delta_{in}$, $\delta_{out}$, $\alpha_{in}$ and $\alpha_{out}$ as a function of time, for simulation where both $\delta_{in}$, $\delta_{out}$, $\alpha_{in}$ and $\alpha_{out}$ was allowed to evolve. At $t = 0$, $\delta_{in} = \delta_{out} = \alpha_{in} = \delta_{out} = 1$. Offspring values for these parameters was allowed to take normal distributed steps away from the parent value with mean $\mu_{phage} = 0.05$ for $\delta_{out}$ and $\alpha_{out}$ and $\mu_{bacteria} = 0.5$ for $\delta_{in}$ and $\alpha_{in}$ respectively, (but not to go below zero). (Since grid size was small we used large evolutionary steps in order to ensure a reasonable short simulation time). **B:** Yellow show sites occupied by healthy bacteria, red sites with infected bacteria and green sites with diffusing phage. Grid size: $40 \times 40$. Initial conditions was randomly scattered bacteria and bacteria infected with phage.

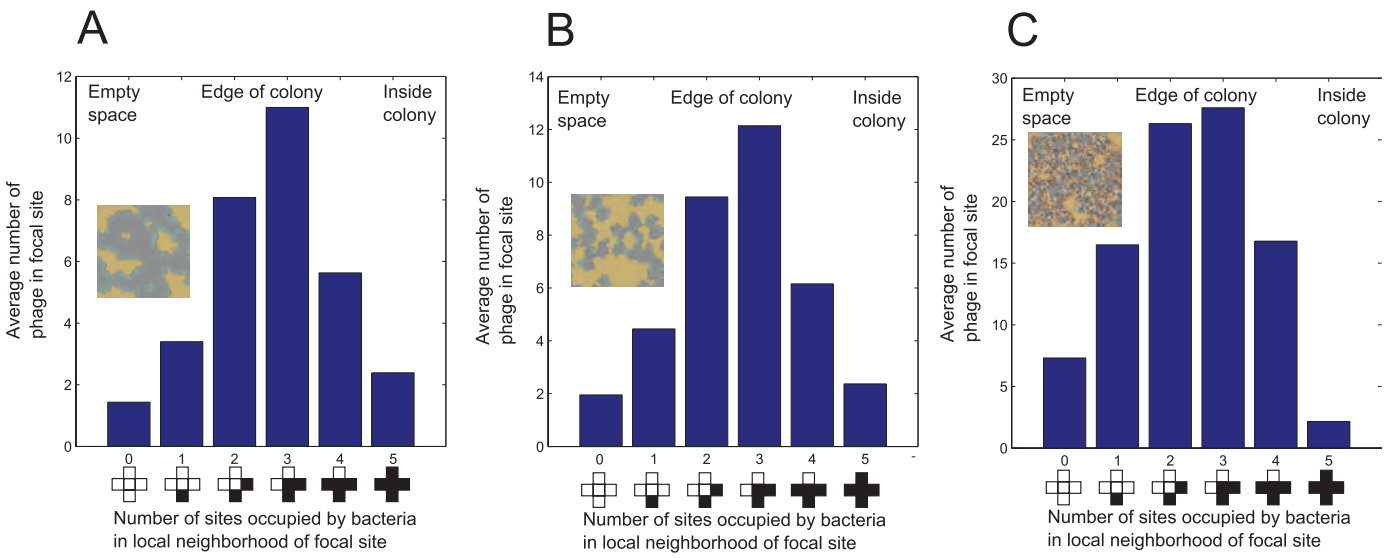


Figure 5.21: **Phage are co-localized with colony edges.** Average number of phage per site as a function of the fraction of sites occupied by bacteria in the local neighborhood of the site. The probability of finding phage at sites with both empty and occupied sites in the vicinity is higher than the probability of finding phage in sites where all sites in the vicinity are either completely occupied or completely empty. This signifies that phage are most abundant at the colony edges. Grid size: $200 \times 200$. Initial conditions was randomly scattered bacteria and bacteria infected with phage. **A:** $\alpha_{out} = \alpha_{in} = 1 \cdot 10^{-1} min^{-1}$ and $\delta_{in} = 100 \cdot 10^{-1} min^{-1}$ and $\delta_{out} = 0.04 \cdot 10^{-1} min^{-1}$. **B:** $\alpha_{out} = \alpha_{in} = 1 \cdot 10^{-1} min^{-1}$ and $\delta_{in} = 10 \cdot 10^{-1} min^{-1}$ and $\delta_{out} = 0.05 \cdot 10^{-1} min^{-1}$. **C:** $\alpha_{out} = \alpha_{in} = 1 \cdot 10^{-1} min^{-1}$ and $\delta_{in} = 3.3 \cdot 10^{-1} min^{-1}$ and $\delta_{out} = 0.8 \cdot 10^{-1} min^{-1}$.

# Appendix 3: Supplementary information for Chapter 3

### 5.8.1 Finding the steady state distribution around a point source of molecules which diffuse and decay uniformly

For a single cell excreting a common good molecule $E$ at a constant rate $\sigma_E$, the change of $E$ in time at a point $\mathbf{r} = (x, y, z)$ at the time $t$ can be described by the partial differential equation:

$$\frac{\partial E}{\partial t} = D\frac{\partial^2 E}{\partial \mathbf{r}^2} - \gamma_E E(\mathbf{r}, t) + \delta(\mathbf{r} - \mathbf{r}_0)\sigma_E \tag{5.35}$$

where the diffusion rate of the molecule is $D$ and degradation rate $\gamma_E$. In most cases we can assume that the time scales of cell division and cell movement is far slower than that of diffusion and degradation of the common good molecules. We set $\frac{\partial E}{\partial t} = 0$ and solve the ordinary differential equation:

$$D\frac{d^2 E_{ss}}{dx^2} = \gamma_E E_{ss}(x) - \delta(x - x_0)\sigma_E \tag{5.36}$$

If we Fourier transform both sides of eq. 5.36 we get:

$$D(i\omega)^2 \tilde{E_{ss}}(\omega) = \gamma_E \tilde{E_{ss}}(\omega) - \frac{\sigma_E}{\sqrt{2\pi}} \exp(-ix_0\omega) \tag{5.37}$$

$$\tilde{E}_{ss}(\omega) = \frac{\sigma_E}{\sqrt{2\pi}} \frac{1}{D\omega^2 + \gamma_E} \exp(-ix_0\omega) \tag{5.38}$$

$E_{ss}(x)$ can thus be found by taking the inverse Fourier transform of eq. 5.38:

$$E_{ss}(x) = \frac{1}{\sqrt{2\pi}} \int_{-\infty}^{\infty} \tilde{E_{ss}}(\omega) \exp(ix\omega)\, d\omega \tag{5.39}$$

$$= \frac{\sigma_E}{2\pi} \int_{-\infty}^{\infty} \frac{1}{D\omega^2 + \gamma_E} \exp(i(x - x_0)\omega)\, d\omega \tag{5.40}$$

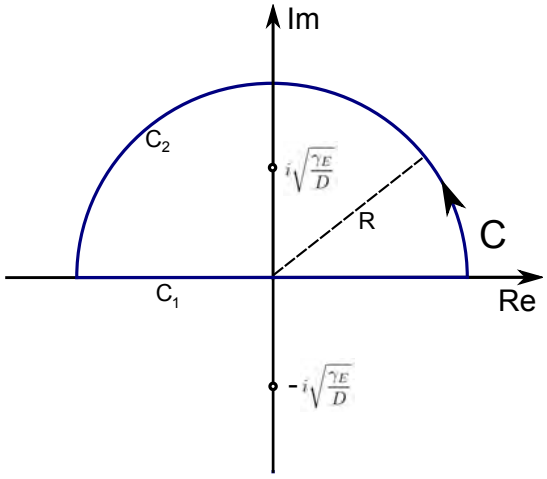


Figure 5.22: The closed path $C$ used in eq. 5.41

the integral eq. 5.40 is equal to the real part of the path integral over the complex valued function $\tilde{E_{ss}}(z) = \frac{\sigma_E}{2\pi}\frac{1}{Dz^2+\gamma_E}\exp(i(x-x_0)z)$:

$$\int_{C_1} \tilde{E_{ss}}(z)dz = \oint_C \tilde{E_{ss}}(z)dz - \int_{C_2} \tilde{E_{ss}}(z)dz \tag{5.41}$$

when $R \to \infty$. (where $z = \omega + iy$ and $C$ is defined in fig. 5.22). Since $\int_{C_2} \tilde{E_{ss}}(z)dz \to 0$ for $R \to \infty$ (because $\frac{1}{Dz^2+\gamma_E} = \frac{1}{DR^2+\gamma_E} \to 0$ for $R \to \infty$), we have:

$$\begin{aligned}
E_{ss}(r) &= \oint_C \tilde{E_{ss}}(z)dz && (5.42)\\
&= \frac{\sigma_E}{2\pi}\oint_C \frac{1}{Dz^2+\gamma_E}\exp(i(x-x_0)z)\,dz && (5.43)\\
&= \frac{\sigma_E}{2\pi}2\pi i\left(\frac{\frac{1}{D}\exp(i(x-x_0)z)}{z+i\sqrt{\frac{\gamma_E}{D}}}\right)_{z=i\sqrt{\frac{\gamma_E}{D}}} && (5.44)\\
&= \frac{\sigma_E}{2\sqrt{D\gamma_E}}\exp\left(-\sqrt{\frac{\gamma_E}{D}}|x-x_0|\right) && (5.45)
\end{aligned}$$

(Where, in the third line, we use Cauchy's integral formula which states that:
$\oint_C \frac{f(z)}{z-z_0}dz = 2\pi i f(z_0)$).

### 5.8.2 Conditions satisfied by global maxima of $\Delta g$

The $\sigma_E^{opt}(C,D)$ which maximizes $\Delta g(C,D)$ for all population sizes, $C$, and diffusion constants $D$ must satisfy $\left.\frac{\partial \Delta g(C,D,\sigma_E)}{\partial \sigma_E}\right|_{\sigma_E=\sigma_E^{opt}} = 0$ , $\left.\frac{\partial^2 \Delta g(C,D,\sigma_E^{opt})}{\partial \sigma_E^2}\right|_{\sigma_E=\sigma_E^{opt}} < 0$, and $\Delta g(C,D,\sigma_E^{opt}) > 0$.

$$\left.\frac{\partial \Delta g(C,D)}{\partial \sigma_E}\right|_{\sigma_E=\sigma_E^{opt}} = 0 \Rightarrow \tag{5.46}$$

$$\left(\frac{B_{max} h K^h}{\sigma_E^{opt}}\right) \frac{\left(\sigma_E^{opt} f(C,D)\right)^h}{\left(\left(\sigma_E^{opt} f(C,D)\right)^h + K^h\right)^2} - p_{cost} = 0 \Rightarrow \tag{5.47}$$

$$\left(\frac{B_{max} h K^h}{p_{cost}}\right) \frac{\left(\sigma_E^{opt} f(C,D)\right)^h}{\left(\left(\sigma_E^{opt} f(C,D)\right)^h + K^h\right)^2} = \sigma_E^{opt} \tag{5.48}$$

from $\left.\frac{\partial^2 \Delta g(C,D)}{\partial \sigma_E^2}\right|_{\sigma_E=\sigma_E^{opt}} < 0$ , we get:

$$\left.\frac{\partial^2 \Delta g(C,D)}{\partial \sigma_E^2}\right|_{\sigma_E=\sigma_E^{opt}} < 0 \Rightarrow \tag{5.49}$$

$$\frac{B_{max} h K^h \left(\sigma_E^{opt} f(C,D)\right)^h \left((h-1)K^h - (h+1)\left(\sigma_E^{opt} f(C,D)\right)^h\right)}{\left(\sigma_E^{opt}\right)^2 \left(K^h + \left(\sigma_E f(C,D)\right)^h\right)^3} < 0 \Rightarrow \tag{5.50}$$

$$(h-1)K^h - (h+1)\left(\sigma_E^{opt} f(C,D)\right)^h < 0 \Rightarrow \tag{5.51}$$

$$\frac{K}{f(C,D)} \sqrt[h]{\frac{h-1}{h+1}} < \sigma_E^{opt,*} \tag{5.52}$$

We note that 5.52 is only defined for $h \geq 1$. For the sigmoidal benefit functions we use in chapter 3 it turns out that the production rate $\sigma_E^{opt,*}$ which satisfies $\frac{K}{f(C,D)} \sqrt[h]{\frac{h-1}{h+1}} = \sigma_E^{opt,*}$ (eq. 5.52) always gives $\Delta g(C,D,\sigma_E^{opt,*}) \leq 0$ so it is the conditions $\Delta g(C,D,\sigma_E^{opt}) > 0$ and $\left.\frac{\partial \Delta g(C,D,\sigma_E)}{\partial \sigma_E}\right|_{\sigma_E=\sigma_E^{opt}} = 0$ alone that determine the critical turn on points, $C_C$ and $D_C$.

### 5.8.3 Limit of $E_{middle}(C,D)$ for $C \to \infty$

For $C \to \infty$,

$$E_{middle}(C,D) = \frac{\sigma_E}{2\sqrt{D\gamma_E}} \left(1 + 2\left(\frac{1 - \exp\left(-\sqrt{\frac{\gamma_E}{D}}\frac{a}{2}(C-1)\right)}{\exp\left(\sqrt{\frac{\gamma_E}{D}}a\right) - 1}\right)\right) \tag{5.53}$$

approaches a constant:

$$\lim_{C\to\infty}\left(E_{middle}(C,D)\right) = \frac{\sigma_E}{2\sqrt{D\gamma_E}} \left(1 + 2\left(\frac{1}{\exp\left(\sqrt{\frac{\gamma_E}{D}}a\right) - 1}\right)\right) \tag{5.54}$$

which for $\sqrt{\frac{\gamma_E}{D}}a \ll 1$ is:

$$\lim_{C\to\infty}(E_{middle}(C,D)) \simeq \frac{\sigma_E}{2\sqrt{D\gamma_E}}\left(1+2\left(\frac{1}{1+\sqrt{\frac{\gamma_E}{D}}a-1}\right)\right) \quad (5.55)$$

$$= \sigma_E\left(\frac{1}{\gamma_E a}+\frac{1}{2\sqrt{D\gamma_E}}\right) \quad (5.56)$$

$$\simeq \frac{\sigma_E}{\gamma_E a} \quad (5.57)$$

(since $\sqrt{\frac{\gamma_E}{D}}a \ll 1 \Leftrightarrow \frac{1}{\gamma_E a} \gg \frac{1}{\sqrt{D\gamma_E}}$). Note that the constant in this limit does not depend on the diffusion constant. This is expected; eq. 5.57, gives what a cell in the middle of an effectively infinite colony feels at steady state, and thus diffusion in and out of the cells local neighborhood should exactly cancel and only production and degradation rates and the density of cells matter.

### 5.8.4 Limit of $\sigma^{opt}_{E,h=1}$ for $D \to 0$ and $C \to \infty$ in the spatial case

Dealing with $D \to 0$ is a bit tricky. We first have to go back and take a look at the partial differential equation which gave us the sst. distribution of common good, $E$, around a single point source (one cell).

$$\frac{\partial E}{\partial t} = D\frac{\partial^2 E}{\partial \mathbf{r}^2} - \gamma_E E(\mathbf{r},t) + \delta(\mathbf{r}-\mathbf{r}_0)\sigma_E \quad (5.58)$$

for $D = 0$ and $\frac{\partial E}{\partial t} = 0$ this gives us:

$$E(\mathbf{r}) = \delta(\mathbf{r}-\mathbf{r}_0)\frac{\sigma_E}{\gamma_E} \quad (5.59)$$

It seem most sensible in this situation to redefine benefit not as a function of $E$ in the exact position of the cell ($\mathbf{r} = \mathbf{r}_0$) but as a function of the integral $\int_{-\epsilon}^{\epsilon} E(\mathbf{r})d\mathbf{r} = \frac{\sigma_E}{\gamma_E}$ (where $1 \gg \epsilon > 0$), which we can think of as the concentration of common good in and around the close vicinity of the cell. (There is no reason to include other cells since with no diffusion they wont feel each others presence anyway...). Since:

$$\sigma^{opt}_{E,h=1} = \sqrt{\frac{1}{f(C,D)}}\sqrt{\frac{B_{max}K}{p_{cost}}} - \frac{K}{f(C,D)} \quad (5.60)$$

$$(5.61)$$

this gives us:

$$\lim\left(\sigma^{opt}_{E,h=1}\right)_{D\to 0} = \sqrt{\gamma_E}\sqrt{\frac{B_{max}K}{p_{cost}}} - K\gamma_E \quad (5.62)$$

This means that for infinitely low diffusion, the optimal production rate of common good approaches a constant low value set by: $\gamma_E$, $K$, and $\frac{B_{max}}{p_{cost}}$. The optimal production rate for $C \to \infty$ is:

$$\lim_{C\to\infty}\left(\sigma^{opt}_{E,h=1}(C)\right) = \sqrt{\frac{1}{\lim_{C\to\infty}(f(C))}}\sqrt{\frac{B_{max}K}{p_{cost}}} - \frac{K}{\lim_{C\to\infty}(f(C))} \quad (5.63)$$

$$= \sqrt{\gamma_E a}\sqrt{\frac{B_{max}K}{p_{cost}}} - K\gamma_E a \quad (5.64)$$

since $\lim_{C\to\infty}(f(C)) = \frac{1}{\gamma_E a}$, (see derivation above).

### 5.8.5 A simple model for polymers degraded by an excreted enzyme

We assume that benefit is directly proportional with the concentration of polymers that has the length which allows transport over the cell membrane, and denote this length 1. We also assume some constant source of polymers of max length $n$, and constant equal degradation of polymers of all lengths. Concentration of a polymer of length $i$ is denoted $N_i$. Longest polymer in system has length $n$. Concentration of enzyme (common good) is denoted $E$. Production rate of polymers of maximal length $n$, is $p$. Degradation rate of all lengths of polymers is $\delta$. Equations describing the change in concentration of polymers for a given level of enzyme $E$ of all lengths are thus as follows:

$$\frac{dN_n}{dt} = p - N_n(E+\delta) \quad (5.65)$$

$$\vdots \quad (5.66)$$

$$\frac{dN_i}{dt} = 2E\sum_{j=i}^{n-1}\frac{N_{j+1}}{j} - N_i(E+\delta) \quad (5.67)$$

$$\vdots \quad (5.68)$$

$$\frac{dN_1}{dt} = 2E\sum_{j=1}^{n-1}\frac{N_{j+1}}{j} - N_1\delta \quad (5.69)$$

$$\text{where} \quad i = 1, 2, \ldots, n \quad (5.70)$$

The steady state concentrations, $N_n^*, \ldots, N_i^*, \ldots, N_1^*$ can be found by setting $\dot{N}_n = \cdots = \dot{N}_i = \cdots = \dot{N}_1 = 0$. For $n = 2$, the steady state concentration of $N_1$ is:

$$N_1^* = 2\frac{Ep}{\delta(\delta+E)} \quad (5.71)$$

For $n = 3$, the steady state concentration of $N_1$ is:

$$N_1^* = \frac{Ep}{\delta(\delta+E)}\left(1 + 2\frac{E}{\delta+E}\right) \quad (5.72)$$

For $n = 4$, the steady state concentration of $N_1$ is:

$$N_1^* = \frac{2}{3}\frac{Ep}{\delta\,(\delta + E)}\left(1 + 3\frac{E}{\delta + E} + 2\frac{E^2}{(\delta + E)^2}\right) \tag{5.73}$$

For $n > 2$ the steady state concentration of $N_1$ is given by:

$$N_1^* = \frac{2}{n-1}\frac{Ep}{\delta(\delta + E)}\left[1 + \left(\frac{2}{n-2} + \sum_{k=2}^{n-2}\frac{1}{k-1}\prod_{j=k}^{n-2}\left(1 + \frac{2}{j}\frac{E}{\delta + E}\right)\right)\frac{E}{\delta + E}\right] \tag{5.74}$$

This expression comes from combining the knowledge that:

$$N_1^* = 2\frac{E}{\delta}\left[\sum_{k=2}^{n}\frac{1}{k-1}N_k^*\right],\ \text{for } n > 2 \tag{5.75}$$

and

$$N_i^* = N_{i+1}^*\left(1 + \frac{2}{i}\frac{E}{\delta + E}\right),\ \text{for } 1 < i < n-1\ \Rightarrow \tag{5.76}$$

$$N_k^* = N_{n-1}^*\prod_{j=k}^{n-2}\left(1 + \frac{2}{j}\frac{E}{\delta + E}\right),\ \text{for } k > 1 \tag{5.77}$$

and

$$N_n^* = \frac{p}{\delta + E} \tag{5.78}$$

$$N_{n-1}^* = \frac{2}{n-1}\frac{E}{\delta + E}N_n^*,\ \text{for } n > 2 \tag{5.79}$$

which follows from setting $\dot{N}_n = \cdots = \dot{N}_i = \cdots = \dot{N}_1 = 0$, solving for $N_n^*, \ldots, N_i^*, \ldots, N_1^*$ .

# Appendix 4: Supplementary information for Chapter 4

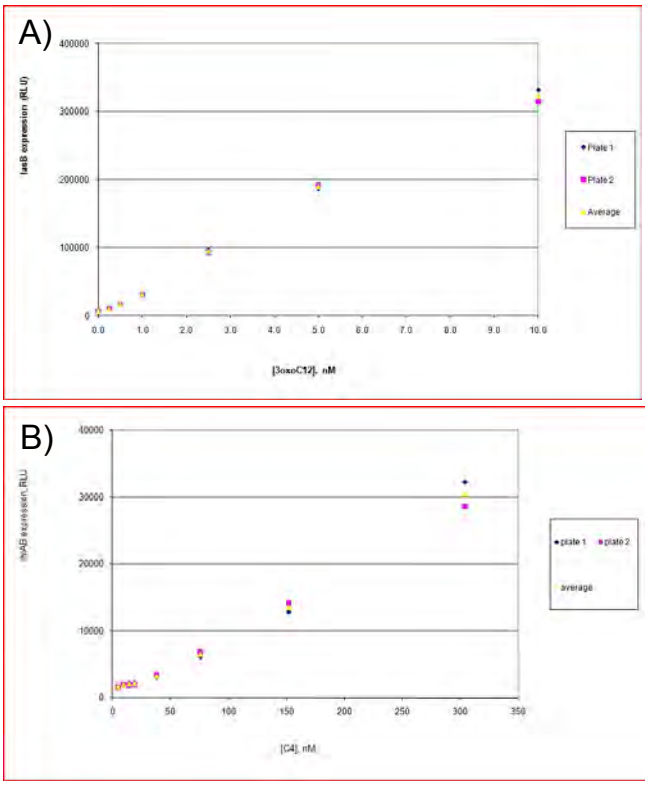


Figure 5.23: **Inducer production curves. A:** Expression level of lasB in response to the concentration of inducer (3OxoC12) in the medium. At higher signal concentrations (not shown) expression level saturates. The expression level of lasI (the gene coding for the inducer molecule) is expected to have a similar shape. Fit to a sigmoidal function gives a hill factor of approx. 1.2. **B:** Expression level of rhlAB in response to the concentration of inducer (C4) in the medium. At higher signal concentrations (not shown) expression level saturates. The expression level of rhlI (the gene coding for the inducer molecule) is expected to have a similar shape. Fit to a sigmoidal function gives a hill factor of approx. 1.3. (Data curtesy of Brooks Peterson UW).

# Part IV

# Papers

JOURNAL OF VIROLOGY, Mar. 2010, p. 3016–3022 Vol. 84, No. 6
0022-538X/10/$12.00 doi:10.1128/JVI.02326-09


# Sustainability of Virulence in a Phage-Bacterial Ecosystem▽†

Silja Heilmann,* Kim Sneppen, and Sandeep Krishna

*Center for Models of Life, Niels Bohr Institute, Copenhagen, Denmark*

Received 4 November 2009/Accepted 31 December 2009

**Virulent phages and their bacterial hosts represent an unusual sort of predator-prey system where each time a prey is eaten, hundreds of new predators are born. It is puzzling how, despite the apparent effectiveness of the phage predators, they manage to avoid driving their bacterial prey to extinction. Here we consider a phage-bacterial ecosystem on a two-dimensional (2-d) surface and show that homogeneous space in itself enhances coexistence. We analyze different behavioral mechanisms that can facilitate coexistence in a spatial environment. For example, we find that when the latent times of the phage are allowed to evolve, selection favors "mediocre killers," since voracious phage rapidly deplete local resources and go extinct. Our model system thus emphasizes the differences between short-term proliferation and long-term ecosystem sustainability.**

The replication strategies of phages fall into two major categories: virulent and temperate. A temperate phage has the ability to integrate its DNA into the host chromosome, where it is then replicated along with the bacterial DNA during cell division. This strategy allows the phage to slow down or completely stop exploitation of the bacteria, thus reducing the risk of driving its host to extinction. A virulent phage lacks this ability, and it is not fully understood how they manage to coexist with their bacterial prey (4, 19). Consider, for example, the highly effective T4 phage. For the sake of argument, let us assume a burst size of 100 offspring upon lysis. On average, not more than a single phage out of each burst of 100 should survive to infect another bacterium, or else the phage would rapidly outgrow the bacteria and drive them to extinction. The half-life ($t_{1/2}$) of a free T4 phage particle has been measured to be approximately 10 days in LB at 37°C (6). Therefore, on average, at least $t_{1/2} \times \log_2(100) \approx 2$ months should pass between infections to prevent runaway phage growth—a time span that seems highly unreasonable for many of the environments where phage and bacteria interact, such as soil or biofilm. Even a more considered calculation, inserting the above half-life measurement into more realistic Lotka-Volterra-like predator-prey models (9) does not change the conclusion that T4 and other virulent phages appear to be far too effective predators for coexistence to be feasible. It is, however, an undisputed fact that virulent phages and bacteria have coexisted for eons and do so still, everywhere around us and inside us. One possible explanation for this puzzle is that bacteria constantly evolve resistance to existing phages and that the phages evolve to attack resistant bacteria in a continuous arms race. This "Red Queen" argument (23) has, however, been criticized on the grounds that the rates of evolution of phages and bacteria are not symmetric (17, 12). Recent measurements support this: in soil, phages appear to be "ahead of the bacteria in the coevolutionary arms race" (24). We therefore wish to explore mechanisms other than bacterial resistance that may promote coexistence between virulent phages and bacteria.

Historically, phage-bacterial ecosystem models have ignored the issue of space, utilizing zero-dimensional approaches, such as ordinary differential equations (e.g., see references 1, 5, 13, 14, 15, and 21). However, many real phage-bacterial ecosystems are found in environments with a complex spatial structure, such as soil, biofilms, or wounds in animal and plant tissue. Schrag and Mittler (20) showed that coexistence between virulent phage and bacteria is feasible in a chemostat but not in serial cultures, due to the heterogeneous nature of the environment in the chemostat. Further, experiments done by Brockhurst et al. (3) indicate that reduced phage dispersal can prolong coexistence for virulent phage and bacteria in spatial environments by creating ephemeral refuges for the bacteria. Kerr et al. (10) introduced a simple cellular automaton to model fragmented populations of phage and bacteria in which coexistence was more easily achieved when migration was spatially restricted. Thus, the main extension to the simple predator-prey framework that we examine will be to add a spatial dimension.

We construct and compare two phage-bacterial ecosystem models: one model where the phage and bacteria exist in a two-dimensional space, such as the surface of an agar gel (referred to as the "spatial model"), and the other model where the phage and bacteria are repeatedly mixed, mimicking serial cultures or a well-mixed broth (referred to as the "well-mixed model"). We show that space does indeed enhance coexistence. We then move on to explore other mechanisms that phage could incorporate into their behavior to further enhance coexistence. These can broadly be classified as "hard-wired" (where every phage follows the same deterministic strategy) versus "adaptive" (where each phage potentially behaves differently, thus allowing the population to explore different options).

We have chosen to look at three specific mechanisms as examples of these categories: (i) phage effectiveness would be reduced if they were unable to register whether they were

* Corresponding author. Mailing address: Niels Bohr Institute, Blegdamsvej 17, Copenhagen, Denmark. Phone: 45 353 25273. Fax: 45 353 25425. E-mail: heilmann@nbi.dk.

† Supplemental material for this article may be found at http://jvi.asm.org/.

▽ Published ahead of print on 13 January 2010.

infecting live, infected, or dead bacteria (a hardwired behavior); (ii) phage could prolong their latent time, concurrently increasing burst size, depending on the number of multiple infections (also a hardwired behavior, but a more "active" sort, where each phage senses and responds to information from the environment; T4 is known to use such a lysis inhibition strategy), and (iii) phage offspring could have altered latent times due to mutations in the holin genes (an adaptive behavior). We will compare each of these mechanisms in the spatial and well-mixed models to investigate whether the heterogeneity possible in a spatial environment affects the outcome.

## METHODS

**Rules of the spatial model.** In the spatial model, virulent phage and bacteria interact on an $L \times L$ grid of locations, or "sites." Each site in the grid can either be empty or occupied by a single bacterium (each grid site thus has a carrying capacity of one bacterium). The bacterium may be healthy or infected. In addition, there can be any number of free phage particles at that site. Time proceeds in discrete steps. Precise timers control bacterial cell division and the lysis of an infected bacterium, which releases a burst of free phage. Other processes are random, e.g., death and diffusion of phage, and are modeled as Poisson processes.

In each time step, the following can happen.

**(i) Bacterial replication.** A bacterium with at least one empty adjacent site will attempt to divide in every time step after the current time has become greater than the value of its replication timer. The probability of replication is set to be proportional to the number of empty neighbor sites. Once a bacterium divides, one daughter cell remains in the original site, and the other is placed randomly in one of the adjacent empty sites. The replication timers of both cells are reset to the current time plus replication time ($T$), a parameter which thus sets the growth rate of the bacteria.

**(ii) Bacterial infection.** A healthy bacterium that shares its site with some free phage may be infected with a probability $p_\alpha$, that depends on the number of phage at the site, the infection rate per phage per bacterium ($\alpha$), and the decay rate of the phage ($\delta$). The number of free phage at that site is then reduced by one, and the lysis timer of the newly infected bacterium is set to $\tau$ (the latent time of the infecting phage) and starts counting down from that value.

**(iii) Bacterial lysis.** An infected bacterium will die when its lysis timer has counted down to zero. The number of phage at that site increases, upon lysis, by the burst size ($\beta$).

**(iv) Phage decay.** Free phage die with a probability $p_\delta$ per phage, which depends on the phage decay rate ($\delta$).

**(v) Phage diffusion.** Each free phage may jump to a neighboring site with a probability $p_\lambda$, which sets the phage diffusion constant.

The burst size increases with latent time: $\beta = \gamma(\tau - \varepsilon)$. This formula models the constant rate of replication ($\gamma$) of phage, after a minimum preparatory time ($\varepsilon$), usually referred to as the eclipse time. The values of the parameters and the size of the basic time step depend on the choice of phage and bacterial species. With *Escherichia coli*, a reasonable choice is a time step of 1 min, a replication time (T) of 30 min (i.e., 30 time steps), and an area of 1 $\mu m^2$ per grid site.

W chose $p_\lambda$ so as to keep the phage diffusion constant ($D$) fixed at $D \approx 1/4$ (site area)/(time step), meaning it would take on average 104 time steps for a phage to move across the grid size of $L = 100$ that we use (too large a diffusion constant would make the system well mixed, negating the purpose of our study). With T4 in mind, we will fix $\varepsilon$ at 10 time steps and $\gamma$ at 7 (time step)$^{-1}$, resulting in (nonzero) burst sizes ranging from 7 (at $\tau = 11$ time steps) to 280 phage (at $\tau = 50$ time steps). However, for the basic spatial model, $\tau$ is fixed at 30 time steps. For the phage infection rate, $\alpha$, we will explore a range of values, between 0.0001 and 5 (site area)/(time step). For T4, for example, an infection rate of $\alpha = 5$ $\mu m^2$ $min^{-1}$ means that a phage closer than 1 $\mu m$ to an *E. coli* bacterium would infect, on average, within 12 s, which is fast but not unrealistic. With this range of $\alpha$ values, we need $\delta$ to be up to 5 (time step)$^{-1}$ to see coexistence, as explained in the Results section below. $p_\alpha$ and $p_\delta$ are calculated from the values of $\delta$ and $\alpha$ by assuming the processes to be Poissonian random processes (see the supplemental material for further details of model rules for bacterial replication, infection, and lysis and for derivation of the probabilities $p_\alpha$, $p_\delta$, and $p_\lambda$).

**Rules of the well-mixed model.** The well-mixed model is very similar to the spatial model, except that (i) upon bacterial cell division, newborn bacteria are placed at random empty grid sites, and (ii) newborn phages, released when an infected bacterium is lysed, are randomly placed all over the grid. This results in continuous mixing of the phage and bacteria populations while at the same time ensuring that the two models are as similar as possible to allow for straightforward comparison.

## RESULTS

**Quantifying coexistence.** The color map in Fig. 1 shows the average steady-state bacterial density per grid site, $B$, for simulations of the spatial model with various combinations of $\delta$ (degradation rate of phage) and $\alpha$ (infection rate per phage per bacterium). In the deep-red region to the right in Fig. 1, the phage are so inefficient that they die out and the bacteria subsequently grow to carrying capacity. In the deep-blue region on the left, the phage are so efficient that they drive the bacteria to extinction and then die out themselves. In the middle region, where $0 < B < 1$, the bacteria and phage coexist stably. The size of this region in the $\delta$-$\alpha$ parameter plane quantifies how easily coexistence is achieved in the models we examine, since $\delta$ and $\alpha$ are the parameters that determine the overall predatory effectiveness of the phage. It is interesting to note that coexistence requires much higher values of $\delta$ (1 to 4 $min^{-1}$ for, say T4) than has been measured in laboratory conditions. This suggests that the effective death rate for phage may be much higher in real ecosystems than in the laboratory.

The typical dynamics of the spatial model involve one or more bacterial colonies that grow at a rate determined by their replication time. These colonies are invaded by phage that move in traveling infection fronts that sweep through the colonies. The speed of the infection front depends on the effectiveness of the phage, i.e., $\alpha$ and $\delta$. If the phage die too quickly or infect very inefficiently, they die out. Conversely, if the phage live a long time or infect quickly, then the infection front may propagate even faster than the bacterial growth front. Within the coexistence region, there is considerable variation in the dynamics of the ecosystem, as shown in the four snapshots in Fig. 1. At point A, right at the edge of the coexistence region, the phage infection front in fact travels faster than the bacterial growth front. Nevertheless, there is coexistence because the infection fronts leave behind healthy bacteria often enough to keep the bacterial population from going extinct. However, at point A, there is considerable variation in bacterial density with time, as the bacteria typically form a small number of big colonies which are then decimated by the fast-moving infection fronts. Increasing $\delta$ or decreasing $\alpha$ from point A moves the system deeper into the coexistence region to points B and C, respectively, where there is a higher average bacterial density. Point B, in stark contrast to point A, is characterized by many small intermixed domains of bacteria and phage, and their populations are quite stable with relatively small fluctuations. At point C, bacteria survive a passing infection front more often than at point A (because of the lower infection rate $\alpha$), and therefore, the bacterial domains are smaller and more dispersed than at point A. Qualitatively similar patterns and dynamics are observed as one moves along isocolor lines (i.e., lines of constant bacterial density) to lower $\alpha$ and $\delta$ values. Thus, the dynamics at point D are very similar to the dynamics at point C. At very small $\delta$ values ($\delta \leq 10^{-4}$), however, the system starts behaving like a well-mixed ecosystem because the phage are able to diffuse across the entire grid before either dying or infecting.

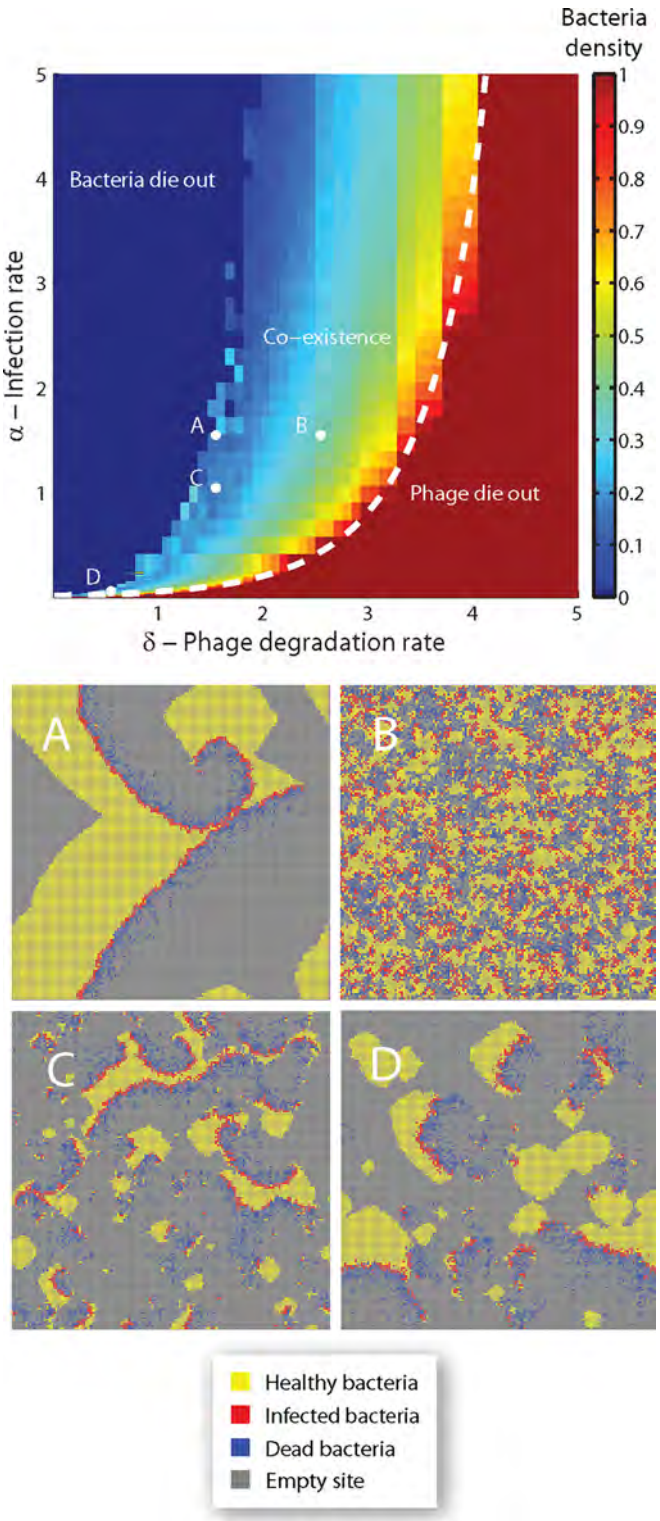


FIG. 1. (Top) Coexistence region in the δ-α plane. δ is the degradation rate of the phage, and α is the infection rate for a phage that occupies the same lattice site as a bacterium (see Methods). The color map shows the average bacterial density in steady state. There is coexistence only in the zone in the middle, where phage are neither too effective nor too ineffective. The white dashed line shows a theoretical estimate for the threshold at which exactly one phage per burst survives long enough to find and infect a bacterium (see the supplemental material). The jaggedness of the boundaries, in this and subsequent plots, arises because only a single simulation was done for each δ-α pair. Doing more simulations does not significantly alter the position and shape of the coexistence region. (Bottom) Snapshots of the ecosystem at the points marked A to D in the top panel. Healthy bacteria, infected bacteria, and dead bacteria are shown. Phage are not shown.

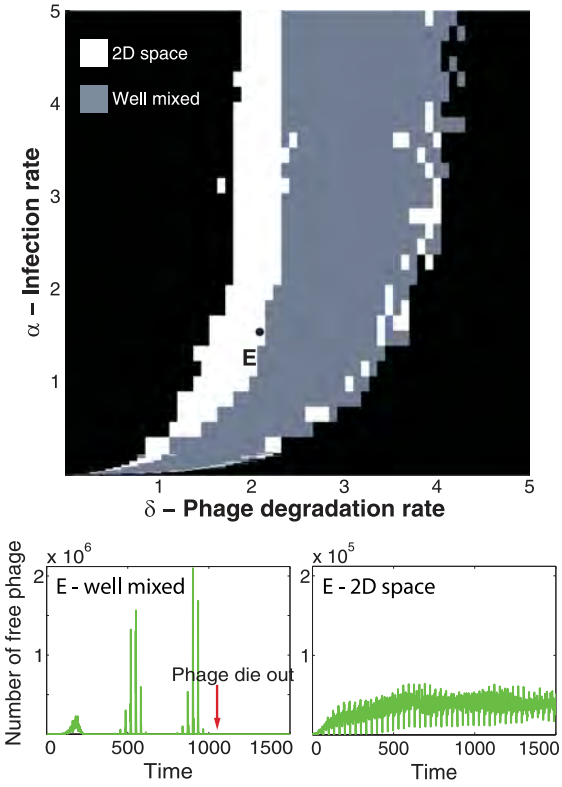


FIG. 2. Space helps coexistence. (Top) Coexistence regions for the spatial and well-mixed models plotted on top of each other. In the white region, there is coexistence only in the spatial model. In the gray region, there is coexistence in both models. The area of the gray region is around 20% smaller than the area of the white region. 2D space, two-dimensional space. (Bottom) The green bars and curves show the total number of free phage in the spatial and well-mixed models as a function of time for the parameters corresponding to the point marked E in the top panel. The population quickly settles at a stable level, with some fluctuations, for the spatial model. In contrast, the well-mixed model exhibits oscillations with increasing amplitude that eventually drive the bacterial population, and subsequently the phage, to extinction.

**Space helps coexistence.** Figure 2 compares the coexistence regions for the spatial and well-mixed models, keeping all parameters other than δ and α fixed at their default values. The coexistence region is approximately 20% smaller for the well-mixed model than for the spatial model. The right boundary of the coexistence region coincides for both models and is situated where the time between infections is so long that on average only one phage per burst survives. The left boundary, however, is situated further to the left for the spatial model than for the well-mixed model, meaning that when there is space, the bacteria can coexist with far more effective phage than in the well-mixed model. In the well-mixed model, the left boundary corresponds, in fact, to the onset of high-amplitude oscillations in the populations. These oscillations cause the

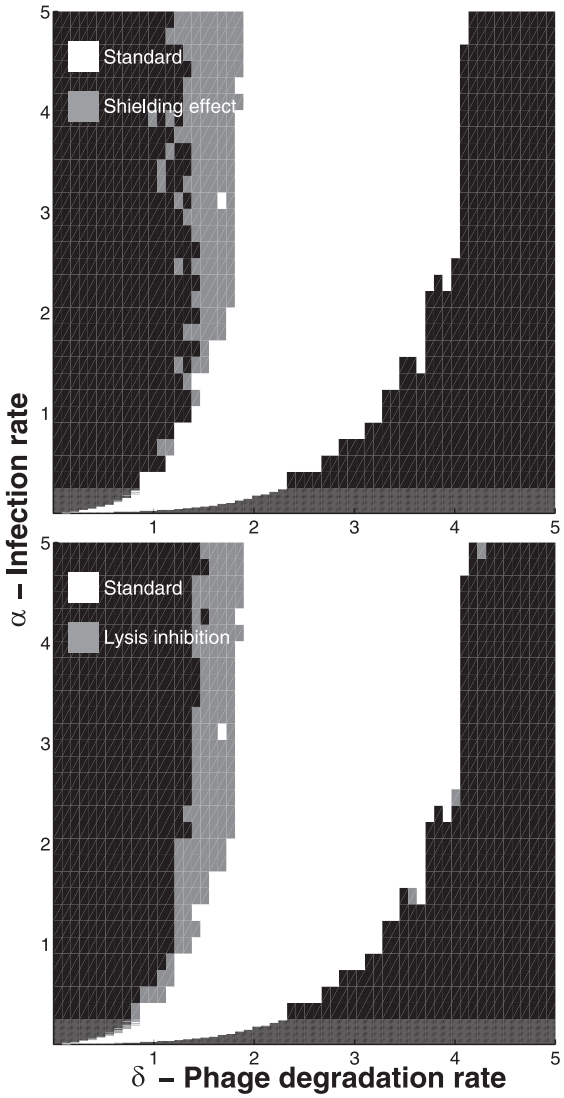


FIG. 3. Effects of two hardwired phage strategies on the coexistence region. (Top) Phage infect live, dead, and infected bacteria alike. (Bottom) Multiple infections of the same bacterial cell result in delayed lysis. In both plots, the white region corresponds to parameters where there is coexistence in the spatial model both with and without the phage strategies, while the gray region shows where there is coexistence only when the corresponding phage strategy is implemented.

bacterial numbers to periodically fall to extremely low levels. When this happens, the few bacteria left have a finite probability of all of the bacteria becoming infected before they divide, so that, sooner or later, the bacteria go extinct. For the same parameter values, the spatial model shows damped or low-amplitude oscillations and therefore coexistence.

**Behavioral mechanism that enhances coexistence. (i) Hardwired phage behavior.** Figure 3 shows the coexistence regions when two hardwired mechanisms are implemented in the spatial model. Both impede phage infection and dispersal, but in different ways. First, the top panel in Fig. 3 shows what happens if phage simply cannot distinguish between healthy and infected/dead bacteria—they infect whatever they come into contact with, and when that is a dead or previously infected bacterium, the phage dies. (We extended the spatial model to keep dead bacteria around for a certain characteristic time, before the site holding them becomes empty [see the supplemental material].) Traditionally, phage-bacterial models ignore the interaction of phage with dead and infected bacteria (16, 13, 21, 5). It has, however, been proposed that the build up of bacterial debris could hinder phage diffusion, protect live bacteria, and enhance coexistence (1, 17). This is indeed the effect we see in the top panel in Fig. 3 at the left boundary of the coexistence region. In contrast, the right boundary is unaffected because here the phage population is relatively low, on the verge of extinction, while the bacterial population is very close to the carrying capacity so infection of previously infected or dead bacteria is rare.

The bottom panel in Figure 3 shows the effect of a more "active" strategy, where the phage can detect multiple infections and delay lysis. T4 is known to use such lysis inhibition (2, 7). Through a mechanism involving the anti-holin rI, T4 delays lysis by 5 to 10 min whenever the cell becomes superinfected with other T4 phage (Ryland Young, personal communication). (We implement this in the spatial model by allowing phage to infect already infected cells. Whenever this happens, lysis is postponed by 8 time steps. However, we set an upper limit of 200 time steps beyond which lysis cannot be postponed. This gives a maximum burst size of 1,330 phage, which approximately corresponds to the phage production allowed by the resources available in a single bacterium [7].) This mechanism also boosts coexistence, as shown in the bottom panel in Fig. 3. Again, the right boundary is unaffected because superinfections are rare here.

The behavior of infecting dead and infected bacteria effectively increases $\delta$ for the phage, whereas delaying lysis upon superinfection effectively decreases $\alpha$ (by reducing burst size per phage). Either way, the result is to shift the boundary of the coexistence region to the left compared to the basic spatial model.

**(ii) Adaptive phage behavior.** Another strategy we explored was to allow the latent times of the phage to mutate. The phage proteins that cause lysis, holins, control the time of lysis with very high precision ($\pm$ 1 min), and point mutations within the holin gene can significantly alter the lysis time without changing the precision (26). We allowed a small fraction of phage progeny to mutate to have a different latent time (and therefore also a different burst size) from the parent phage. (The latent times of 0.5% of the phage from each burst are chosen randomly and uniformly from the range 0 to 50 time steps. The other 99.5% inherit the same latent time as the parent phage. Additionally, 0.5% of the bursts are comprised entirely of latent time mutants [see the supplemental material for the biological reasoning behind these rules].) The top panel in Fig. 4 shows that implementing this adaptive mechanism enhances coexistence in the spatial model.

It is not intuitively obvious why this strategy helps. Consider that if the bacterial density is kept fixed, the phage will evolve to all have the same "optimal" latent time that maximizes the rate with which they spread in that density (see the supplemental material, where we show how the optimal latent time depends on the bacterial density; also see reference 9). At the maximum bacterial density of one per site, which is what an infection front typically encounters in the spatial model, the

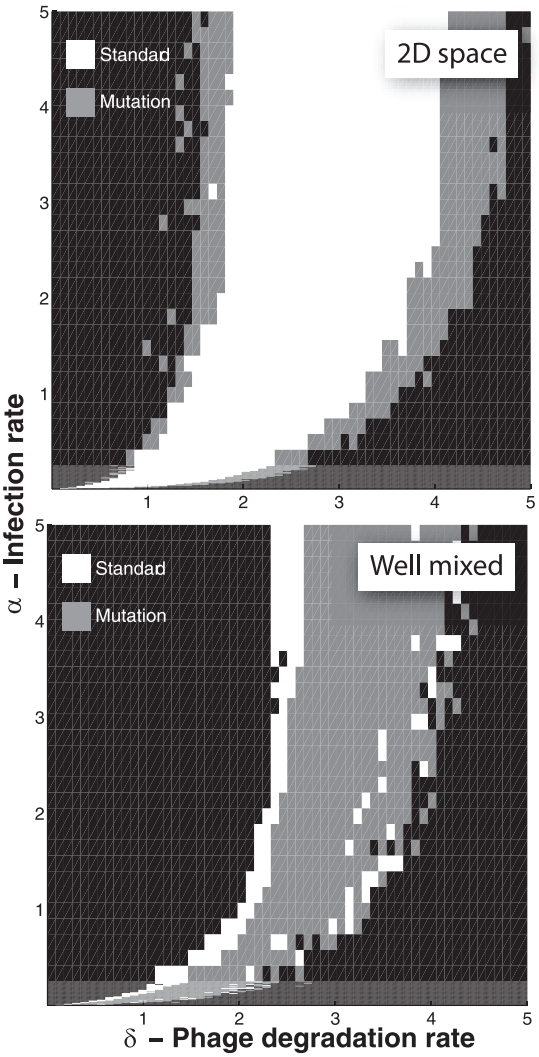


FIG. 4. Effect of an adaptive phage strategy where latent times are allowed to mutate. (Top) The white region corresponds to parameters where there is coexistence in the spatial model both with and without latent time mutability, while the gray region shows where there is coexistence only when latent time mutability is implemented. (Bottom) The gray region corresponds to parameters where there is coexistence in the well-mixed model both with and without latent time mutability, while the white region shows where there is coexistence only when latent time mutability is not implemented.

infection front of the optimal phage actually moves faster than the growth front of the bacterial colony.

One then wonders why the host population is not wiped out by the appearance of these optimal "efficient killers," resulting in an overall reduction of coexistence compared to the standard spatial model.

The reason this does not happen is that when an "optimal" phage mutant arises in a colony, it quickly wipes it out and subsequently goes extinct if it cannot quickly find another colony nearby to infect. Thus, when the bacterial population is split into many small colonies, there is effective selection against very efficient phage. In turn, the very existence of phage with different latent times makes the system self-organize to have a larger number of small bacterial colonies compared to the basic spatial model, as shown in Fig. 5d.

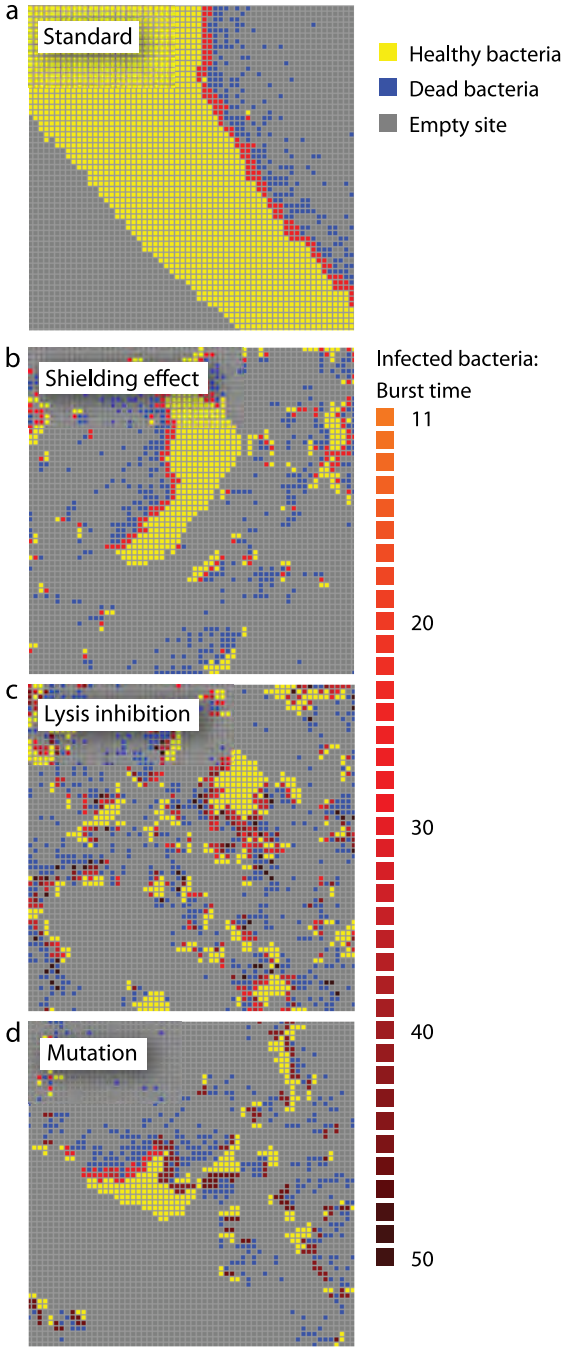


FIG. 5. Close-up views of ecosystem snapshots of the spatial model for parameters corresponding to point A in Fig. 1. (a) Basic spatial model (phage latent time is fixed at $\tau = 30$). (b) Phage infect live, dead, and infected bacteria alike (phage latent time is fixed at $\tau = 30$). (c) Basic spatial model with delayed lysis upon superinfection (phage latent time is $\tau = 30$ but increases with 8 time steps upon each super infection). (d) Basic spatial model with latent time mutability (phage latent time $\tau$ can mutate to any value in the range 11 to 50 time steps). Light red/orange cells are bacteria infected by phage with shorter latent times, while dark red/brown cells are bacteria infected by phage with long latent times. Free phage are not shown.

In contrast, in the well-mixed model, overefficient phage that arise have access to the entire bacterial population, so there is no negative selection to restrain them. This, along with the increased oscillations we observe when implementing the

adaptive strategy in the well-mixed model, makes coexistence harder to achieve than in the absence of latent time mutability (Fig. 4, bottom panel).

## DISCUSSION

**Spatial heterogeneity boosts coexistence.** The comparison between the spatial and well-mixed models shows that space boosts coexistence—even uniform two-dimensional space, without any built-in heterogeneities, such as permanent bacterial refuges. Spatial heterogeneity arises spontaneously as a result of the dynamic interaction between the bacterial growth front and the propagating phage infection front and is crucial for enhancing coexistence. In the well-mixed model, which lacks this heterogeneity, the infection and burst events are more prone to happen in sync for the whole system, often resulting in large-amplitude oscillations that destroy coexistence. In the spatial model, each small bacterial colony might experience oscillations or big population fluctuations, but on a larger spatial scale, these average out because the life cycles of the phage attacking separate colonies quickly become desynchronized and uncorrelated.

Looking at Fig. 1, moving from point A deeper into the coexistence region, to point B (by increasing $\delta$) or point C (by decreasing $\alpha$), results in more heterogeneity in a snapshot of the system. When phage infect dead or previously infected bacteria, their $\delta$ is effectively increased, and when phage delay lysis upon superinfection, their $\alpha$ is effectively decreased. Thus, one would expect both behavioral mechanisms to increase heterogeneity compared to the basic spatial model. This is exactly what we see in Fig. 5, which shows snapshots of the ecosystem for the basic spatial model and the different strategies, for the same parameter values.

That shielding by dead bacteria enhances coexistence has been observed before in models that lack space (1, 17). However, in these models, to see a significant effect, the dead bacteria must remain in the system for quite long times. In our spatial model, the enhancement of coexistence is much more dramatic. Even when the degradation rate of the dead bacteria is such that we cannot see any enhancement of coexistence in the well-mixed model (see the supplemental material), we still see a distinct enhancement in the spatial model. This is because the free phage and dead bacteria are typically colocalized here—both are "created" by the same events.

The mechanism of lysis inhibition also works in slightly different ways in the spatial and well-mixed models. It has been previously argued that this mechanism could enhance coexistence in the following way: the original infecting phage interpret superinfection as a sign that phage outnumber host cells in the external environment (18), whereupon delaying lysis gives the few bacteria left alive out there an additional chance to reproduce, thereby reducing the risk of driving them to extinction (22). This reasoning breaks down in the well-mixed case because lysis inhibition also creates ticking "time bombs"; multiply superinfected bacteria that release a huge number of phage when they eventually burst, which counteract the effect of allowing bacteria more time to replicate. In the spatial model, however, these time bombs are typically left behind by the moving infection front, so when they do lyse and release a huge number of phage, these phage are generally relatively far from susceptible bacteria. (We observe some enhancement of coexistence in the well-mixed model also when lysis inhibition is implemented [see the supplemental material], which occurs because the strategy of delaying lysis desynchronizes burst events and therefore dampens oscillations.)

**Survival of the mediocre killers.** One of the most interesting aspects of the adaptive strategy in a spatial setting is that it exhibits selection against the most efficient killers since these deplete resources locally and subsequently die out. This part of our study thus emphasizes that one must be careful in assessing what is "optimal" behavior for a phage. Calculations that try to determine optimal latent times, for instance, often take the short-term view of maximizing the phage population growth rate (25, 27). Recognizing the risks of making assumptions of this kind has led others to suggest extending the notion of fitness to include "environmental inheritance" (8). Our study supports this point of view: for long-term survival in a spatial environment, virulent phage must ensure that their offspring inherit an environment with sufficient resources. Space promotes survival of mediocre killers.

## ACKNOWLEDGMENTS

This work was funded by the Danish National Research Foundation.

We thank Ryland Young for fruitful discussions during the construction of the model.

## REFERENCES

1. **Aviram, I., and A. Rabinovitch.** 2008. Dynamical types of bacteria and bacteriophages interaction: shielding by debris. J. Theor. Biol. **251:**121–136.
2. **Bode, W.** 1967. Lysis inhibition in Escherichia coli infected with bacteriophage T4. J. Virol. **1:**948–955.
3. **Brockhurst, M. A., A. Buckling, and P. B. Rainey.** 2006. Spatial heterogeneity and the stability of host-parasite coexistence. J. Evol. Biol. **19:**374–379.
4. **Campbell, A.** 1961. Conditions for the existence of bacteriophage. Evolution **15:**153–165.
5. **Carletti, M.** 2007. Mean-square stability of a stochastic model for bacteriophage infection with time delays. Math. Biosci. **210:**395–414.
6. **De Paepe, M., and F. Taddei.** 2006. Viruses—life history: towards a mechanistic basis of a trade-off between survival and reproduction among phages. PLoS Biol. **4:**e193.
7. **Dressman, H. K., and J. W. Drake.** 1999. Lysis and lysis inhibition in bacteriophage T4: rV mutations reside in the holin t gene. J. Bacteriol. **181:** 4391–4396.
8. **Goodnight, C., E. Rauch, H. Sayama, M. A. M. de Aguiar, M. Baranger, and Y. Bar-Yam.** 2008. Evolution in spatial predator-prey models and the "prudent predator": the inadequacy of steady-state organism fitness and the concept of individual and group selection. Complexity **13:**23–44.
9. **Heilmann, S.** 2009. Survival of the mediocre killers—space and mutability in phage-bacteria ecosystems. Master's thesis. Copenhagen University, Copenhagen, Denmark. http://www.nbi.dk/heilmann/silja/thesisdownload.php.
10. **Kerr, B., C. Neuhauser, B. J. M. Bohannan, and A. M. Dean.** 2006. Local migration promotes competitive restraint in a host-pathogen "tragedy of the commons." Nature **442:**75–78.
11. Reference deleted.
12. **Lapchin, L., and T. Guillemaud.** 2005. Asymmetry in host and parasitoid diffuse coevolution: when the red queen has to keep a finger in more than one pie. Front. Zool. **2:**4–8.
13. **Levin, B. R., F. M. Stewart, and L. Chao.** 1977. Resource-limited growth, competition, and predation: a model and experimental studies with bacteria and bacteriophage. Am. Nat. **111:**3–24.
14. **Levin, B. R., and J. J. Bull.** 1996. Phage therapy revisited: the population biology of a bacterial infection and its treatment with bacteriophage and antibiotics. Am. Nat. **147:**881–898.
15. **Middelboe, M.** 2000. Bacterial growth rate and marine virus-host dynamics. Microb. Ecol. **40:**114–124.
16. **Ortega-Cejas, V., J. Fort, V. Méndez, and D. Campos.** 2004. Approximate solution to the speed of spreading viruses. Phys. Rev. E Stat. Nonlin. Soft Matter. Phys. **69:**031909.
17. **Rabinovitch, A., I. Aviram, and A. Zaritskyc.** 2003. Bacterial debris—an ecological mechanism for coexistence of bacteria and their viruses. J. Theor. Biol. **224:**377–383.
18. **Ramanculov, E., and R. Young.** 2001. Genetic analysis of the T4 holin: timing and topology. Gene **265:**25–36.

19. **Rosvall, M., I. B. Dodd, S. Krishna, and K. Sneppen.** 2006. Network models of phage-bacteria coevolution. Phys. Rev. E Stat. Nonlin. Soft Matter. Phys. **74:**066105.
20. **Schrag, S. J., and J. E. Mittler.** 1996. Host-parasite coexistence: the role of spatial refuges in stabilizing bacteria-phage interactions. Am. Nat. **148:**348–377.
21. **Stewart, F. M., and B. R. Levin.** 1984. The population biology of bacterial viruses: why be temperate. Theor. Popul. Biol. **26:**93–117.
22. **Streips, U. N., and R. E. Yasbin.** 2002. Modern microbial genetics. Wiley-Liss, New York, NY.
23. **Van Valen, L.** 1973. A new evolutionary law. Evol. Theory **1:**1–30.
24. **Vos, M., P. J. Birkett, E. Birch, R. I. Griffiths, and A. Buckling.** 2009. Local adaptation of bacteriophages to their bacterial hosts in soil. Science **325:**833.
25. **Wang, I.-N., D. E. Dykhuizen, and L. B. Slobodkin.** 1996. The evolution of phage lysis timing. Evol. Ecol. **10:**545–558.
26. **Wang, I.-N., D. L. Smith, and R. Young.** 2000. Holins: the protein clocks of bacteriophage infections. Annu. Rev. Microbiol. **54:**799–825.
27. **Zheng, Y., D. K. Struck, C. A. Dankenbring, and R. Young.** 2008. Evolutionary dominance of holin lysis systems derives from superior genetic malleability. Microbiology **154:**1710–1718.

# Coexistence of phage and bacteria on the boundary of self-organized refuges

Silja Heilmann[a,1], Kim Sneppen[a], and Sandeep Krishna[b]

[a]Center for Models of Life, Niels Bohr Institute, University of Copenhagen, 2100 Copenhagen, Denmark; and [b]National Center for Biological Sciences, GKVK, Bangalore 560065, India

Edited by Sankar Adhya, National Institutes of Health, National Cancer Institute, Bethesda, MD, and approved June 21, 2012 (received for review January 19, 2012)

**Bacteriophage are voracious predators of bacteria and a major determinant in shaping bacterial life strategies. Many phage species are virulent, meaning that infection leads to certain death of the host and immediate release of a large batch of phage progeny. Despite this apparent voraciousness, bacteria have stably coexisted with virulent phages for eons. Here, using individual-based stochastic spatial models, we study the conditions for achieving coexistence on the edge between two habitats, one of which is a bacterial refuge with conditions hostile to phage whereas the other is phage friendly. We show how bacterial density-dependent, or quorum-sensing, mechanisms such as the formation of biofilm can produce such refuges and edges in a self-organized manner. Coexistence on these edges exhibits the following properties, all of which are observed in real phage–bacteria ecosystems but difficult to achieve together in nonspatial ecosystem models: (*i*) highly efficient virulent phage with relatively long lifetimes, high infection rates and large burst sizes; (*ii*) large, stable, and high-density populations of phage and bacteria; (*iii*) a fast turnover of both phage and bacteria; and (*iv*) stability over evolutionary timescales despite imbalances in the rates of phage vs. bacterial evolution.**

prey | heterogeneity



Virulent phage are remarkably efficient predators. For every bacterial infection, they produce on the order of 100 copies of themselves, in just a time span of around one bacterial generation (1). Such a high predator–prey conversion factor is unheard of for most macroscopic ecosystems. Questions related to phage bacteria coexistence, population dynamics, and evolution have been studied extensively both theoretically and experimentally, e.g., in refs. 2–8. However, it remains a puzzle exactly how virulent phage avoid driving their bacterial prey to extinction (9–11).

Perhaps the most prominent explanation for how virulent phage manage to coexist with their bacterial hosts is that they are continuously engaged in a balanced coevolutionary arms race where bacteria constantly avoid disaster by evolving resistance to existing phage and the phage then counterevolve to attack resistant bacteria. This "Red Queen" argument (12) has, however, been criticized by some on the grounds that the rates of evolution of phage and bacteria are not necessarily symmetric (13, 14). Recent measurements support this: In soil, phage appear to be "ahead of the bacteria in the coevolutionary arms race" (ref. 15, p. ■■■). For the Red Queen argument to work it is necessary that at every stage the phage and bacteria must coexist, without one or the other becoming extinct, for long enough to allow resistant bacteria to evolve. In our view, therefore, although coevolution is responsible for very long-term coexistence between virulent phage and bacteria (e.g., refs. 5 and 7), it is important to explore nonevolutionary mechanisms that can stabilize predator–prey populations. In this paper we focus on spatial heterogeneity as one such mechanism and show how enhanced coexistence in the short term ties in to stability of the longer-term coevolutionary arms race.

The degree of spatial heterogeneity is high in many typical phage bacteria environments, for example in soil and biofilm, and it has been suggested that spatial bacteria refuges aid coexistence to some degree in these milieus: Schrag and Mittler (16) showed that coexistence between virulent phage and bacteria is feasible in a chemostat but not in serial cultures, due to biofilm refuge formation. Experiments done by Brockhurst et al. (17) indicate that reduced phage dispersal can prolong coexistence for virulent phage and bacteria in spatial environments by creating ephemeral refuges for the bacteria. The impact of spatial heterogeneity on phage–bacteria coexistence has been explored computationally by Kerr et al. (6). Using a simple cellular automaton, modeling fragmented populations of phage and bacteria, they showed that coexistence was more easily achieved when the phage migration pattern induced spatial heterogeneity. In macroecology, it has been argued theoretically that prey refuges may help stabilize predator–prey interactions (18, 19). The formation of a spatial refuge invariably leads to the formation of a boundary zone or edge between two different environments and studies of natural macroecosystems have shown that there is an increased biodiversity on edges between different types of habitats (e.g., ref. 20).

Here we use an individual-based stochastic spatial model to explore the effect of bacterial refuges on coexistence of virulent phage and their bacterial hosts. We further explore density-dependent mechanisms, such as quorum-sensing–triggered biofilm formation, that allow bacteria to create refuges in a self-organized manner. Both for spatially fixed refuges and for self-organized ones, we find that the phage and bacteria can coexist along the edges of the refuges and that this coexistence is remarkably robust to changes of parameters that affect phage efficiency and to alterations in the details of the model rules. (Henceforth we use the term "phage efficiency" to mean the phage growth rate in an environment where the bacterial density is kept constant. Parameters that influence phage efficiency are, for example, the infection rate $\alpha$, the burst size $\beta$, the phage degradation rate $\delta$, and the phage diffusion constant.

Finally, we explore evolutionary models where phage efficiency can evolve and find that the possibility of creating spatial refuges pushes the system toward more stable coexistence.

## Results

**Coexistence in the Basic Model Occurs only for a Narrow Range of Parameters.** In a previous study (11), we established which parameter ranges allow stable coexistence in a 2D phage–bacteria ecosystem model (the basic model described in *Materials and Methods*). Fig. 1 shows that coexistence is possible only in a narrow

Author contributions: S.H., K.S., and S.K. designed research; S.H. performed research; S.H., K.S., and S.K. analyzed data; and S.H. and S.K. wrote the paper.

The authors declare no conflict of interest.

This article is a PNAS Direct Submission.

[1]To whom correspondence should be addressed. E-mail: heilmann.silja@gmail.com.

This article contains supporting information online at www.pnas.org/lookup/suppl/doi:10.1073/pnas.1200771109/-/DCSupplemental.

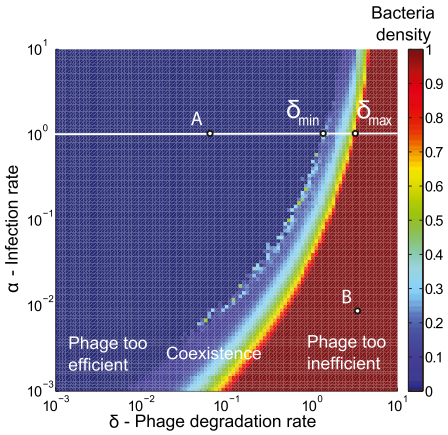


**Fig. 1.** Narrow coexistence region for basic model. Colors shows average bacterial density for simulations after 1,000 bacterial generations have passed as a function of phage infection rate (α) and degradation rate (δ). Dark red is the maximal bacterial density of one, and dark blue is zero; colors in between signify that bacteria and phage coexist. For each value of α there exists an interval $[\delta_{min}, \delta_{max}]$, outside of which there will be no coexistence. Here these points are marked for $\alpha = 1 \cdot 10^{-1}$ min$^{-1}$. Points *A* and *B* show the parameters used for the simulation shown in Fig. 4. The grid size used in these simulations was 100 × 100, and initial conditions were randomly scattered uninfected bacteria (at density 0.05) and bacteria infected with phage (at density 0.005).

range of the phage degradation rate (δ) and infection rate (α) values. (We define coexistence to mean that neither phage nor bacteria go extinct for up to 1,000 bacterial generations. The number 1,000 was chosen for practical reasons only—so simulations are completed in a reasonable time with the computational resources at our disposal—but is also long enough for our overall aim of testing mechanisms to determine whether they can stabilize the populations for long enough to allow bacteria to evolve resistance.)

On either side of this region, phage and bacteria cannot coexist for two different reasons. On the right side (red region), phage are too inefficient and die out even at high bacterial density. On the left side (blue region), phage are too efficient; they drive the bacteria to extinction and subsequently die out themselves. In the narrow region in the middle, coexistence is possible because the degradation rate is high enough and/or the search times for new bacterial hosts are long enough to ensure that most phage offspring die before they can find and successfully infect a new host. Hence, for these parameters, the phage and bacteria can coexist despite the large phage burst size. However, the narrowness of the region indicates that coexistence in this basic model is fine-tuned and may not be robust to evolutionary or environmental changes that perturb the parameter values affecting phage efficiency.

**Bacterial Refuges Enhance Coexistence.** To test whether bacterial refuges can stabilize phage–bacteria coexistence, we begin by introducing a spatial refuge in the basic model. We divide the plane in two halves and allow phage efficiency to take on different values in the two halves (see *Materials and Methods* for details). As expected, when parameter values in either one of the half-planes are chosen from within the coexistence region in Fig. 1 of the basic model, we get coexistence here too, whereas if parameters of both half-planes lie in the same noncoexistence region, then we do not observe coexistence.

Whenever parameters for one half are chosen from the right *non*-coexistence region of Fig. 1 (where phage are too inefficient to coexist in the basic model), whereas parameters in the other half are chosen from the left *non*-coexistence region (where phage are too efficient to coexist in the basic model), a more interesting phenomenon is seen. In this case, we observe coexistence of phage and bacteria, which is stable for at least 1,000 bacterial generations. The phage exist only in a zone around the edge between the two halves. The dynamics and width of this zone vary considerably, as seen in Fig. 2, which shows snapshots from three different simulations of the fixed bacterial refuge model where only δ, the phage degradation rate, differs between the two half-planes. The same is observed when the phage infection rate α is varied between the two half-planes, keeping all other parameters fixed, or when combinations of δ, α, β (burst size), and the phage diffusion constant are varied between the half-planes. It is interesting that it is thus possible to obtain long coexistence when the parameters in each half-plane in isolation would lead to fast extinction of phage or bacteria. The only condition required for long coexistence is that one half-plane must be a bacterial refuge (i.e., the parameter values there make phage too inefficient to survive), whereas the other is phage friendly. Thus, this stabilization of coexistence occurs for parameter values spanning many orders of magnitude: a vast set compared with the narrow band of parameters that allows coexistence in the basic model.

**Density-Dependent Mechanisms Can Create Self-Organized Bacterial Refuges.** In the above model, the bacterial refuge is determined before the simulation and occupies a fixed position in space. We wanted to test whether the same enhancement of coexistence is possible if bacterial refuges instead form dynamically. In particular, we examined whether mechanisms that create phage unfriendly conditions in areas of high bacterial density are sufficient to produce robust coexistence.

Substantial evidence exists in the literature that conditions for phage can be more difficult inside a dense bacterial colony. Nutrient depletion and limitation change the physiological condition for the cells and make them down-regulate receptors for phage adsorption (21, 22). Further, murein, which forms the cell wall, becomes hypercross-linked and richer in covalently bound

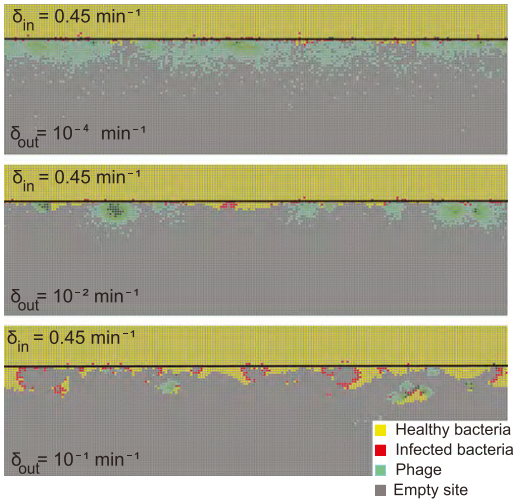


**Fig. 2.** Snapshots of fixed bacterial refuge simulations. The plane is divided into two halves. The upper part is a bacterial refuge where phage cannot sustain themselves for long because of a high phage degradation rate. The three snapshots show simulations with three different $\delta_{out}$ values in the lower part of the system. The $\delta_{in}$ value in the upper part of the system (the bacterial refuge) is kept constant at $\delta_{in} = 0.45$ min$^{-1}$. Grid size: 150 × 150. Initial conditions: upper plane was filled with uninfected bacteria and one line of infected bacteria was placed on the boundary between the two halves. (*Top*) $\delta_{out} = 10^{-4}$ min$^{-1}$. (*Middle*) $\delta_{out} = 10^{-2}$ min$^{-1}$. (*Bottom*) $\delta_{out} = 10^{-1}$ min$^{-1}$.

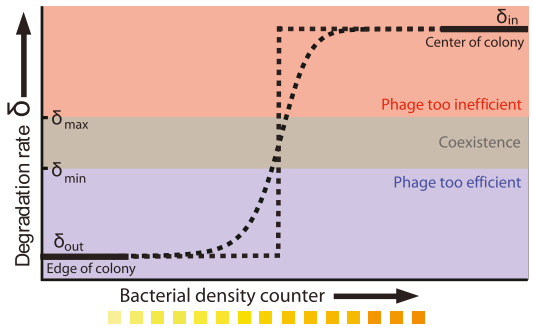


**Fig. 3.** Phage degradation rate dependence on bacterial density counter. One way of implementing the self-organized bacterial refuge model is by making phage degradation rate an increasing function of the bacterial density counter. Thereby, bacteria that are young or alone occupy sites where the phage degradation rate is low, whereas bacteria that have spent some time at high density are at sites with high phage degradation rates. The plot shows schematically how this method may be done. The degradation rate at zero and maximal density counter values are denoted $\delta_{out}$ and $\delta_{in}$, respectively. Also shown schematically is the region between $\delta_{min}$ and $\delta_{max}$, where phage and bacteria would coexist in the basic model. $\delta_{out}$ and $\delta_{in}$ can be chosen without restriction, but phage–bacteria coexistence is enhanced when they are chosen as shown, with $\delta_{out} < \delta_{min}$ and $\delta_{in} > \delta_{max}$. The dotted lines signify that we have also tried smoother, sigmoidal, functions and this method gives similar results.

lipoprotein (23), which may alter the kinetics of phage infection. Reduced infection rates, for cells in stationary phase, have for this reason also been used in other model studies (8). Reduced burst size and prolonged latent times have also been observed for cells with low growth rate/low metabolic activity, as well as for cells in stationary phase, in several studies (24–29). Another challenge for phage in high cell density is that bacterial quorum-sensing systems may trigger production of biofilm. Diffusibility inside a biofilm is locally significantly reduced due to high density of exopolymers produced by bacteria (30). Inside a biofilm, tight cell–cell binding may directly block phage receptors (31) and this action could also reduce phage infection. Also biofilms often contain proteolytic enzymes as well as endoglycanases that can lead to phage inactivation (26).

**Self-Organized Bacterial Refuges also Enhance Coexistence.** To test the effect of density-dependent formation of bacterial refuges, we constructed another version of the basic model where parameters such as the infection rate α and phage degradation rate δ can be different at different spatial locations. However, unlike the fixed bacterial refuge model, the values are not prespecified at each point in space. Instead they depend on local bacterial density as it develops dynamically during the course of the simulation (*Materials and Methods*). We implement the density-dependent effect by assigning to each bacterium a "density counter." Each counter is an integer number that is incremented every time step that the bacterium spends with three or more neighbors and decremented otherwise. The value of these counters thus correlates with how long a bacterium has spent recently in high density. We then let the parameters of a specific site in the grid depend on the density counter of the bacterium that occupies that site, such that when the bacteria are young or alone, and thus have a low density-counter value, they are more susceptible to phage. Fig. 3 shows schematically how this method can be done by making the phage degradation rate δ an increasing function of the density-counter value. Similarly phage infection rate or burst size or diffusion $(\alpha, \beta, \lambda)$, or combinations of all of these, can be made a decreasing function of the density counter. In this model we observe long-lived coexistence: Bacterial refuges self-organized and the system developed an almost static pattern of bacterial islands, with phage proliferating on new bacteria produced on the edges of the islands (Fig. 4). This phenomenon occurs for a huge range of parameter values and is stable against many changes in the model rules (see *SI Appendix* for details on this process). Fig. 5 shows the duration of coexistence as a function of $\delta_{out}$ and $\delta_{in}$, for simulations where only δ depends on the density counter ($\delta_{out}$ and $\delta_{in}$ are the values of δ for sites with minimal and maximal density-counter values, respectively) (Fig. 3). In the region where $\delta_{in} > \delta_{max}$ and $\delta_{out} < \delta_{min}$, we find that coexistence times rise steeply compared with the values outside this region (Fig. 3 shows simulations that last at most 1,000 bacterial generations, but on the basis of a few longer simulations we suspect that coexistence times are much larger for parameter values deeper within this region). What is required for long-lived coexistence on the edge of bacterial refuges is merely that the bacteria in the center of the colony are so resilient that phage cannot sustain themselves in there, whereas recently divided bacteria on the edge of the colonies are (possibly very) susceptible to phage infection.

**Evolution of Bacterial Refuges.** We next extended the self-organized refuge model to allow both bacteria and phage to evolve. Fig. 6 shows the results of one such implementation, where $\delta_{in}$ was a property that bacteria pass on to their offspring and $\delta_{out}$ a property inherited by phage offspring from their parents, and both were allowed to mutate (*Materials and Methods* and *SI Appendix*, Figs. S15–S18). The colored trajectories in Fig. 6 starting at different initial conditions each show, as time progresses, the changing values of $\delta_{in}$ and $\delta_{out}$, averaged over all phage and bacteria at that time. We see how the average parameters of the system are all pushed deeper into the blue-shaded region, toward more long-lived coexistence, by bacteria evolving to increase $\delta_{in}$ and phage evolving to decrease $\delta_{out}$. Note that we chose the initial values of $\delta_{in}$ and $\delta_{out}$ in these simulations to be outside the coexistence region. Thus, in the absence of evolution, coexistence would not have lasted very long. A similar pattern is seen when we allow the infection rates, $\alpha_{in}$ and $\alpha_{out}$, to mutate instead (*SI Appendix*, Fig. S18). Interestingly, this pattern was also maintained when the mean mutation step sizes of phage and bacteria were very different. For example, we observed that evolution of $\delta_{in}$ and $\delta_{out}$ from the initial condition of $\delta_{in} = \delta_{out} = 1.0 \cdot 10^{-1} \text{min}^{-1}$ was able to bring the system into the

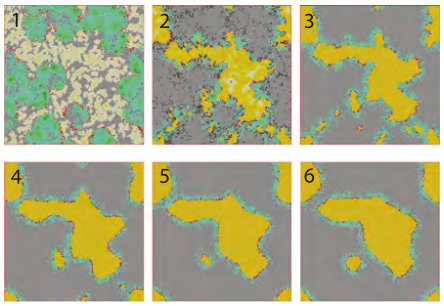


**Fig. 4.** Snapshots of simulations of the self-organized bacterial refuge model. After awhile bacteria in the center of colonies reach the maximal density-counter value and grid sites inside colonies become phage unfriendly (bacteria with low density counters are light yellow and bacteria with increasingly higher density counters are colored darker shades of yellow). New bacteria with density counter equal to zero are produced at the colony edges. Parameters were $(\delta_{out}, \alpha_{out}) = (0.05 \cdot 10^{-1}\ \text{min}^{-1},\ 1.0 \cdot 10^{-1}\ \text{min}^{-1})$ and $(\delta_{in}, \alpha_{in}) = (5.0 \cdot 10^{-1}\ \text{min}^{-1},\ 0.01 \cdot 10^{-1}\ \text{min}^{-1})$ marked by *A* and *B* in Fig. 1. The initial condition was randomly distributed bacteria with density counter equal to zero and a few infected with phage. Grid size: 200 × 200. 1, snapshot taken 4 bacterial generations (bac. gen.) after $t = 0$; 2, after 8 bac. gen.; 3, after 70 bac. gen.; 4, after 500 bac. gen.; 5, after 1,000 bac. gen.; and 6, after 2,000 bac. gen.

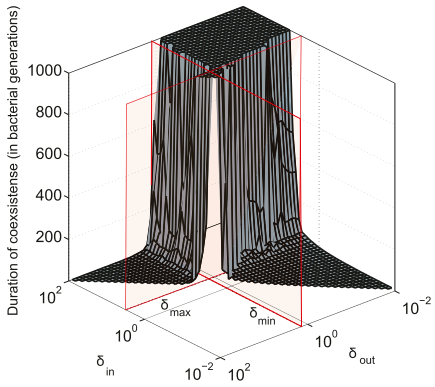


**Fig. 5.** Long-lived coexistence for a broad range of $\delta_{in}$ and $\delta_{out}$. Shown is duration of coexistence as a function of $\delta_{in}$ and $\delta_{out}$ ($\alpha_{in} = \alpha_{out} = 1.0 \cdot 10^{-1}$ min$^{-1}$). Red lines mark $\delta_{min}$ and $\delta_{max}$ for $\alpha = 11.0 \cdot 10^{-1}$ min$^{-1}$ in the basic model. If time reached 1,000 bacterial generations while there was still coexistence (i.e., both phage and bacteria were present), then the simulation was stopped. Only parameter sets where $\delta_{out} \leq \delta_{in}$ were considered. Within the region where $\delta_{in} > \delta_{max}$ and $\delta_{out} < \delta_{min}$ the phage and bacteria coexisted for durations much longer than the bacterial generation time. In this region, the average infection front speeds were also relatively low (*SI Appendix*). When $\delta_{in} > \delta_{max}$ and $\delta_{out} > \delta_{min}$, the phage live for a short time on the edge of the expanding bacterial colony before dying out. When $\delta_{in} < \delta_{max}$ and $\delta_{out} < \delta_{min}$, the phage infection fronts rapidly eat into the colonies and eventually wipe out the bacteria. In the small region where both $\delta_{in}$ and $\delta_{out}$ are within the narrow range of $[\delta_{min}, \delta_{max}]$, there is stable coexistence. Grid size: 100 × 100. Initial conditions: upper half-plane filled by uninfected bacteria and a single line of infected bacteria on the boundary between the upper part and the empty lower half-plane.

blue region of Fig. 6 both when $\mu_{phage}/\mu_{bacteria} = 0.1$ and when $\mu_{phage}/\mu_{bacteria} = 5$.

## Discussion

In this paper we explore bacterial refuges and their formation by density-dependent mechanisms as a mechanism for enhancing phage–bacteria coexistence. We find that coexistence between a virulent phage and its bacterial host is remarkably stable and robust on boundaries between habitats within each of which coexistence is not possible—provided one habitat is a bacterial refuge where conditions are hostile to phage, whereas the other is phage friendly. We further show that this enhancement of coexistence also stabilizes the long-term coevolution between phage and bacteria.

Spatial heterogeneity is a prominent feature of many real phage–bacteria ecosystems. This heterogeneity is reflected in the fact that soil or biofilms, and even ocean data, show high variability of phage and bacteria density over small length scales (32). In oceans, heterogeneity could be self-organized by cyanobacteria making colonies in the form of sheets and mats (33).

Many bacteria can at high density create a heterogenous and somewhat phage-hostile environment by themselves. One such density-dependent mechanism is the use of quorum-sensing systems to trigger biofilm formation. Biofilm is not invincible to phage attack (30) but many factors contribute to make phage existence in biofilm harsher as discussed earlier. Costerton et al. (34) report that *Escherichia coli* persist in the intestinal tract by adhering to tissue surfaces and food particles, where they live in encapsulated microcolonies akin to biofilms. Sternberg et al. (35) report that within biofilms, cells typically form clusters (microcolonies) with the most metabolically active cells located on the periphery of each microcolony. This formation resembles the self-organized bacterial clusters formed in our simulations. Corbin et al. (30) observe ongoing phage proliferation and sustained coexistence of bacteria and phage populations of T4 in *E. coli* glucose-limited biofilm. They suggest that virulent phage multiply only in the part of the *E. coli* biofilm population where bacteria are not in stationary phase. Other studies have also reported that phage may alter biofilm morphology but that bacteria and virulent phage are able to coexist stably inside biofilm (26, 36).

**Characteristics of Phage–Bacteria Coexistence on Edges of Refuges.** In our simulations, we found that density-dependent, or quorum-sensing, mechanisms are a robust way of forming self-organized bacterial refuges. And having stable refuges is in turn a robust way to enhance phage–bacteria coexistence. We found that coexistence, in these simulations, has the following characteristics: (*i*) Phage and bacterial densities are quite high with phage being concentrated on the edges of dense bacterial colonies, (*ii*) phage can outnumber bacteria by easily an order of magnitude without destabilizing the system, and (*iii*) there is a high turnover of the phage population and also of the bacterial population at the edge of colonies (*SI Appendix*, Figs. S11–S13). And all this coexistence happens despite the phage being intrinsically very efficient predators, with a large burst size, long lifetimes, and high infection rates outside the bacterial refuge. In the absence of refuges, coexistence between phage and bacteria is difficult to obtain and has very different characteristics because a higher phage efficiency is incompatible with stable and high bacterial density and high turnover of both phage and bacteria populations. The only way to get coexistence with an efficient phage in the absence of refuges is to have a sufficiently low bacterial density so that it takes so long to find new host bacteria that on average only a single phage from a burst survives long enough to infect a new bacterium (11). Data from soil (37) and marine (38)

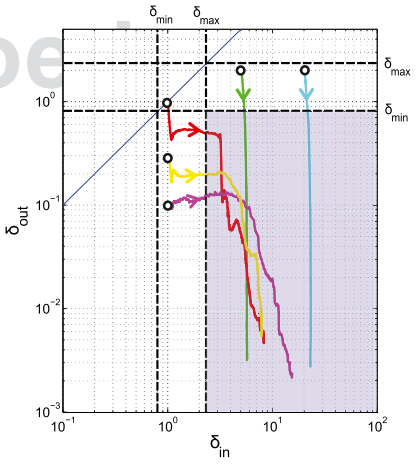


**Fig. 6.** Evolution pushes the self-organized bacterial refuge system deeper into the parameter region with long-lived coexistence. Trajectories show how the system averages of $\delta_{in}$ and $\delta_{out}$ change during five different simulations (each lasting 3,000 time steps) in the self-organized bacterial refuge model when bacteria and phage are permitted to evolve ($\delta_{in}$ was an inheritable characteristic of the bacteria whereas $\delta_{out}$ was an inheritable characteristic of the phage, both passed on vertically to offspring with the chance of small changes; new offspring values were picked from a normal distribution with a mean equal to the parent value and a variance of $\mu_{bacteria} = 0.07$ and $\mu_{phage} = 0.1$, respectively). We see that selection tends to push $\delta_{in}$ to higher values and $\delta_{out}$ toward lower values. This process drives the system deeper into the parameter region where $\delta_{in} > \delta_{max}$ and $\delta_{out} < \delta_{min}$ (the light blue region), where the phage and bacteria coexist for much longer than the bacteria generation time. Grid size: 150 × 150. Initial conditions: randomly scattered uninfected bacteria and a few infected. Purple start point: $(\delta_{in}, \delta_{out}) = (1.0 \cdot 10^{-1}$ min$^{-1}, 0.1 \cdot 10^{-1}$ min$^{-1})$. Yellow start point: $(\delta_{in}, \delta_{out}) = (1.0 \cdot 10^{-1}$ min$^{-1}, 0.3 \cdot 10^{-1}$ min$^{-1})$. Red start point: $(\delta_{in}, \delta_{out}) = (1.0 \cdot 10^{-1}$ min$^{-1}, 1.0 \cdot 10^{-1}$ min$^{-1})$. Green start point: $(\delta_{in}, \delta_{out}) = (5.0 \cdot 10^{-1}$ min$^{-1}, 2.0 \cdot 10^{-1}$ min$^{-1})$. Blue start point: $(\delta_{in}, \delta_{out}) = (20.0 \cdot 10^{-1}$ min$^{-1}, 2.0 \cdot 10^{-1}$ min$^{-1})$.

phage–bacteria ecosystems seem to match the characteristics of the refuge model better; the population densities of both phage and bacteria are observed to be relatively high and the phage:bacteria ratio is around 10:1. Moreover, stable populations numbers and a high turnover rate of phage and bacteria are also observed: Virulent phage are estimated to kill $\approx 20-40\%$ of the bacteria in the oceans on a daily basis (38).

Our results suggest that it would be particularly interesting to measure parameters that affect phage efficiency, such as phage lifetime, infection rate, and diffusion constant, in natural ecosystems where such phage have been observed to coexist with bacteria. The lifetimes of nine different virulent phage were measured in laboratory conditions with bacteria growing on LB and found to be of the order of 10 d on average (39). However, the corresponding numbers are not known in natural ecosystems in soil or oceans. If measured parameters are found to lie outside the coexistence region of the basic model, that result would strongly suggest that there must be additional mechanisms that allow coexistence. The specific mechanism of coexistence along the edge of refuges also predicts that the variance of these parameters should be large, even over very short length scales. It would, for example, be interesting to know the variance of burst sizes in a biofilm instead of just the mean burst size. This is a qualitative prediction at the moment, but as more accurate measurements of parameters are made the more quantitative such predictions of our models will become.

The jump from our simple models to real phage–bacteria ecosystems is a substantial one, and any predictions should be treated with caution and first confirmed in simpler laboratory experiments with isogenic phage and bacteria. However, it is encouraging that the model behavior is robust to many alterations in the dynamical rules. In addition to the variants described above, we have also found qualitatively similar refuge formation and enhancement of coexistence when we added a third dimension, density-dependent bacterial growth, bacterial diffusion, and hydrodynamic flows that make bacteria and phage drift in a specific direction (*SI Appendix*, Figs. S14, S19, and S20).

**Bacterial Refuges and the Coevolutionary Arms Race.** Bacterial refuges alone are not necessarily sufficient to ensure very long-term coexistence of phage and bacteria. In real ecosystems, very long-term coexistence certainly involves bacteria evolving to become resistant to phage and phage counter-evolving strategies to infect resistant bacteria. However, such a coevolutionary arms race cannot be stable if at any time conditions arise where either the phage or the bacteria rapidly die out. For example, if a particularly efficient phage arises, it could rapidly wipe out the whole system before bacteria have time to evolve resistance. Therefore, any nonevolutionary mechanisms that enhance coexistence could play a crucial role in allowing sufficient time for evolution to occur. Self-organized bacterial refuges are one of several such possible mechanisms. We have shown that, for a very broad region of parameter space, such refuges can slow down the rate of extinction immensely, while maintaining a high density of both phage and bacteria, for time spans of at least 1,000 times longer than the bacterial generation time. The evolutionary simulations we have done complete the second part of this argument. We found that even when the system starts with parameter values that do not allow coexistence for very long, evolution of the phage and bacteria pushes these parameter values into regions that do allow coexistence. Interestingly, this outcome was true both when the phage mutated faster than the bacteria and vice versa. As one of the referees pointed out, irrespective of the particular values chosen for the mutation rates, the self-organized refuges result in an asymmetry in the evolutionary rates of phage and bacteria. Bacterial mutations occur more often at the edges of colonies because that is where new bacteria are formed, but these mutations are often quickly eliminated by phage infections. On the other hand, phage mutations (which also occur mainly at the edges) can persist and spread through the population. This process likely explains the shape of the evolutionary trajectories shown in Fig. ■■■ and in *SI Appendix*: Changes in bacterial parameters typically occur early on when the refuges are still stabilizing, whereas later the trajectory moves mainly in the direction of changing phage parameters. In these evolutionary simulations, the properties of the ecosystem described above are maintained—highly efficient phage living on the edge of almost static refuges, with a high turnover of both phage and bacterial populations—and there is continuous evolution of phage that are more efficient and bacteria that create better refuges. A very interesting direction to take these models in the future would be to include multiple phage and bacteria species with a complex network of infection and immunity interactions between them.

To summarize, we have shown that self-organized bacterial refuge formation might be a mechanism that can help facilitate coexistence and perhaps resolve several apparently paradoxical features of the phage–bacteria coexistence observed in the real world. We have shown that self-organized bacterial refuges can produce coexistence with features similar to those observed in real-world ecosystems by concentrating phage–bacteria interaction to the edges of the refuges and have argued that selection pressures will push the system toward more robust coexistence.

## Materials and Methods

**Basic Model.** We use the simple virulent phage and bacteria ecosystem model introduced in ref. 11. Phage and bacteria interact on a 2D $L \times L$ grid of "sites". Each site in the grid can be either occupied or unoccupied by a single bacterium. The bacterium may be uninfected or infected. In addition, there can be any number of free phage at that site. Time proceeds in discrete steps. Precise timers control bacterial cell division and the lysis of an infected bacterium, which releases a burst of free phage. Other processes are random, e.g., death and diffusion of phage, and are modeled as Poisson processes. In each time step the following can happen:

*i*) Bacterial replication: A bacterium with at least one empty adjacent site will attempt to divide in every time step after the current time has become greater than the value of its replication timer. The probability of replication is set proportional to the number of empty neighbor sites. Once a bacterium divides, one daughter cell remains in the original site and the other is placed randomly in one of the adjacent empty sites. The replication timers of both cells are reset to the current time plus $T$, a parameter that thus sets the growth rate of the bacteria.

*ii*) Bacterial infection: An uninfected bacterium at the same site as free phage may be infected with a probability that is set by the infection rate per phage per bacterium, $\alpha$. When an infection occurs, then the number of free phage at that site is reduced by one, and the lysis timer of the newly infected bacterium is set to $\tau$ (the latent time of the infecting phage) time steps ahead. (Note that we disallow superinfection—phage can infect only uninfected bacteria in all of the models used in this paper.)

*iii*) Bacterial lysis: An infected bacterium dies when its lysis time is reached. The number of phage at that site then increases by the burst size, $\beta$.

*iv*) Phage degradation: Free phage die with a probability determined by the phage degradation rate $\delta$.

*v*) Phage diffusion: Each free phage may jump to a neighboring site with a probability set by the phage jump rate $\lambda$ (which thus sets the phage diffusion constant).

The values of the parameters and the size of the time step depend on the choice of phage and bacteria species (see *SI Appendix*, Table S1 for explanation of symbols and parameters). For *E. coli* with a replication time of 300 min, a reasonable choice of time step would be 10 min, and each grid site would have an area of $\sim 1\ \mu m^2$. We choose $\lambda$ to keep the phage diffusion constant fixed at $D \approx 1/4$ (site area)/(time step), meaning that a phage on average will use $10^4$ time steps to move across a grid size of $L = 100$. (For the choice of *E. coli* this number would correspond to at phage diffusion constant of $2.510^{-2}\ \mu m^2/min$, which is relatively low.) See *SI Appendix* and ref. 11 for further details of model rules for bacterial replication, phage diffusion, infection, and lysis.

**Fixed Bacterial Refuge Model.** We extend the basic model to include a bacterial refuge by dividing the $L \times L$ grid into two halves. Grid points in one half are assigned one set of $\alpha, \delta, \beta$, and $\lambda$ values that make this half phage hostile—this is the bacterial refuge part of the grid. The other half is given another set of parameter values that make it phage friendly. This division is in contrast to the basic model where parameters are the same all over the grid. Phage-hostile and phage-friendly parts of the plane can be created in many ways. The simplest is where only a single phage parameter is changed. For example, $\delta$ could be high in the phage-hostile half and low in the phage-friendly half. Bacterial growth rate is the same throughout the system.

**Self-Organized Bacterial Refuge Model.** In the self-organized bacterial refuge model we again allow $\alpha, \delta, \beta$, and $\lambda$ to have different values for different grid points. However, unlike those in the fixed-refuge model, these values are not preassigned to each point. Instead they are determined dynamically during the course of simulation in a manner dependent on the density of bacteria. The rules that govern this determination mimic the formation of a biofilm within which phage efficiency is reduced. Each bacterium has a density counter, which is an integer number that goes up every time step that the bacterium spends with three neighbors or more and down each time step it spends with two neighbors or less (the counter stops increasing at a certain maximum value and never goes below zero). These counters thus keep track of how long a bacterium has spent recently in high cell density, which we assume is correlated to its being within the biofilm protection. We explore different ways, described in the main text, of making phage parameters depend on the biofilm protection, i.e., on the value of the density counter of the bacterium that occupies a site.

**Evolutionary Version of Self-Organized Refuge Model.** In this variant, the parameter values at each grid point are again determined by the value of the density counter there, but additionally the function of the density counter from which the value is computed varies across grid points (unlike the self-organized refuge model where this function was the same for all grid points). The function used is determined by the bacteria and phage that occupy that grid point. The value chosen when the density counter is maximal is an inheritable property of the bacterium, whereas the value chosen when the density counter is zero is an inheritable property of each phage. When bacteria or phage replicate, the offspring properties are normally distributed around the parent properties with variance $\mu_{\text{bacteria}}$ and $\mu_{\text{phage}}$, respectively. We have implemented several variants of this method, and an algorithmic description of the different models can be found in *SI Appendix*. A Java applet implementing the self-organized refuge model is available from S.H. The applet is interactive and allows the user to modify phage degradation and infection rates.

**ACKNOWLEDGMENTS.** We thank Ian Dodd, Keith Shearwin, Steen Pedersen, and Namiko Mitarai for fruitful discussions. We also thank the anonymous referees for suggesting several instructive variants of the models and for many useful comments. This work was funded by the Danish National Research Foundation.

1. Kutter E, Sulakvelidze A (2005) *Bacteriophages: Biology and Applications, Illustrated Edition*. (CRC, Boca Raton, FL).
2. Coberly LC, et al. (2009) Space, time, and host evolution facilitate coexistence of competing bacteriophages: Theory and experiment. *Am Nat* 173:E121–E138.
3. Thingstad TF, Lignell R (1997) Theoretical models for the control of bacterial growth rate, abundance, diversity and carbon demand. *Aquat Microb Ecol* 13:19–27.
4. Jessup CM, Forde SE (2008) Ecology and evolution in microbial systems: The generation and maintenance of diversity in phage-host interactions. *Res Microbiol* 159:382–389.
5. Buckling A, Rainey PB (2002) Antagonistic coevolution between a bacterium and a bacteriophage. *Proc Biol Sci* 269:931–936.
6. Kerr B, Neuhauser C, Bohannan BJM, Dean AM (2006) Local migration promotes competitive restraint in a host-pathogen 'tragedy of the commons'. *Nature* 442: 75–78.
7. Weitz JS, Hartman H, Levin SA (2005) Coevolutionary arms races between bacteria and bacteriophage. *Proc Natl Acad Sci USA* 102:9535–9540.
8. Weitz J, Dushoff J (2008) Alternative stable states in host-phage dynamics. *Theor Ecol* 1:13–19.
9. Campbell A (1961) Conditions for the existence of bacteriophage. *Evolution* 15: 153–165.
10. Rosvall M, Dodd IB, Krishna S, Sneppen K (2006) Network models of phage-bacteria coevolution. *Phys Rev E Stat Nonlin Soft Matter Phys* 74:066105.
11. Heilmann S, Sneppen K, Krishna S (2010) Sustainability of virulence in a phage-bacterial ecosystem. *J Virol* 84:3016–3022.
12. van Valen L (1973) A new evolutionary law. *Evol Theory* 1:1–30.
13. Rabinovitch A, Aviram I, Zaritsky A (2003) Bacterial debris-an ecological mechanism for coexistence of bacteria and their viruses. *J Theor Biol* 224:377–383.
14. Lapchin L, Guillemaud T (2005) Asymmetry in host and parasitoid diffuse coevolution: When the red queen has to keep a finger in more than one pie. *Front Zool* 2:4–8.
15. Vos M, Birkett PJ, Birch E, Griffiths RI, Buckling A (2009) Local adaptation of bacteriophages to their bacterial hosts in soil. *Science* 325:833.
16. Schrag SJ, Mittler JE (1996) Host-parasite coexistence: The role of spatial refuges in stabilizing bacteria-phage interactions. *Am Nat* 148:348–377.
17. Brockhurst MA, Buckling A, Rainey PB (2006) Spatial heterogeneity and the stability of host-parasite coexistence. *J Evol Biol* 19:374–379.
18. Kareiva P, Mullen A, Southwood R (1990) Population dynamics in spatially complex environments: Theory and data. *Philos Trans R Soc Lond B Biol Sci* 330:175–190.
19. Comins HN, Blatt DWE (1974) Prey-predator models in spatially heterogeneous environments. *J Theor Biol* 48:75–83.
20. Hufkens K, Scheunders P, Ceulemans R (2009) Ecotones in vegetation ecology: Methodologies and definitions revisited. *Ecol Res* 24:977–986.
21. Chapman-McQuiston E, Wu XL (2008) Stochastic receptor expression allows sensitive bacteria to evade phage attack. Part I: Experiments. *Biophys J* 94:4525–4536.
22. Death A, Notley L, Ferenci T (1993) Derepression of LamB protein facilitates outer membrane permeation of carbohydrates into Escherichia coli under conditions of nutrient stress. *J Bacteriol* 175:1475–1483.
23. Pisabarro AG, de Pedro MA, Vázquez D (1985) Structural modifications in the peptidoglycan of Escherichia coli associated with changes in the state of growth of the culture. *J Bacteriol* 161:238–242.
24. Sillankorva S, Oliveira R, Vieira MJ, Sutherland I, Azeredo J (2004) Pseudomonas fluorescens infection by bacteriophage PhiS1: The influence of temperature, host growth phase and media. *FEMS Microbiol Lett* 241:13–20.
25. Rabinovitch A, Fishov I, Hadas H, Einav M, Zaritsky A (2002) Bacteriophage T4 development in Escherichia coli is growth rate dependent. *J Theor Biol* 216:1–4.
26. Azeredo J, Sutherland IW (2008) The use of phages for the removal of infectious biofilms. *Curr Pharm Biotechnol* 9:261–266.
27. Middelboe M (2000) Bacterial growth rate and marine virus-host dynamics. *Microb Ecol* 40:114–124.
28. Parada V, Herndl GJ, Weinbauer MG (2006) Viral burst size of heterotrophic prokaryotes in aquatic systems. *J Mar Biol Assoc* 86:613–621.
29. Moebus K (1996) Marine bacteriophage reproduction under nutrient-limited growth of host bacteria. I. Investigations with six phage-host systems. *Mar Ecol Prog Ser* 144: 1–12.
30. Corbin BD, McLean RJ, Aron GM (2001) Bacteriophage T4 multiplication in a glucose-limited Escherichia coli biofilm. *Can J Microbiol* 47:680–684.
31. Rickard AH, Gilbert P, High NJ, Kolenbrander PE, Handley PS (2003) Bacterial coaggregation: An integral process in the development of multi-species biofilms. *Trends Microbiol* 11:94–100.
32. Suttle CA (2007) Marine viruses—major players in the global ecosystem. *Nat Rev Microbiol* 5:801–812.
33. Stal LJ (2000) *Cyanobacterial Mats and Stromatolites* (Kluwer Academic, Dordrecht, The Netherlands), pp 61–120.
34. Costerton JW, et al. (1987) Bacterial biofilms in nature and disease. *Annu Rev Microbiol* 41:435–464.
35. Sternberg C, et al. (1999) Distribution of bacterial growth activity in flow-chamber biofilms. *Appl Environ Microbiol* 65:4108–4117.
36. Tait K, Skillman LC, Sutherland IW (2002) The efficacy of bacteriophage as a method of biofilm eradication. *Biofouling* 18:305–311.
37. Ashelford KE, Day MJ, Fry JC (2003) Elevated abundance of bacteriophage infecting bacteria in soil. *Appl Environ Microbiol* 69:285–289.
38. Suttle CA (2005) Viruses in the sea. *Nature* 437:356–361.
39. De Paepe M, Taddei F (2006) Viruses' life history: Towards a mechanistic basis of a trade-off between survival and reproduction among phages. *PLoS Biol* 4:e193.

The ISME Journal (2012), 1–10

www.nature.com/ismej

ORIGINAL ARTICLE

# Acyl-homoserine lactone-dependent eavesdropping promotes competition in a laboratory co-culture model

Josephine R Chandler[1], Silja Heilmann[2], John E Mittler[1] and E Peter Greenberg[1]
[1]*Department of Microbiology, University of Washington School of Medicine, Seattle, WA, USA and*
[2]*Center for Models of Life, Niels Bohr Institute, University of Copenhagen, Copenhagen, Denmark*

**Many *Proteobacteria* use acyl-homoserine lactone (AHL)-mediated quorum sensing to activate the production of antibiotics at high cell density. Extracellular factors like antibiotics can be considered public goods shared by individuals within a group. Quorum-sensing control of antibiotic production may be important for protecting a niche or competing for limited resources in mixed bacterial communities. To begin to investigate the role of quorum sensing in interspecies competition, we developed a dual-species co-culture model using the soil saprophytes *Burkholderia thailandensis* (*Bt*) and *Chromobacterium violaceum* (*Cv*). These bacteria require quorum sensing to activate the production of antimicrobial factors that inhibit growth of the other species. We demonstrate that quorum-sensing-dependent antimicrobials can provide a competitive advantage to either *Bt* or *Cv* by inhibiting growth of the other species in co-culture. Although the quorum-sensing signals differ for each species, we show that the promiscuous signal receptor encoded by *Cv* can sense signals produced by *Bt*, and that this ability to eavesdrop on *Bt* can provide *Cv* an advantage in certain situations. We use an *in silico* approach to investigate the effect of eavesdropping in competition, and show conditions where early activation of antibiotic production resulting from eavesdropping can promote competitiveness. Our work supports the idea that quorum sensing is important for interspecies competition and that promiscuous signal receptors allow eavesdropping on competitors in mixed microbial habitats.**
*The ISME Journal* (2012) **0,** 000–000. doi:10.1038/ismej.2012.69
**Subject Category:** microbe–microbe and microbe–host interactions
**Keywords:** *Burkholderia*; *Chromobacterium*; cell–cell communication; microbial competition; quorum sensing; eavesdropping; evolution

Q6



## Introduction

Quorum sensing affords bacteria the ability to control the expression of specific genes in a cell density-dependent manner (Fuqua *et al.*, 1994, 2001; Bassler, 2002; Waters and Bassler, 2005). Many species of *Proteobacteria* use small molecules, acylated homoserine lactones (AHLs), as quorum-sensing signals. AHLs are produced by LuxI family synthases, and specifically interact with cytoplasmic LuxR family transcription factors to influence gene expression. AHL specificity is defined by the nature of the acyl side group. AHLs can diffuse through lipid bilayers and thus can move out of and into cells by diffusion. Because of the signal diffusibility, AHLs must reach a critical environmental concentration before they cause changes in gene expression. It is common that the AHL synthase gene is among the genes activated, creating a positive feedback loop that results in increased production of signal (Engebrecht *et al.*, 1983; Seed *et al.*, 1995; Latifi *et al.*, 1996; Duerkop *et al.*, 2009; Stauff and Bassler, 2011). Thus, AHL signaling can coordinate population-wide changes in a cell-density-dependent manner.

Quorum-sensing-regulated genes are predominated by those required for the production of shared 'public goods', such as secreted or excreted factors. One commonly occurring example is antimicrobials. Quorum-controlled antimicrobials have been described in many saprophytic *Proteobacteria* including *Erwinia carotovora* (Bainton *et al.*, 1992), *Pseudomonas aeruginosa* (Kownatzki *et al.*, 1987; Bainton *et al.*, 1992; Gallagher and Manoil, 2001; Ran *et al.*, 2003; Schuster and Greenberg, 2006), *Burkholderia thailandensis* (*Bt*) (Duerkop *et al.*, 2009) and *Chromobacterium violaceum* (*Cv*) (Latifi *et al.*, 1995; McClean *et al.*, 1997). Although some groups have proposed that antimicrobial activity of

Correspondence: EP Greenberg, Department of Microbiology, University of Washington School of Medicine, 1705 North East Pacific Street, Campus Box 357242, Seattle, WA 98195-7242, USA.
E-mail: epgreen@u.washington.edu
Received 30 January 2012; revised 3 May 2012; accepted 10 May 2012

secondary metabolites is a side effect and the primary function of these compounds is as signals (Davies *et al.*, 2006; Yim *et al.*, 2007), the classic view is that they are used for competition with other strains or species in multi-species environments. This classic view suggests that quorum sensing may be important for interspecies competition. Quorum sensing is best understood in the context of virulence, and few studies have addressed its importance in competition (Mazzola *et al.*, 1992; Moons *et al.*, 2005, 2006; An *et al.*, 2006). The advantage of using quorum sensing to control the production of antimicrobials is unknown, but it may allow a population to coordinate delivery of a sudden killing dose that deprives competitors of the ability to adapt during exposure to subinhibitory antimicrobial concentrations (Hibbing *et al.*, 2010, D An and M Parsek, unpublished). Quorum sensing may also defer production of an antimicrobial to minimize the metabolic cost of production.

We are interested in the connection between quorum sensing and production of antibiotics, and specifically whether quorum-sensing-controlled antibiotics are important for interspecies competition. Thus, we developed a dual-bacterial species model with two soil saprophytes, *Bt* and *Cv*. Although it is not unlikely that these species coexist in nature, we selected this pair of bacteria because we have a base of knowledge about their quorum-sensing systems, about quorum-sensing control of antibiotic synthesis and because these species exhibit similar laboratory growth characteristics. The *Bt* genome encodes three LuxR–LuxI pairs. The BtaI1–R1 pair produces and responds to octanoyl-HSL (C8-HSL). Little is known about the genes controlled by this system, but it facilitates clumping under some conditions (Chandler *et al.*, 2009). BtaI3 is a 3-hydroxy-octanoyl-HSL synthase, but little is known about BtaI3–R3 (Chandler *et al.*, 2009). Finally, BtaR2–I2 senses and produces 3-hydroxy-octanoyl-HSL and 3-hydroxy-decanoyl-HSL (Duerkop *et al.*, 2009). The BtaR2–I2 system activates *btaI2* and a set of genes responsible for the production of a family of hydrophilic antibiotics, the bactobolins, that have activity against a broad range of bacterial species (Duerkop *et al.*, 2009; Seyedsayamdost *et al.*, 2010; Carr *et al.*, 2011) including *Cv* (see below). The most potent of these is bactobolin A (Carr *et al.*, 2011).

*Cv* has a single AHL circuit, the CviR–CviI quorum-sensing system. This circuit activates genes required for the production of a purple pigment called violacein and related compounds that have broad-spectrum antimicrobial activity (McClean *et al.*, 1997). We found that *Bt* is resistant to purified violacein, but shows sensitivity to other quorum-sensing-dependent factors produced by *Cv*. The CviI-produced AHL signal is hexanoyl-HSL (C6-HSL), and although CviR is a C6-HSL-responsive transcription factor, it is promiscuous and also responds to a number of different AHL signals (McClean *et al.*, 1997; Swem *et al.*, 2009). This promiscuity may allow *Cv* to eavesdrop on other AHL-producing species. There are now a number of examples of *Proteobacteria* with promiscuous LuxR homologs (Pierson *et al.*, 1998; Riedel *et al.*, 2001; Steidle *et al.*, 2001; Venturi *et al.*, 2004; Dulla and Lindow, 2009; Ahlgren *et al.*, 2011; Hosni *et al.*, 2011). It is not known if AHL receptor promiscuity provides any advantage over more signal-specific receptors.

We report here that quorum-sensing-dependent production of antimicrobials can provide a competitive advantage to either *Bt* or *Cv* by inhibiting growth of the other species in co-culture. We also present evidence that although *Bt* and *Cv* produce different AHLs, the promiscuous signal receptor of *Cv* can sense *Bt* signals, and that this ability to eavesdrop on *Bt* can provide a competitive advantage to *Cv*. We describe a mathematical model of our dual species system and use this model to show that eavesdropping can promote fitness during competition as long as the population can produce sufficient antibiotic to kill the competitor. Our results support the idea that quorum sensing is important for interspecies competition and that promiscuous signal receptors promote fitness in some situations by enabling eavesdropping on AHLs produced by competitors.



## Materials and methods

*Bacterial strains and growth*

Strains and plasmids are described in the Supplementary Text and Supplementary Table S1. All bacteria were grown in Luria–Bertani (LB) broth containing morpholinepropanesulfonic acid (50 mM; pH 7). Bactobolin A was generously supplied by Jon Clardy (Seyedsayamdost *et al.*, 2010) and dissolved in filter-sterilized water. Synthetic C6-HSL and purified violacein were purchased from Sigma-Aldrich (St Louis, MO, USA) and dissolved in acidified ethyl acetate ($0.1\,ml\,l^{-1}$ glacial acetic acid) or in dimethylformamide, respectively. AHLs were prepared from the *Bt* bactobolin$^-$ strain BD20 by extracting stationary-phase ($OD_{600}$ 8–10) culture fluid with two equal volumes of acidified ethyl acetate and drying to completion under a stream of nitrogen gas. The dried extracts were dissolved in volumes of media equivalent to the volumes from which they were extracted. The extracts did not affect growth of *Bt* or *Cv*. Extracts similarly prepared from cultures of an AHL$^-$, bactobolin$^-$ double mutant had no effect on the outcome of co-culture experiments. Co-cultures and cultures for AHL preparation were grown at 30 °C. All other growth was at 30 °C for *Cv* and 37 °C for *Bt*. Pure cultures and co-cultures containing visibly aggregated cells of *Cv* were dispersed by homogenization or water-bath sonication before plating for viable counts. Gentamicin was used at $10\,\mu g\,ml^{-1}$ (*Cv* and

*Escherichia coli*) or 100 μg ml$^{-1}$ (*Bt*) and trimethoprim was used at 100 μg ml$^{-1}$. For selection of *Bt* and *Cv* transconjugants, gentamicin was at 10 μg ml$^{-1}$ and trimethoprim was at 100 μg ml$^{-1}$.

*Antimicrobial susceptibility testing*

We determined the minimum inhibitory concentration of bactobolin or violacein using a protocol modified from the 2003 guidelines of the Clinical and Laboratory Standards Institute (CLSI, formerly NCCLS). Inocula were prepared from logarithmic-phase cultures and suspended to $5 \times 10^6$ cells in 1 ml morpholinepropanesulfonic acid-buffered LB containing dilutions of antibiotic compounds. The minimum inhibitory concentration was defined as the lowest concentration (μg ml$^{-1}$) that prevented visible growth of bacteria after 24 h. To assess susceptibility to cell culture fluid, bacteria were similarly suspended in a broth with 10% (*Bt*) or 75% (*Cv*) (vol vol$^{-1}$) filtered fluid from stationary-phase cultures grown for 24 or 16 h, respectively. Culture fluid was filtered through a 0.22-μm pore-size membrane and tested immediately. Fluid from cultures of *Cv* was diluted into 4 × concentrated LB to a 1 × final LB concentration. *Cv* and *Bt* were treated for 24 and 10 h, respectively, before plating for viability. All antimicrobial susceptibility testing was at 30 °C with shaking.

*Co-culture experiments*

To inoculate co-cultures, pure cultures were grown to mid-logarithmic phase, subcultured to fresh medium at an optical density at 600 nm ($OD_{600}$) 0.05 and grown an additional 3 h before combining at the appropriate ratios in 10 ml (Figures 1 and 2) or 20 ml (Figures 3 and 4) of medium in 125-ml culture flasks. The initial $OD_{600}$ of the co-culture was 0.05 ($2–4 \times 10^7$ cells per ml) for *Bt* and 0.005 ($2–4 \times 10^6$ cells per ml) for *Cv*. Co-cultures were incubated with shaking at 250 r.p.m. Colony-forming units (CFUs) of each species were determined by using differential antibiotic selection on LB agar plates. *Bt* was selected with gentamicin and *Cv* was selected with trimethoprim.

## Results

*Antibiotic sensitivities*

As a first step in developing our binary culture model, we needed to test the sensitivity of *Cv* to bactobolin and the sensitivity of *Bt* to violacein. Thus, we used purified antibiotics to determine the minimum inhibitory concentrations. The minimum inhibitory concentration of bactobolin A for *Cv* was 8 μg ml$^{-1}$, and at concentrations exceeding 8 μg ml$^{-1}$, *Cv* was killed during treatment (data not shown). This bactobolin was estimated to be at 5.3 μg ml$^{-1}$ in pure *Bt* culture fluid in growth conditions similar to those we use (Seyedsayamdost *et al*., 2010). *Bt* produces at least seven other bactobolin compounds (Seyedsayamdost *et al*., 2010; Carr *et al*., 2011). To test if *Bt*-produced bactobolins in cell culture fluid are sufficient to kill *Cv*, we assessed *Cv* viability after treatment with filtered fluid from a stationary-phase ($OD_{600}$ 8–10) *Bt* culture. After treatment with 10% (vol vol$^{-1}$) culture fluid from a wild-type *Bt* culture diluted into fresh broth, we were unable to recover viable *Cv*. After similar treatment with 10% (vol vol$^{-1}$) culture fluid from a *Bt* bactobolin-defective mutant (*btaK*$^-$)

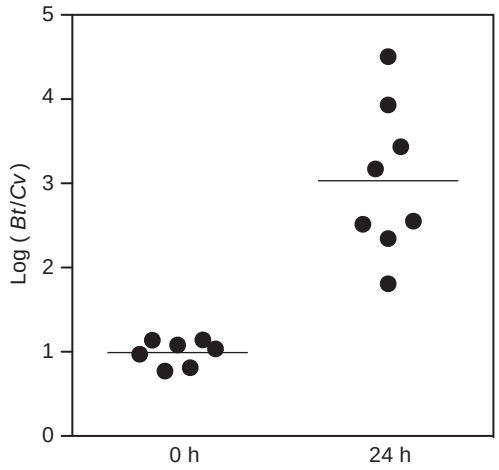


**Figure 1** *B. thailandensis–C. violaceum* competition. Initial cell densities were $2–4 \times 10^7$ *B. thailandensis* (*Bt*) cells per ml and $2–4 \times 10^6$ *C. violaceum* (*Cv*) cells per ml. The initial and final cell densities of *Bt* and *Cv* were determined for each independent experiment by selective plating and colony counts. Each data point represents the log-transformed average of the ratios of the two species from duplicate measurements of an independent co-culture experiment. The lines represent the mean of all of the experiments in each set.

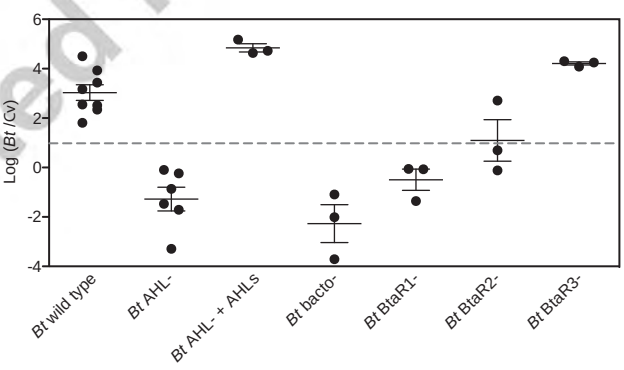


**Figure 2** Competition in co-cultures of wild-type *C. violaceum* (*Cv*) and wild-type or mutant *B. thailandensis* (*Bt*) strains. The dashed line indicates the starting 10:1 ratio of *Bt* to *Cv*. The ratio of *Bt* to *Cv* after 24 h was determined by selective plating and colony counts. The co-culture results with wild-type *Bt* are also shown in Figure 1 and the final average CFU of each species is also partially represented in Table 2. *Bt* AHLs were extracted from culture fluid of a *Bt* bactobolin mutant (see Materials and methods) and added to culture medium. The solid lines represent means for each group. The vertical bars show the standard error of the mean for each group.

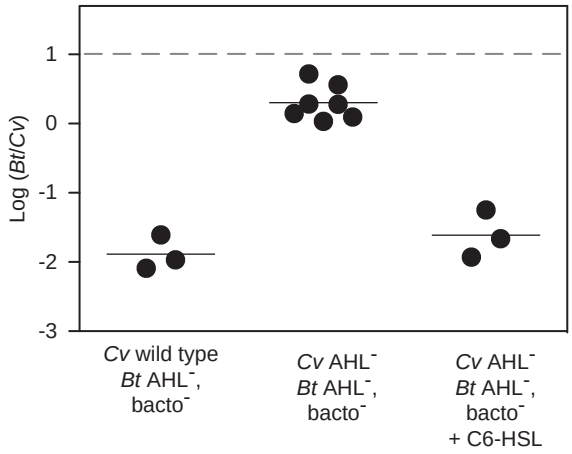


**Figure 3** Co-cultures of the *C. violaceum* (*Cv*) wild-type Cv017 or the AHL mutant Cv026 and the *B. thailandensis* (*Bt*) competition-impaired AHL⁻, bactobolin double mutant JBT125. The dashed line shows the initial ratio of *Bt* to *Cv*. After 24 h, the ratio of *Bt* to *Cv* was determined by colony counts on selective agar. Co-cultures were grown in 20 ml medium. C6-HSL was added before inoculation where indicated (250 nM final concentration). The solid lines represent the means of each group.

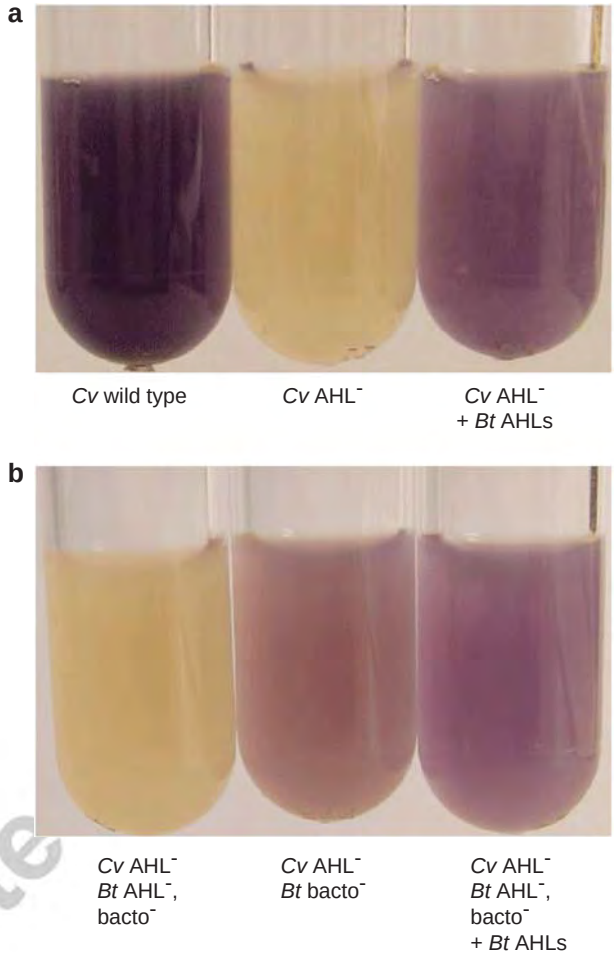


**Figure 4** *Cv* quorum sensing is activated by *Bt* AHLs. Quorum-sensing activation is indicated by the *Cv* quorum-sensing-dependent purple pigment, violacein, in stationary-phase cultures. (**a**) *Cv* wild-type (Cv017) and the AHL mutant (Cv026) with or without added *Bt* AHLs. (**b**) Co-cultures of the *Cv* AHL mutant and *Bt* strains as indicated (AHL mutant JBT112; AHL, bactobolin double mutant JBT125). AHLs were extracted from stationary-phase cultures of *Bt* BD20, a bactobolin mutant.

or in broth alone, *Cv* grew to 2–3 × $10^9$ CFU per ml (Table 1). Our results show that stationary-phase *Bt* cultures produce sufficient bactobolins to kill *Cv*.

*Bt* was resistant to violacein at the highest concentration tested, 125 μg $ml^{-1}$ (data not shown), which is in excess of amounts produced by *Cv* (Tobie, 1935; Strong, 1944). *Cv* codes for other putative antimicrobial factors, including phenazines and hydrogen cyanide (Brazilian National Genome Project Consortium, 2003). To test whether *Cv* produces quorum-sensing-dependent antimicrobials with activity against *Bt*, we incubated *Bt* with filtered fluid from *Cv* wild-type or mutant stationary-phase cultures ($OD_{600}$ 4–5). After 10 h, *Bt* grew modestly to 3 × $10^8$ in the presence of wild-type *Cv* culture fluid, but grew to 2 × $10^9$ in the presence of fluid from the AHL synthesis mutant (Table 2). This indicates that *Cv* quorum sensing regulates production of extracellular factors that inhibit growth of *Bt*, and that this inhibition is not due to violacein alone.

*The Bt–Cv co-culture model*

In pure culture, the doubling times of all *Bt* strains were 60 min ± 5% and *Cv* strains were 48 min ± 5% (see Supplementary Table S2), and both species reached densities of about 3 × $10^9$ cells per ml in early stationary phase. Because of the modest growth-rate discrepancy, we used an inoculum of 2–4 × $10^7$ *Bt* per ml and 2–4 × $10^6$ *Cv* per ml in our co-culture experiments. Wild-type *Bt* outcompetes wild-type *Cv*, increasing in relative abundance by about 100-fold in 24 h (Figure 1). To study the competition further, we enumerated bacteria during logarithmic, early stationary and late stationary growth phases. In logarithmic and early stationary

**Table 1** Sensitivity of *C. violaceum* (*Cv*) strains to *B. thailandensis* (*Bt*) culture fluid

| Bt *culture fluid tested*[a] | Cv *(CFU per ml)*[b] | |
|---|---|---|
| | *Wild type* | *AHL⁻* |
| Wild type | <100 | <100 |
| AHL⁻ | 3 × $10^9$ | 2 × $10^9$ |
| Bactobolin⁻ | 2 × $10^9$ | 2 × $10^9$ |
| No added culture fluid | 2 × $10^9$ | 1 × $10^9$ |

[a]Sensitivity was assessed by growing *Cv* in the presence of filtered culture fluid from stationary-phase (24 h) *Bt* cultures as described in the Materials and methods. The *Bt* AHL⁻ (*btaI1*, *I2*, *I3*) mutant JBT125 and the bactobolin⁻ (*btaK*) mutant BD20 were used. The *Cv* AHL⁻ (*cviI*) mutant Cv026 was used. Experiments were carried out in duplicate and in all cases the ranges did not exceed 10%.
[b]*Bt* cell culture fluid was added to a final concentration of 10% (vol $vol^{-1}$) in 90% (vol $vol^{-1}$) in 1 ml Luria–Bertani-morpholinepropanesulfonic acid broth.

**Table 2** Sensitivity of *B. thailandensis* (*Bt*) strains to *C. violaceum* (*Cv*) culture fluid

| Cv *culture fluid tested*[a] | Bt *(CFU per ml)*[b] | | |
|---|---|---|---|
| | *Wild type* | *AHL*$^-$ | *Bactobolin*$^-$ |
| Wild type | $3 \times 10^8$ | $2 \times 10^8$ | $3 \times 10^8$ |
| AHL$^-$ | $2 \times 10^9$ | $2 \times 10^9$ | $1 \times 10^9$ |
| No added culture fluid | $7 \times 10^9$ | $8 \times 10^9$ | $8 \times 10^9$ |

[a]Sensitivity was assessed by growing *Bt* in the presence of filtered culture fluid from stationary-phase (16 h) *Cv* cultures as described in the Materials and methods. The *Bt* AHL$^-$ (*btaI1*, *I2*, *I3*) mutant JBT125 and the bactobolin$^-$ (*btaK*) mutant BD20 were used. The *Cv* AHL$^-$ (*cvil*) mutant Cv026 was used. Experiments were carried out in duplicate and in all cases the ranges did not exceed 10%.
[b]*Cv* cell culture fluid was added to a final concentration of 75% (vol vol$^{-1}$) in 25% (vol vol$^{-1}$) concentrated Luria–Bertani-morpholinepropanesulfonic acid broth in 1 ml.

phase, both species reached densities in co-culture that were identical to the densities in pure culture ($2–5 \times 10^9$ cells per ml). However, the final densities of both species in late stationary phase (24 h) was lower in co-culture than in pure culture (Table 3). The final cell density of *Cv* decreased over three logs from $5 \times 10^9$ cells per ml in early stationary phase to $1 \times 10^6$ cells per ml at 24 h. There was no significant decrease in *Cv* density in pure culture (Table 3). The final density of *Bt* was 10-fold lower in co-culture than in pure culture (Table 2). Our results are consistent with the hypothesis that both species produce quorum-sensing-controlled antimicrobials during stationary phase that inhibit growth of or kill the other species.

*Quorum-sensing-controlled bactobolin synthesis promotes Bt competitiveness in binary culture*

To test the hypothesis that quorum sensing promotes *Bt* competitiveness in co-culture, we assessed competition with a *Bt* AHL mutant and wild-type *Cv*. We also assessed the competitiveness of a *Bt* bactobolin mutant. In co-culture conditions where wild-type *Bt* had a robust competitive advantage, either the *Bt* AHL or bactobolin mutant were outcompeted by *Cv* (Figure 2). We could rescue competitiveness of the AHL mutant by supplementing our co-cultures with *Bt* AHLs that were obtained by ethyl acetate extraction of culture fluid from a stationary-phase ($OD_{600}$ 8–10) *Bt* bactobolin mutant (Materials and methods). These results demonstrate that quorum sensing and quorum-sensing-dependent bactobolin production are critical for the competitive success of *Bt* in our co-culture model.

Bactobolin production is controlled by the BtaI2–R2 quorum-sensing system (Duerkop *et al.*, 2009). Next, we assessed the importance of BtaI2–R2 and each of the other two *Bt* quorum-sensing systems, BtaI1–R1 and BtaI3–R3, to the competitiveness of *Bt* in our co-culture model. For this, we used *Bt* strains harboring individual deletions in

**Table 3** Final yields of *B. thailandensis* (*Bt*) and *C. violaceum* (*Cv*) in pure culture and co-culture

| *Strain(s)* | *Final growth yield (CFU per ml)*[a,b] | |
|---|---|---|
| | Bt | Cv |
| *Pure culture* | | |
| *Bt* wild type | $1.4 (\pm 0.7) \times 10^{10}$ | |
| *Bt* AHL$^-$ | $1.0 (\pm 0.9) \times 10^{10}$ | |
| *Cv* wild type | | $9.9 (\pm 8.4) \times 10^8$ |
| *Co-culture (with wild-type Cv)*[c] | | |
| *Bt* wild type | $1.3 (\pm 0.8) \times 10^9$ | $1.4 (\pm 2.0) \times 10^6$ |
| *Bt* AHL$^-$ | $2.3 (\pm 2.6) \times 10^8$ | $2.1 (\pm 1.2) \times 10^9$ |
| *Bt* bactobolin$^-$ | $1.0 (\pm 1.5) \times 10^8$ | $2.7 (\pm 0.5) \times 10^9$ |

[a]The values are the means of at least three independent experiments with ranges indicated within parantheses. The *Bt* signal synthase (*btaI1*, *I2*, *I3*) mutant JBT125 and the bactobolin (*btaK*) mutant BD20 were used.
[b]The growth yield in early stationary phase (9 h) of *Bt* and *Cv* in pure and co-culture was $1–3 \times 10^9$.
[c]Co-culture data from individual experiments are also represented in Figure 1.

each of the AHL receptor genes *btaR1*, *btaR2* or *btaR3* (Figure 2). Not surprisingly, the *btaR2* mutant competed poorly with *Cv*. Results were similar to those with the bactobolin mutant and the AHL synthesis mutant. The outcome with the *btaR3* mutant was identical to wild type, indicating that BtaR3 is not important for competition in our model. The *btaR1* mutant showed an intermediate ability to compete with *Cv*, suggesting that this regulator may be important for the production of bactobolin or production of other factors that enhance competition or bactobolin activity. In support of the former, we found that expression of a bactobolin *btaK-lacZ* transcriptional fusion is delayed in a *btaR1* mutant (data not shown), suggesting that BtaR1 may advance the production of bactobolin. We also tested the competitiveness of strains with individual mutations in each of the AHL synthase genes. All three individual AHL synthase mutants outcompeted *Cv* with results similar to competitions with wild-type *Bt* (data not shown). These findings suggest that the AHL synthases have overlapping abilities to induce expression of bactobolin. This is supported by our previous finding that BtaR2 can respond to both 3-hydroxy-octanoyl-HSL and 3-hydroxy-decanoyl-HSL, which are produced by the BtaI3 and BtaI2 synthases, respectively (Duerkop *et al.*, 2009).

*Quorum sensing can promote competitiveness of Cv*

Our results indicate that *Cv* also produces quorum-sensing-dependent antimicrobial factors that inhibit growth of *Bt* (Table 1). Thus, we hypothesized that quorum sensing promotes competitiveness of *Cv* as it does for *Bt*. To address this, we compared the competitiveness of the *Cv* wild-type and AHL mutant strains in co-culture with *Bt*. We modified

our experiment to give wild-type *Cv*, a competitive advantage by using a competition-defective *Bt* AHL, bactobolin double mutant, and we increased the co-culture volume to 20 ml because we observed that this further improves *Cv* competitiveness for reasons that are unknown (data not shown). In these conditions, wild-type *Cv* strongly outcompeted the *Bt* mutant, whereas the *Cv* AHL mutant barely outcompeted the *Bt* mutant (Figure 3). Competitiveness could be restored to the *Cv* AHL mutant by the addition of C6-HSL (the AHL produced by *Cv*) (Figure 3). These results show that quorum sensing can promote the competitiveness of *Cv*. Because violacein does not have any antimicrobial activity against *Bt*, we note that this is not due to violacein, but must be caused by as-yet undefined quorum-sensing-dependent factors.

*Cv can sense and respond to Bt AHLs*

The *Cv* AHL receptor CviR can be activated by a range of AHLs including at least one of the AHLs produced by *Bt*, C8-HSL (McClean *et al*., 1997; Swem *et al*., 2009). We hypothesized that *Bt* AHLs can activate the *Cv* quorum-sensing receptor CviR and that this promotes competitiveness of *Cv* in co-culture with *Bt*. We first tested whether a pure culture of *Cv* can sense and respond to *Bt* AHLs; these AHLs were ethyl acetate extracted and concentrated from stationary-phase ($OD_{600}$ 8–10) culture fluid and added to *Cv* cultures to match concentrations in the culture from which they were extracted. As a read-out for quorum-sensing activation, we followed the purple pigment violacein. The *Cv* AHL mutant is not pigmented, but pigmentation can be restored by supplementing the culture medium with *Bt* AHL extracts (Figure 4a). This result shows that *Cv* can sense and respond to physiological levels of *Bt* AHLs.

Next, we tested whether the *Cv* AHL mutant can respond to *Bt* AHLs during co-culture growth. Because *Cv* is killed by *Bt*-produced bactobolin in co-culture (Table 1), we used the *Bt* bactobolin mutant BD20 for these experiments (Figure 4b). When in co-culture with a *Bt* AHL, bactobolin double mutant, the *Cv* AHL mutant did not turn purple. However, in co-culture with the AHL-producing *Bt* bactobolin mutant BD20, or with exogenously supplied *Bt* AHLs, the co-culture turned purple. This finding indicates that the *Cv* CviR responds to *Bt* AHLs. We conclude that *Bt* AHLs are cues that alter the behavior of *Cv*, although they did not evolve for that purpose (Keller and Surette, 2006). In our experiment, the *Cv* AHL synthase mutant can eavesdrop on *Bt*.

*Eavesdropping promotes competitiveness of Cv*

To determine whether eavesdropping can influence competitiveness of *Cv*, we enumerated *Bt* and *Cv* in co-cultures (Figure 5). As in our previous experiments, we grew the *Cv* AHL mutant with the *Bt* bactobolin mutant or an AHL, bactobolin double mutant. The *Cv* AHL mutant was more competitive with the *Bt* bactobolin mutant than it was with the double mutant. As a control, we added *Bt* AHLs to the co-culture with the *Bt* double mutant and observed that this improved the competitiveness of *Cv*. These results suggest that eavesdropping on *Bt* AHLs promotes *Cv* competitiveness. As an additional control, we tested whether the *Cv* AHL receptor CviR is required for eavesdropping. To address this, we constructed a *Cv* AHL synthase, receptor double mutant. We found that CviR is required for the competitive advantage provided to *Cv* by eavesdropping on *Bt* AHLs (Figure 5).

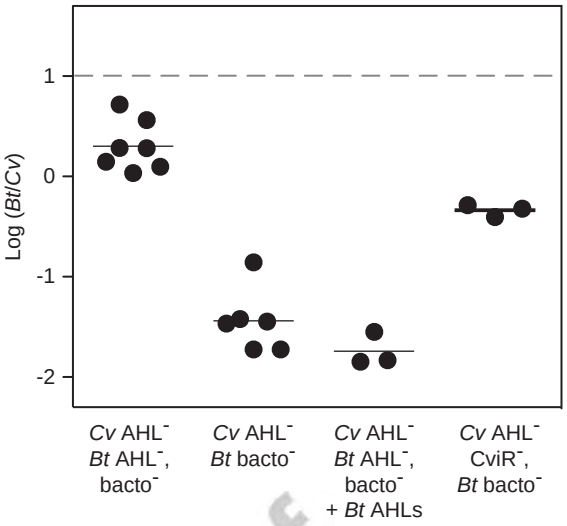


**Figure 5** Eavesdropping promotes competitiveness of *Cv* in co-cultures with a *B. Bt* bactobolin mutant. After 24 h of co-culture, the ratio of *Bt* to *Cv* was determined. Co-cultures of the *Cv* AHL mutant (Cv026), or the *Cv* AHL synthase, receptor double mutant (Cv026R) and the *Bt* strains as indicated and described in Figure 4 legend. Co-cultures were grown in 20 ml volumes. The dashed line indicates the initial ratio of *Bt* to *Cv*. The solid lines represent the means for each group. AHLs were obtained as described for Figure 4.

*An in silico eavesdropping model*

Our experimental approach has limitations and with the conditions we used, we could not observe an affect of eavesdropping with wild-type strains (data not shown). However, we suspect there may be conditions where eavesdropping provides an advantage to wild-type *Cv*. This may be as the population nears the critical density required for quorum-sensing activation. At this density, AHLs produced by a nearby competitor may cause early activation of quorum-sensing-dependent antibiotics and would improve competitiveness of the eavesdropping microbe.

To explore this hypothesis further, we developed a mathematical model of our binary culture system (see Supplementary Text and Supplementary Table S3). The model accounts for two wild-type species

that produce antibiotics in response to AHL signals in a well-mixed environment, similar to species *Bt* and *Cv* in our experimental system. *In silico*, the antibiotic produced by each species has equal killing efficiency towards the competing species, but no influence on the producing species. The two species in our *in silico* model also have identical growth rates, rates of antibiotic and AHL production, and antibiotic-production costs. However, as we observed experimentally, in some conditions one species (which we refer to here as species C) can eavesdrop on the other (species B). In the *in silico* model, we assume that antibiotic production accelerates once the inducer reaches a critical threshold concentration. However, antibiotic-production rates eventually level off as AHL concentrations exceed the quorum-sensing threshold. We use several different activation thresholds in our analysis.

Our *in silico* model has a bistable dynamic where one species completely dominates under most conditions. In the absence of eavesdropping, the outcome favors the species that is numerically dominant at the beginning (Figure 6). When we vary the activation thresholds for antibiotic production (by varying $K_B$ and $K_C$ of B and C, respectively, see Supplementary Text and Supplementary Table S3), there is an optimal value ($K^{optimal}$) where one species can dominate the other; if we fix $K_B$ at this value, B can dominate C at any value of $K_C$ (other than when $K_C$ was equal to $K^{optimal}$), and the same is true for C if $K_C$ is set at $K^{optimal}$ (see Supplementary Figure S1). For every set of parameter values we explored, we find that $K^{optimal}$ is greater than zero. Thus, waiting until a population reaches a quorum provides a fitness benefit for antibiotic-producing bacteria.

We then investigated eavesdropping in our *in silico* model when species B and C had identical thresholds above (high), equal to (optimal) and below (low) the optimal threshold. At a relatively high threshold, eavesdropping provided a distinct advantage to C by allowing it to invade B from lower starting frequencies (Figure 6a), supporting our initial hypothesis. However, with an optimal or low threshold, eavesdropping was disadvantageous (Figures 6b and c). We posit that in the latter two cases, the eavesdropping population activates production of antibiotic too early to accumulate a sufficient killing dose and antibiotic production is an ineffective metabolic burden. To test this hypothesis, we kept the same conditions as in Figure 6c and increased the toxicity of the antibiotic of both species. In these conditions, eavesdropping provides an advantage (Figure 6d), supporting our hypothesis. Furthermore, eavesdropping is also advantageous if the antibiotic cost is decreased (Supplementary Figures S2 and S3). However, these changes in toxicity and cost alter the optimal threshold (Supplementary Figure S1B and data not shown), effectively resetting the system so that antibiotic production is induced after the optimal

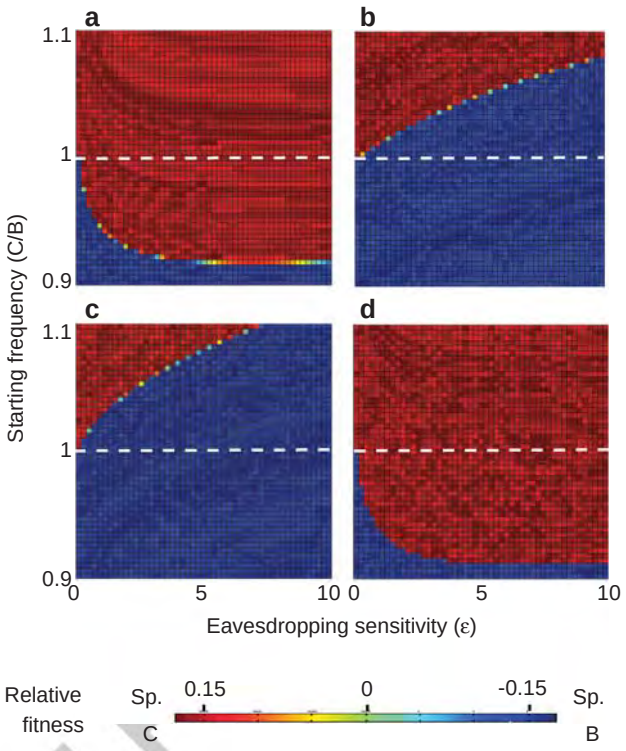


**Figure 6** *In silico* modeling. Our model accounts for two species with quorum-sensing-controlled antibiotics, similar to our experimental model of *Bt* and *Cv*. As in our experimental model, our *in silico* model accounts for two species (B and C) that produce antibiotics in a density-dependent manner. In our model, species C can eavesdrop on species B (see Supplementary Text). We show relative fitness of each species as a function of the initial ratio (C/B) and the eavesdropping sensitivity ($\varepsilon$) of C. The fitness of C relative to B was measured using the log relative fitness measure given in Wu *et al.* (2006) and is indicated by the color spectrum on the far right. (**a**) The inducer concentration required for production of antibiotic (activation threshold, $K_B$ and $K_C$) is relatively high for both species (0.01, see text). (**b**) The activation threshold is lower (0.003898) and corresponds to an optimal threshold for each species that gives it an advantage over the other species regardless of the other species' threshold. (**c**) Both species have an activation threshold lower than the optimal threshold (0.003). (**d**) The same parameters were used as in (**c**); however, the antibiotic toxicity is raised 10-fold. This changes the optimal activation threshold to 0.001113, which is below the activation threshold value used (0.003) (see Supplementary Figure S1).

threshold is achieved. Thus, eavesdropping-dependent early production of antibiotics promotes competition in a population that has already reached a sufficient density to produce a killing dose.

## Discussion

We have developed a dual-species competition model with two soil saprophytes, *Bt* and *Cv*, which both use quorum sensing to control production of antimicrobial factors. We show that both of these species can gain a competitive advantage over the other with success dependent on quorum sensing. The advantage of quorum-sensing control of antimicrobials has also been shown in other laboratory

co-culture models (Moons *et al.*, 2005, 2006; An *et al.*, 2006). The previous reports, together with the results reported here, support the idea that quorum-sensing regulation is important in multi-species competition. Our results indicate that competitiveness of *Bt* relies on the *btaI2-R2*-controlled antibiotic bactobolin and *Cv* uses as-yet unidentified quorum-sensing-dependent factors for competition. The bactobolin biosynthetic genes and *btaI2-R2* are encoded within a large (120-kb) DNA element that is absent from a close relative, the host-adapted pathogen *Burkholderia mallei*. That this element is retained in *Bt* supports the view that *btaI2-R2* and bactobolin are important for competition during saprophytic growth.

Why do bacteria use quorum sensing to regulate antibiotic production? Our *in silico* model provides some possible clues. The results indicate that when antibiotic production is costly, early production slows population growth without effectively killing the competitor. Thus, quorum sensing defers the cost of antibiotic production until a sufficient killing dose can be delivered. We do not include in our model the additional possibility that sublethal concentrations of antibiotics may induce in the competitor an adaptation to higher concentrations of antibiotic. Both of these possibilities can be further explored with our experimental co-culture model. An alternative hypothesis is that deferred production may also protect the producing population against the emergence of non-producing cheaters. Cheaters can exploit public goods producers by utilizing the available goods without incurring the cost of their production. In a recent study by Xavier *et al.* (2011), delayed production of an exploitable public good, surfactant, protected the producing population against the emergence of cheaters. This strategy maximized growth of the producing population, thereby increasing its ability to compete with cheaters. Quorum-sensing regulation may similarly promote competitiveness with non-producing cheaters.

Our experimental model also showed that cross-species AHL activation of the *Cv* broad-specificity AHL receptor can promote the competitiveness of *Cv* (Figure 5). In addition to *Cv*, there are several other species with broad-specificity AHL receptors and these are also saprophytes: *E. carotovora* (ExpR2)(Sjoblom *et al.*, 2006); *P. aeruginosa* (QscR)(Lee *et al.*, 2006); and receptors encoded by two species of *Bradyrhizobium* (BraR and BjaR) (Ahlgren *et al.*, 2011; Lindemann *et al.*, 2011). ExpR2 and QscR are both orphan receptors without a cognate AHL synthase gene (Cui *et al.*, 2006; Fuqua, 2006; Sjoblom *et al.*, 2006). The potential role of each of these receptors in competition has not been determined. AHL receptor specificity can be easily altered by single amino-acid changes (Collins *et al.*, 2005; Hawkins *et al.*, 2007; Chen *et al.*, 2011; Lintz *et al.*, 2011), suggesting that AHL recognition may be very adaptable in nature. In contrast to these broad-specificity AHL receptors, the receptor of the squid symbiont *Vibrio fischeri* is quite specific for its cognate AHL (Visick and Ruby, 1999). *V. fischeri* Q3 activates quorum-sensing-dependent functions when it is at high cell densities in its squid host; in this environment it rarely encounters other bacterial species (Visick and McFall-Ngai, 2000). Thus, AHL receptors may evolve broad signal specificity in specific environments where eavesdropping might be of use, although the role of these receptors in inter-species competition and eavesdropping requires further study.

In the conditions of our experimental model, eavesdropping did not provide an observable fitness advantage to wild-type strains during competition. However in another study, AHLs produced by epiphytic bacteria on plant leaves altered the quorum-sensing-regulated virulence phenotype of a wild-type *Pseudomonas syringae* strain (Dulla and Lindow, 2009), suggesting that wild-type strains can be responsive to AHLs from other species in natural environments. Our co-culture model may provide a limited view of the possible interactions between species in nature, for example, Dulla *et al.* (2010) Q4 identified several epiphytic species that produce 10-fold more AHL than their laboratory *P. syringae* strain. High-level signal producers may play a significant role in cross-species induction.

Our mathematical model allowed a simple assessment of the costs and benefits of eavesdropping between competing wild-type strains. For the model, we made the basic assumption that detection of exogenous AHLs can cause early quorum-sensing-dependent activation of antibiotic genes. We have observed this experimentally in *Bt* with a transcriptional fusion to the bactobolin biosynthetic gene *btaK* (data not shown), but it is more difficult to address with *Cv* because we do not yet know what quorum-controlled genes are involved in competition, and during early logarithmic phase the activity of the antimicrobials is too low for our methods of detection. The *in silico* model indicates that eavesdropping can promote competition in certain conditions where production of antibiotic occurs relatively late during growth. However, eavesdropping can also be detrimental if the activation threshold is relatively low. We observed similar results in other variations of this model (data not shown). Our results suggest that receptors would evolve broad specificity only in particular circumstances where eavesdropping is beneficial. Our bias is that specificity is the more evolved trait and that highly specific receptors likely arose from receptors with less specificity.



## Acknowledgements

This work was funded by a National Institute of Allergy and Infectious Disease (NIAID) award to the Northwest Regional Center of Excellence for Biodefense and Emerging Infectious Diseases (U54AI057141) to EPG.

JRC was funded by the NIAID (NRSA 1 F32 AI073027-01A2), SH was funded by the Danish National Research Foundation and JEM was funded by the UW Royalty Research Grant. We thank Drs Ajai Dandekar, Snow Brook Peterson, Ben Kerr and Matt Parsek for helpful discussions regarding this manuscript.

## References

Ahlgren NA, Harwood CS, Schaefer AL, Giraud E, Greenberg EP. (2011). Aryl-homoserine lactone quorum sensing in stem-nodulating photosynthetic bradyrhizobia. *Proc Natl Acad Sci USA* **108**: 7183–7188.

An D, Danhorn T, Fuqua C, Parsek MR. (2006). Quorum sensing and motility mediate interactions between *Pseudomonas aeruginosa* and *Agrobacterium tumefaciens* in biofilm cocultures. *Proc Natl Acad Sci USA* **103**: 3828–3833.

Bainton NJ, Bycroft BW, Chhabra SR, Stead P, Gledhill L, Hill PJ *et al.* (1992). A general role for the *lux* autoinducer in bacterial cell signalling: control of antibiotic biosynthesis in *Erwinia*. *Gene* **116**: 87–91.

Bassler BL. (2002). Small talk. Cell-to-cell communication in bacteria. *Cell* **109**: 421–424.

Brazilian National Genome Project Consortium (2003). The complete genome sequence of *Chromobacterium violaceum* reveals remarkable and exploitable bacterial adaptability. *Proc Natl Acad Sci USA* **100**: 11660–11665.

Carr G, Seyedsayamdost MR, Chandler JR, Greenberg EP, Clardy J. (2011). Sources of diversity in bactobolin biosynthesis by *Burkholderia thailandensis* E264. *Org Lett* **13**: 3048–3051.

Chandler JR, Duerkop BA, Hinz A, West TE, Herman JP, Churchill ME *et al.* (2009). Mutational analysis of *Burkholderia thailandensis* quorum sensing and self-aggregation. *J Bacteriol* **191**: 5901–5909.

Chen G, Swem LR, Swem DL, Stauff DL, O'Loughlin CT, Jeffrey PD *et al.* (2011). A strategy for antagonizing quorum sensing. *Mol Cell* **42**: 199–209.

Collins CH, Arnold FH, Leadbetter JR. (2005). Directed evolution of *Vibrio fischeri* LuxR for increased sensitivity to a broad spectrum of acyl-homoserine lactones. *Mol Microbiol* **55**: 712–723.

Cui Y, Chatterjee A, Hasegawa H, Chatterjee AK. (2006). *Erwinia carotovora* subspecies produce duplicate variants of ExpR, LuxR homologs that activate *rsmA* transcription but differ in their interactions with *N*-acylhomoserine lactone signals. *J Bacteriol* **188**: 4715–4726.

Davies J, Spiegelman GB, Yim G. (2006). The world of subinhibitory antibiotic concentrations. *Curr Opin Microbiol* **9**: 445–453.

Duerkop BA, Varga J, Chandler JR, Peterson SB, Herman JP, Churchill ME *et al.* (2009). Quorum-sensing control of antibiotic synthesis in *Burkholderia thailandensis*. *J Bacteriol* **191**: 3909–3918.

Dulla GF, Lindow SE. (2009). Acyl-homoserine lactone-mediated cross talk among epiphytic bacteria modulates behavior of *Pseudomonas syringae* on leaves. *ISME J* **3**: 825–834.

Engebrecht J, Nealson K, Silverman M. (1983). Bacterial bioluminescence: isolation and genetic analysis of functions from *Vibrio fischeri*. *Cell* **32**: 773–781.

Fuqua C. (2006). The QscR quorum-sensing regulon of *Pseudomonas aeruginosa*: an orphan claims its identity. *J Bacteriol* **188**: 3169–3171.

Fuqua C, Parsek MR, Greenberg EP. (2001). Regulation of gene expression by cell-to-cell communication: acyl-homoserine lactone quorum sensing. *Annu Rev Genet* **35**: 439–468.

Fuqua WC, Winans SC, Greenberg EP. (1994). Quorum sensing in bacteria: the LuxR–LuxI family of cell density-responsive transcriptional regulators. *J Bacteriol* **176**: 269–275.

Gallagher LA, Manoil C. (2001). *Pseudomonas aeruginosa* PAO1 kills *Caenorhabditis elegans* by cyanide poisoning. *J Bacteriol* **183**: 6207–6214.

Hawkins AC, Arnold FH, Stuermer R, Hauer B, Leadbetter JR. (2007). Directed evolution of *Vibrio fischeri* LuxR for improved response to butanoyl-homoserine lactone. *Appl Environ Microbiol* **73**: 5775–5781.

Hibbing ME, Fuqua C, Parsek MR, Peterson SB. (2010). Bacterial competition: surviving and thriving in the microbial jungle. *Nat Rev Microbiol* **8**: 15–25.

Hosni T, Moretti C, Devescovi G, Suarez-Moreno ZR, Fatmi MB, Guarnaccia C *et al.* (2011). Sharing of quorum-sensing signals and role of interspecies communities in a bacterial plant disease. *ISME J* **5**: 1857–1870.

Keller L, Surette MG. (2006). Communication in bacteria: an ecological and evolutionary perspective. *Nat Rev Microbiol* **4**: 249–258.

Kownatzki R, Tummler B, Doring G. (1987). Rhamnolipid of *Pseudomonas aeruginosa* in sputum of cystic fibrosis patients. *Lancet* **1**: 1026–1027.

Latifi A, Foglino M, Tanaka K, Williams P, Lazdunski A. (1996). A hierarchical quorum-sensing cascade in *Pseudomonas aeruginosa* links the transcriptional activators LasR and RhIR (VsmR) to expression of the stationary-phase sigma factor RpoS. *Mol Microbiol* **21**: 1137–1146.

Latifi A, Winson MK, Foglino M, Bycroft BW, Stewart GS, Lazdunski A *et al.* (1995). Multiple homologues of LuxR and LuxI control expression of virulence determinants and secondary metabolites through quorum sensing in *Pseudomonas aeruginosa* PAO1. *Mol Microbiol* **17**: 333–343.

Lee JH, Lequette Y, Greenberg EP. (2006). Activity of purified QscR, a *Pseudomonas aeruginosa* orphan quorum-sensing transcription factor. *Mol Microbiol* **59**: 602–609.

Lindemann A, Pessi G, Schaefer AL, Mattmann ME, Christensen QH, Kessler A *et al.* (2011). Isovaleryl-homoserine lactone, an unusual branched-chain quorum-sensing signal from the soybean symbiont *Bradyrhizobium japonicum*. *Proc Natl Acad Sci USA* **108**: 16765–16770.

Lintz MJ, Oinuma K, Wysoczynski CL, Greenberg EP, Churchill ME. (2011). Crystal structure of QscR, a *Pseudomonas aeruginosa* quorum sensing signal receptor. *Proc Natl Acad Sci USA* **108**: 15763–15768.

Mazzola M, Cook RJ, Thomashow LS, Weller DM, Pierson LS III. (1992). Contribution of phenazine antibiotic biosynthesis to the ecological competence of fluorescent pseudomonads in soil habitats. *Appl Environ Microbiol* **58**: 2616–2624.

McClean KH, Winson MK, Fish L, Taylor A, Chhabra SR, Camara M *et al.* (1997). Quorum sensing and *Chromobacterium violaceum*: exploitation of violacein production and inhibition for the detection of

*N*-acylhomoserine lactones. *Microbiology* **143** (Part 12) 3703–11.

Moons P, Van Houdt R, Aertsen A, Vanoirbeek K, Engelborghs Y, Michiels CW. (2006). Role of quorum sensing and antimicrobial component production by *Serratia plymuthica* in formation of biofilms, including mixed biofilms with *Escherichia coli*. *Appl Environ Microbiol* **72**: 7294–7300.

Moons P, Van Houdt R, Aertsen A, Vanoirbeek K, Michiels CW. (2005). Quorum sensing dependent production of antimicrobial component influences establishment of *E. coli* in dual species biofilms with *Serratia plymuthica*. *Commun Agric Appl Biol Sci* **70**: 195–198.

Pierson EA, Wood DW, Cannon JA, Blachere FM, Pierson LS 3rd. (1998). Interpopulation signaling via *N*-acyl-homoserine lactones among bacteria in the wheat rhizosphere. *Mol Plant Microbe Interact* **11**: 1078–1084.

Ran H, Hassett DJ, Lau GW. (2003). Human targets of *Pseudomonas aeruginosa* pyocyanin. *Proc Natl Acad Sci USA* **100**: 14315–14320.

Riedel K, Hentzer M, Geisenberger O, Huber B, Steidle A, Wu H *et al.* (2001). *N*-acylhomoserine-lactone-mediated communication between *Pseudomonas aeruginosa* and *Burkholderia cepacia* in mixed biofilms. *Microbiology* **147**: 3249–3262.

Schuster M, Greenberg EP. (2006). A network of networks: quorum-sensing gene regulation in *Pseudomonas aeruginosa*. *Int J Med Microbiol* **296**: 273–81.

Seed PC, Passador L, Iglewski BH. (1995). Activation of the *Pseudomonas aeruginosa lasI* gene by LasR and the *Pseudomonas* autoinducer PAI: an autoinduction regulatory hierarchy. *J Bacteriol* **177**: 654–659.

Seyedsayamdost MR, Chandler JR, Blodgett JA, Lima PS, Duerkop BA, Oinuma K *et al.* (2010). Quorum-sensing-regulated bactobolin production by *Burkholderia thailandensis* E264. *Org Lett* **12**: 716–719.

Sjoblom S, Brader G, Koch G, Palva ET. (2006). Cooperation of two distinct ExpR regulators controls quorum sensing specificity and virulence in the plant pathogen *Erwinia carotovora*. *Mol Microbiol* **60**: 1474–1489.

Stauff DL, Bassler BL. (2011). Quorum sensing in *Chromobacterium violaceum*: DNA recognition and gene regulation by the CviR receptor. *J Bacteriol* **193**: 3871–3878.

Steidle A, Sigl K, Schuhegger R, Ihring A, Schmid M, Gantner S *et al.* (2001). Visualization of *N*-acylhomoserine lactone-mediated cell–cell communication between bacteria colonizing the tomato rhizosphere. *Appl Environ Microbiol* **67**: 5761–5770.

Strong FM. (1944). Isolation of violacein. *Science* **100**: 287.

Swem LR, Swem DL, O'Loughlin CT, Gatmaitan R, Zhao B, Ulrich SM *et al.* (2009). A quorum-sensing antagonist targets both membrane-bound and cytoplasmic receptors and controls bacterial pathogenicity. *Mol Cell* **35**: 143–153.

Tobie WC. (1935). The pigment of *Bacillus violaceus*: I. The production, extraction, and purification of violacein. *J Bacteriol* **29**: 223–227.

Venturi V, Friscina A, Bertani I, Devescovi G, Aguilar C. (2004). Quorum sensing in the *Burkholderia cepacia* complex. *Res Microbiol* **155**: 238–244.

Visick KL, Ruby EG. (1999). The emergent properties of quorum sensing: consequences to bacteria of autoinducer signaling in their natural environment. In: Winans GMDaSC (ed.) *Cell–Cell Signaling in Bacteria*. ASM Press: Washington, DC, pp 333–352.

Visick KL, McFall-Ngai MJ. (2000). An exclusive contract: specificity in the *Vibrio fischeri*–Euprymna scolopes partnership. *J Bacteriol* **182**: 1779–1787.

Waters CM, Bassler BL. (2005). Quorum sensing: cell-to-cell communication in bacteria. *Annu Rev Cell Dev Biol* **21**: 319–346.

Wu H, Huang Y, Dykes C, Liu D, Ma J, Perelson AS *et al.* (2006). Modeling and estimation of replication fitness of human immunodeficiency virus type 1 *in vitro* experiments by using a growth competition assay. *J Virol* **80**: 2380–2389.

Xavier JB, Kim W, Foster KR. (2011). A molecular mechanism that stabilizes cooperative secretions in *Pseudomonas aeruginosa*. *Mol Microbiol* **79**: 166–179.

Yim G, Wang HH, Davies J. (2007). Antibiotics as signalling molecules. *Philos Trans R Soc Lond Ser B* **362**: 1195–1200.

Supplementary Information accompanies the paper on The ISME Journal website (http://www.nature.com/ismej)

# Bibliography


[1] Stephen T Abedon, T. D. Herschler, and D. Stopar. Bacteriophage Latent-Period Evolution as a Response to Resource Availability. *Applied and Environmental Microbiology*, 67(9):4233–4241, September 2001.

[2] Stephen T Abedon, P. Hyman, and C. Thomas. Experimental Examination of Bacteriophage Latent-Period Evolution as a Response to Bacterial Availability. *Applied and Environmental Microbiology*, 69(12):7499–7506, December 2003.

[3] Nathan A Ahlgren, Caroline S Harwood, Amy L Schaefer, Eric Giraud, and E Peter Greenberg. Aryl-homoserine lactone quorum sensing in stem-nodulating photosynthetic bradyrhizobia. *Proceedings of the National Academy of Sciences of the United States of America*, 108(17):7183–7188, 2011.

[4] Aylin Alin. Simpson's paradox. *Wiley Interdisciplinary Reviews Computational Statistics*, 2(April):247–250, 2010.

[5] Ding Ding An, Thomas Danhorn, Clay Fuqua, and Matthew R Parsek. Quorum sensing and motility mediate interactions between Pseudomonas aeruginosa and Agrobacterium tumefaciens in biofilm cocultures. *Proceedings of the National Academy of Sciences of the United States of America*, 103(10):3828–3833, 2006.

[6] Kevin E Ashelford, Martin J Day, and John C Fry. Elevated Abundance of Bacteriophage Infecting Bacteria in Soil. *Applied and Environmental Microbiology*, 69(1):285–289, 2003.

[7] Ira Aviram and Avinoam Rabinovitch. Dynamical types of bacteria and bacteriophages interaction: shielding by debris. *Journal of Theoretical Biology*, 251(1):121–136, 2008.

[8] Joana Azeredo and Ian W Sutherland. The use of phages for the removal of infectious biofilms. *Current pharmaceutical biotechnology*, 9(4):261–6, August 2008.

[9] N J Bainton, P Stead, S R Chhabra, B W Bycroft, G P Salmond, G S Stewart, and P Williams. N-(3-oxohexanoyl)-L-homoserine lactone regulates carbapenem antibiotic production in Erwinia carotovora. *The Biochemical journal*, 288(Pt 3):997–1004, 1992.

[10] Ken Binmore. *Playing for Real: A Text on Game Theory*. Oxford University Press, USA, 2007.

[11] W Bode. Lysis inhibition in Escherichia coli infected with bacteriophage T4. *Journal of virology*, 1(5):948–55, October 1967.

[12] Michael A Brockhurst, A Buckling, and P B Rainey. Spatial heterogeneity and the stability of host-parasite coexistence. *Journal of evolutionary biology*, 19(2):374–9, March 2006.

[13] Michael A Brockhurst, Angus Buckling, Dan Racey, and Andy Gardner. Resource supply and the evolution of public-goods cooperation in bacteria. *BMC Biology*, 6(20):20, 2008.

[14] M R W Brown and J H Scott Foster. A simple diagnostic milk medium for Pseudomonas aeruginosa. *Journal of Clinical Pathology*, 23(2):172–177, 1970.

[15] Sam P Brown and François Taddei. The Durability of Public Goods Changes the Dynamics and Nature of Social Dilemmas. *PLoS ONE*, 2(7):7, 2007.

[16] Angus Buckling and Paul B Rainey. Antagonistic coevolution between a bacterium and a bacteriophage. *Proceedings of the Royal Society B Biological Sciences*, 269(1494):931–936, 2002.

[17] A Campbell. Conditions for the existence of bacteriophage. *Evolution*, 15(2):153–165, 1961.

[18] Margherita Carletti. Mean-square stability of a stochastic model for bacteriophage infection with time delays. *Mathematical biosciences*, 210(2):395–414, December 2007.

[19] Josephine R Chandler, Silja Heilmann, John E Mittler, and E Peter Greenberg. Acyl-homoserine lactone-dependent eavesdropping promotes competition in a laboratory co-culture model. *The ISME Journal (2012)*, (in press):1–10, 2012.

[20] E Chapman-McQuiston and X L Wu. Stochastic receptor expression allows sensitive bacteria to evade phage attack. Part I: experiments. *Biophysical Journal*, 94(11):4525–4536, 2008.

[21] L Caitlin Coberly, Wei Wei, Koffi Y Sampson, Jack Millstein, Holly A Wichman, and Stephen M Krone. Space, time, and host evolution facilitate coexistence of competing bacteriophages: theory and experiment. *The American naturalist*, 173(4):E121–E138, 2009.

[22] H N Comins and D W Blatt. Prey-predator models in spatially heterogeneous environments. *Journal of Theoretical Biology*, 48(1):75–83, 1974.

[23] Jodi L Connell, Aimee K Wessel, Matthew R Parsek, Andrew D Ellington, Marvin Whiteley, and Jason B Shear. Probing Prokaryotic Social Behaviors with Bacterial "Lobster Traps". *mBio*, 1(4):1–8, 2010.

[24] Brian D. Corbin, Robert J.C. McLean, and Gary M. Aron. Bacteriophage T4 multiplication in a glucose-limited Escherichia coli biofilm. *Canadian Journal of Microbiology*, 47(7):680–684, 2001.

[25] J W Costerton, K J Cheng, G G Geesey, T I Ladd, J C Nickel, M Dasgupta, and T J Marrie. Bacterial biofilms in nature and disease. *Annual Review of Microbiology*, 41(1):435–464, 1987.

[26] T. Czaran and R. F. Hoekstra. A spatial model of the evolution of quorum sensing regulating bacteriocin production. *Behavioral Ecology*, 18(5):866–873, July 2007.

[27] Julian Davies, George B Spiegelman, and Grace Yim. The world of subinhibitory antibiotic concentrations. *Current Opinion in Microbiology*, 9(5):445–453, 2006.

[28] Marianne De Paepe and François Taddei. Viruses' life history: towards a mechanistic basis of a trade-off between survival and reproduction among phages. *PLoS Biology*, 4(7):e193, July 2006.

[29] A Death, L Notley, and T Ferenci. Derepression of LamB protein facilitates outer membrane permeation of carbohydrates into Escherichia coli under conditions of nutrient stress. *Journal Of Bacteriology*, 175(5):1475–1483, 1993.

[30] John J Dennehy, Stephen T Abedon, and Paul E Turner. Host density impacts relative fitness of bacteriophage Phi6 genotypes in structured habitats. *Evolution; international journal of organic evolution*, 61(11):2516–27, November 2007.

[31] Stephen P Diggle, Andy Gardner, Stuart a West, and Ashleigh S Griffin. Evolutionary theory of bacterial quorum sensing: when is a signal not a signal? *Philosophical transactions of the Royal Society of London. Series B, Biological sciences*, 362(1483):1241–9, July 2007.

[32] Michael Doebeli, Christoph Hauert, and Timothy Killingback. The evolutionary origin of cooperators and defectors. *Science (New York, N.Y.)*, 306(5697):859–62, October 2004.

[33] Holly Kloos Dressman and John W Drake. Lysis and lysis inhibition in bacteriophage T4: rV mutations reside in the holin t gene. *Journal Of Bacteriology*, 181(14):4391–4396, 1999.

[34] Breck A Duerkop, John Varga, Josephine R Chandler, Snow Brook Peterson, Jake P Herman, Mair E A Churchill, Matthew R Parsek, William C Nierman, and E Peter Greenberg. Quorum-sensing control of antibiotic synthesis in Burkholderia thailandensis. *Journal Of Bacteriology*, 191(12):3909–3918, 2009.

[35] Glenn F J Dulla and Steven E Lindow. Acyl-homoserine lactone-mediated cross talk among epiphytic bacteria modulates behavior of Pseudomonas syringae on leaves. *The ISME journal*, 3(7):825–834, 2009.

[36] B J Finlay, S C Maberly, and J I Cooper. Microbial diversity and ecosystem function. *Oikos*, 80(2):209–213, 1997.

[37] C Fuqua, Matthew R Parsek, and E Peter Greenberg. Regulation of gene expression by cell-to-cell communication: acyl-homoserine lactone quorum sensing. *Annual review of genetics*, 35:439–68, January 2001.

[38] Larry A Gallagher and Colin Manoil. Pseudomonas aeruginosa PAO1 Kills Caenorhabditis elegans by Cyanide Poisoning. *Journal Of Bacteriology*, 183(21):6207–6214, 2001.

[39] Andy Gardner and Kevin R Foster. The Evolution and Ecology of Cooperation- History and Concepts. In J H Korb and J Heinze, editors, *Ecology of Social Evolution*, chapter 1, pages 1–36. Springer, 2008.

[40] C Goodnight, E Rauch, H Sayama, M A M D E Aguiar, and M Baranger. Evolution in Spatial Predator-Prey Models and the Prudent Predator: The Inadequacy of Steady-State Organism Fitness and the Concept of Individual and Group Selection. *Complexity*, 13(5):23–44, 2008.

[41] Jan O Haerter, Ala Trusina, and Kim Sneppen. Bacterial CRISPR defense system buffers phage diversity. *Journal of Virology*, 85(20):10554–60, 2011.

[42] Oskar Hallatschek, Pascal Hersen, Sharad Ramanathan, and David R Nelson. Genetic drift at expanding frontiers promotes gene segregation. *Proceedings of the National Academy of Sciences of the United States of America*, 104(50):19926–30, December 2007.

[43] W.D. Hamilton. The genetical evolution of social behaviour. I. *Journal of Theoretical Biology*, 7(1):1–16, July 1964.

[44] F Harrison and A Buckling. Cooperative production of siderophores by Pseudomonas aeruginosa. *Frontiers in Bioscience*, Volume(14):4113, 2009.

[45] Eric L Haseltine and Frances H Arnold. Implications of rewiring bacterial quorum sensing. *Applied and environmental microbiology*, 74(2):437–45, January 2008.

[46] Silja Heilmann. Survival of the mediocre killers - Space and Mutability in Phage/Bacteria Ecosystems, Master Thesis, 2009.

[47] Richard H Heineman, James J Bull, and T Hansen. TESTING OPTIMALITY WITH EXPERIMENTAL EVOLUTION: LYSIS TIME IN A BACTERIOPHAGE. *Evolution: International Journal of Organic Evolution*, 61(7):1695–1709, 2007.

[48] Burkhard a Hense, Christina Kuttler, Johannes Müller, Michael Rothballer, Anton Hartmann, and Jan-Ulrich Kreft. Does efficiency sensing unify diffusion and quorum sensing? *Nature reviews. Microbiology*, 5(3):230–9, March 2007.

[49] R Hoge, A Pelzer, F Rosenau, and S Wilhelm. Weapons of a pathogen : Proteases and their role in virulence of Pseudomonas aeruginosa. *In Vitro*, 45:383–395, 2010.

[50] Taha Hosni, Chiaraluce Moretti, Giulia Devescovi, Zulma Rocio Suarez-Moreno, M Barek Fatmi, Corrado Guarnaccia, Sandor Pongor, Andrea Onofri, Roberto Buonaurio, and Vittorio Venturi. Sharing of quorum-sensing signals and role of interspecies communities in a bacterial plant disease. *The ISME journal*, 5(12):1–14, 2011.

[51] Koen Hufkens, Paul Scheunders, and Reinhart Ceulemans. Ecotones in vegetation ecology: methodologies and definitions revisited. *Ecological Research*, 24(5):977–986, 2009.

[52] Paul Hyman and Stephen T Abedon. Practical methods for determining phage growth parameters. *Methods In Molecular Biology Clifton Nj*, 501:175–202, 2009.

[53] Christine M Jessup and Samantha E Forde. Ecology and evolution in microbial systems: the generation and maintenance of diversity in phage-host interactions. *Research in microbiology*, 159(5):382–9, June 2008.

[54] Mario Juhas, Leo Eberl, and Burkhard Tummler. Quorum sensing: the power of cooperation in the world of Pseudomonas. *Environmental Microbiology*, 7(4):459–471, 2005.

[55] Tomer Kalisky, Erez Dekel, and Uri Alon. Cost-benefit theory and optimal design of gene regulation functions. *Physical Biology*, 4(4):229–45, 2007.

[56] Peter Kareiva, A Mullen, and R Southwood. Population Dynamics in Spatially Complex Environments: Theory and Data [and Discussion]. *Philosophical Transactions Biological Sciences*, 330(1257):175–190, 1990.

[57] Daniel B Kearns. A field guide to bacterial swarming motility. *Nature Reviews Microbiology*, 8(9):634–644, 2010.

[58] J. K. Kelly. Restricted Migration and the Evolution of Altruism by Kelly, J. K.: Evolution. 46(5):1492-1495. No - Bibliomania!, 1992.

[59] Benjamin Kerr, Claudia Neuhauser, Brendan J M Bohannan, and Antony M Dean. Local migration promotes competitive restraint in a host-pathogen 'tragedy of the commons'. *Nature*, 442(7098):75–8, July 2006.

[60] E Kessler, M Safrin, W R Abrams, J Rosenbloom, and D E Ohman. Inhibitors and specificity of Pseudomonas aeruginosa LasA. *The Journal of Biological Chemistry*, 272(15):9884–9889, 1997.

[61] Thilo Köhler, Angus Buckling, and Christian van Delden. Cooperation and virulence of clinical Pseudomonas aeruginosa populations. *Proceedings of the National Academy of Sciences of the United States of America*, 106(15):6339–44, May 2009.

[62] R Kownatzki, B Tümmler, and G Döring. Rhamnolipid of Pseudomonas aeruginosa in sputum of cystic fibrosis patients., 1987.

[63] Rolf Kümmerli and Sam P Brown. Molecular and regulatory properties of a public good shape the evolution of cooperation. *Proceedings of the National Academy of Sciences of the United States of America*, 107(44):18921–18926, 2010.

[64] Rolf Kümmerli, N Jiricny, L S Clarke, S A West, and A S Griffin. Phenotypic plasticity of a cooperative behaviour in bacteria. *Journal of Evolutionary Biology*, 22(3):589–598, 2009.

[65] Elizabeth Kutter and Alexander Sulakvelidze. *Bacteriophages: Biology and Applications*. CRC Press, 2004.

[66] Laurent Lapchin and Thomas Guillemaud. Asymmetry in host and parasitoid diffuse coevolution: when the red queen has to keep a finger in more than one pie. *Frontiers in Zoology*, 2(1):4, 2005.

[67] Joon-Hee Lee, Yannick Lequette, and E Peter Greenberg. Activity of purified QscR, a Pseudomonas aeruginosa orphan quorum-sensing transcription factor. *Molecular Microbiology*, 59(2):602–609, 2006.

[68] B R Levin and James J Bull. Phage therapy revisited: the population biology of a bacterial infection and its treatment with bacteria and antiobiotics. *The American Naturalist*, 147:881–898, 1996.

[69] B R Levin, F M Stewart, and L Chao. Resource-limited growth, competition, and predation: a model and experimental studies with bacteria and bacteriophage. *The American Naturalist*, 111(977):3–24, 1977.

[70] Yanjun Li, M Hong Nguyen, Shaoji Cheng, Stephan Schmidt, Li Zhong, Hartmut Derendorf, and Cornelius J Clancy. A pharmacokinetic/pharmacodynamic mathematical model accurately describes the activity of voriconazole against Candida spp. in vitro. *International journal of antimicrobial agents*, 31(4):369–74, April 2008.

[71] Tao Long, Kimberly C Tu, Yufang Wang, Pankaj Mehta, N P Ong, Bonnie L Bassler, and Ned S Wingreen. Quantifying the integration of quorum-sensing signals with single-cell resolution. *PLoS biology*, 7(3):e68, March 2009.

[72] M. E. Santos and J. W. Drake. Rates of Spontaneous Mutation in Bacteriophage T4 Are Independent of Host Fidelity Determinants, 1994.

[73] R Craig MaClean, Ayari Fuentes-Hernandez, Duncan Greig, Laurence D Hurst, and Ivana Gudelj. A mixture of "cheats" and "co-operators" can enable maximal group benefit. *PLoS biology*, 8(9), January 2010.

[74] J Maynard Smith and G R Price. The logic of animal conflict. *Nature*, 246(5427):15–18, 1973.

[75] M Mazzola, R J Cook, L S Thomashow, D M Weller, and L S Pierson III. Contribution of phenazine antibiotic biosynthesis to the ecological competence of fluorescent pseudomonads in soil habitats. *Appl environ microbiol*, 58(8):2616–2624, 1992.

[76] K H McClean, M K Winson, L Fish, A Taylor, S R Chhabra, M Camara, M Daykin, J H Lamb, S Swift, B W Bycroft, G S A B Stewart, and P Williams. Quorum sensing and Chromobacterium violaceum: exploitation of violacein production and inhibition for the detection of N-acylhomoserine lactones. *Microbiology*, 143(12):3703–3711, 1997.

[77] Pontus Melke, Patrik Sahlin, Andre Levchenko, and Henrik Jönsson. A cell-based model for quorum sensing in heterogeneous bacterial colonies. *PLoS computational biology*, 6(6):e1000819, June 2010.

[78] M Middelboe. Bacterial growth rate and marine virus-host dynamics. *Microbial Ecology, Vol. 40, No. 2 (Aug., 2000), pp. 114-124*, pages 114–124, 2000.

[79] M Milinski. TIT-FOR-TAT IN STICKLEBACKS AND THE EVOLUTION OF COOPERATION. *Nature*, 325(6103):433–435, 1987.

[80] M B Miller and Bonnie L Bassler. Quorum sensing in bacteria. *Annual Review of Microbiology*, 55(1):165–199, 2001.

[81] K Moebus. Marine bacteriophage reproduction under nutrient-limited growth of host bacteria. I. Investigations with six phage-host systems. *Marine Ecology Progress Series*, 144:1–12, 1996.

[82] Pieter Moons, R Van Houdt, A Aertsen, K Vanoirbeek, and C W Michiels. Quorum sensing dependent production of antimicrobial component influences establishment of E. coli in dual species biofilms with Serratia plymuthica. *Communications in Agricultural and Applied Biological Sciences*, 70(2):195–198, 2005.

[83] Pieter Moons, Rob Van Houdt, Abram Aertsen, Kristof Vanoirbeek, Yves Engelborghs, and Chris W Michiels. Role of quorum sensing and antimicrobial component production by Serratia plymuthica in formation of biofilms, including mixed biofilms with Escherichia coli. *Applied and environmental microbiology*, 72(11):7294–300, November 2006.

[84] Johan W Mouton, Nieko Punt, and Alexander A Vinks. Concentration-effect relationship of ceftazidime explains why the time above the MIC is 40 percent for a static effect in vivo. *Antimicrobial agents and chemotherapy*, 51(9):3449–51, September 2007.

[85] Carey D Nadell, Kevin R Foster, and João B Xavier. Emergence of spatial structure in cell groups and the evolution of cooperation. *PLoS computational biology*, 6(3):e1000716, March 2010.

[86] Carey D Nadell, Joao B Xavier, Simon a Levin, and Kevin R Foster. The evolution of quorum sensing in bacterial biofilms. *PLoS biology*, 6(1):e14, January 2008.

[87] J B Neilands. Siderophores of bacteria and fungi. *Microbiological sciences*, 1(1):9–14, 1984.

[88] Wai-Leung Ng and Bonnie L Bassler. Bacterial quorum-sensing network architectures. *Annual review of genetics*, 43:197–222, January 2009.

[89] Vicente Ortega-Cejas, Joaquim Fort, Vicenç Méndez, and Daniel Campos. Approximate solution to the speed of spreading viruses. *Physical Review E - Statistical, Nonlinear and Soft Matter Physics*, 69(3 Pt 1):031909, 2004.

[90] Parada Veronica, Herndl Gerhard J., Weinbauer Markus G., P Parada, Gerhard J Herndl, Markus G Weinbauer O, and Nl-A B Den Burg. Viral burst size of heterotrophic prokaryotes in aquatic systems, 2006.

[91] E A Pierson, D W Wood, J A Cannon, F M Blachere, and L S Pierson. Interpopulation signaling via N-acyl-homoserine lactones among bacteria in the wheat rhizosphere. *Molecular PlantMicrobe Interactions*, 11(11):1078–1084, 1998.

[92] M Pirhonen, D Flego, R Heikinheimo, and E T Palva. A small diffusible signal molecule is responsible for the global control of virulence and exoenzyme production in the plant pathogen Erwinia carotovora. *the The European Molecular Biology Organization Journal*, 12(6):2467–2476, 1993.

[93] a G Pisabarro, M a de Pedro, and D Vázquez. Structural modifications in the peptidoglycan of Escherichia coli associated with changes in the state of growth of the culture. *Journal of bacteriology*, 161(1):238–42, January 1985.

[94] Seth D Pollak. Origins of Altruism and Cooperation. *Prospects*, pages 333–341, 2011.

[95] Cassie F Pope, Timothy D McHugh, and Stephen H Gillespie. Methods to determine fitness in bacteria. *Methods In Molecular Biology Clifton Nj*, 642:113–21, 2010.

[96] W H Press, S A Teukolsky, W T Vetterling, and B P Flannery. *Numerical Recipes in C: The Art of Scientific Computing*, volume 9. Cambridge University Press, 1992.

[97] Avinoam Rabinovitch, Ira Aviram, and Arieh Zaritsky. Bacterial debris-an ecological mechanism for coexistence of bacteria and their viruses. *Journal of Theoretical Biology*, 224(3):377–383, 2003.

[98] Avinoam Rabinovitch, Itzhak Fishov, Hilla Hadas, Monica Einav, and Arieh Zaritsky. Bacteriophage T4 development in Escherichia coli is growth rate dependent. *Journal of theoretical biology*, 216(1):1–4, May 2002.

[99] Erlan Ramanculov and Ry Young. Genetic analysis of the T4 holin: timing and topology. *Gene*, 265(1-2):25–36, March 2001.

[100] Huimin Ran, Daniel J Hassett, and Gee W Lau. Human targets of Pseudomonas aeruginosa pyocyanin. *Proceedings of the National Academy of Sciences of the United States of America*, 100(24):14315–14320, 2003.

[101] Rosemary J Redfield. Is quorum sensing a side effect of diffusion sensing? *Trends in microbiology*, 10(8):365–70, August 2002.

[102] Alexander H Rickard, Peter Gilbert, Nicola J High, Paul E Kolenbrander, and Pauline S Handley. Bacterial coaggregation: an integral process in the development of multi-species biofilms. *Trends in Microbiology*, 11(2):94–100, February 2003.

[103] K Riedel, M Hentzer, O Geisenberger, B Huber, A Steidle, H Wu, N Hø iby, M Givskov, S Molin, and L Eberl. N-acylhomoserine-lactone-mediated communication between Pseudomonas aeruginosa and Burkholderia cepacia in mixed biofilms. *Microbiology (Reading, England)*, 147(Pt 12):3249–62, December 2001.

[104] Martin Rosvall, Ian B Dodd, Sandeep Krishna, and Kim Sneppen. Network Models of Phage-Bacteria Coevolution. *Physical Review E - Statistical, Nonlinear and Soft Matter Physics*, 74(6 Pt 2):066105, 2006.

[105] Kelsi M Sandoz, Shelby M Mitzimberg, and Martin Schuster. Social cheating in Pseudomonas aeruginosa quorum sensing. *Proceedings of the National Academy of Sciences of the United States of America*, 104(40):15876–81, October 2007.

[106] J Andy Schaber, Nancy L Carty, Naomi A McDonald, Eric D Graham, Rajkumar Cheluvappa, John A Griswold, and Abdul N Hamood. Analysis of quorum sensing-deficient clinical isolates of Pseudomonas aeruginosa. *Journal of Medical Microbiology*, 53(Pt 9):841–853, 2004.

[107] S Schauder and Bonnie L Bassler. The languages of bacteria. *Genes & Development*, 15(12):1468–80, 2001.

[108] Michael P Schlüsener and Kai Bester. Persistence of antibiotics such as macrolides, tiamulin and salinomycin in soil. *Environmental Pollution*, 143(3):565–571, 2006.

[109] S J Schrag and J E Mittler. Host-parasite coexistence: the role of spatial refuges in stabilizing bacteria-phage interactions. *The American Naturalist*, 148(2):348–377, 1996.

[110] Martin Schuster and E Peter Greenberg. A network of networks: quorum-sensing gene regulation in Pseudomonas aeruginosa. *International journal of medical microbiology IJMM*, 296(2-3):73–81, 2006.

[111] Martin Schuster, C. P. Lostroh, Tomoo Ogi, and E Peter Greenberg. Identification, Timing, and Signal Specificity of Pseudomonas aeruginosa Quorum-Controlled Genes: a Transcriptome Analysis. *Journal of Bacteriology*, 185(7):2066–2079, April 2003.

[112] Yongping Shao and Ing-Nang Wang. Bacteriophage adsorption rate and optimal lysis time. *Genetics*, 180(1):471–82, September 2008.

[113] Kennon M Sheldon. Learning the lessons of tit-for-tat: Even competitors can get the message. *Journal of Personality*, 77(6):1245–1253, 1999.

[114] Sankale Shompole, Kim T Henon, Linda E Liou, Katarzyna Dziewanowska, Gregory A Bohach, and Kenneth W Bayles. Biphasic intracellular expression of Staphylococcus aureus virulence factors and evidence for Agr-mediated diffusion sensing. *Molecular Microbiology*, 49(4):919–927, 2003.

[115] Sanna Sillankorva, Rosário Oliveira, Maria João Vieira, Ian W Sutherland, and Joana Azeredo. Bacteriophage Phi S1 infection of Pseudomonas fluorescens planktonic cells versus biofilms. *Biofouling*, 20(3):133–8, June 2004.

[116] E H Simpson. The Interpretation of Interaction in Contingency Tables. *Journal of the Royal Statistical Society Series B Methodological*, 13(2):238–241, 1951.

[117] Lucas J Stal. Cyanobacterial mats and stromatolites. In Brian A Whitton and Malcom Potts, editors, *Ecology*, chapter 4, pages 61–120. Kluwer Academic Publishers, 2000.

[118] A Steidle, K Sigl, R Schuhegger, A Ihring, M Schmid, S Gantner, M Stoffels, K Riedel, M Givskov, A Hartmann, C Langebartels, and L Eberl. Visualization of N-acylhomoserine lactone-mediated cell-cell communication between bacteria colonizing the tomato rhizosphere. *Applied and environmental microbiology*, 67(12):5761–70, December 2001.

[119] Claus Sternberg, B B Christensen, T Johansen, a Toftgaard Nielsen, Jens Bo Andersen, M Givskov, and S Molin. Distribution of bacterial growth activity in flow-chamber biofilms. *Applied and environmental microbiology*, 65(9):4108–17, October 1999.

[120] Ann M Stevens, Martin Schuster, and Kendra P Rumbaugh. Working together for the common good: cell-cell communication in bacteria. *Journal of bacteriology*, 194(9):2131–41, May 2012.

[121] F M Stewart and B R Levin. The population biology of bacterial viruses: why be temperate. *Theoretical Population Biology*, 26(1):93–117, 1984.

[122] Uldis N Streips and Ronald E Yasbin, editors. *Modern Microbial Genetics*. Wiley-Liss, New York, 2nd edition, 2002.

[123] Curtis a Suttle. Viruses in the sea. *Nature*, 437(7057):356–61, September 2005.

[124] Curtis a Suttle. Marine viruses–major players in the global ecosystem. *Nature reviews. Microbiology*, 5(10):801–12, October 2007.

[125] Lee R Swem, Danielle L Swem, Colleen T O'Loughlin, Raleene Gatmaitan, Bixiao Zhao, Scott M Ulrich, and Bonnie L Bassler. A quorum-sensing antagonist targets both membrane-bound and cytoplasmic receptors and controls bacterial pathogenicity. *Molecular Cell*, 35(2):143–153, 2009.

[126] Karen Tait, L C Skillman, and Ian W Sutherland. The efficacy of bacteriophage as a method of biofilm eradication. *Biofouling*, 18(4):305–311, January 2002.

[127] TF Thingstad and R Lignell. Theoretical models for the control of bacterial growth rate, abundance, diversity and carbon demand, 1997.

[128] D S Toder, S J Ferrell, J L Nezezon, L Rust, and B H Iglewski. lasA and lasB genes of Pseudomonas aeruginosa: analysis of transcription and gene product activity. *Infection and Immunity*, 62(4):1320–1327, 1994.

[129] M L Urbanowski, C P Lostroh, and E P Greenberg. Reversible Acyl-Homoserine Lactone Binding to Purified Vibrio fischeri LuxR Protein. *Journal Of Bacteriology*, 186(3):631–637, 2004.

[130] L Van Valen. A new evolutionary law. *Theory*, 1:1–30, 1973.

[131] Vittorio Venturi, Arianna Friscina, Iris Bertani, Giulia Devescovi, and Claudio Aguilar. Quorum sensing in the Burkholderia cepacia complex. *Research in Microbiology*, 155(4):238–244, 2004.

[132] P F Verhulst. Notice sur la loi que la population suit dans son accroissement. *Corr Math et Phys*, 10(10):113–121, 1838.

[133] J Von Neumann and O Morgenstern. *Theory of Games and Economic Behaviour*, volume 2. Princeton University Press, 1944.

[134] Michiel Vos, Philip J Birkett, Elizabeth Birch, Robert I Griffiths, and Angus Buckling. Local adaptation of bacteriophages to their bacterial hosts in soil. *Science*, 325(5942):833, 2010.

[135] Barbara Vu, Miao Chen, Russell J Crawford, and Elena P Ivanova. Bacterial extracellular polysaccharides involved in biofilm formation. *Molecules Basel Switzerland*, 14(7):2535–2554, 2009.

[136] Joe Yuichiro Wakano, Martin A Nowak, and Christoph Hauert. Spatial dynamics of ecological public goods. *Proceedings of the National Academy of Sciences of the United States of America*, 106(19):7910–7914, 2009.

[137] I N Wang, D L Smith, and R Young. Holins: the protein clocks of bacteriophage infections. *Annual Review of Microbiology*, 54(1):799–825, 2000.

[138] Ya-Juan Wang and Jared Renton Leadbetter. Rapid acyl-homoserine lactone quorum signal biodegradation in diverse soils. *Applied and Environmental Microbiology*, 71(3):1291–1299, 2005.

[139] Christopher M Waters and Bonnie L Bassler. Quorum Sensing : Communication in Bacteria. *Communication*, 21(1):319–46, 2005.

[140] R Weiner, S Langille, and E Quintero. Structure, function and immunochemistry of bacterial exopolysaccharides. *Journal Of Industrial Microbiology*, 15:339–346, 1995.

[141] J S Weitz, H Hartman, and S A Levin. Coevolutionary arms races between bacteria and bacteriophage. *Proceedings of the National Academy of Sciences of the United States of America*, 102(27):9535–9540, 2005.

[142] Joshua S Weitz and Jonathan Dushoff. Alternative stable states in host-phage dynamics. *Theoretical Ecology*, 1(1):13–19, 2008.

[143] William B Whitman, David C Coleman, and William J Wiebe. Prokaryotes : The unseen majority Notes : Perspective Prokaryotes : The unseen majority. *PNAS*, 95(January):6578–6583, 2007.

[144] Cara N Wilder, Stephen P Diggle, and Martin Schuster. Cooperation and cheating in Pseudomonas aeruginosa: the roles of the las, rhl and pqs quorum-sensing systems. *The ISME journal*, 5(8):1332–43, August 2011.

[145] Klaus Winzer and Paul Williams. Quorum sensing and the regulation of virulence gene expression in pathogenic bacteria. *International journal of medical microbiology IJMM*, 291(2):131–143, 2001.

[146] João B Xavier and Kevin R Foster. Cooperation and conflict in microbial biofilms. *Proceedings of the National Academy of Sciences of the United States of America*, 104(3):876–81, January 2007.

[147] João B Xavier, Wook Kim, and Kevin R Foster. A molecular mechanism that stabilizes cooperative secretions in Pseudomonas aeruginosa. *Molecular microbiology*, 79(1):166–79, January 2011.

[148] Grace Yim, Helena Huimi Wang, and Julian Davies Frs. Antibiotics as signalling molecules. *Philosophical Transactions of the Royal Society of London - Series B: Biological Sciences*, 362(1483):1195–1200, 2007.

[149] Yi Zheng, Douglas K Struck, Chelsey A Dankenbring, and Ry Young. Evolutionary dominance of holin lysis systems derives from superior genetic malleability. *Microbiology*, 154(Pt 6):1710–1718, 2008.

[150] Jun Zhu, Melissa B Miller, Russell E Vance, Michelle Dziejman, Bonnie L Bassler, and John J Mekalanos. Quorum-sensing regulators control virulence gene expression in Vibrio cholerae. *Proceedings of the National Academy of Sciences of the United States of America*, 99(5):3129–3134, 2002.

[151] Jun Zhu and Stephen C Winans. Autoinducer binding by the quorum-sensing regulator TraR increases affinity for target promoters in vitro and decreases TraR turnover rates in whole cells. *Proceedings of the National Academy of Sciences of the United States of America*, 96(9):4832–4837, 1999.